DE[redacted]IED

Copy 20
RM SL56K21

NACA

AUTHORITY
NACA TO LEBOW
MEMO DATED 12/13/6

Declassified by authority of NASA
Classification Change Notices No. 43
Dated ** 12/29/65

RESEARCH MEMORANDUM

for the

Bureau of Aeronautics, Department of the Navy

INVESTIGATION OF DRAG AND STATIC LONGITUDINAL AND LATERAL STABILITY CHARACTERISTICS OF A 1/15-SCALE MODEL OF THE GRUMMAN F11F-1F AIRPLANE AT MACH NUMBERS OF 1.56, 1.76, 2.06, AND 2.53

TED. NO. NACA AD 3125

By Kenneth L. Turner and Roger H. Fournier

Langley Aeronautical Laboratory
Langley Field, Va.

SERVICE REPORT

[redacted]

N66 81477
(ACCESSION NUMBER)
177
(PAGES)
(NASA CR OR TMX OR AD NUMBER)
(THRU)
(CODE)
(CATEGORY)
FACILITY FORM 602

TIONAL ADVISORY COMMITTEE
FOR AERONAUTICS
WASHINGTON

NOV 30 1956

[redacted]

 DEC[redacted]IFIED

NATIONAL ADVISORY COMMITTEE FOR AERONAUTICS

RESEARCH MEMORANDUM

for the

Bureau of Aeronautics, Department of the Navy

INVESTIGATION OF DRAG AND STATIC LONGITUDINAL AND LATERAL STABILITY CHARACTERISTICS OF A 1/15-SCALE MODEL OF THE GRUMMAN F11F-1F AIRPLANE AT MACH NUMBERS OF 1.56, 1.76, 2.06, AND 2.53

TED. NO. NACA AD 3125

By Kenneth L. Turner and Roger H. Fournier

AUTHORITY
DROBKA TO LEBOW
MEMO DATED 12/13/65

DECLASSIFIED
ATS 430

SUMMARY

An investigation was made in the Langley Unitary Plan wind tunnel to determine the drag and static longitudinal and lateral stability characteristics of a 1/15-scale model of the Grumman F11F-1F airplane at Mach numbers of 1.56, 1.76, 2.06, and 2.53. The effects on performance and stability of modifications consisting of a wing-root leading-edge fillet and horizontal tails with negative dihedral of 10° and 30° are included in this investigation. The Reynolds numbers of this test, based on the mean aerodynamic chord of the wing, are 1.33×10^{6}, 1.25×10^{6}, 1.10×10^{6}, and 0.87×10^{6} at Mach numbers of 1.56, 1.76, 2.06, and 2.53, respectively.

INTRODUCTION

At the request of the Bureau of Aeronautics, Department of the Navy, an investigation of the aerodynamic characteristics of a 1/15-scale model of the Grumman F11F-1F airplane at supersonic speeds has been undertaken by the National Advisory Committee for Aeronautics.

[redacted]

Declassified by authority of NASA
Classification Change Notices No. 45
Dated ** 12/29/63

This paper contains results obtained at Mach numbers of 1.56, 1.76, 2.06, and 2.53 for angles of attack from -4° to 12° and for angles of sideslip from -2° to 6°. The effect on performance and stability of model modifications consisting of a wing-root leading-edge fillet and horizontal-tail negative dihedral of 10° and 30° is also included.

COEFFICIENTS AND SYMBOLS

The results of these tests are presented as coefficients of forces and moments referred to the stability-axes system. All aerodynamic moments were taken about the center of gravity which is longitudinally located at the 0.25 mean aerodynamic chord and at a station 0.661 inch below the wing-root chord. Symbols used in this paper are as follows:

b wing span, in.

c local chord

$\bar{c}$ mean aerodynamic chord, in.

C_D' drag coefficient, F_D'/qS

C_{D_b}' base-drag coefficient, $-\dfrac{A_b \cos \alpha}{qS}$

C_{D_c}' chamber-drag coefficient, $-\dfrac{A_c \cos \alpha}{qS}$

C_{D_e} net external drag

ΔC_{D_t} change in drag due to fixing transition

C_{D_i}' internal-duct drag coefficient, $\dfrac{A_i \cos \alpha + \dfrac{m_D}{m_S} S_1 q \sin^2 \alpha}{qS}$

C_L lift coefficient, L/qS

C_m pitching-moment coefficient, $m/qS\bar{c}$

[redacted]

C_l	rolling-moment coefficient, l/qSb
C_n	yawing-moment coefficient, n/qSb
C_Y	lateral-force coefficient, Y/qS
F_D'	force along X-axis, lb
A_b	base axial force, lb
A_c	chamber axial force, lb
A_i	internal-duct axial force, lb
L	lift, lb
m	pitching moment, in-lb
l	rolling moment, in-lb
n	yawing moment, in-lb
Y	lateral force, lb
M	free-stream Mach number
p	free-stream static pressure, lb/sq ft
q	free-stream dynamic pressure, $0.7pM^2$, lb/sq ft
m_E	weight flow through duct, lb/sec
m_1	weight flow based on inlet area and free-stream conditions, lb/sec
V	free-stream velocity, ft/sec
S	wing area including body intercept, sq ft
S_1	duct-inlet area, sq ft
i_t	stabilator angle, deg
α	angle of attack of wing chord line, deg
β	angle of sideslip of fuselage center line, deg

APPARATUS AND METHODS

Tunnel

The tests were made in the low Mach number test section of the Langley Unitary Plan wind tunnel. This tunnel is a variable-pressure, continuous, return-flow type. The test section is 4 feet square and approximately 7 feet in length. The nozzle leading to the test section is of the asymmetric sliding-block type and Mach number may be varied continuously through a Mach number range from approximately 1.56 to 2.80 without tunnel shutdown.

Model and Support System

The 1/15-scale steel model was constructed by Grumman Aircraft Engineering Corp. A three-view drawing of the airplane is presented as figure 1. Photographs of the model as tested are presented in figure 2. Figure 3 shows the modifications used in tests of this model. The basic model had a wing with 35° sweepback of the quarter chord, an aspect ratio of 4, a taper ratio of 0.5, and dihedral of -2.5°. The geometric characteristics of the model are presented in table I. The model had the cambered leading-edge modification described in reference 1 installed during all the tests.

The model was attached to the forward end of an enclosed, six-component, electrical strain-gage balance. This balance was attached, by means of a sting, to the tunnel central support system. Balance and read-out equipment were supplied by the National Advisory Committee for Aeronautics.

An additional component of the model support system was a remotely operated, adjustable coupling that enabled tests to be performed at variable sideslip angles concurrently with variable angles of attack. This coupling was placed between the model sting and the tunnel central support system. The adjustable coupling permits vertical angular variations of approximately ±20°.

Measurements and Accuracy

Tests were made through an angle-of-attack range from approximately -4° to 12° for 0° sideslip angle. At angles of attack of approximately 0°, 5°, and 10°, sideslip angles from approximately -2° to 6° were tested. All angles of attack and angles of sideslip were corrected for the deflection of the sting and balance under static load conditions. These angles

are estimated to be accurate within ±0.1°. All basic model tests were performed with a stabilator incidence of 0°. The maximum deviation of local Mach number in the portion of the tunnel occupied by the model was ±0.015 from the average values given.

The dewpoint temperature for all tests was maintained below -30° F. The stagnation temperature was approximately 125° F and the stagnation pressure was maintained at approximately 9 pounds per square inch.

The tunnel, as yet, has not been completely calibrated, and any flow angularity that might exist in the tunnel has not been determined. Tunnel pressure gradients in the region of the model have been determined and are sufficiently small so as not to induce any buoyancy effect on the model.

The accuracy of the force and moment coefficients, based on balance calibration and reproducibility of data, is estimated to be within the following limits:

C_L	±0.002
C_D	±0.001
C_m	±0.001
C_l	±0.0002
C_n	±0.0005
C_Y	±0.0015

The drag data have been adjusted to correspond to zero-balance chamber-drag coefficient $\left(C_{D_C} = 0\right)$. Several examples of these drag-coefficient corrections are presented in figure 4 in order to show the relative magnitudes of these coefficients for this model.

Internal-duct drag and base drag of the model were obtained for all test points and have been subtracted out of the drag data, thus leaving all drag coefficients in terms of net external drag. The internal-duct drag was obtained by measuring the mass flow in the duct with a calibrated total- and static-pressure rake. The mass flow in collaboration with measurement of Mach number and pressure at the duct exit determines the internal drag of the duct. Several curves showing the variation of internal-duct-drag coefficient and base-drag coefficient with angle of attack and Mach number are presented in figure 5 in order to give an example of the relative magnitude of these coefficients.

In order to assure turbulent flow over the model, a few tests were performed with transition fixed on the model. For this condition, a

transition strip was placed around the fuselage, 1 inch rearward of the model nose, and on the 10 percent chord of the wing, full span, top and bottom. These transition strips were 0.25 inch wide and consisted of no. 60 carborundum grains imbedded in shellac with approximately 15 grains per 0.25 square inch. The results of these tests are presented in figures 6 and 7.

In order to obtain net external drag, the drag coefficients shown in the characteristic plots must be increased by the incremental difference in drag coefficient shown in figure 6 at the same model attitude $\left(C_{D_e} = C_D' + \Delta C_{D_t}\right)$. A small part of the drag caused by fixing transition is due to the wave drag of the transition strips. It is believed, however, that this is more than offset by the differences in smoothness between the model and the full-scale airplane.

Figures 8 and 9 present plots of mass-flow ratio against angle of attack and sideslip, respectively, at all test Mach numbers. It may be noted that some of the mass-flow ratios are greater than one. The mass flows were computed from values taken from an internally mounted pressure rake which was calibrated statically at a zero angle of attack. This calibration may not be perfectly correct under test conditions, thus leading to errors in measurements.

A study of the force data in conjunction with the schlieren photographs (fig. 10) indicates wall-reflected shock waves striking the model tail at $\alpha = 12^{\circ}$ and $\beta = 6^{\circ}$ at a Mach number of 1.56. The data indicate, however, that the effect of these shock reflections is relatively minor.

PRESENTATION OF RESULTS

The results of the investigation are presented in the following figures:

	Figure
Effect of horizontal and vertical tails on aerodynamic characteristics in pitch ($\beta = 0^{\circ}$)	11
Effect of root leading-edge wing fillets on aerodynamic characteristics in pitch ($\beta = 0^{\circ}$)	12
Effect of horizontal-tail negative dihedral on aerodynamic characteristics in pitch ($\beta = 0^{\circ}$)	13
Effect of flaperon on aerodynamic characteristics in pitch ($\beta = 0^{\circ}$)	14
Effect of ventral fins on aerodynamic characteristics in pitch ($\beta = 0^{\circ}$)	15
Effect of mass-flow ratio on aerodynamic characteristics in pitch ($\beta = 0^{\circ}$)	16

[redacted]

Figure

Effect of faired duct inlets on aerodynamic characteristics in pitch ($\beta = 0^{\circ}$) 17
Effect of horizontal and vertical tails on aerodynamic characteristics in sideslip 18
Effect of root leading-edge wing fillets on aerodynamic characteristics in sideslip 19
Effect of horizontal-tail negative dihedral on aerodynamic characteristics in sideslip 20
Effect of ventral fins on aerodynamic characteristics in sideslip 21
Effect of mass-flow ratio on aerodynamic characteristics in sideslip 22
Effect of faired duct inlets on aerodynamic characteristics in sideslip 23

RESULTS

This is a data report and the basic results are presented without analysis; however, some general observations relative to the data are as follows:

1. The net external minimum drag coefficients for the basic model configuration at Mach numbers of 1.56, 1.76, 2.06, and 2.53 are 0.046, 0.046, 0.044, and 0.044, respectively. Fixing transition on the model increases minimum drag coefficient approximately 0.004 at all Mach numbers tested.

2. The neutral points for the basic model configuration at Mach numbers of 1.56, 1.76, 2.06, and 2.53 are located at 60, 57, 54, and 52 percent of the mean aerodynamic chord, respectively. With the tails off, the neutral points at Mach numbers of 1.56, 1.76, and 2.06 are located at 37, 36, and 33 percent of the mean aerodynamic chord, respectively. The two negative-dihedral tails and the flaperon moved the neutral point rearward for all test Mach numbers, whereas use of a wing-root leading-edge fillet caused the neutral point to move forward at all test Mach numbers.

3. The results indicate positive static directional stability for all tail-on model configurations at angles of attack up to 10.6° for all test Mach numbers. Increases in angle of attack or Mach number lead to decreased directional stability. Adding negative dihedral to the horizontal tail or use of ventral fins increases the positive static directional stability at all Mach numbers tested.

[redacted]

4. Positive effective dihedral is indicated for the basic model configuration at all test Mach numbers. Increasing horizontal-tail negative dihedral or use of ventral fins decreases the positive effective dihedral. Increases in angle of attack also lead to less positive effective dihedral.

Langley Aeronautical Laboratory,
National Advisory Committee for Aeronautics,
Langley Field, Va., October 25, 1956.

Kenneth L. Turner

Kenneth L. Turner
Aeronautical Research Engineer

Roger H. Fournier

Roger H. Fournier
Aeronautical Research Engineer

Approved: Herbert A. Wilson
Herbert A. Wilson
Chief of Unitary Wind Tunnel

ccb

REFERENCE

1. Palazzo, Edward B., and Spearman, M. Leroy: Static Longitudinal and Lateral Stability and Control Characteristics of a Model of a 35° Swept-Wing Airplane at a Mach Number of 1.41. NACA RM L54G08, 1955.

[redacted]

TABLE I.- GEOMETRIC CHARACTERISTICS OF THE 1/15-SCALE GRUMMAN F11F-1F AIRPLANE MODEL

Center-of-gravity location (3.15 percent M.A.C. above fuselage reference line)	$\bar{c}/4$
Wing:	
Loading, lb/sq ft	72.4
Area (theoretical), sq ft	1.11
Span, in.	25.310
Aspect ratio	4
Taper ratio	0.5
Sweepback of quarter-chord line, deg	35
Dihedral, deg	-2.5
Incidence, deg	0
Geometric twist, deg	0
Airfoil section:	
Root	NACA 65A006
Tip	NACA 65A004
Root chord, in.	8.440
Tip chord, in.	4.220
Root-chord location:	
Longitudinal (behind nose at fuselage station 108), in.	15.567
Vertical (above fuselage reference line), in.	0.867
Mean aerodynamic chord:	
Length, in.	6.55
Location:	
Longitudinal (at leading edge):	
Behind nose, in.	19.972
Behind root leading edge, in.	4.405
Lateral, in.	5.621
Vertical (above fuselage reference line), in.	0.524
Fuselage:	
Length, in.	35.400
Width, in.	4.68
Depth, in.	4.55
Frontal area, sq in.	15.365
Overall fineness ratio	9.761
Side area, sq in.	129.61
Volume, cu in.	270.46
Base annulus area, sq in.	3.05
Horizontal tail:	
Area:	
Theoretical, sq ft	0.3043
Exposed, sq ft	0.1898
Span, in.	12.500
Aspect ratio	3.56
Taper ratio	0.393
Root-chord length, in.	5.036
Mean aerodynamic chord:	
Length, in.	3.730
Location:	
Longitudinal (at fuselage station 431.45)	c/4
Lateral, in.	2.671
Vertical (below fuselage reference line) in.	0.2000
Tail length, in.	10.185
Sweepback of quarter-chord line, deg	35
Dihedral, deg	0
Geometric twist, deg	0
Airfoil section:	
Root	65A006.04
Tip	65A004
Tip-chord length, in.	1.980
Vertical tail:	
Area exposed, sq ft	0.2004
Span, in.	6.733
Aspect ratio	1.40
Taper ratio	0.286
Root-chord length (on 3° bias), in.	7.467
Airfoil section:	
Root	NACA 16005.62
Tip	NACA 16005.62
Tip-chord length (on 3° bias), in.	2.133
Duct areas:	
Inlet, sq in.	2.44
Compressor inlet, sq in.	≈3.60
Exit (normal choke), sq in.	2.34
Exit (low mass-flow choke), sq in.	2.07

[redacted]

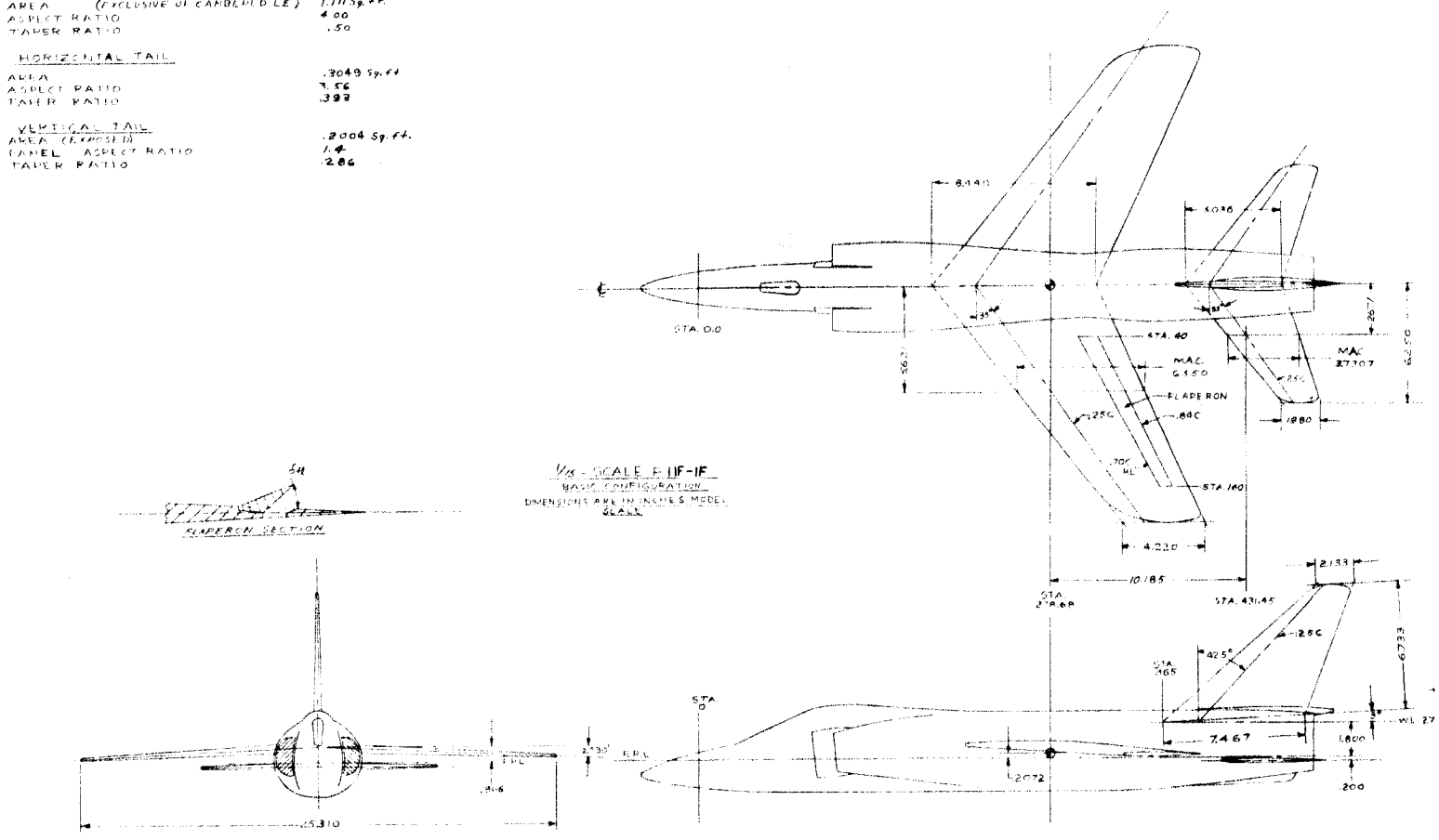

Figure 1.- Three-view drawing of 1/15-scale model of the Grumman F11F-1F airplane.

DECLASSIFIED

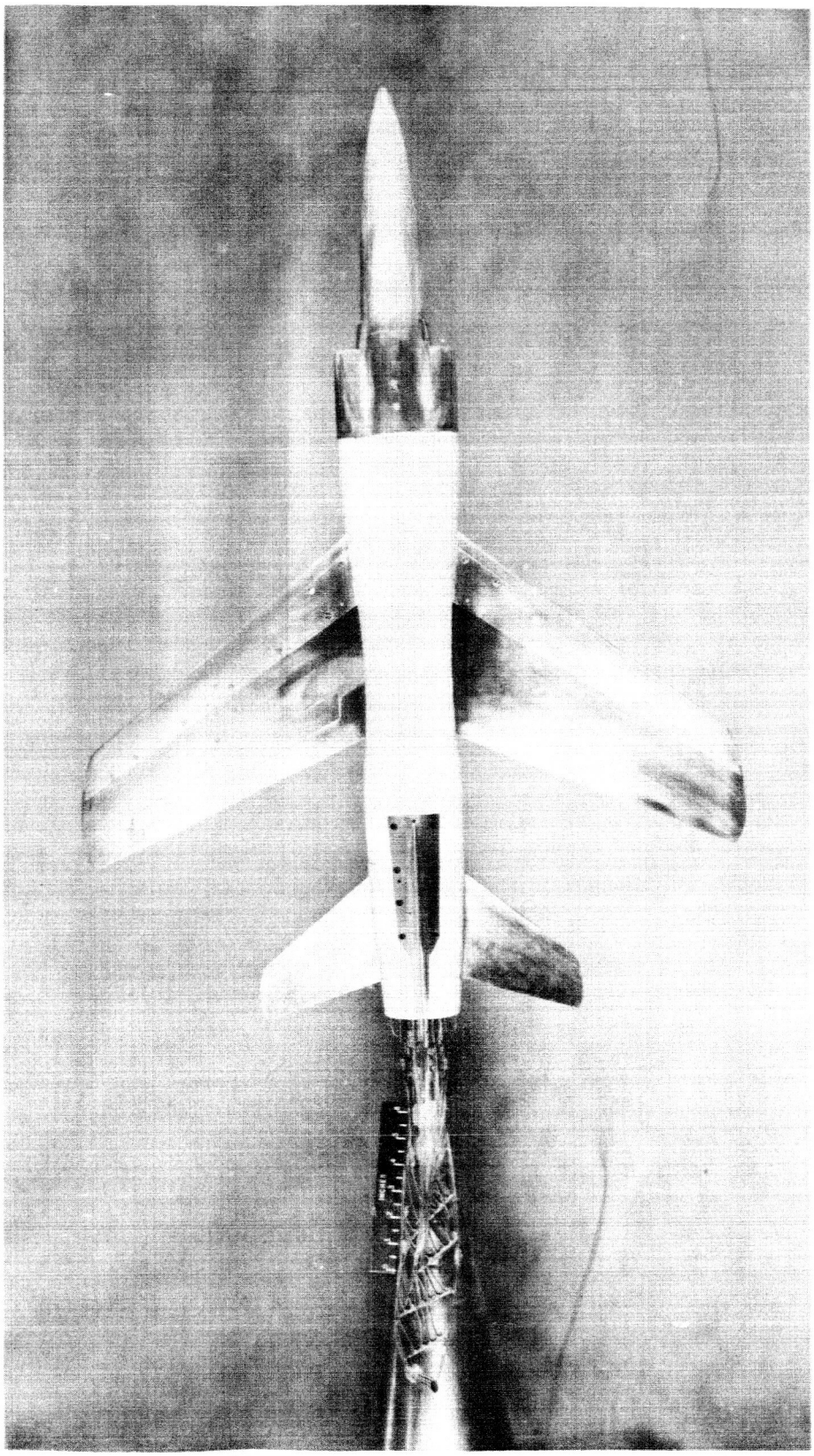

L-93706

(a) Top view.

Figure 2.- Photographs of the 1/15-scale model of the Grumman F11F-1F airplane.

DECLASSIFIED

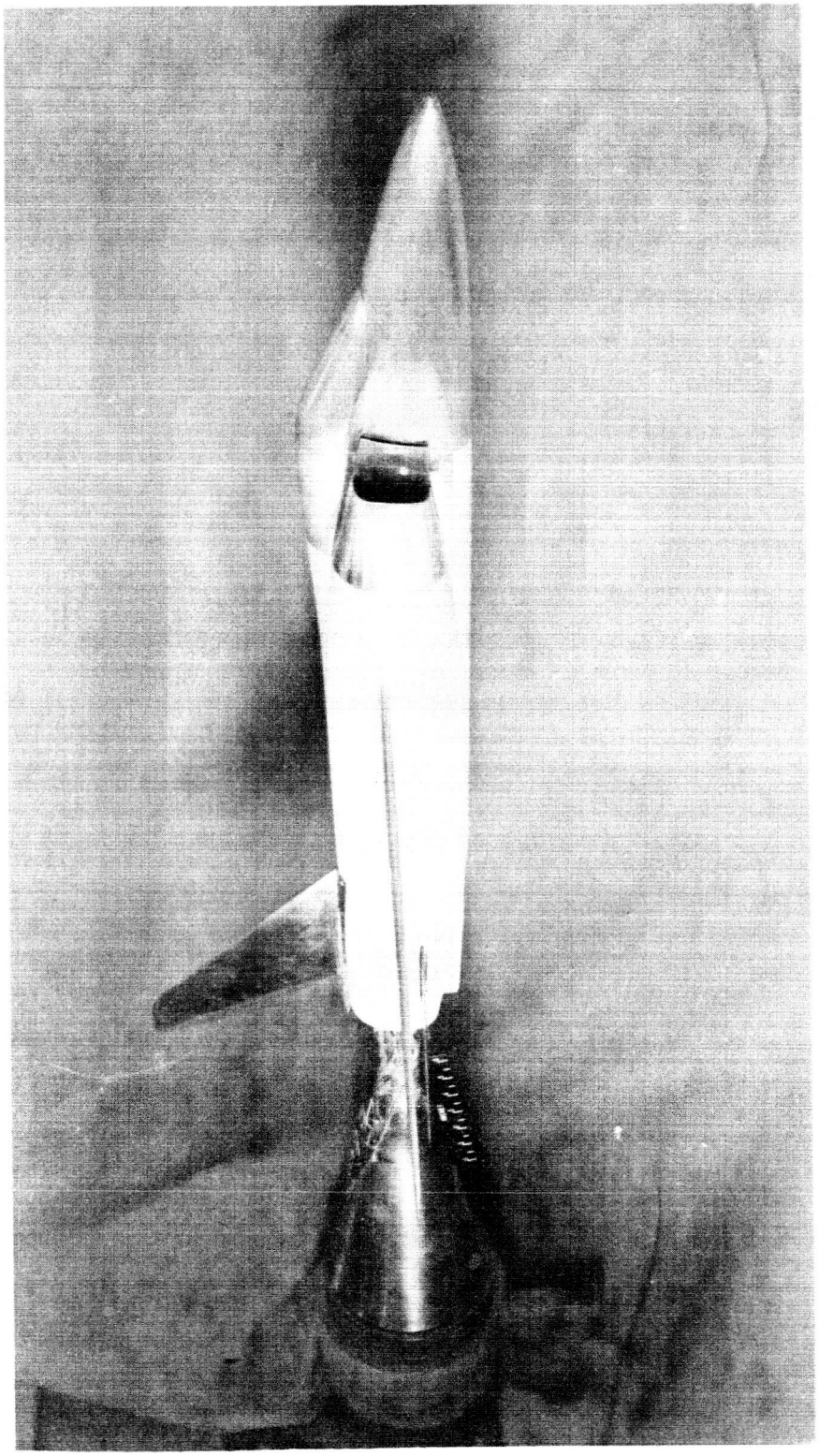

L-93712

(b) Three-quarter front view.

Figure 2.- Continued.

DECLASSIFIED

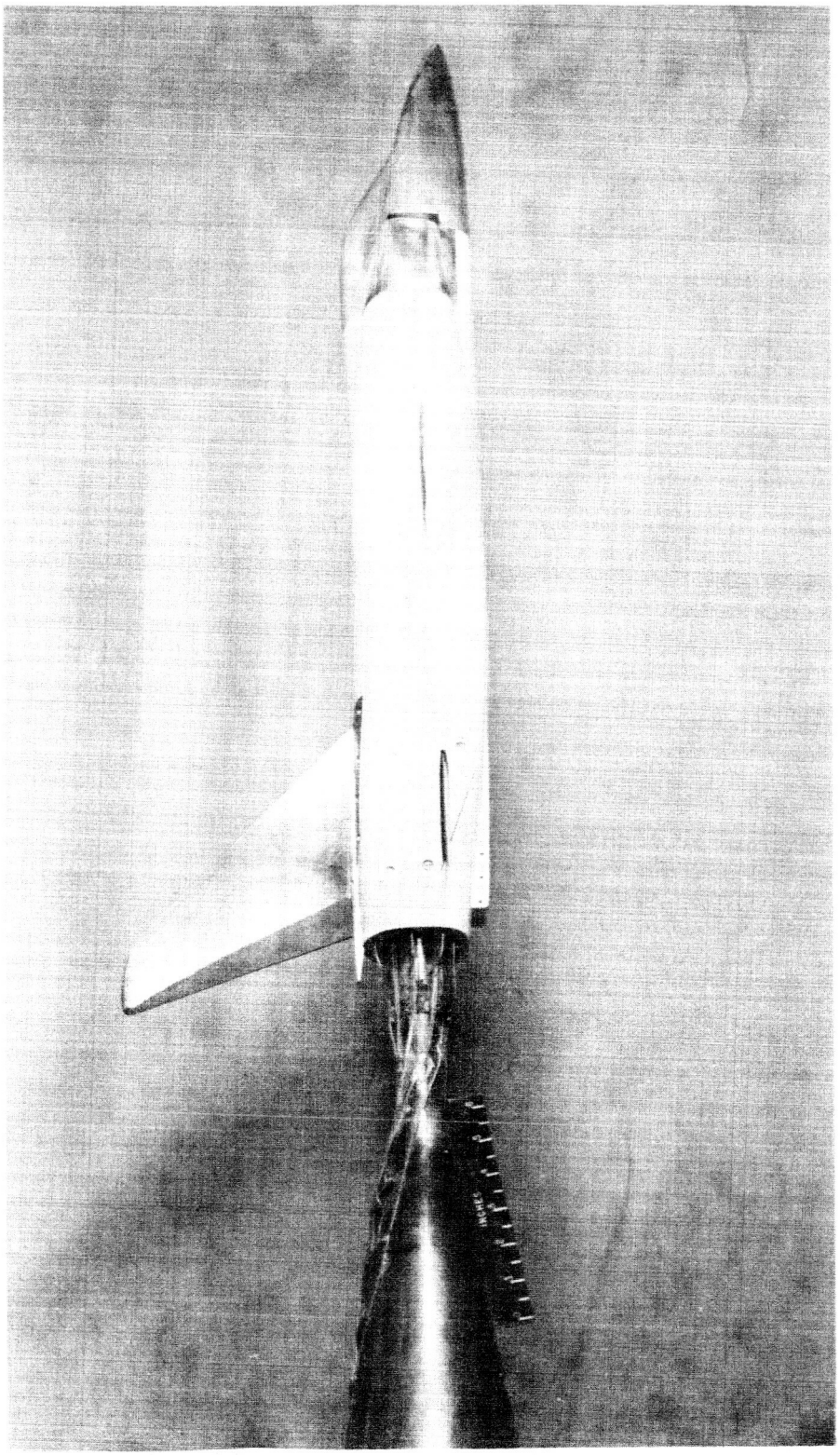

(c) Three-quarter rear view with 0° dihedral tail. L-93703

Figure 2.- Continued.

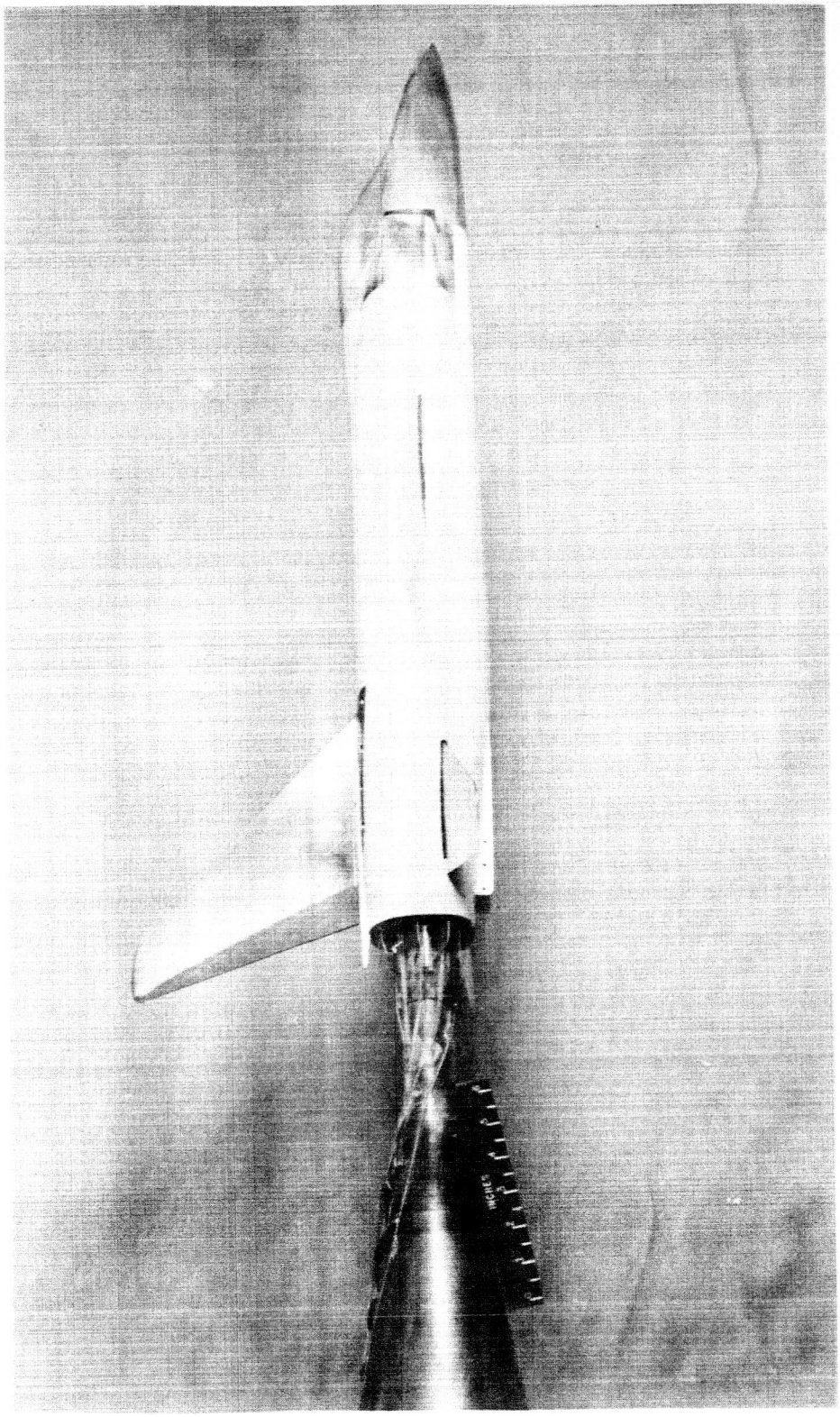

(d) Three-quarter rear view with 10° negative-dihedral tail. L-93701

Figure 2.- Continued.

[redacted]

DECLASSIFIED

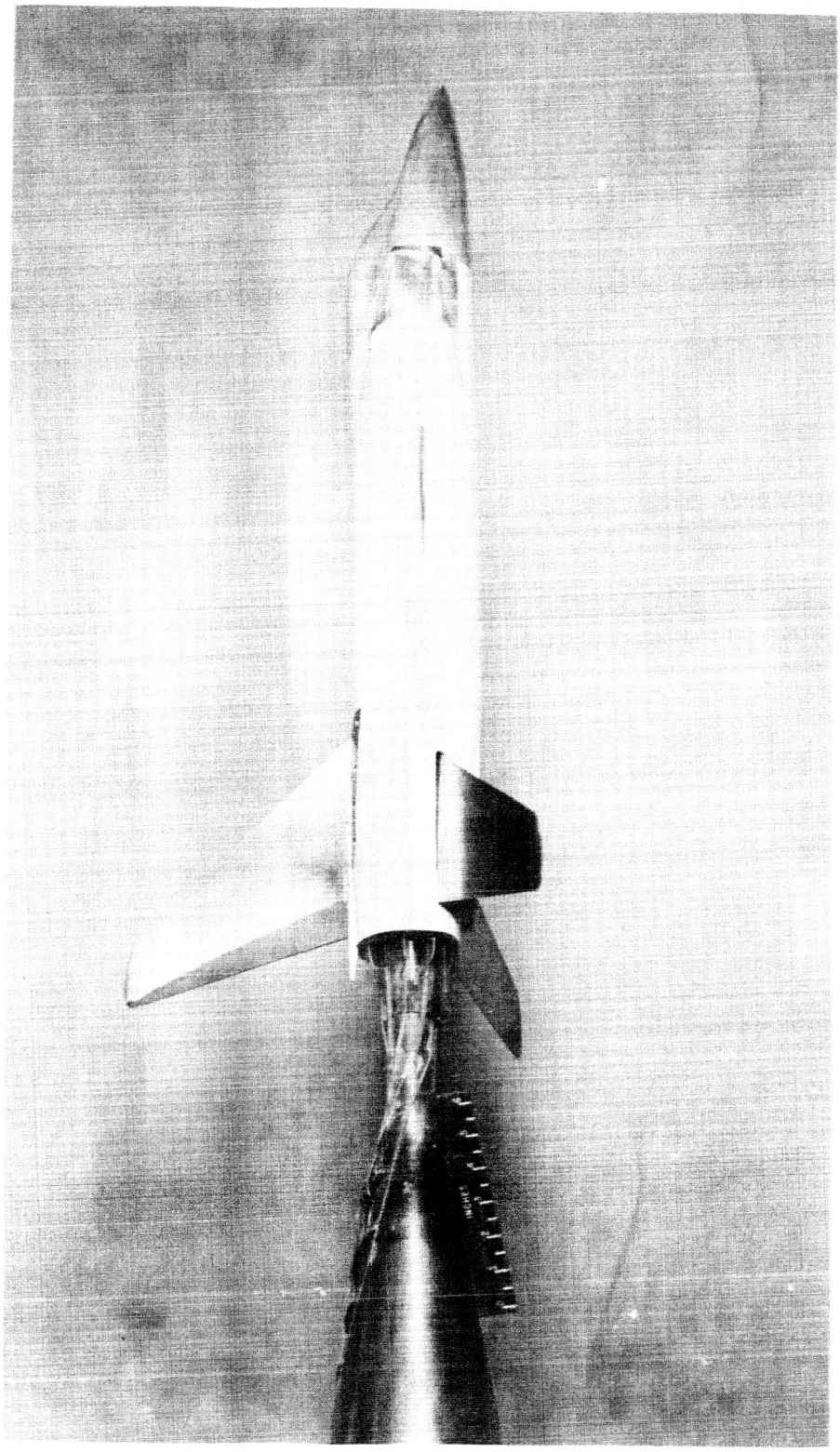

(e) Three-quarter rear view with 30° negative-dihedral tail. L-93702

Figure 2.- Continued.

[redacted]

DECLASSIFIED

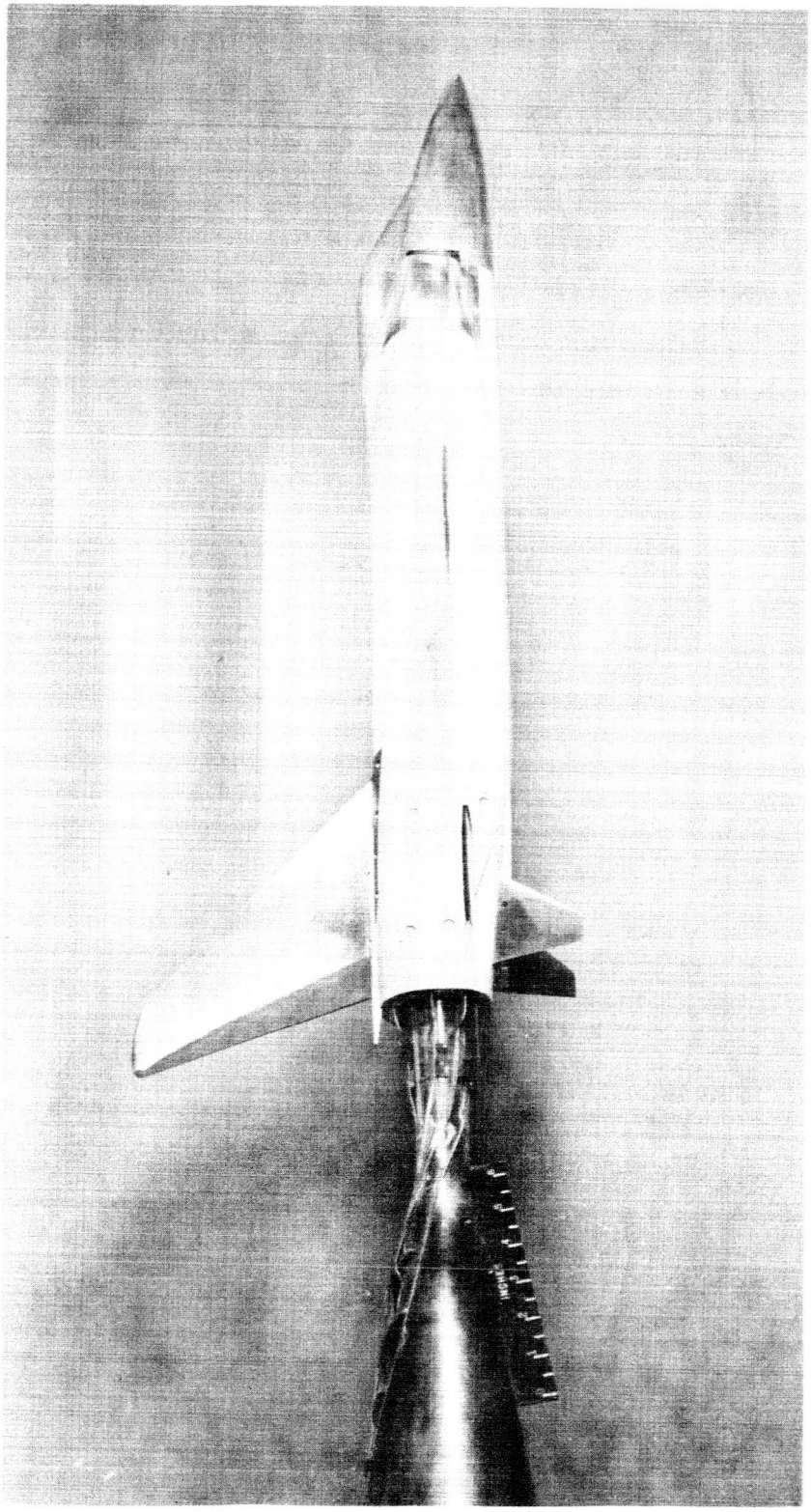

(f) Three-quarter rear view with ventral fins. L-93704

Figure 2.- Concluded.

[redacted]

DECLASSIFIED

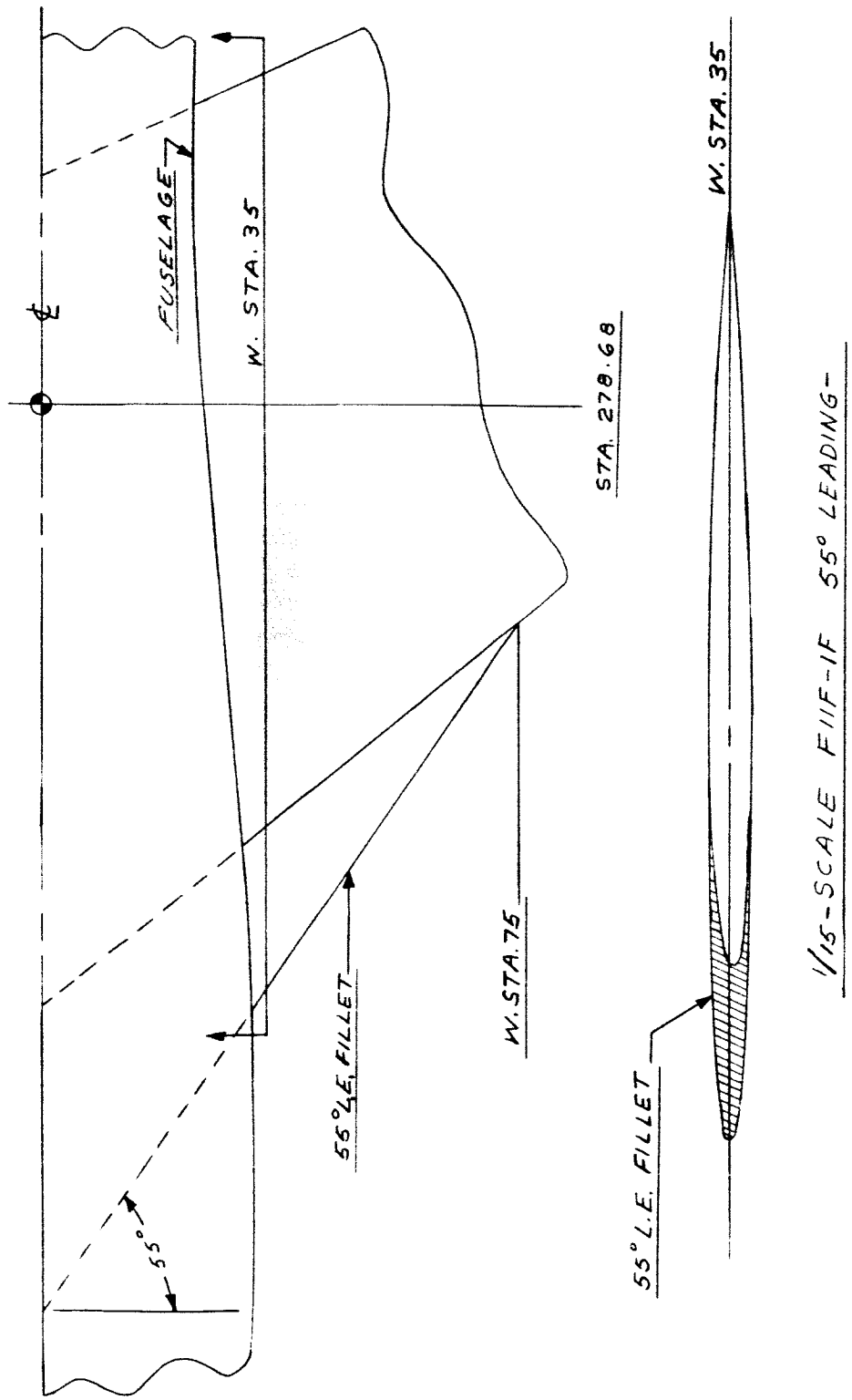

(a) Wing-root leading-edge fillet.

Figure 3.- Modifications used in model tests.

[redacted]

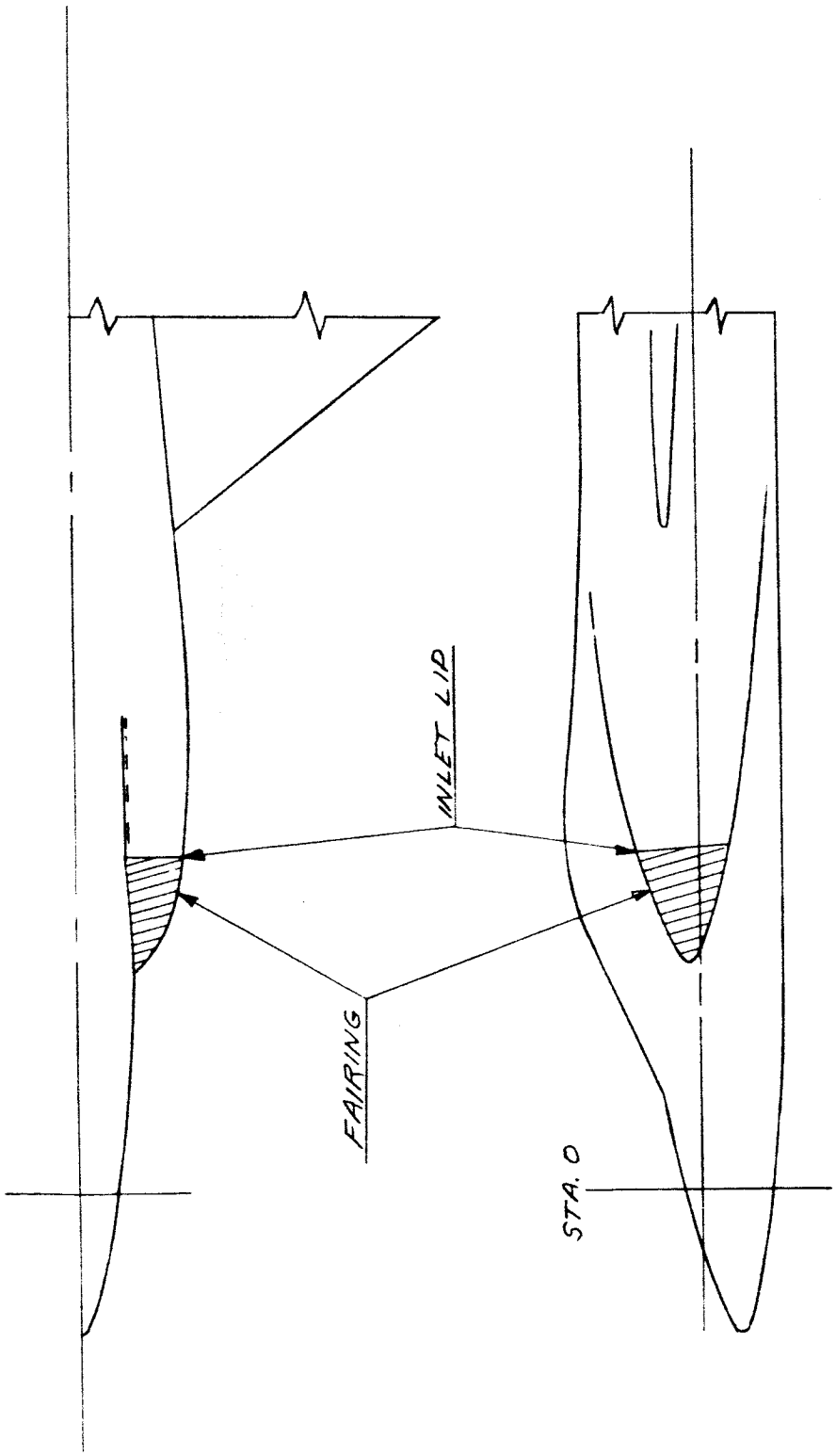

(b) Duct-inlet fairing.

Figure 3.- Continued.

DECLASSIFIED

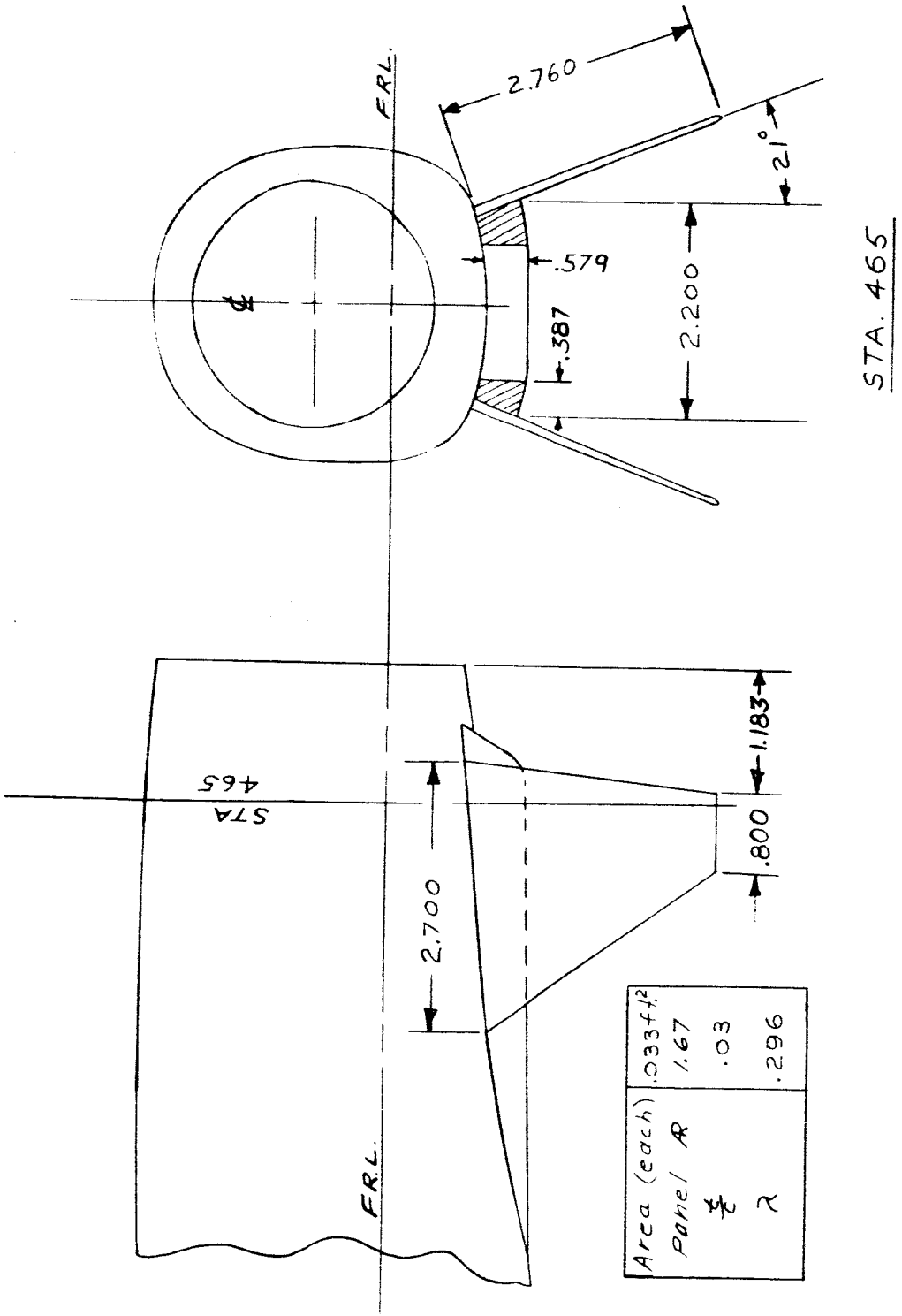

(c) Ventral fins.

Figure 3.- Concluded.

[redacted]

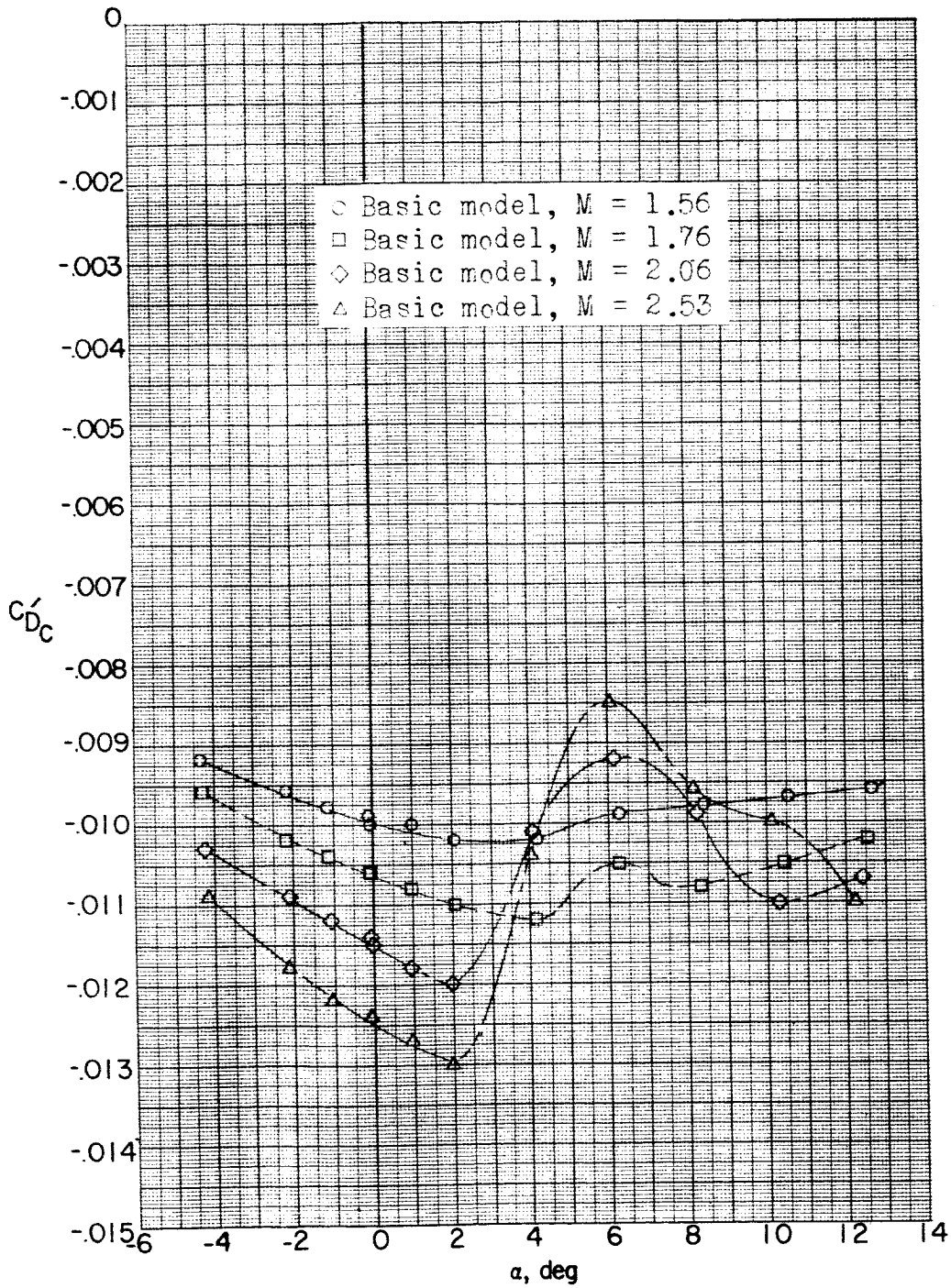

Figure 4.- Typical examples of variation of balance-chamber-drag coefficient with angle of attack. $\beta = 0^{\circ}$. Flagged symbols denote wall-reflected shock waves striking the tail.

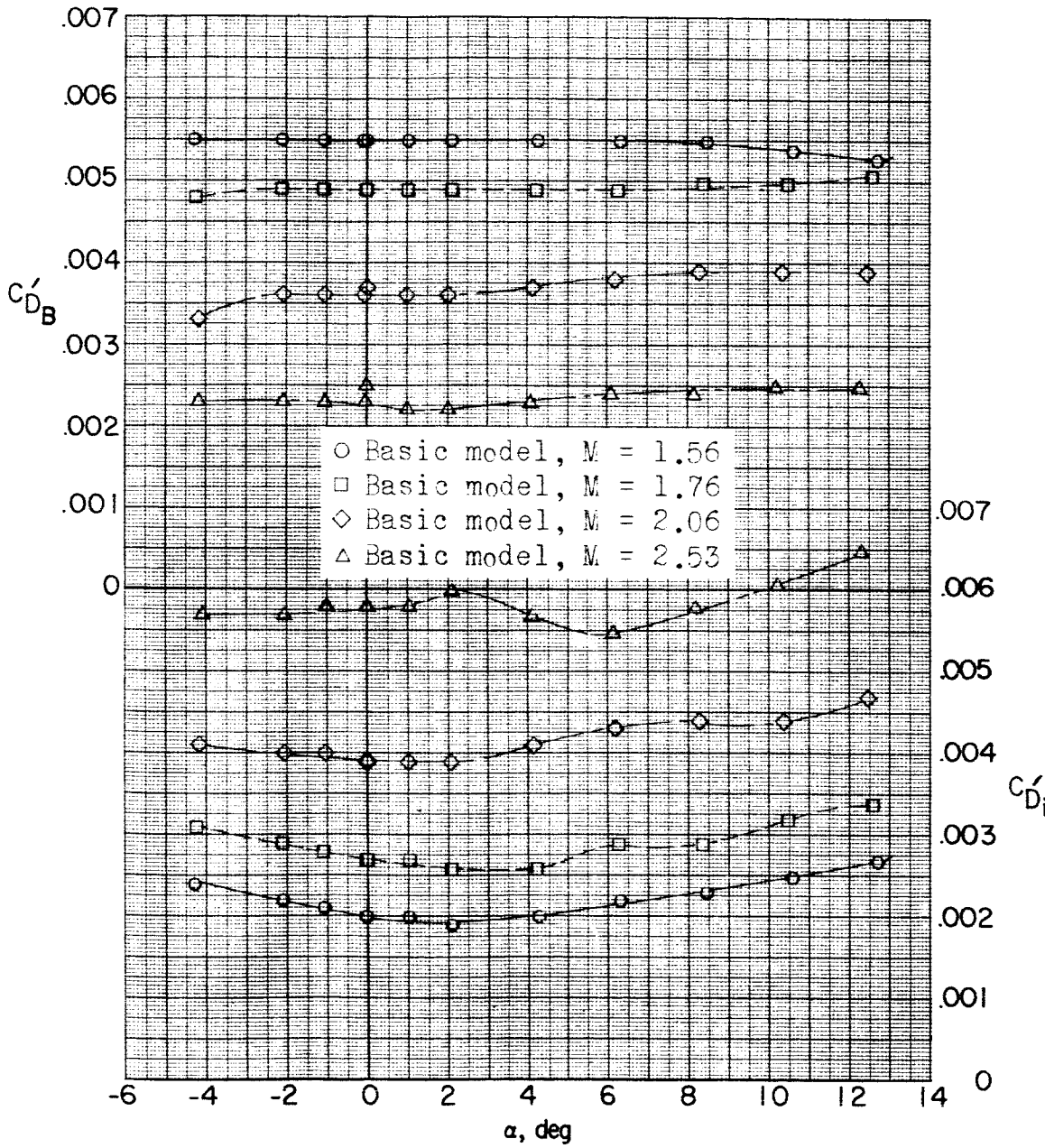

Figure 5.- Typical examples of variation of base-drag coefficient and internal-duct-drag coefficient with angle of attack. $\beta = 0^{\circ}$. Flagged symbols denote wall-reflected shock waves striking the tail.

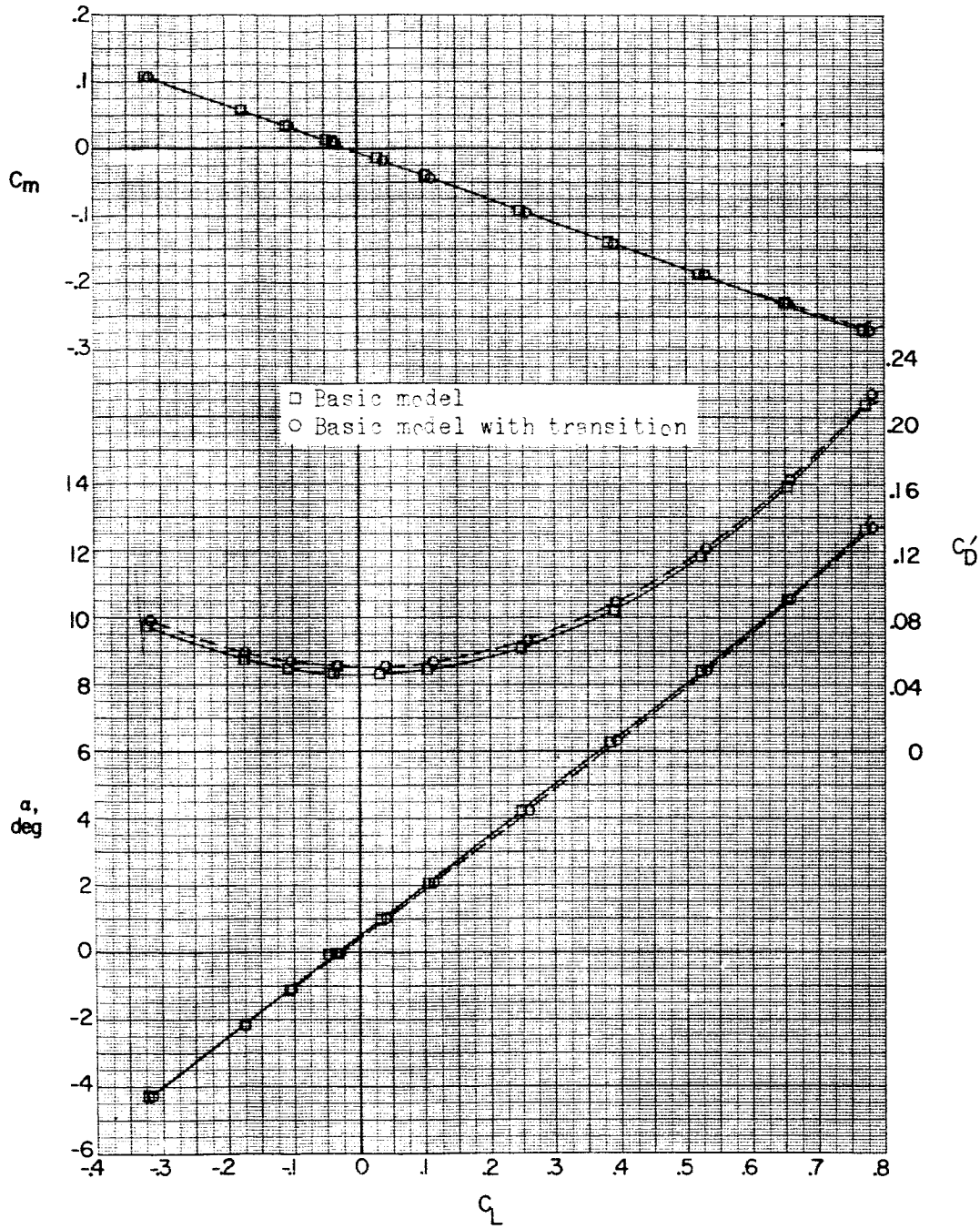

(a) M = 1.56.

Figure 6.- Effect of fixed transition on aerodynamic characteristics in pitch. $\beta = 0^{\circ}$. Flagged symbols denote wall-reflected shock waves striking the tail.

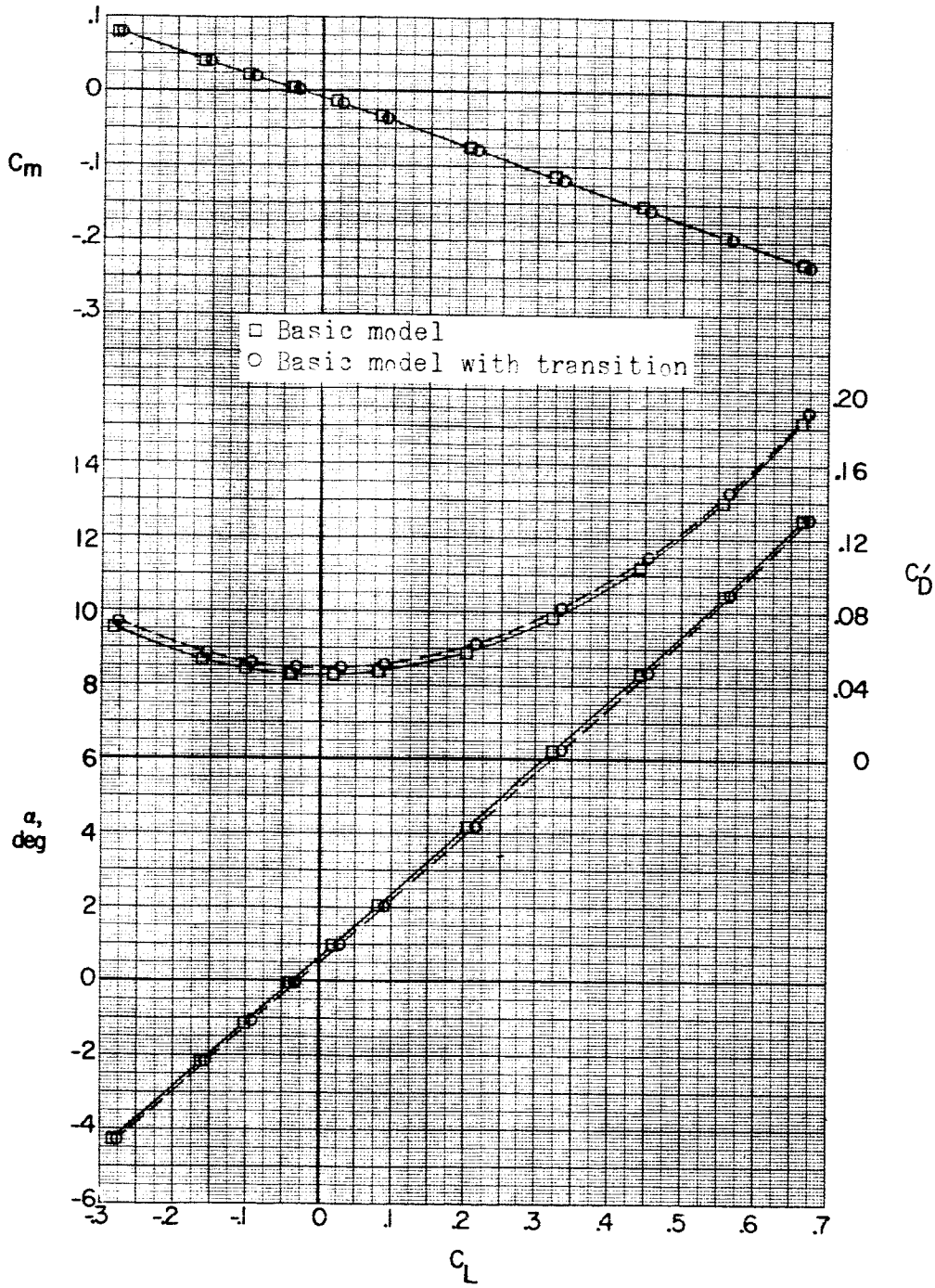

(b) M = 1.76.

Figure 6.- Continued.

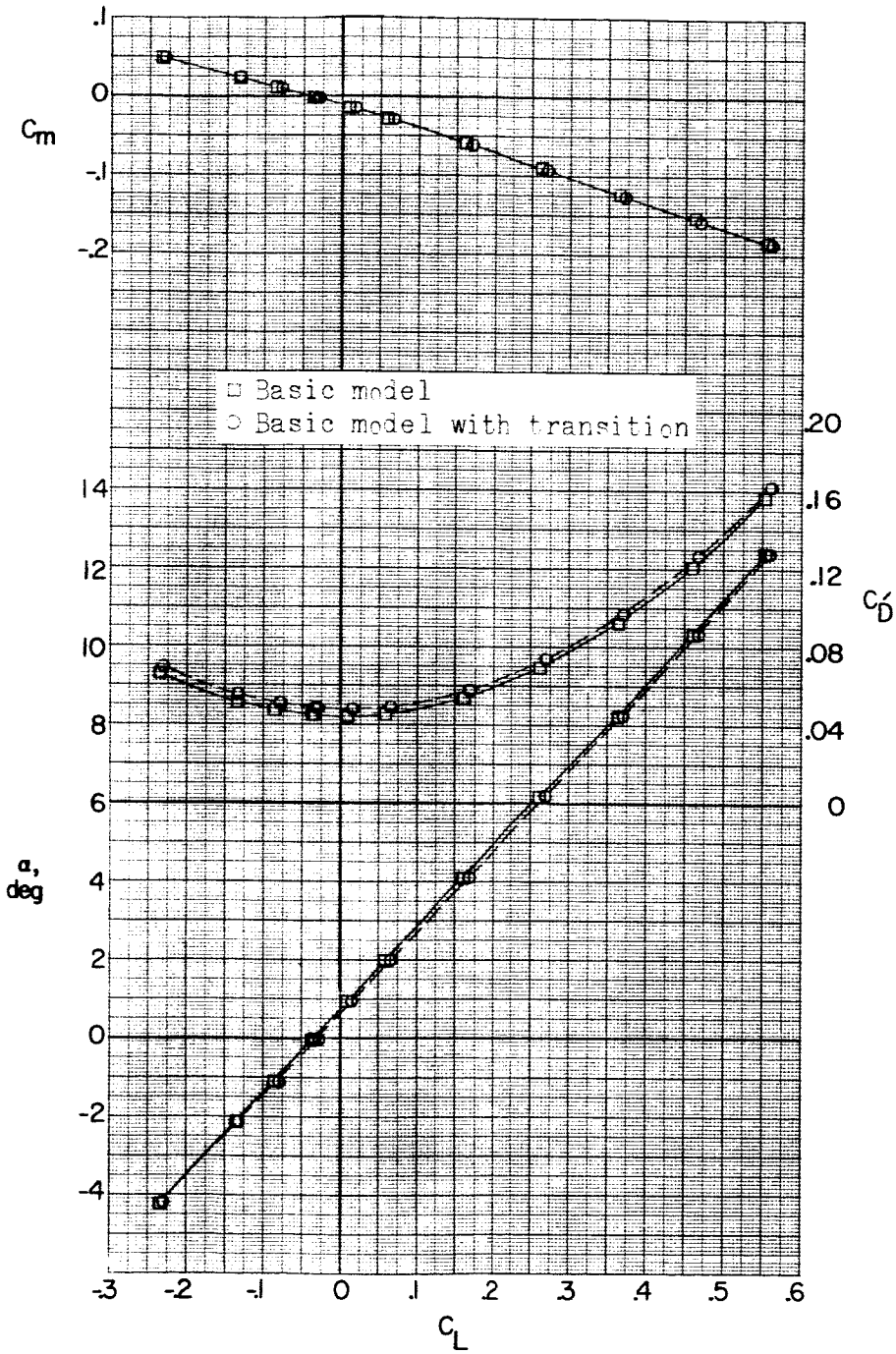

(c) M = 2.06.

Figure 6.- Continued.

[redacted]

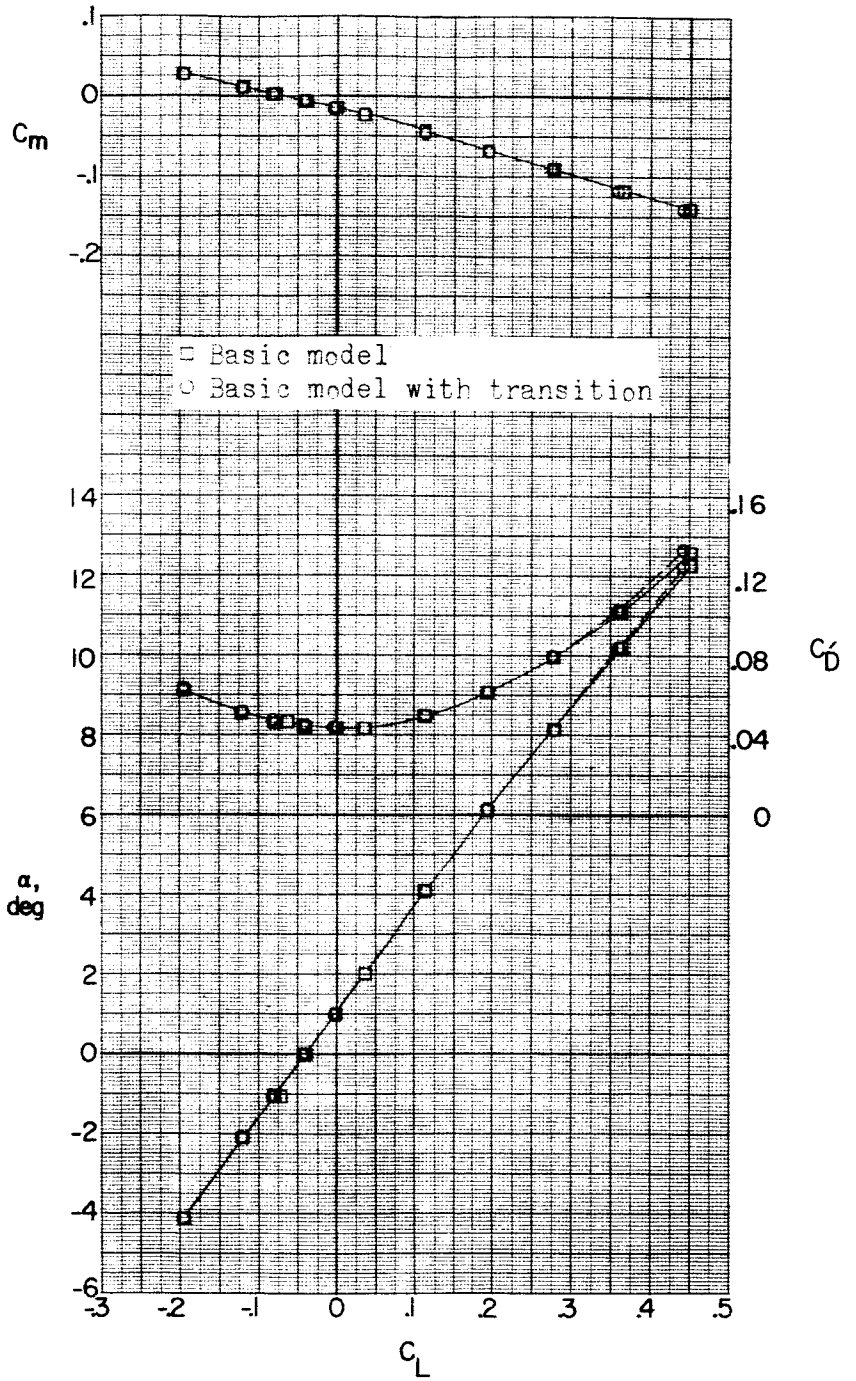

(d) M = 2.53.

Figure 6.- Concluded.

[redacted]

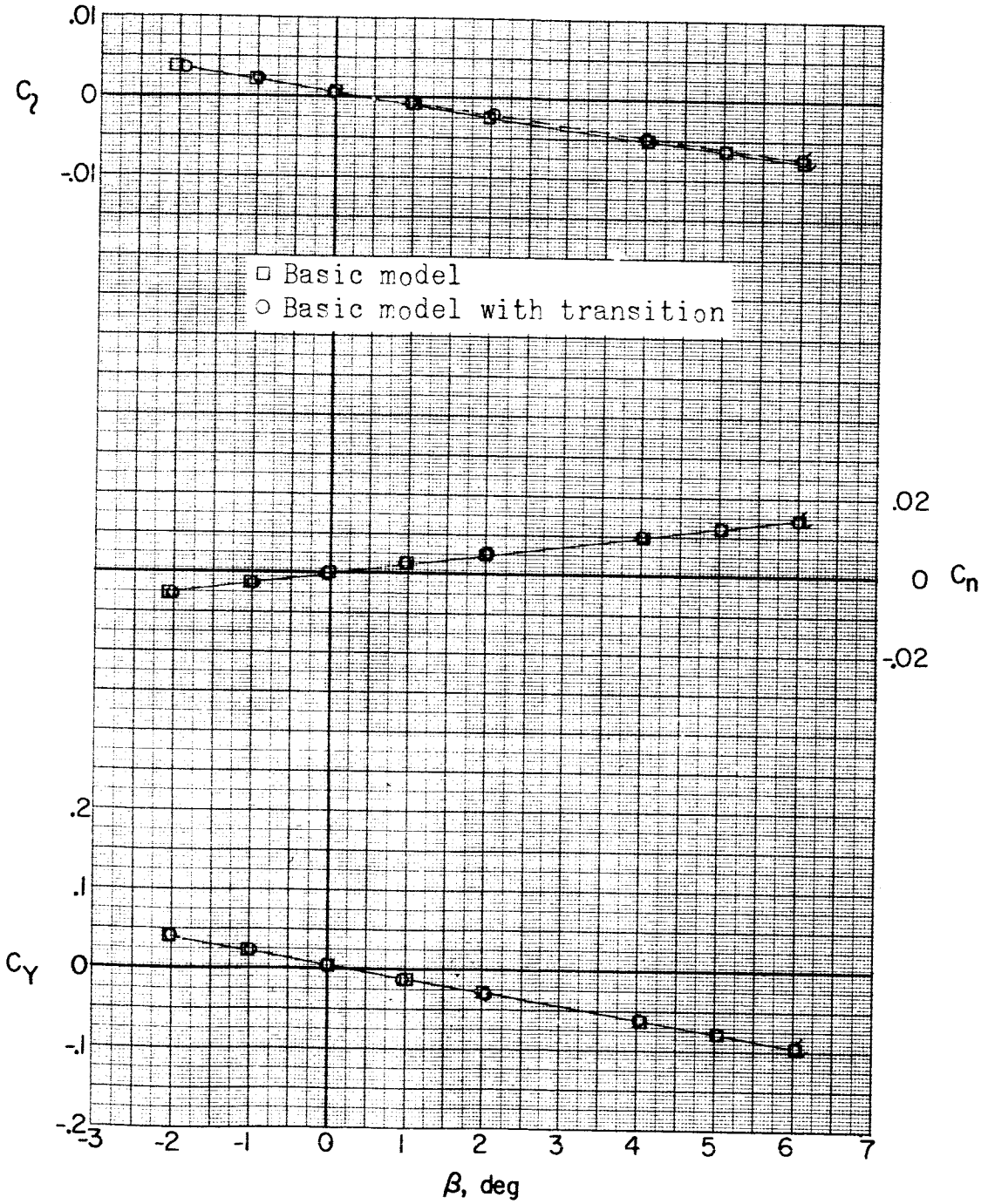

(a) M = 1.56; α = 0°.

Figure 7.- Effect of fixed transition on aerodynamic characteristics in sideslip. Flagged symbols denote wall-reflected shock waves striking the tail.

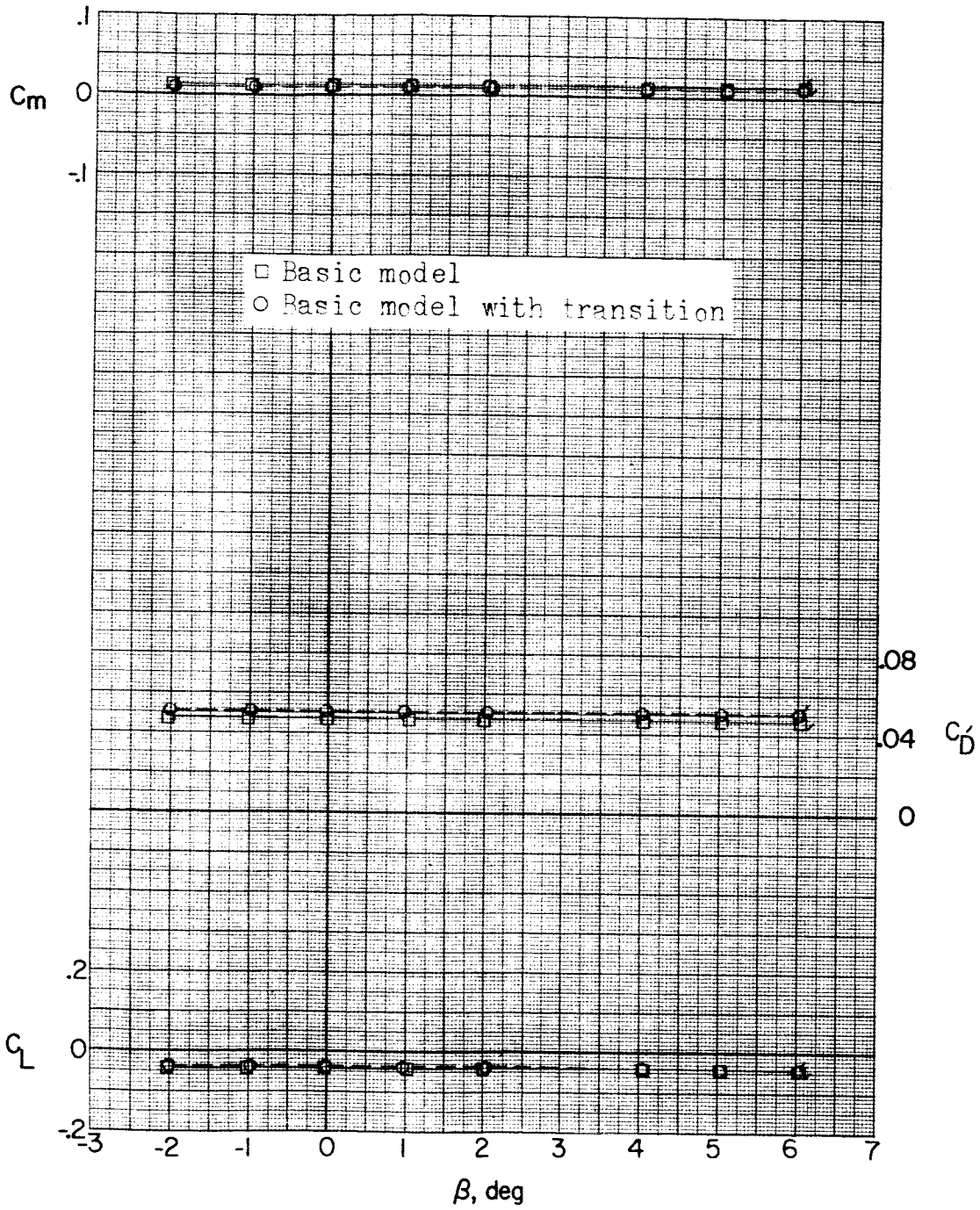

(a) Continued. $\alpha = 0^{\circ}$.

Figure 7.- Continued.

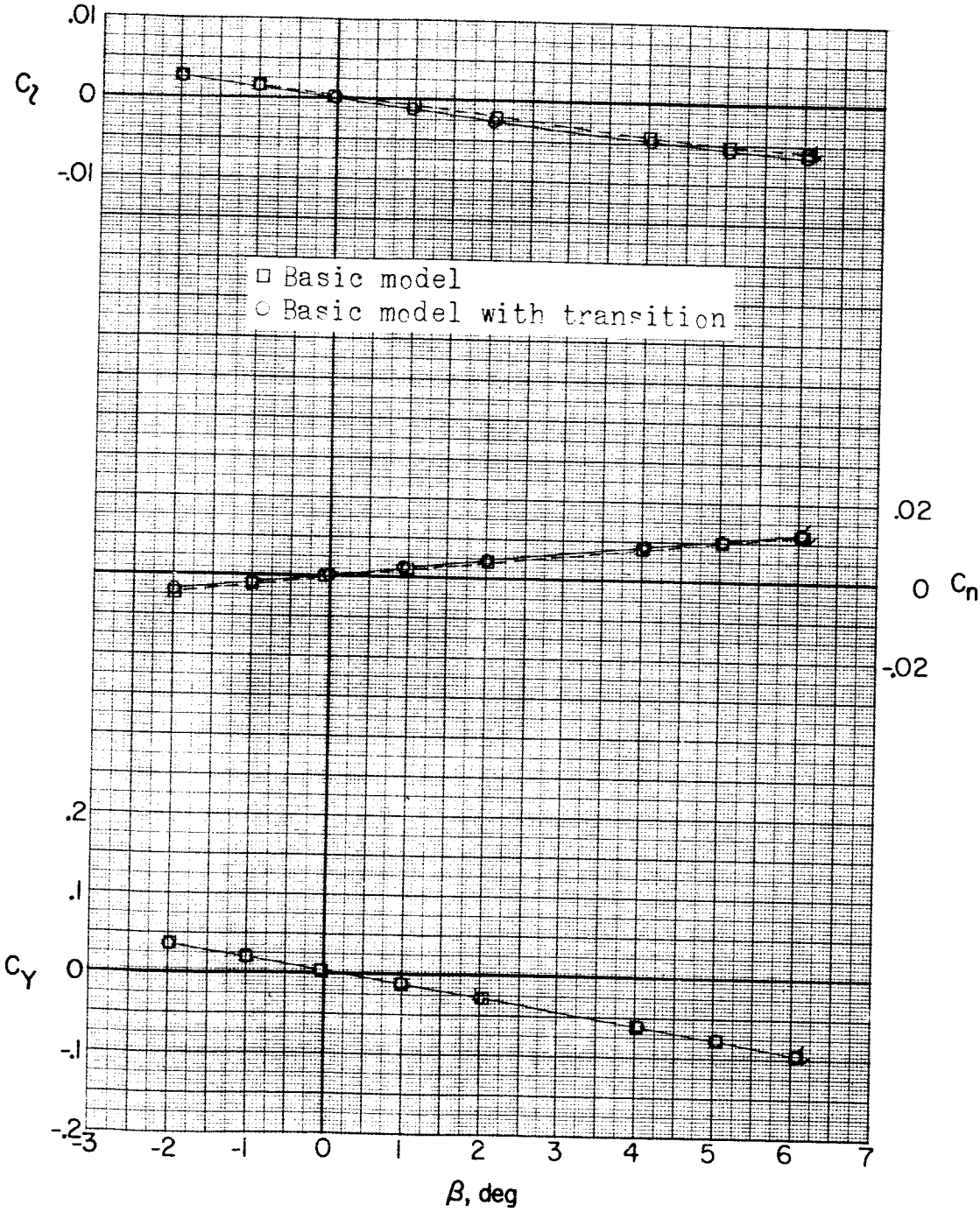

(a) Continued. $\alpha = 5.3^{\circ}$.

Figure 7.- Continued.

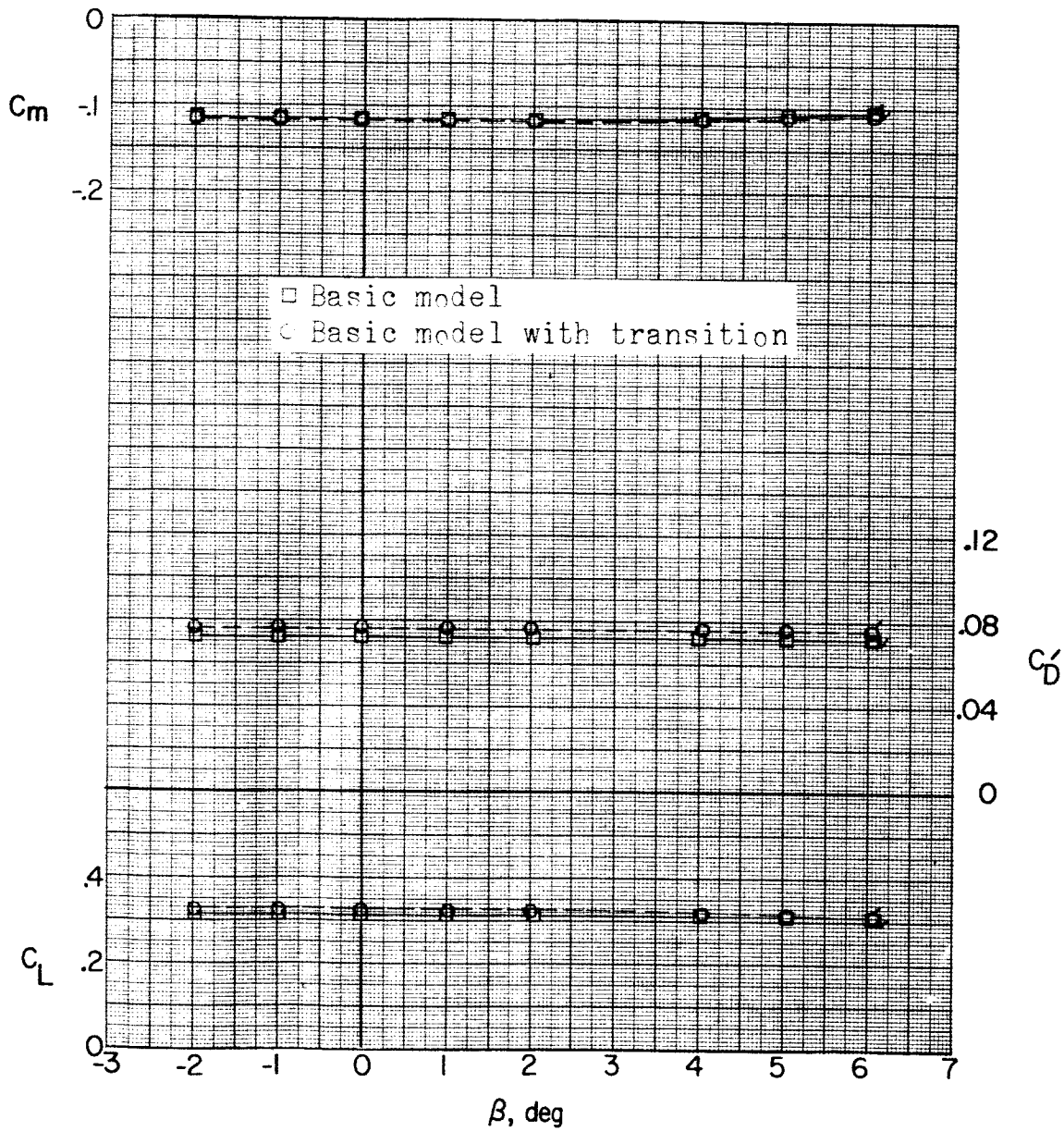

(a) Continued. $\alpha = 5.3^{\circ}$.

Figure 7.- Continued.

[redacted]

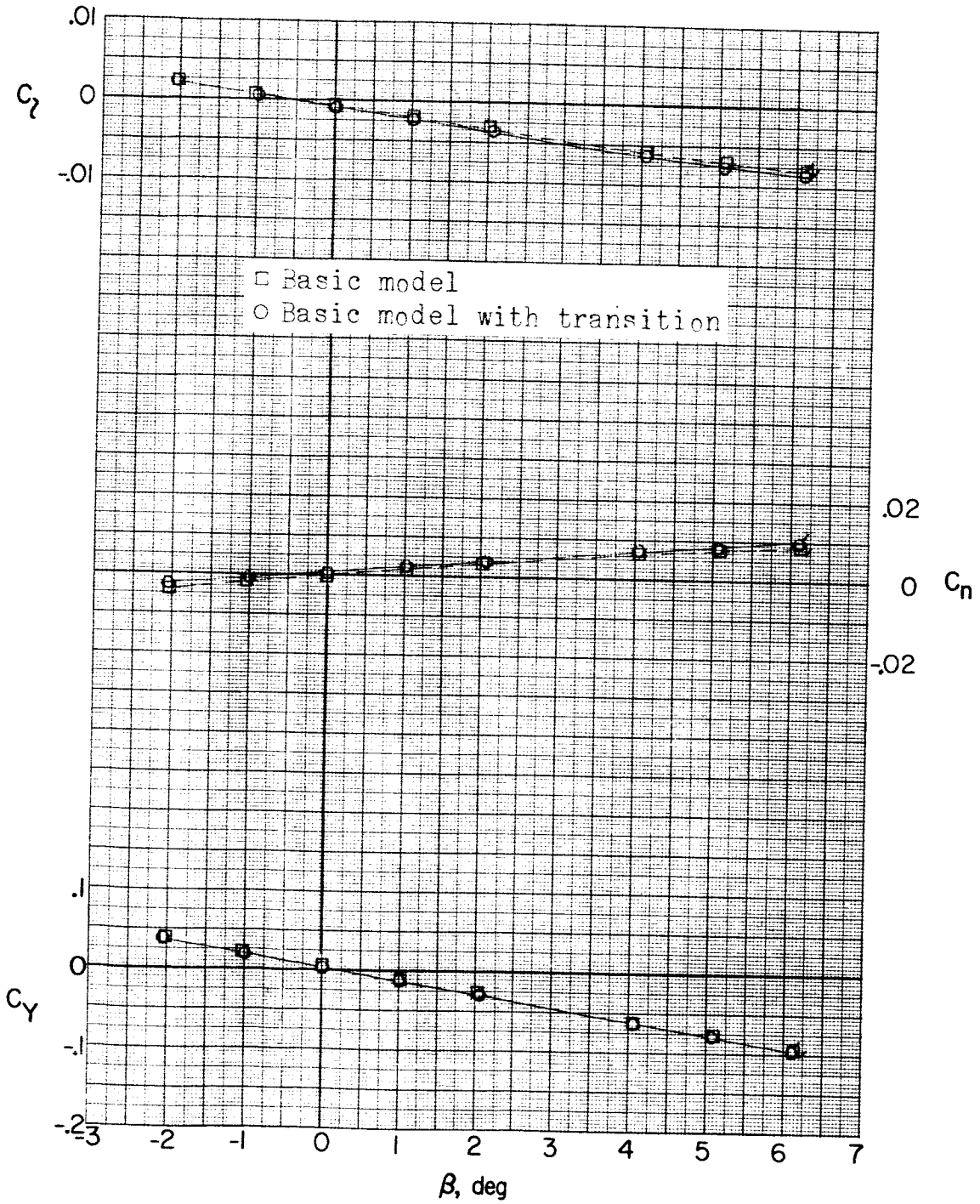

(a) Continued. $\alpha = 10.6^{\circ}$.

Figure 7.- Continued.

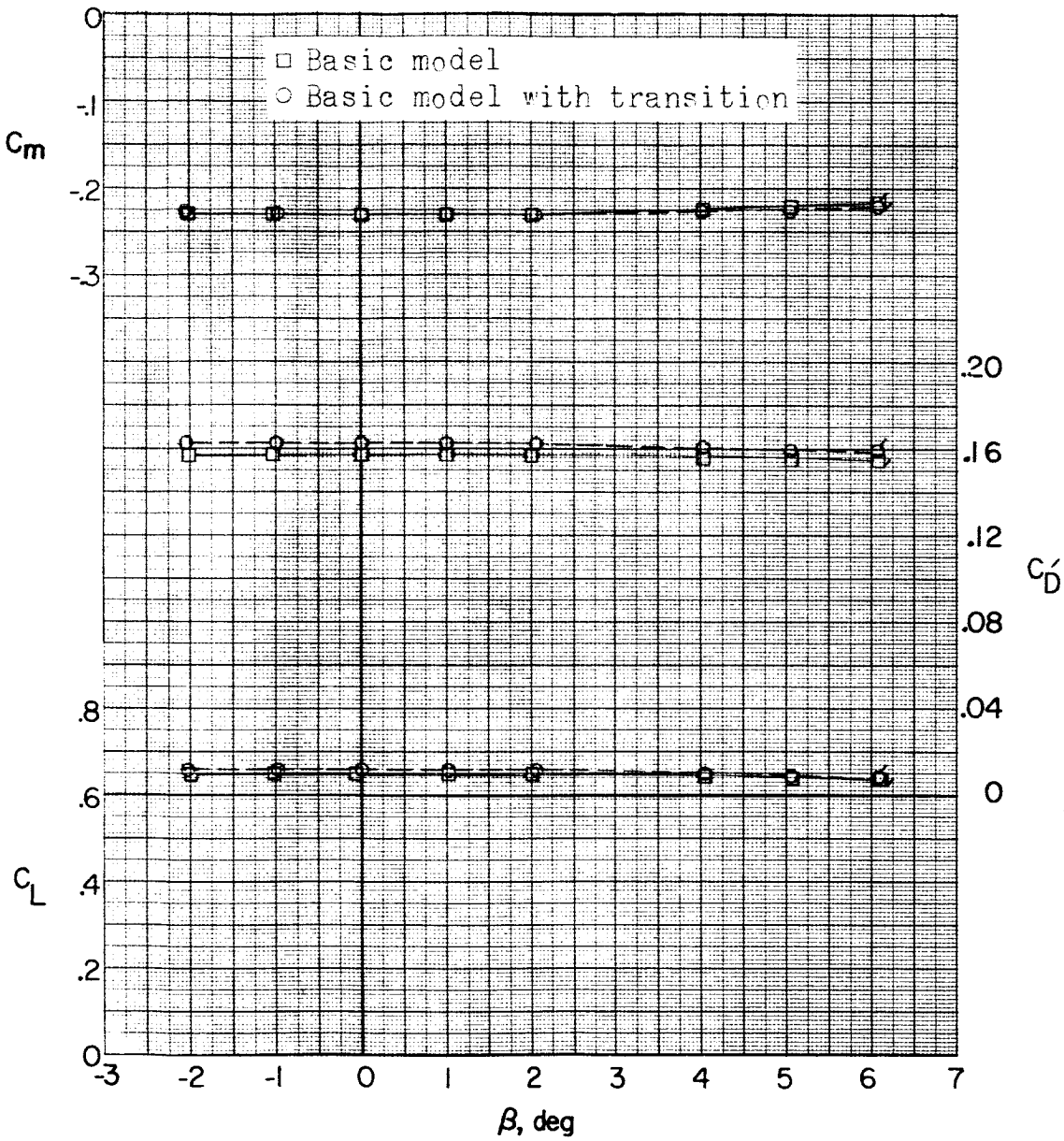

(a) Concluded. $\alpha = 10.6^{\circ}$.

Figure 7.- Continued.

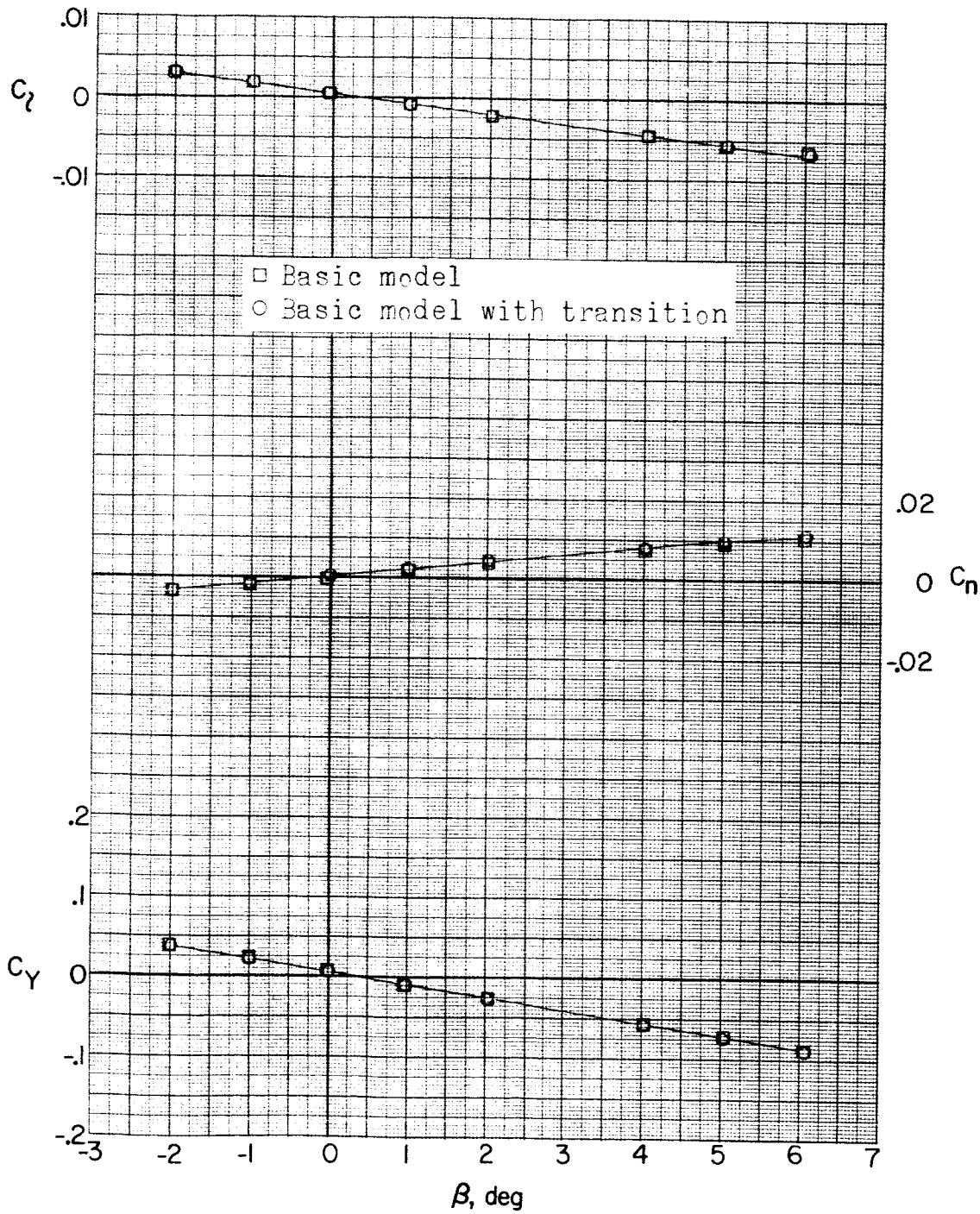

(b) M = 1.76; α = 0°.

Figure 7.- Continued.

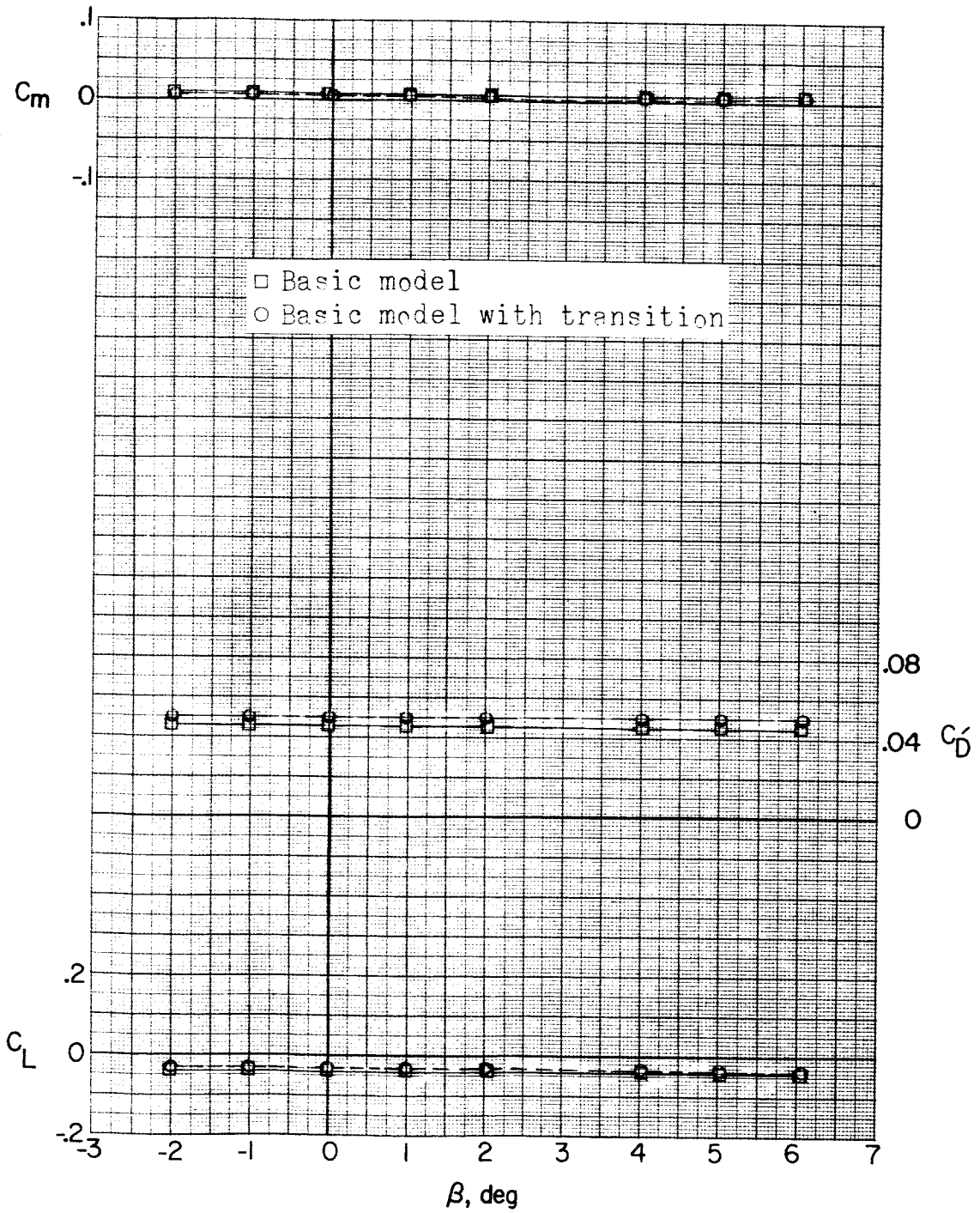

(b) Continued. $\alpha = 0^{\circ}$.

Figure 7.- Continued.

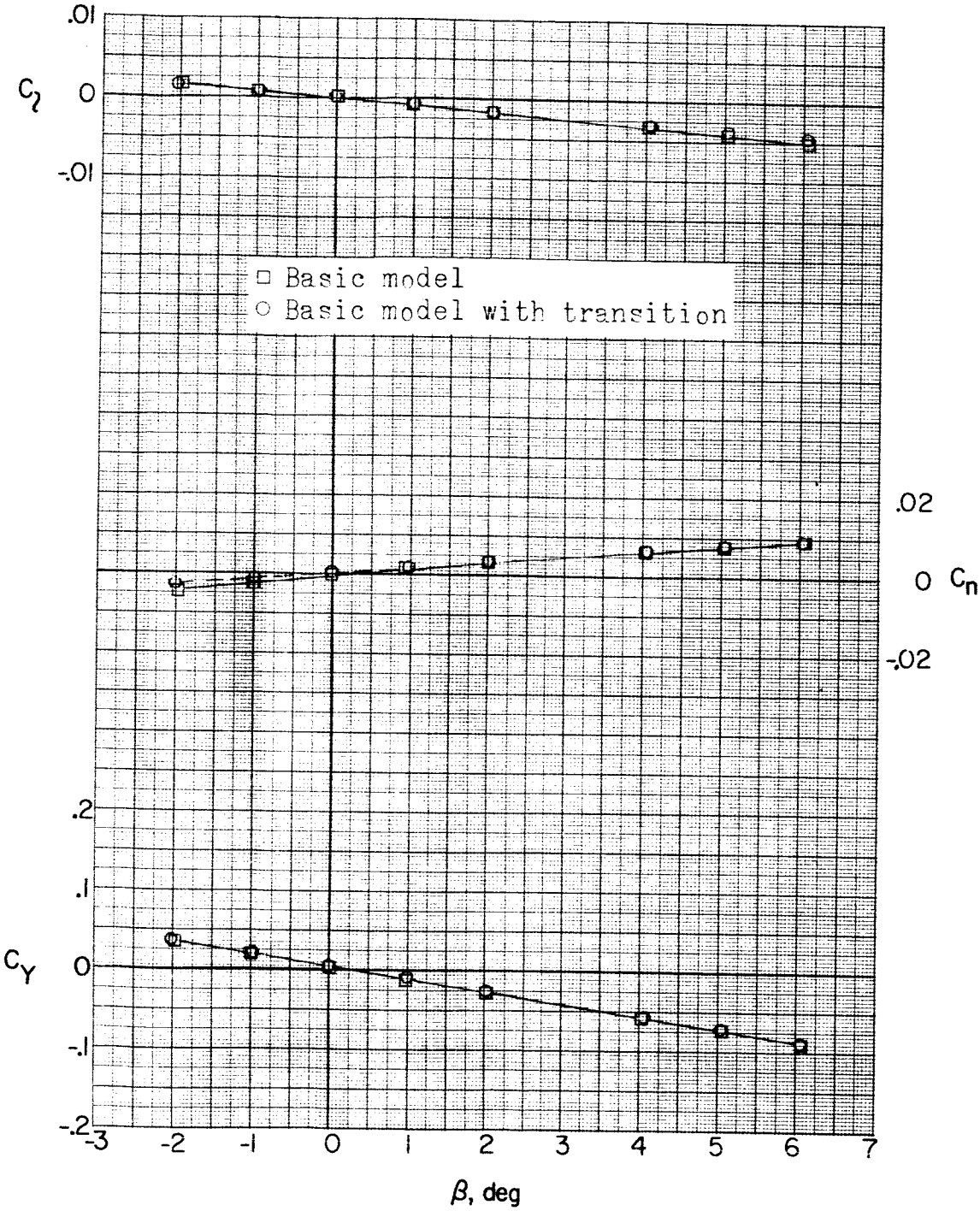

(b) Continued. $\alpha = 5.2^{\circ}$.

Figure 7.- Continued.

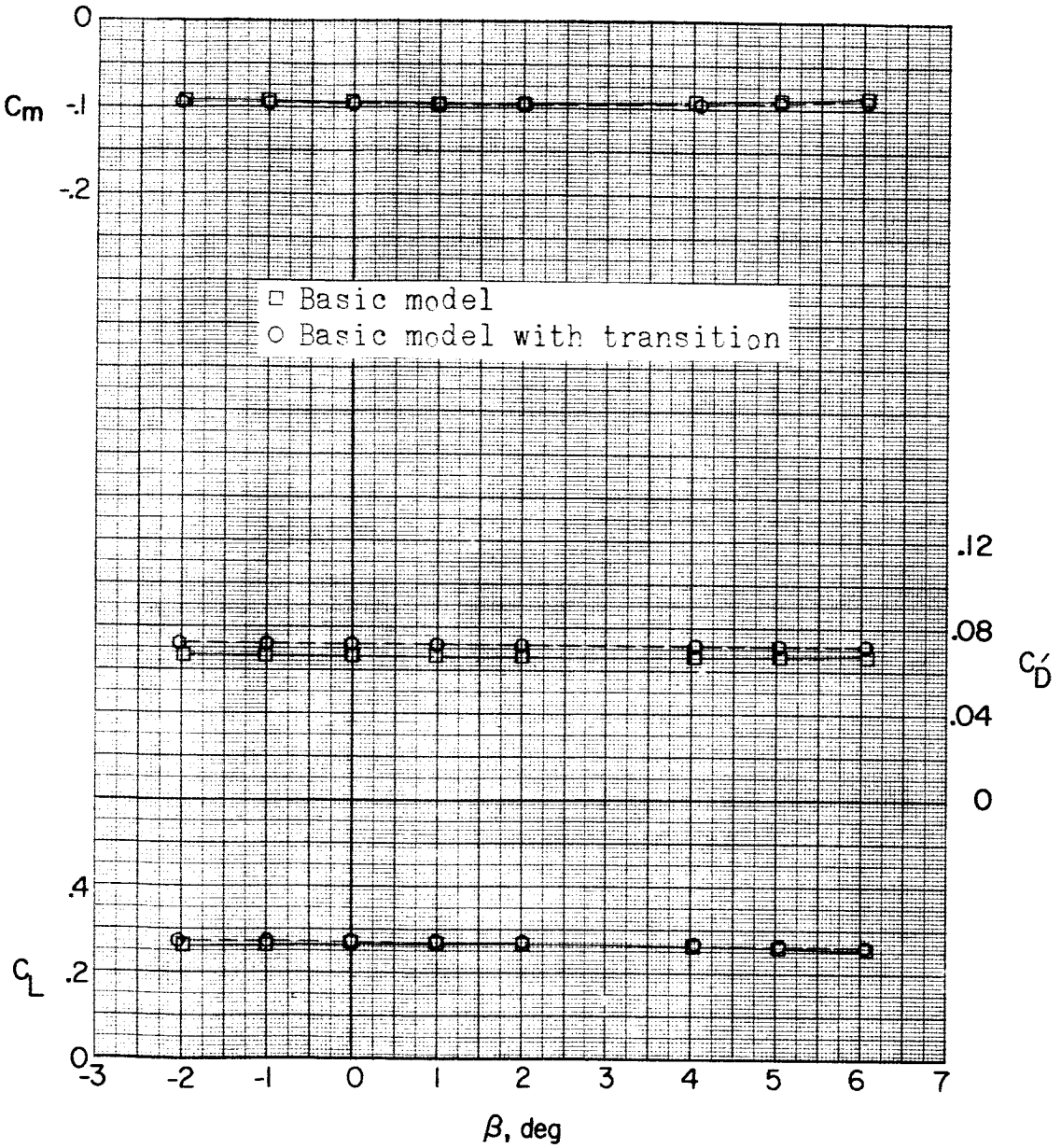

(b) Continued. $\alpha = 5.2^{\circ}$.

Figure 7.- Continued.

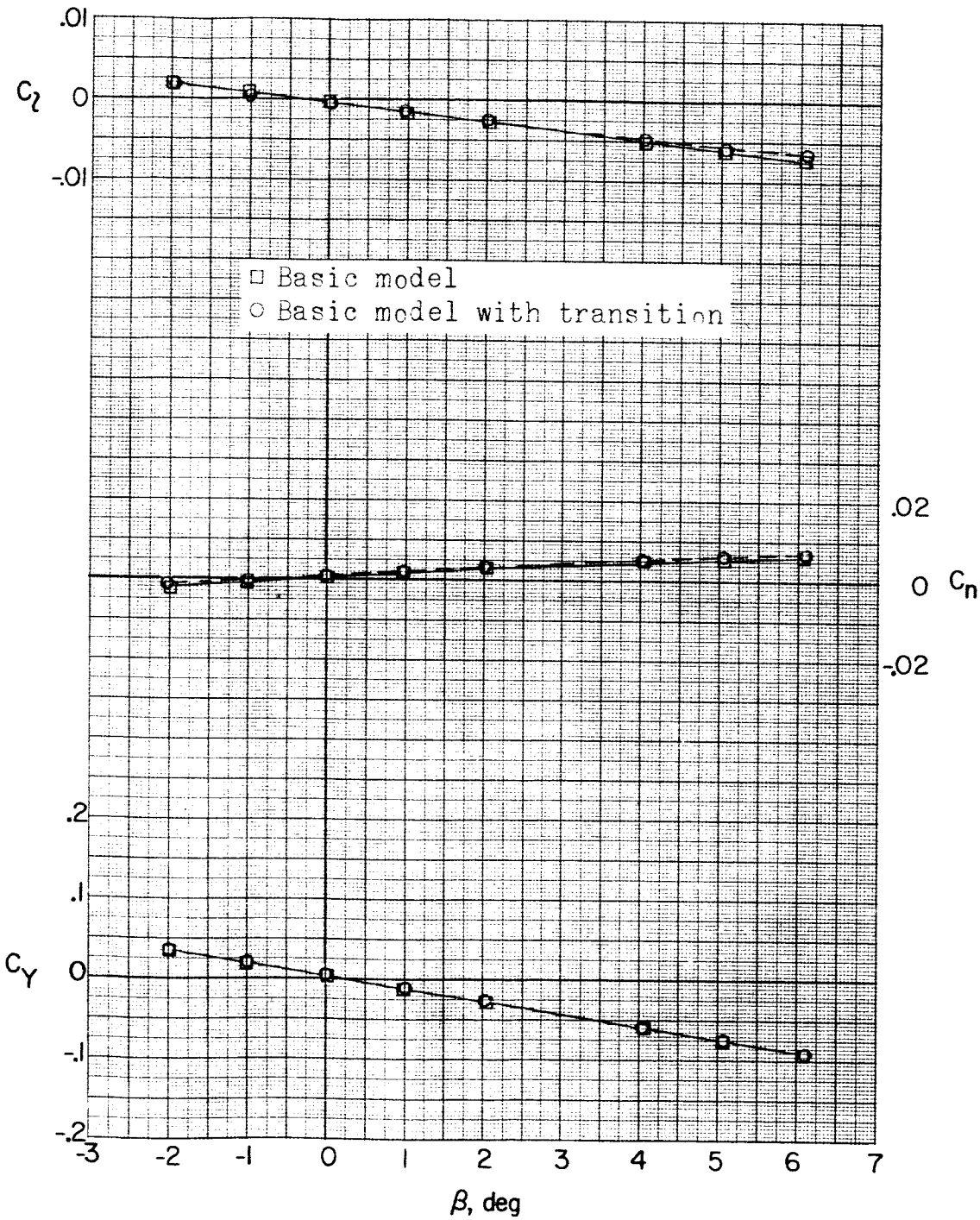

(b) Continued. $\alpha = 10.5^{\circ}$.

Figure 7.- Continued.

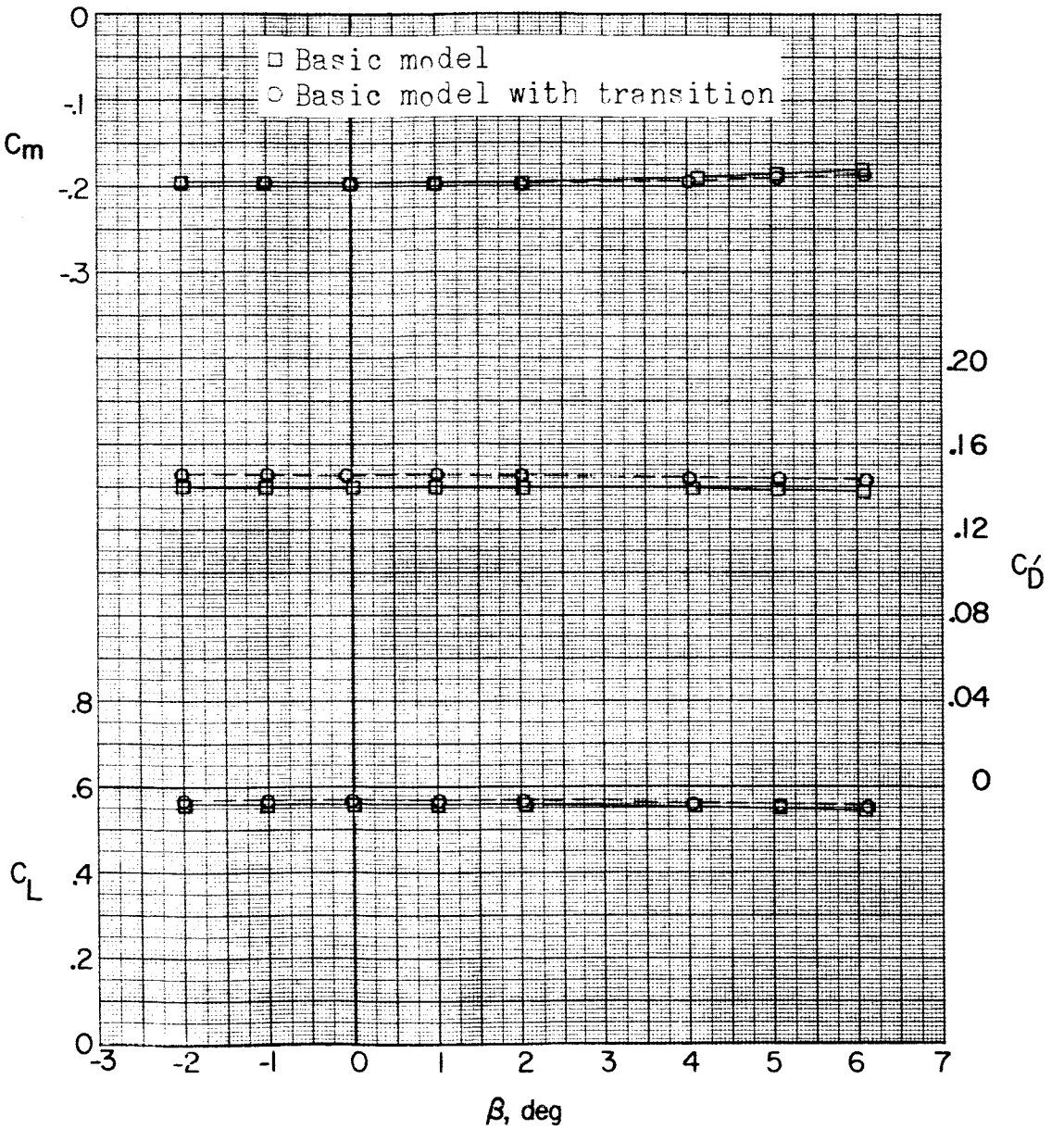

(b) Concluded. $\alpha = 10.5^{\circ}$.

Figure 7.- Continued.

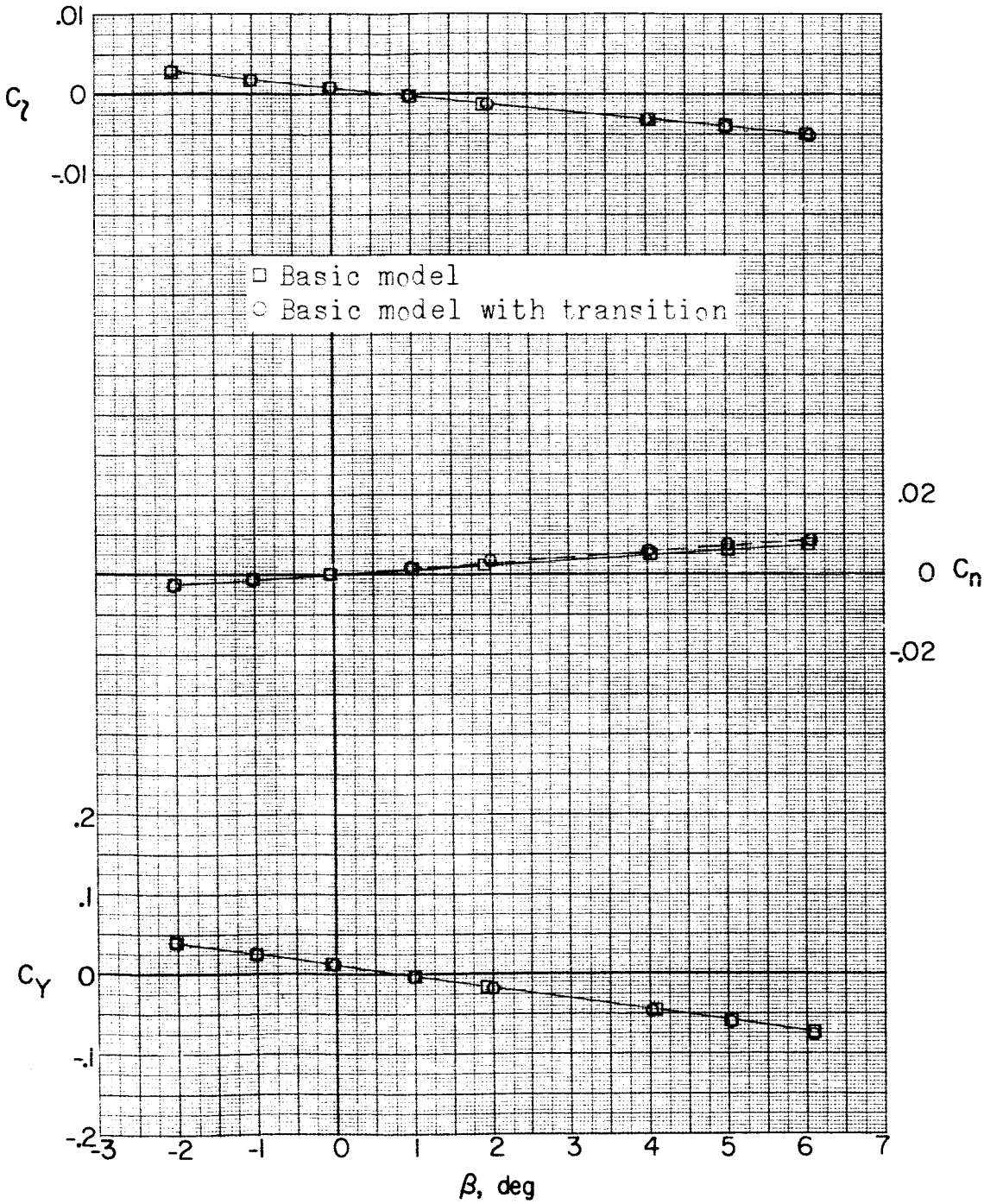

(c) M = 2.06; α = 0°.

Figure 7.- Continued.

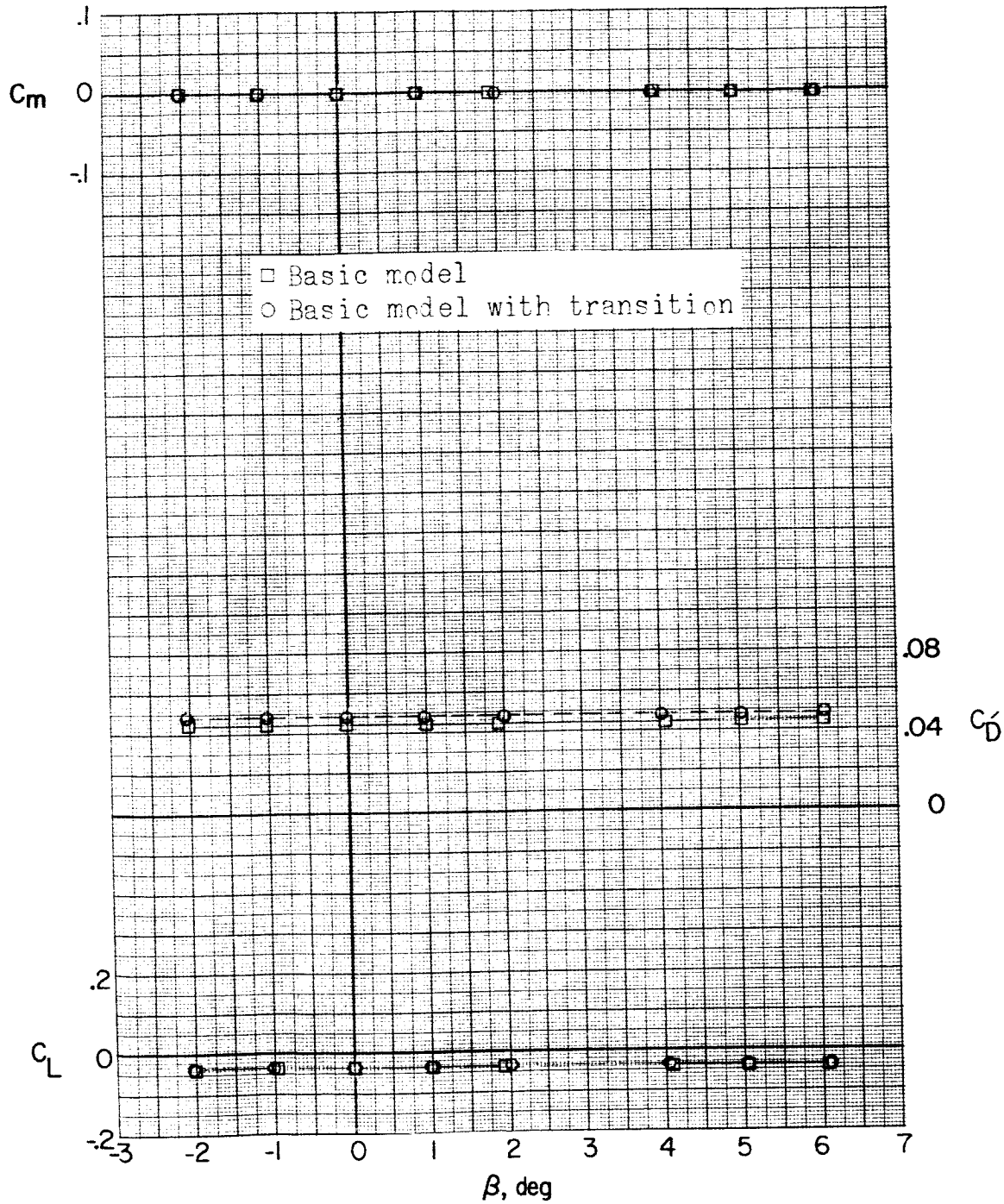

(c) Continued. $\alpha = 0^{\circ}$.

Figure 7.- Continued.

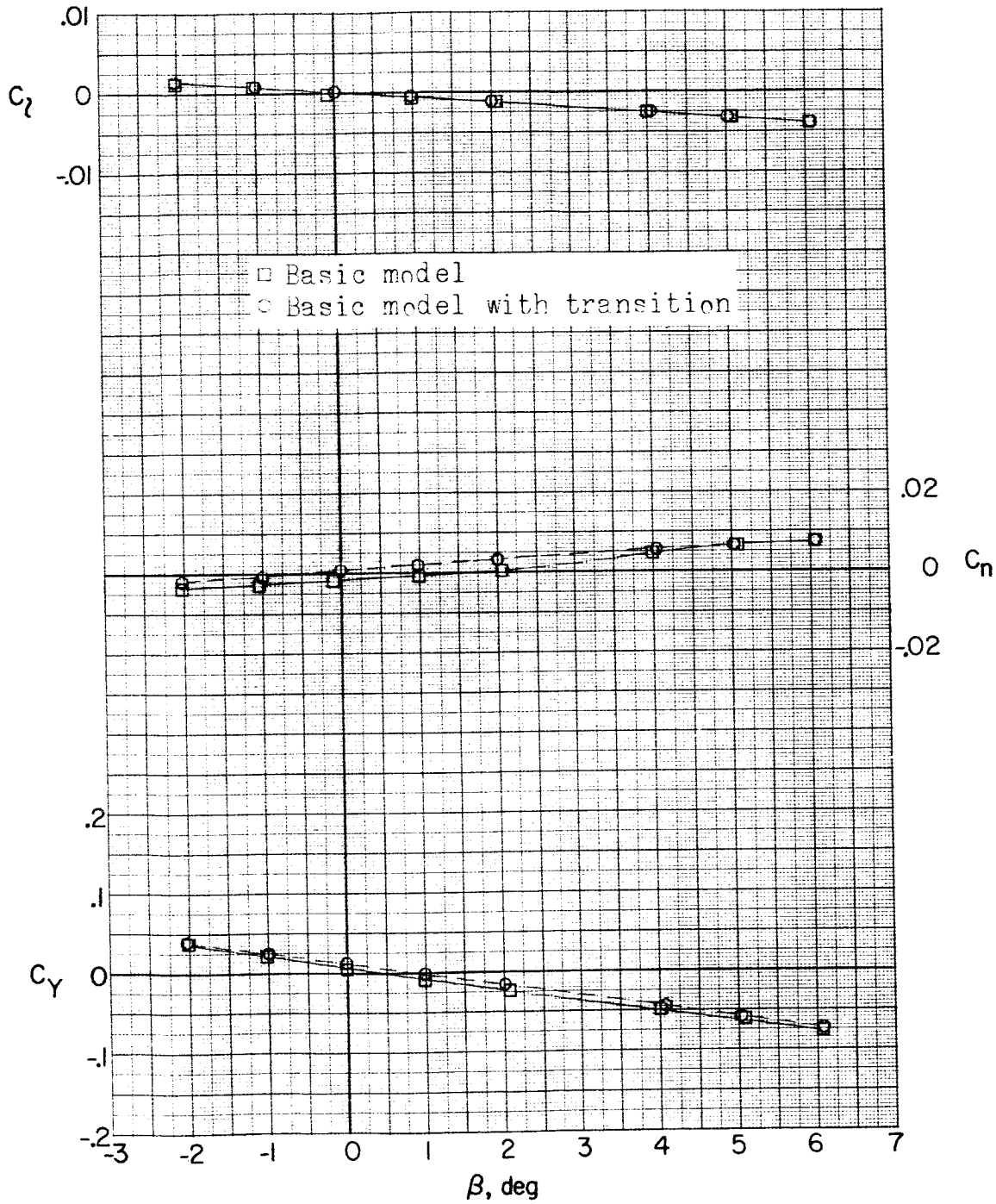

(c) Continued. $\alpha = 5.2^{\circ}$.

Figure 7.- Continued.

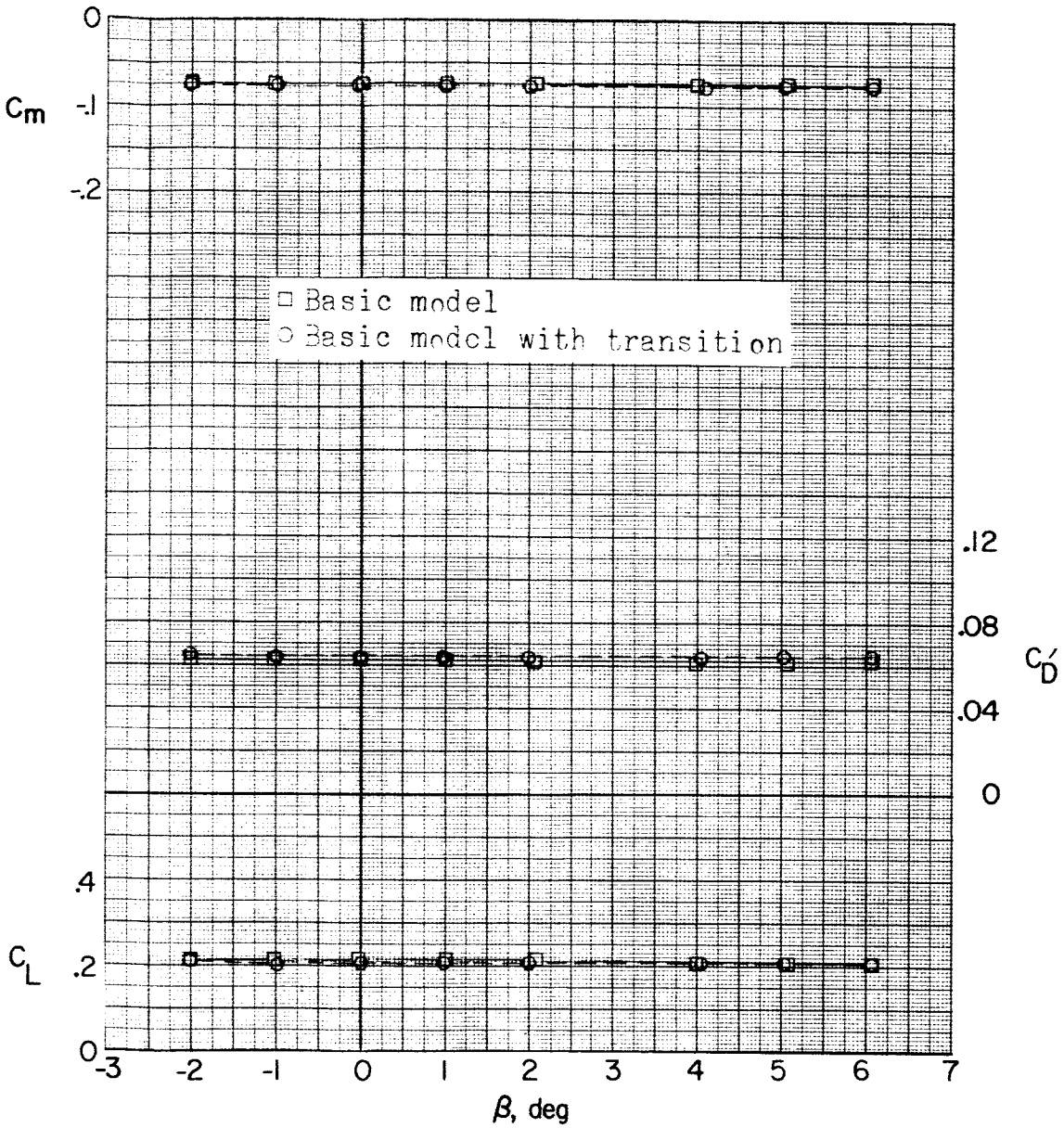

(c) Continued. $\alpha = 5.2^{\circ}$.

Figure 7.- Continued.

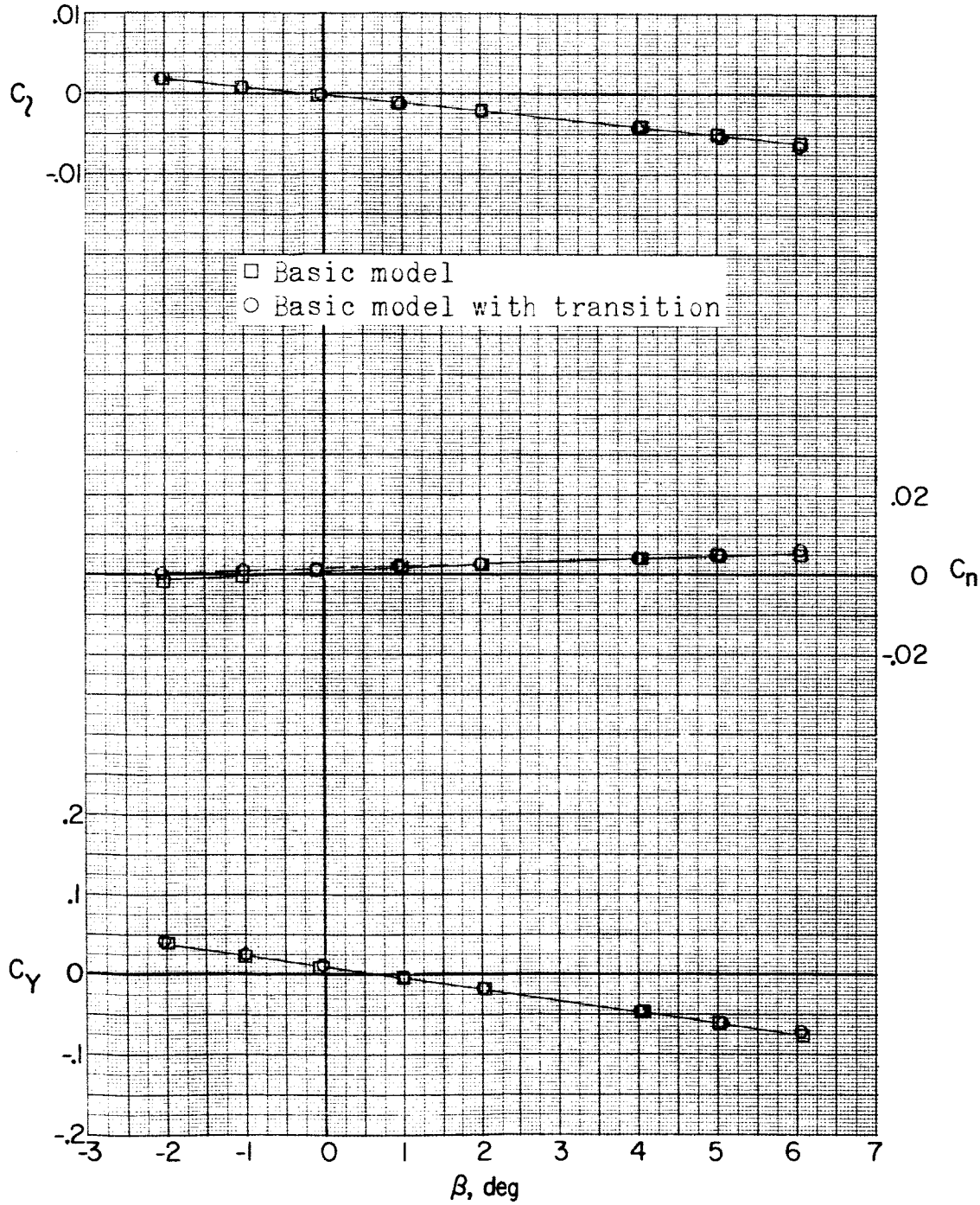

(c) Continued. $\alpha = 10.4^{\circ}$.

Figure 7.- Continued.

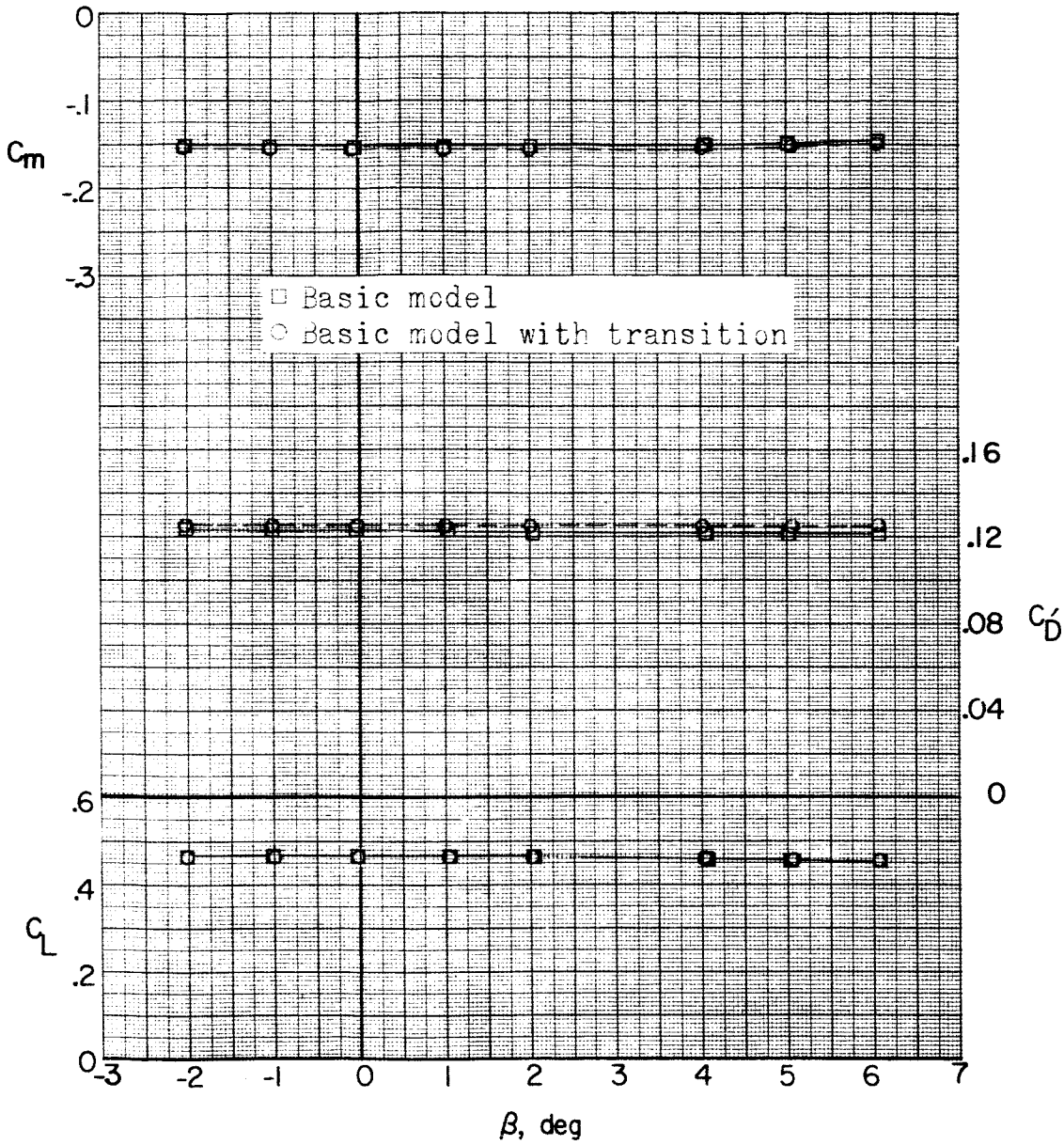

(c) Concluded. $\alpha = 10.4^{\circ}$.

Figure 7.- Concluded.

DECLASSIFIED

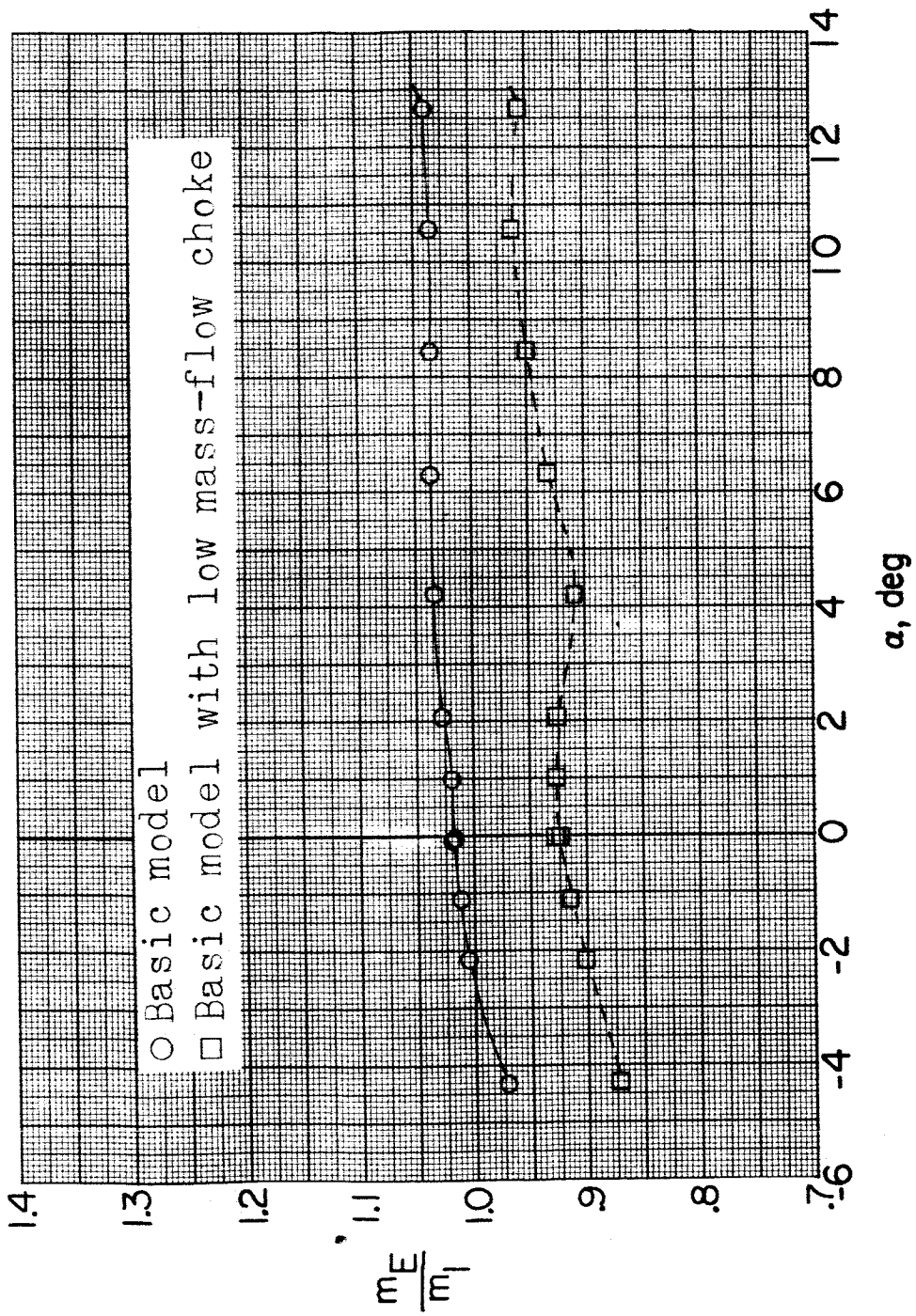

(a) M = 1.56.

Figure 8.- Effect of angle of attack on mass-flow ratio. Flagged symbols denote wall-reflected shock waves striking the tail.

[redacted]

DECLASSIFIED

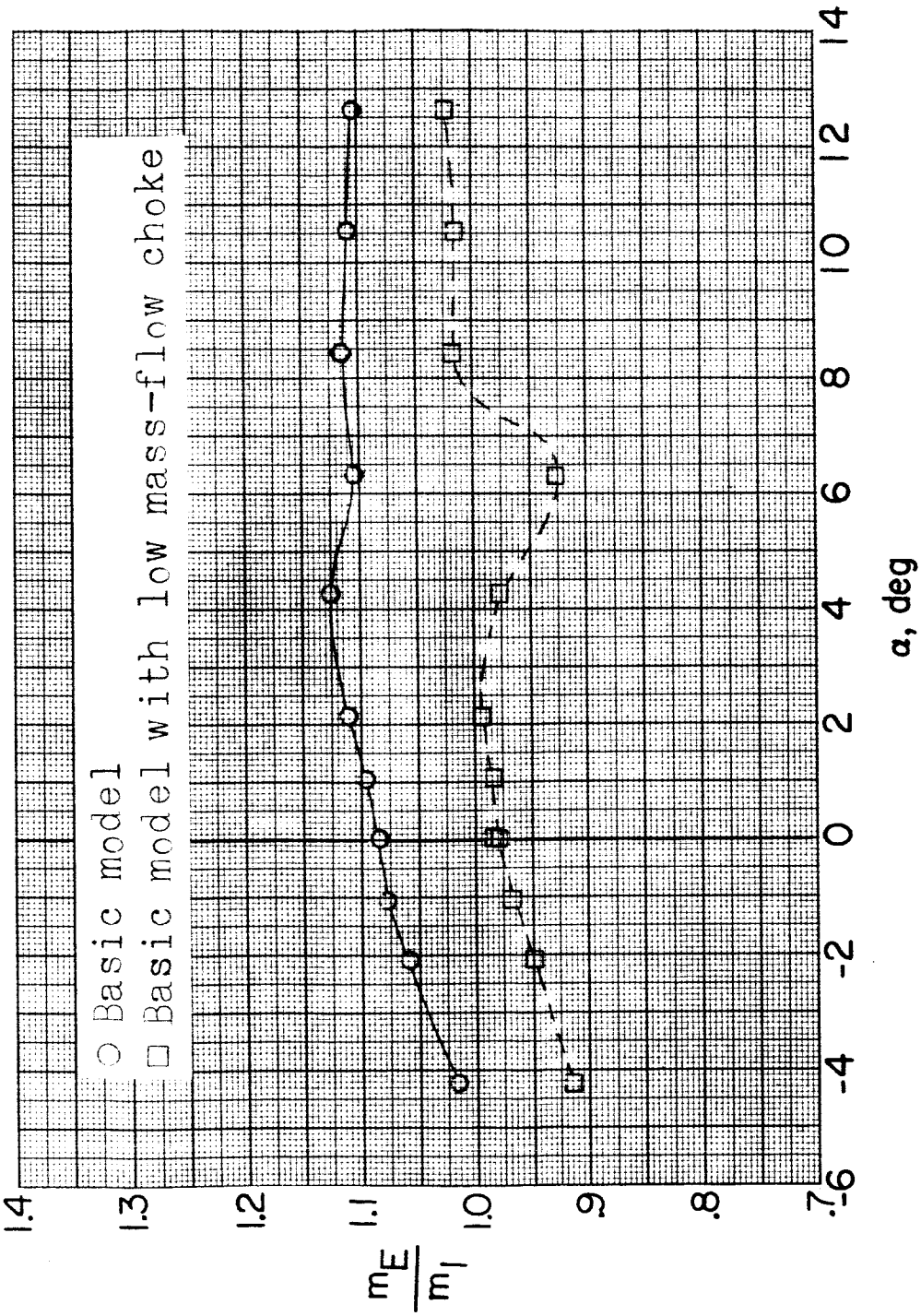

(b) M = 1.76.

Figure 8.- Continued.

[redacted]

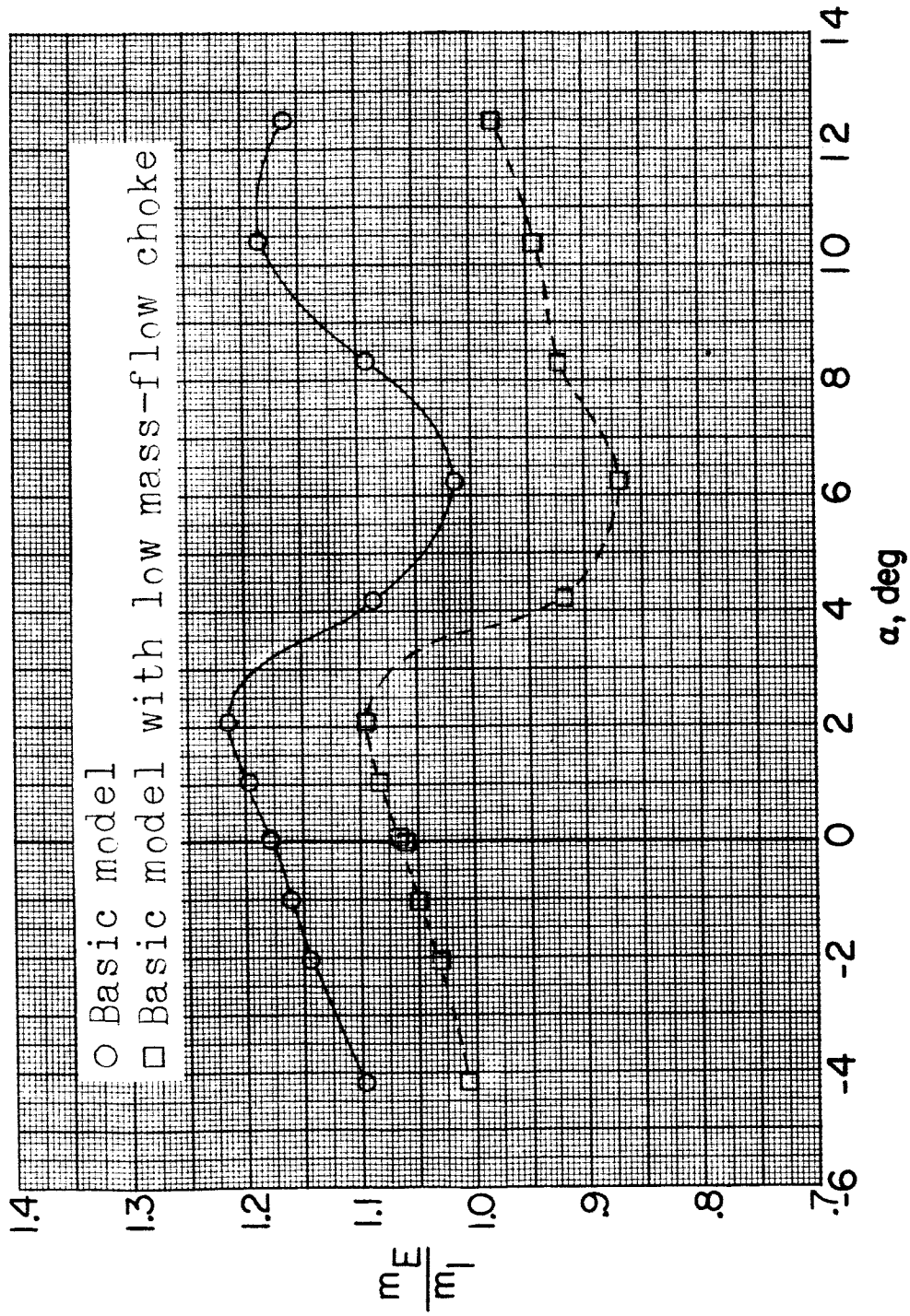

(c) M = 2.06.

Figure 8.- Continued.

[redacted]

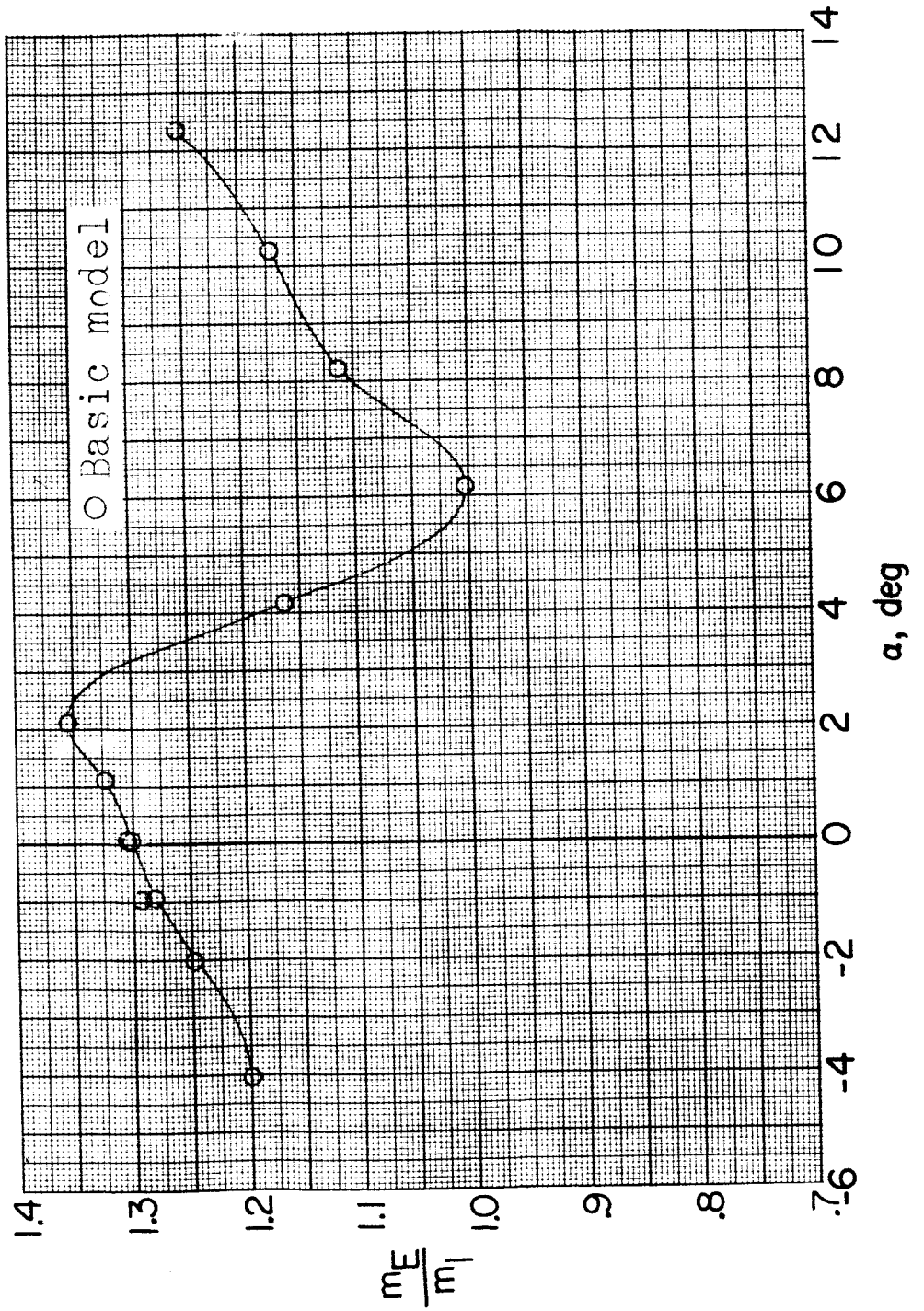

(d) M = 2.53.

Figure 8.- Concluded.

[redacted]

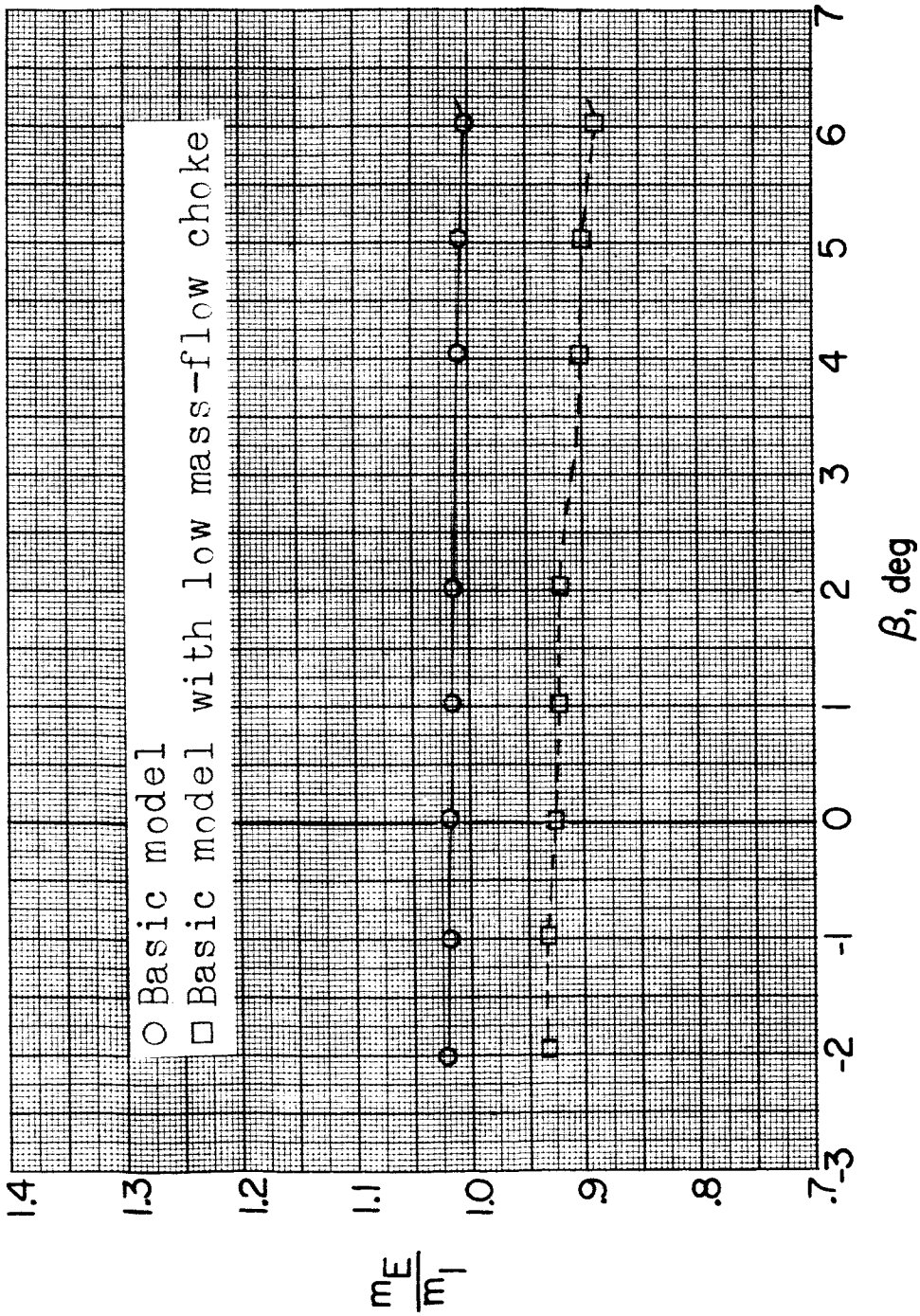

(a) M = 1.56; α = 0°.

Figure 9.- Effect of sideslip on mass-flow ratio. Flagged symbols denote wall-reflected shock waves striking the tail.

[redacted]

DECLASSIFIED

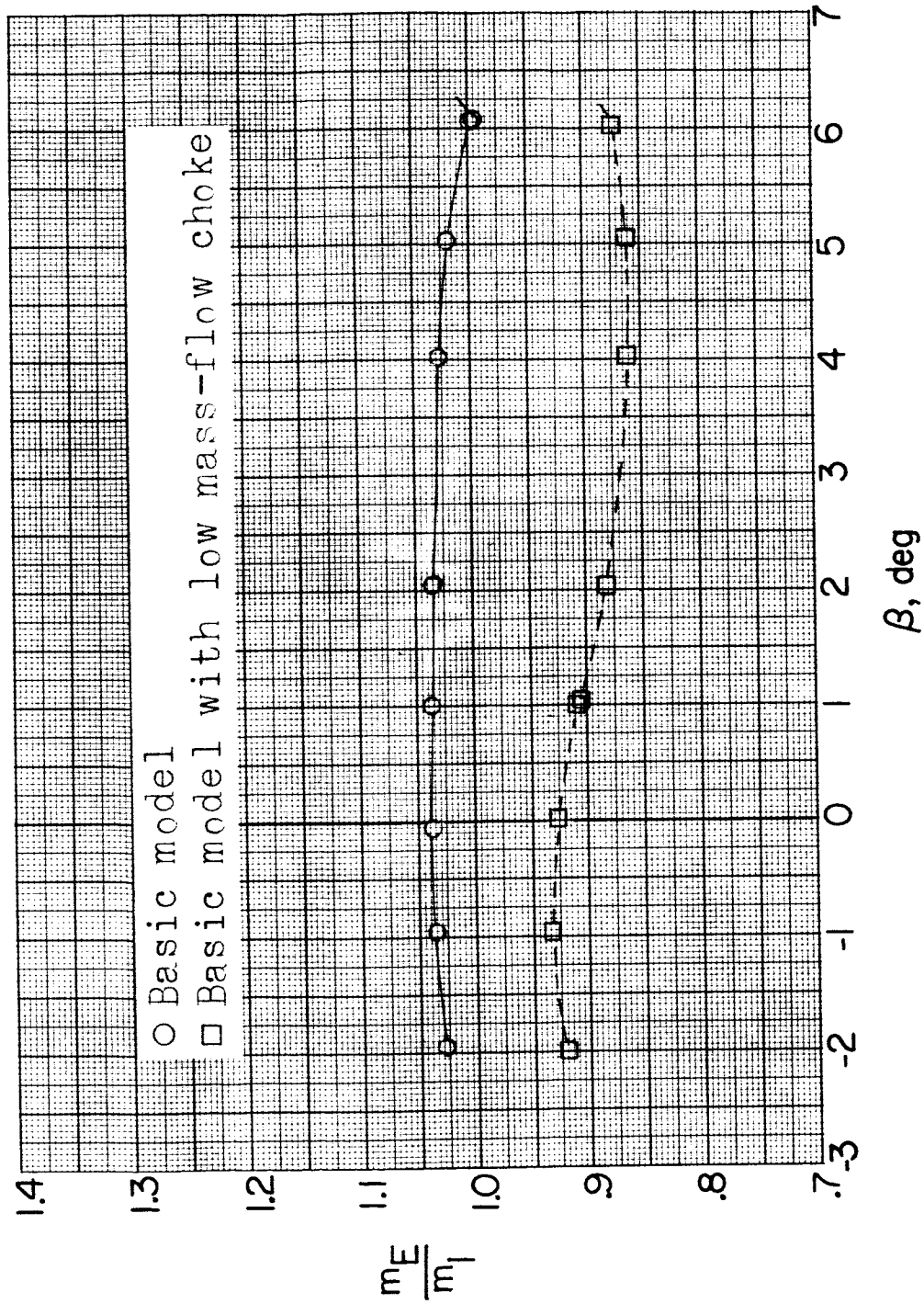

(a) Continued. $\alpha = 5.3^{\circ}$.

Figure 9.- Continued.

[redacted]

DECLASSIFIED

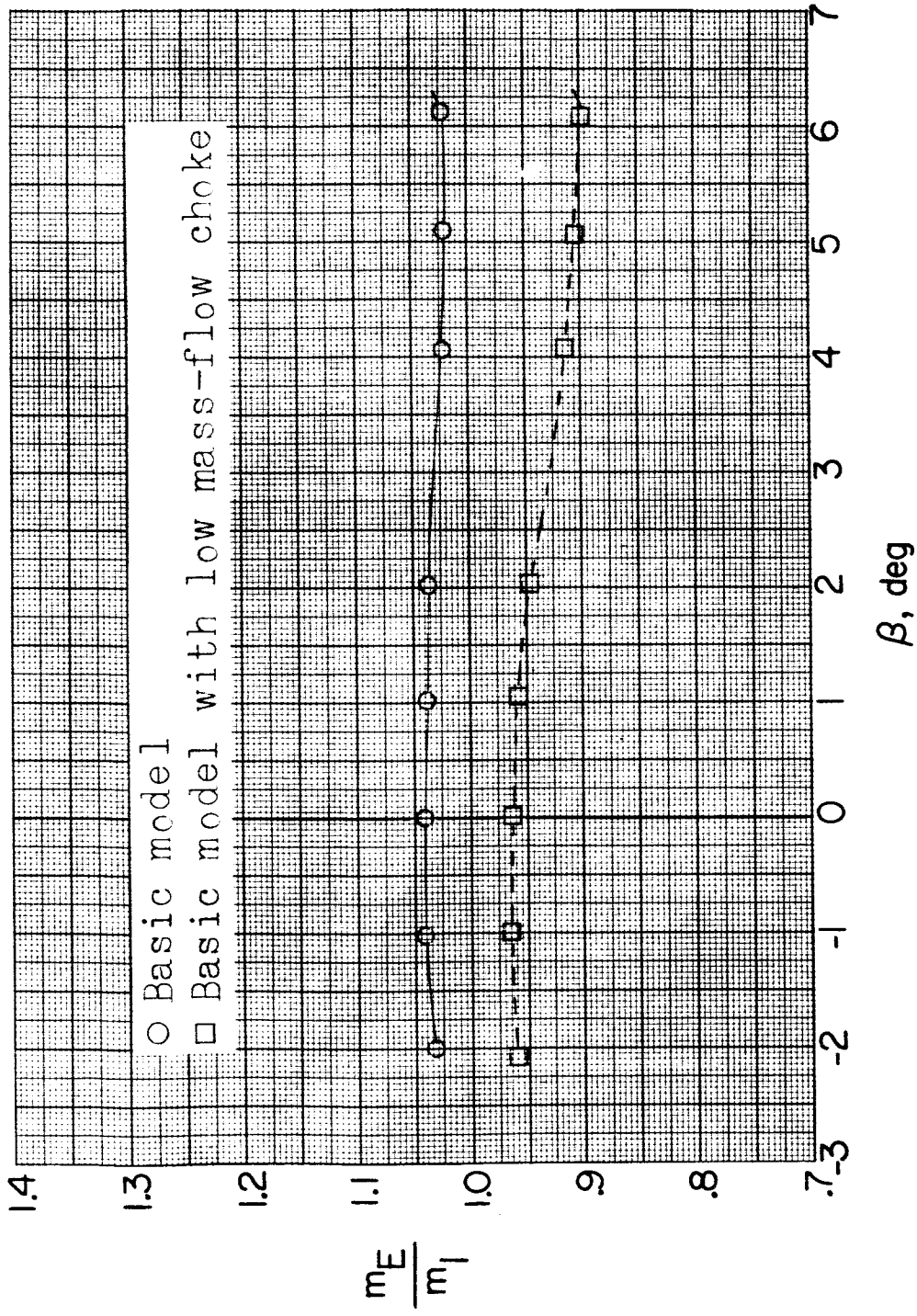

(a) Concluded. $\omega = 10.6^{\circ}$.

Figure 9.- Continued.

[redacted]

DECLASSIFIED

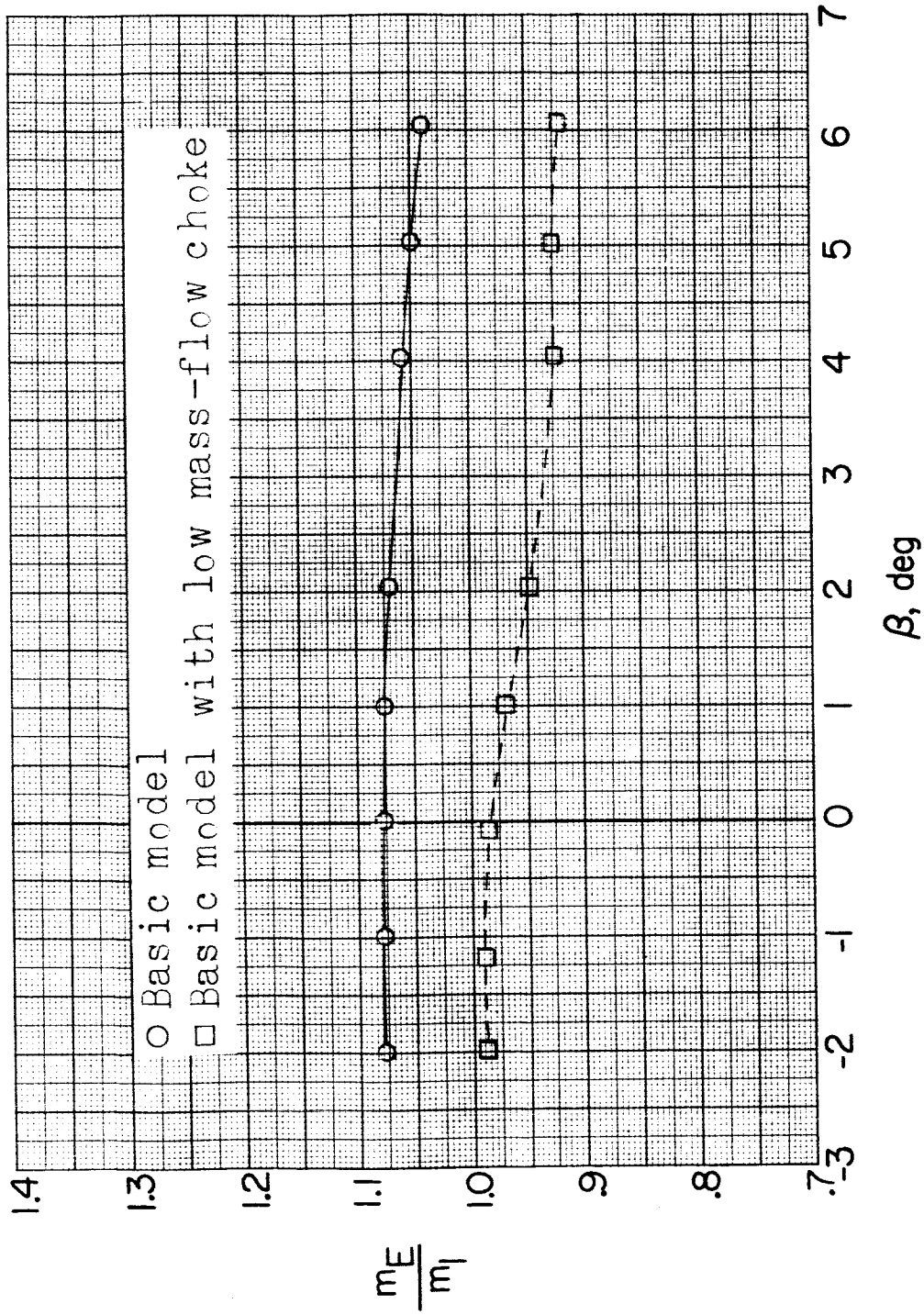

(b) M = 1.76; α = 0°.

Figure 9.- Continued.

[redacted]

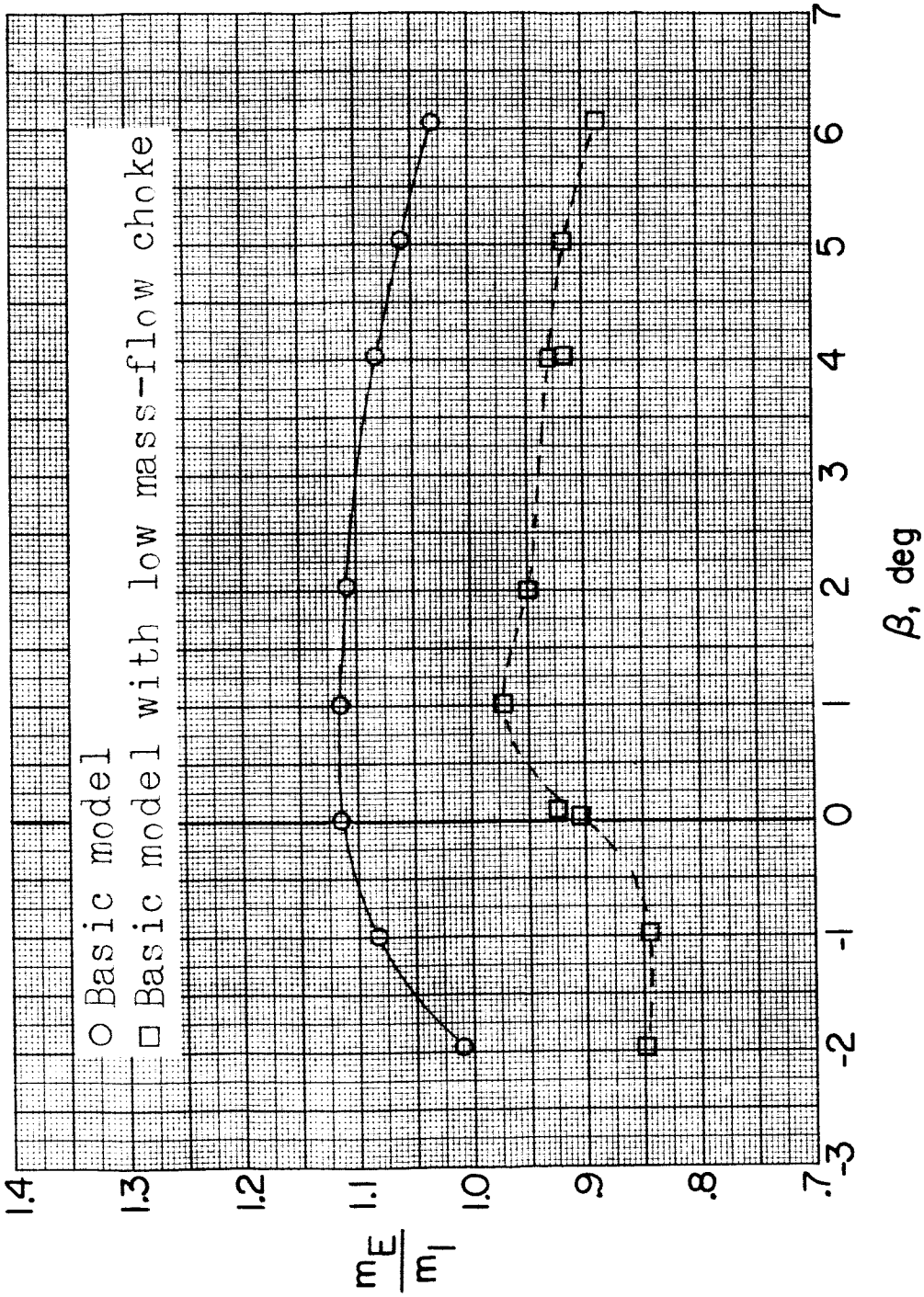

(b) Continued. $\alpha = 5.2^{\circ}$.

Figure 9.- Continued.

[redacted]

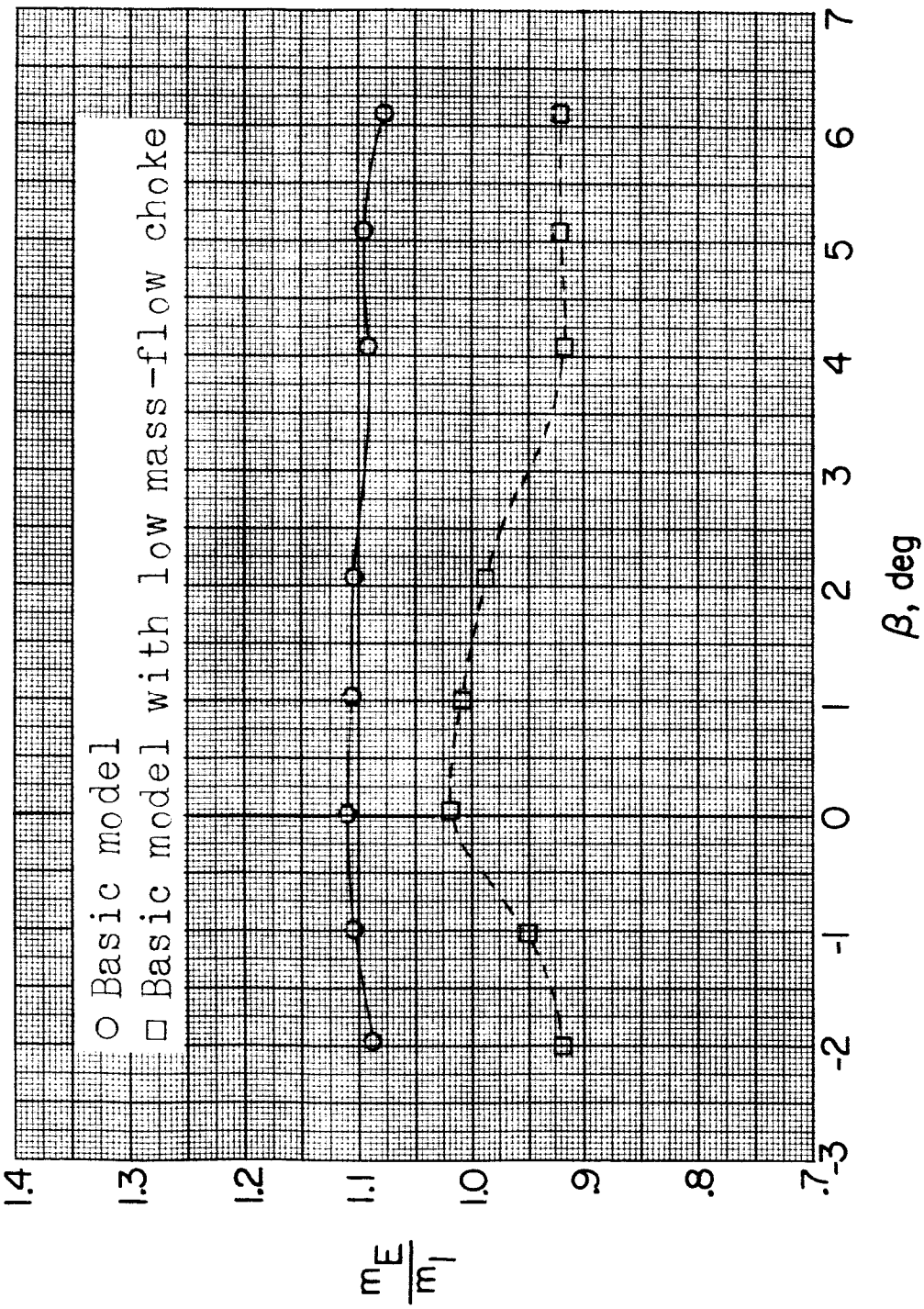

(b) Concluded. $\alpha = 10.5^{\circ}$.

Figure 9.- Continued.

[redacted]

DECLASSIFIED

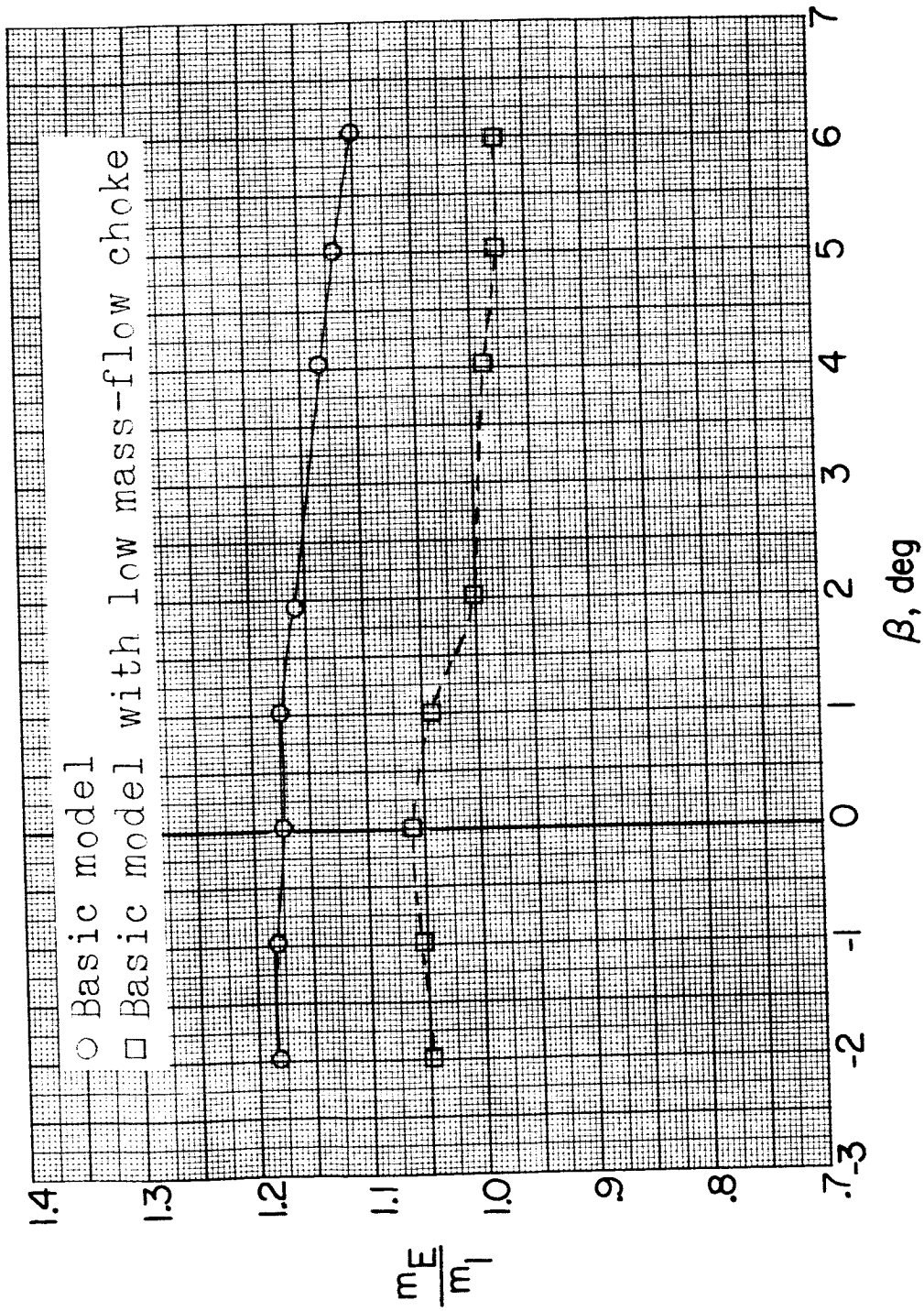

(c) M = 2.06; α = 0°.

Figure 9.- Continued.

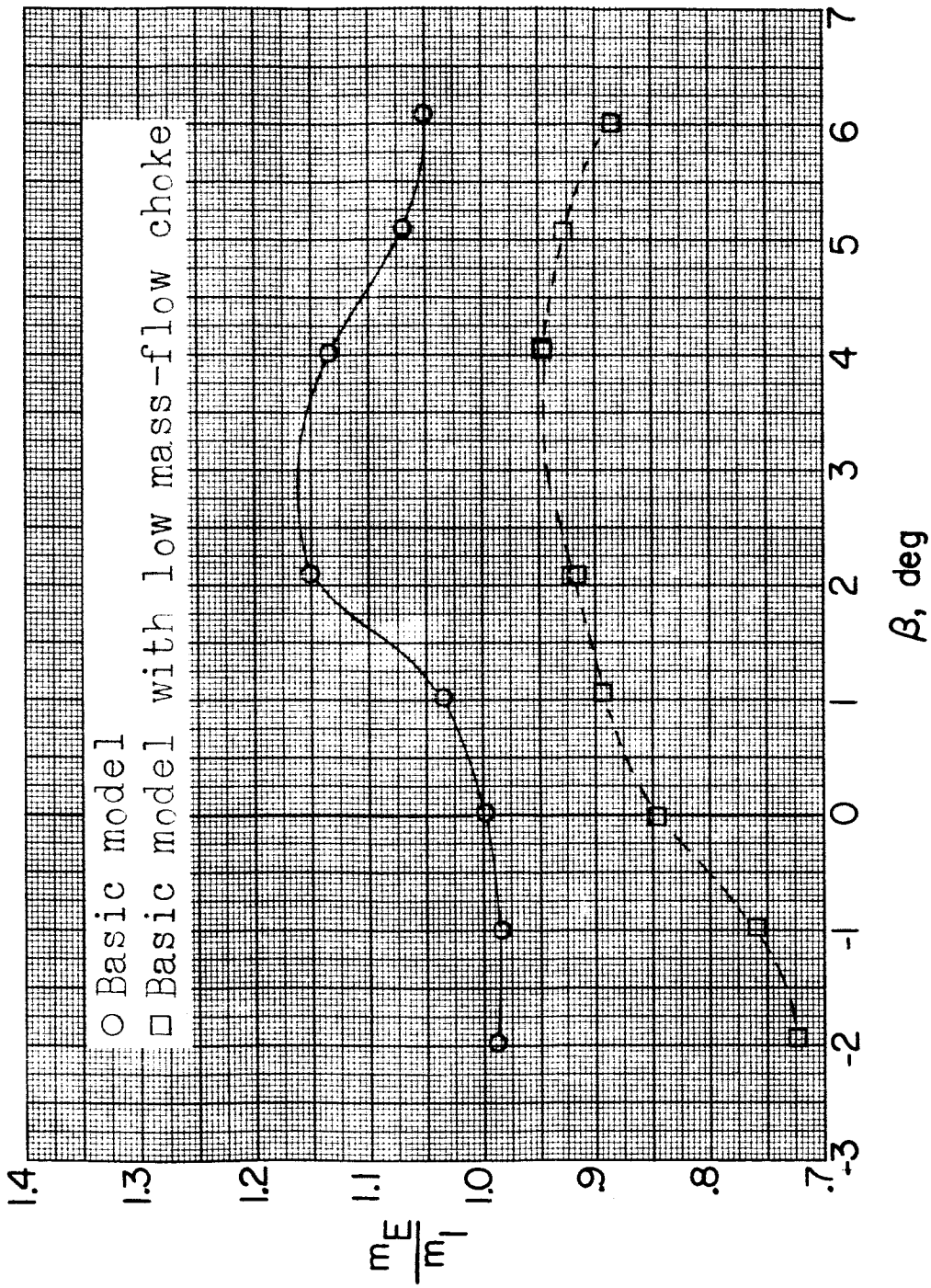

(c) Continued. $\alpha = 5.2^{\circ}$.

Figure 9.- Continued.

[redacted]

DECLASSIFIED

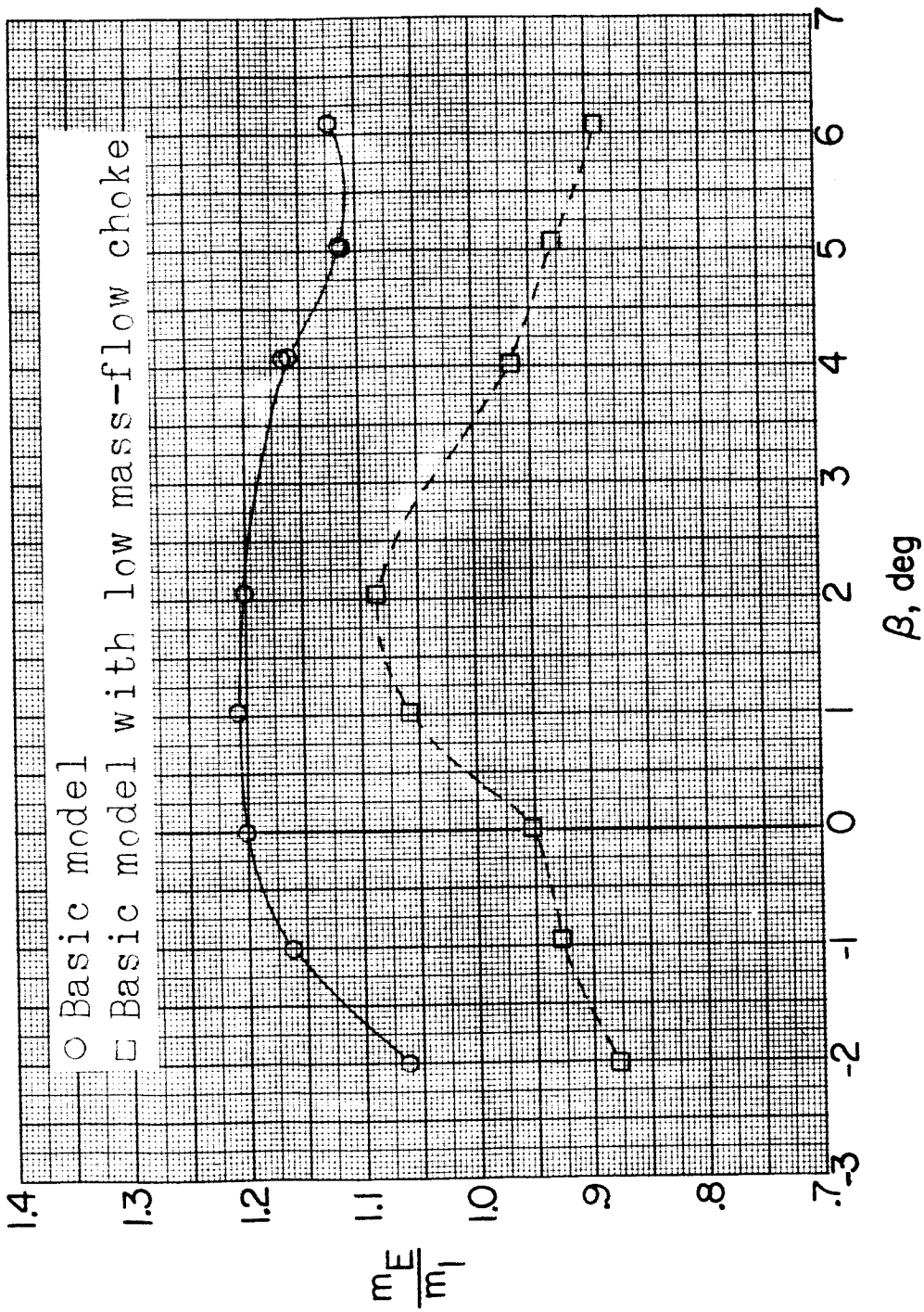

(c) Concluded. $\alpha = 10.4^{\circ}$.

Figure 9.- Continued.

[redacted]

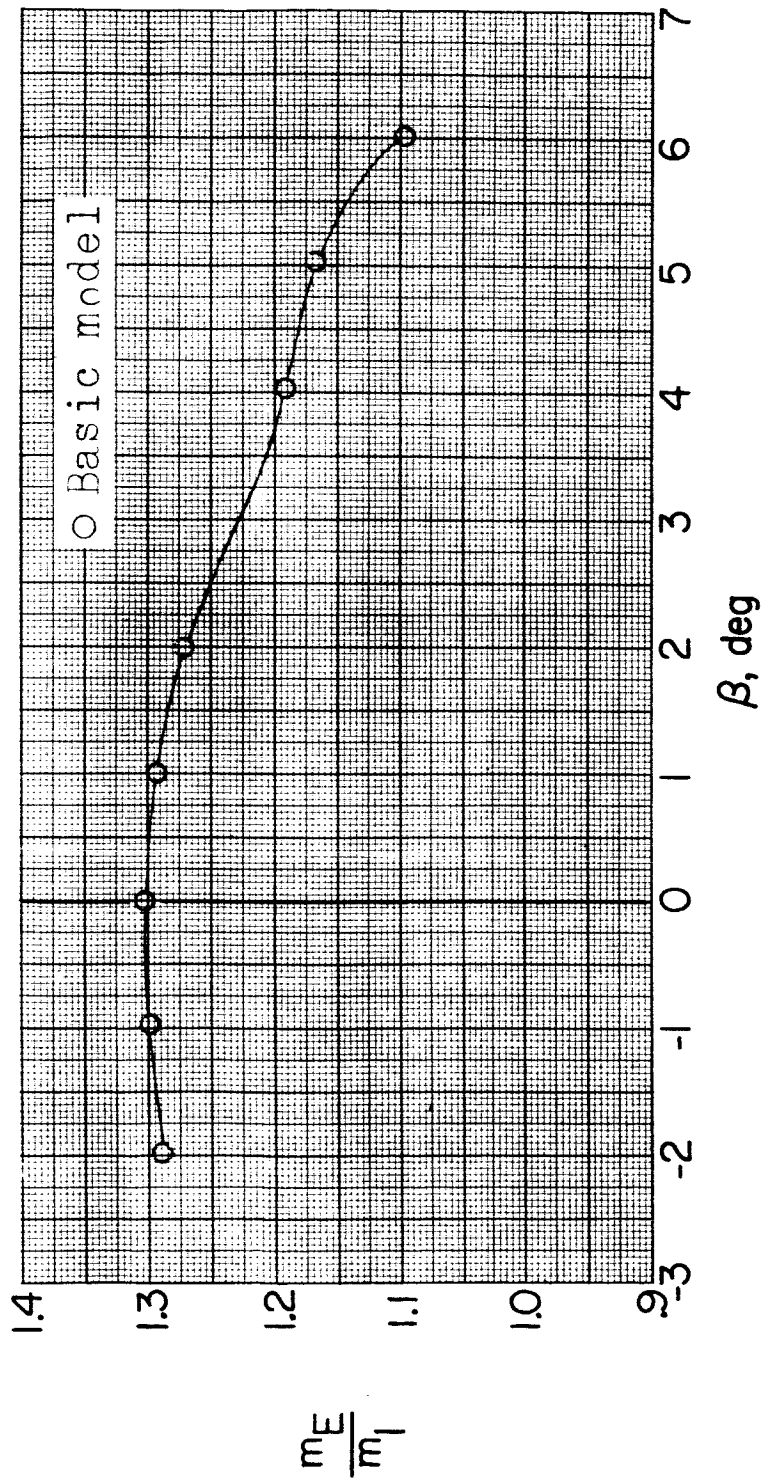

(d) M = 2.53; α = 0°.

Figure 9.- Continued.

[redacted]

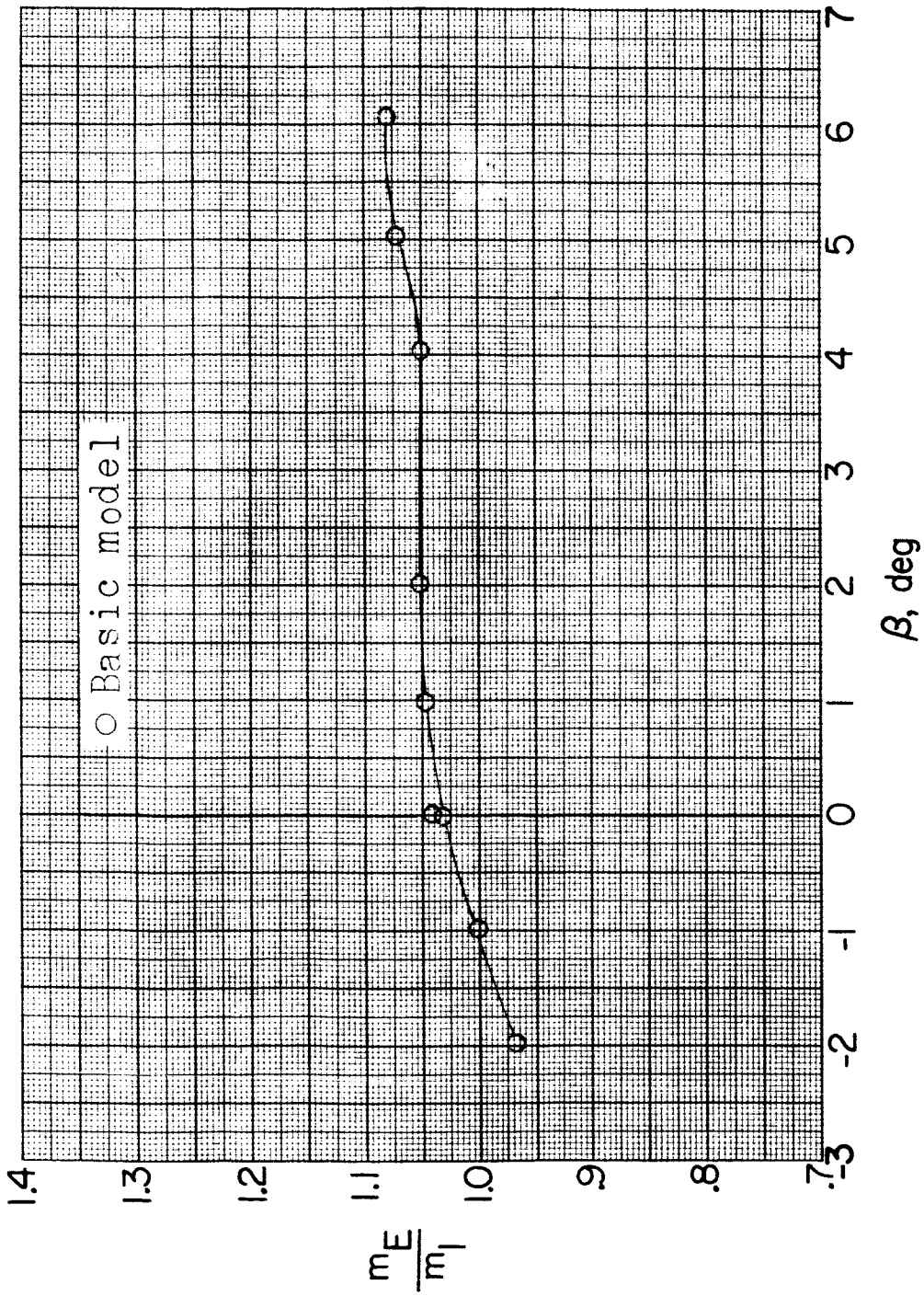

(d) Continued. $\alpha = 5.1^{\circ}$.

Figure 9.- Continued.

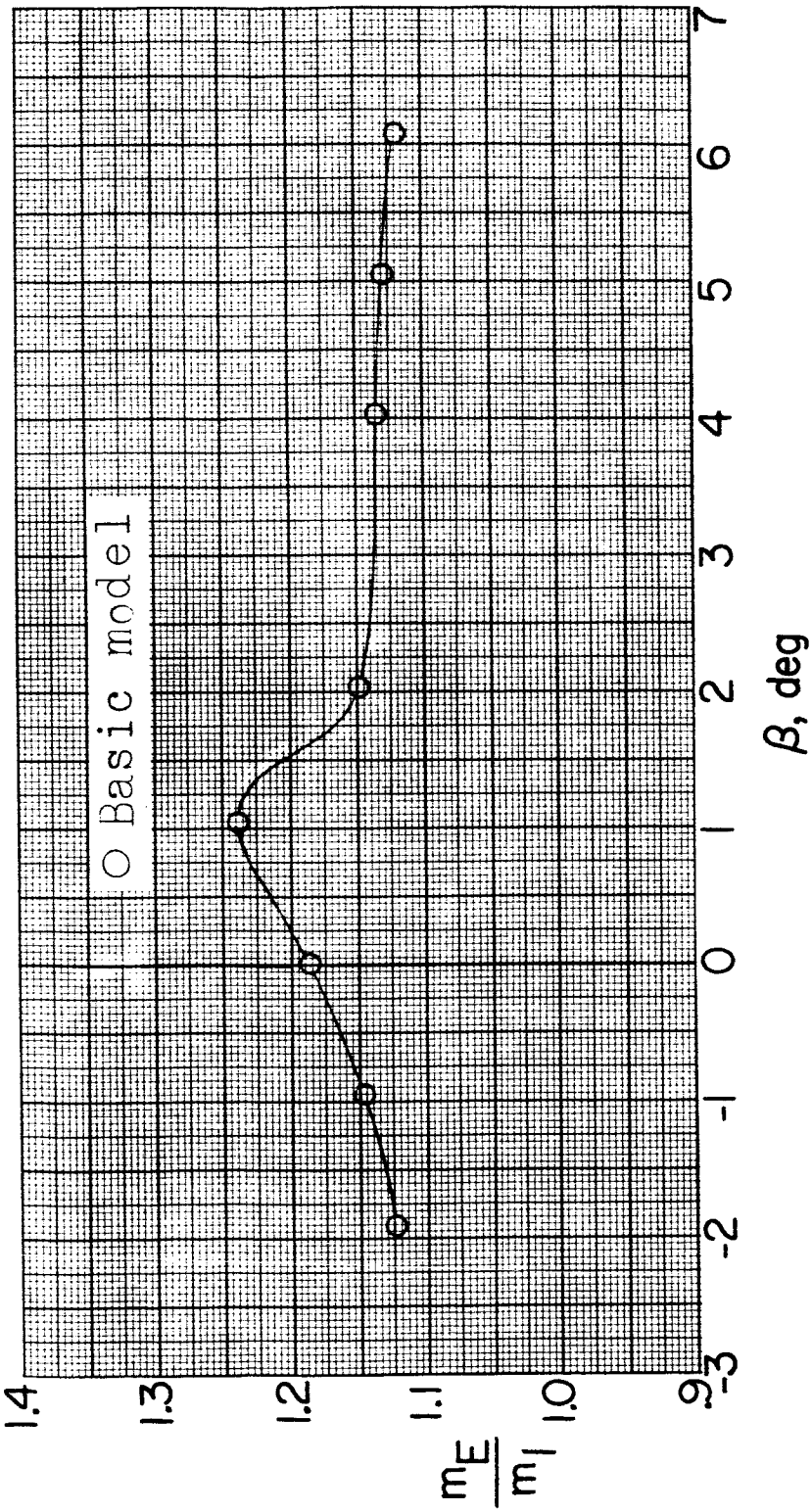

(d) Concluded. $\alpha = 10.2^{\circ}$.

Figure 9.- Concluded.

(a) Basic model.

L-95878

Figure 10.- Typical schlieren photographs of the 1/15-scale model of the Grumman F11F-1F airplane.

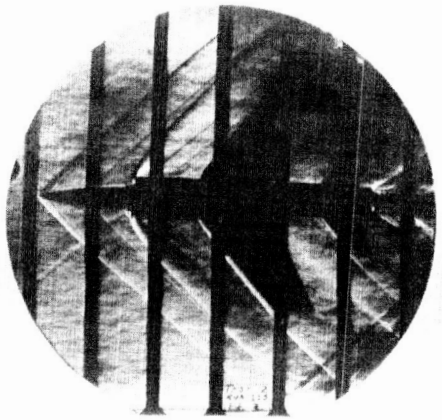

$\alpha = -.04°$
$\beta = -.01°$

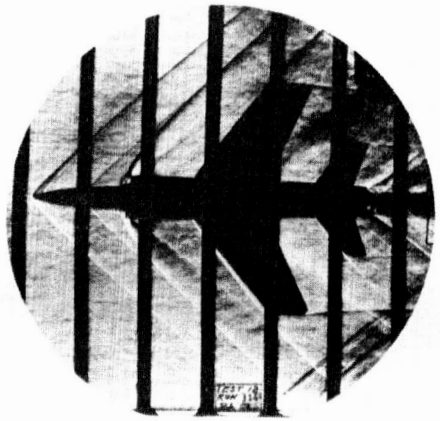

$\alpha = 5.28°$
$\beta = -.01°$

Basic model with transition

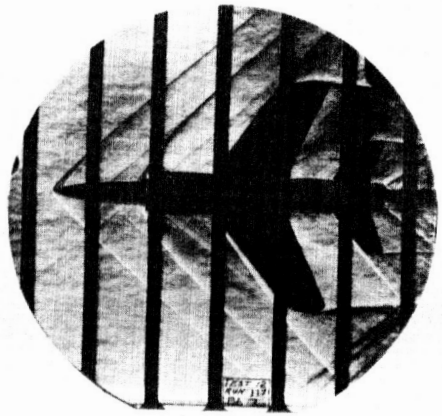

$\alpha = 10.61°$
$\beta = .01°$

$\alpha = -.02°$
$\beta = .01°$

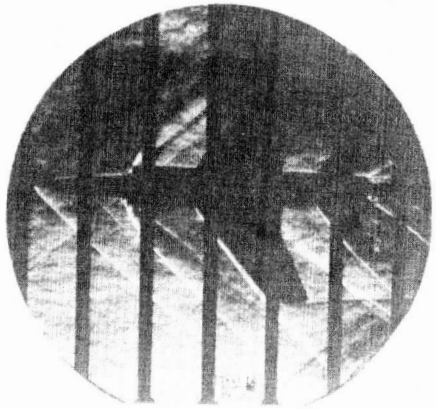

$\alpha = 5.29°$
$\beta = -.03°$

Basic model

(b) Effect of transition. M = 1.56. L-95879

Figure 10.- Continued.

[redacted]

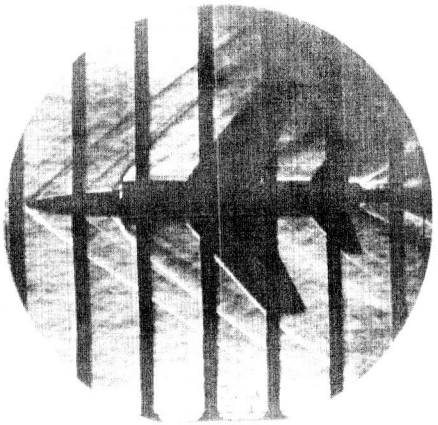

$\alpha = -.02°$
$\beta = .01°$

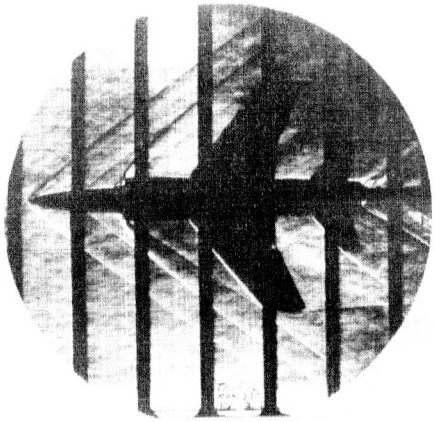

$\alpha = 5.23°$
$\beta = -.01°$

Basic model with transition

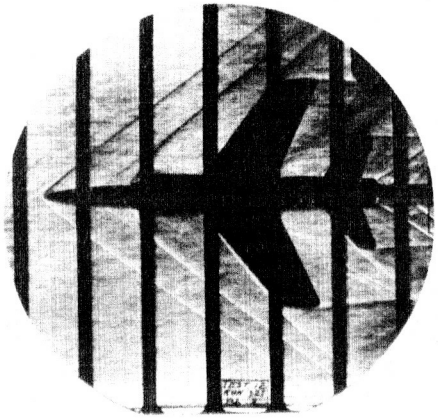

$\alpha = 10.50°$
$\beta = .01°$

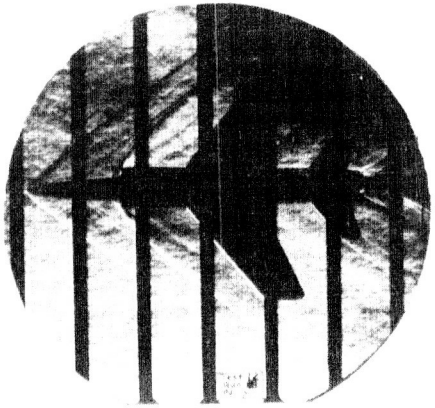

$\alpha = -.03°$
$\beta = -.01°$

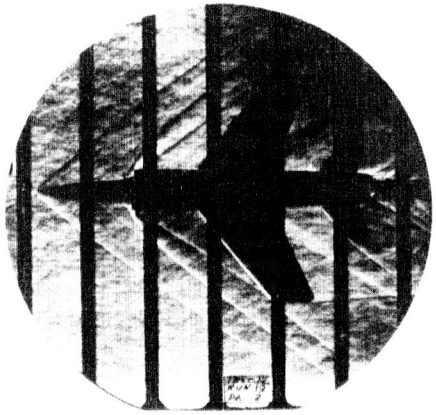

$\alpha = 5.22°$
$\beta = -.01°$

Basic model

(b) Continued. M = 1.76.

L-95880

Figure 10.- Continued.

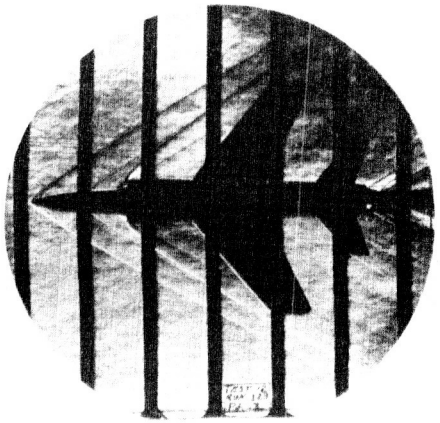

$\alpha = -.02°$
$\beta = .00°$

$\alpha = 5.17°$
$\beta = .00°$

Basic model with transition

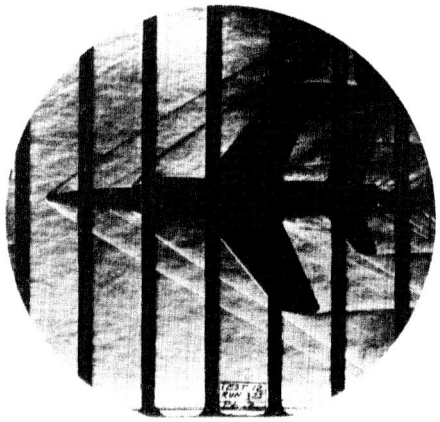

$\alpha = 10.34°$
$\beta = -.02°$

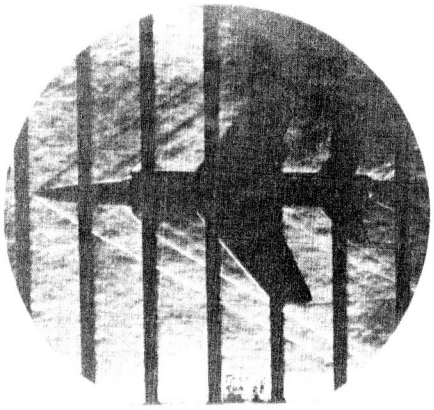

$\alpha = 5.15°$
$\beta = .00°$

Basic model

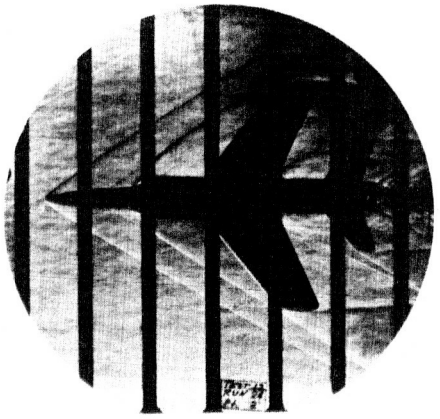

$\alpha = 10.35°$
$\beta = -.03°$

(b) Concluded. M = 2.06. L-95881

Figure 10.- Concluded.

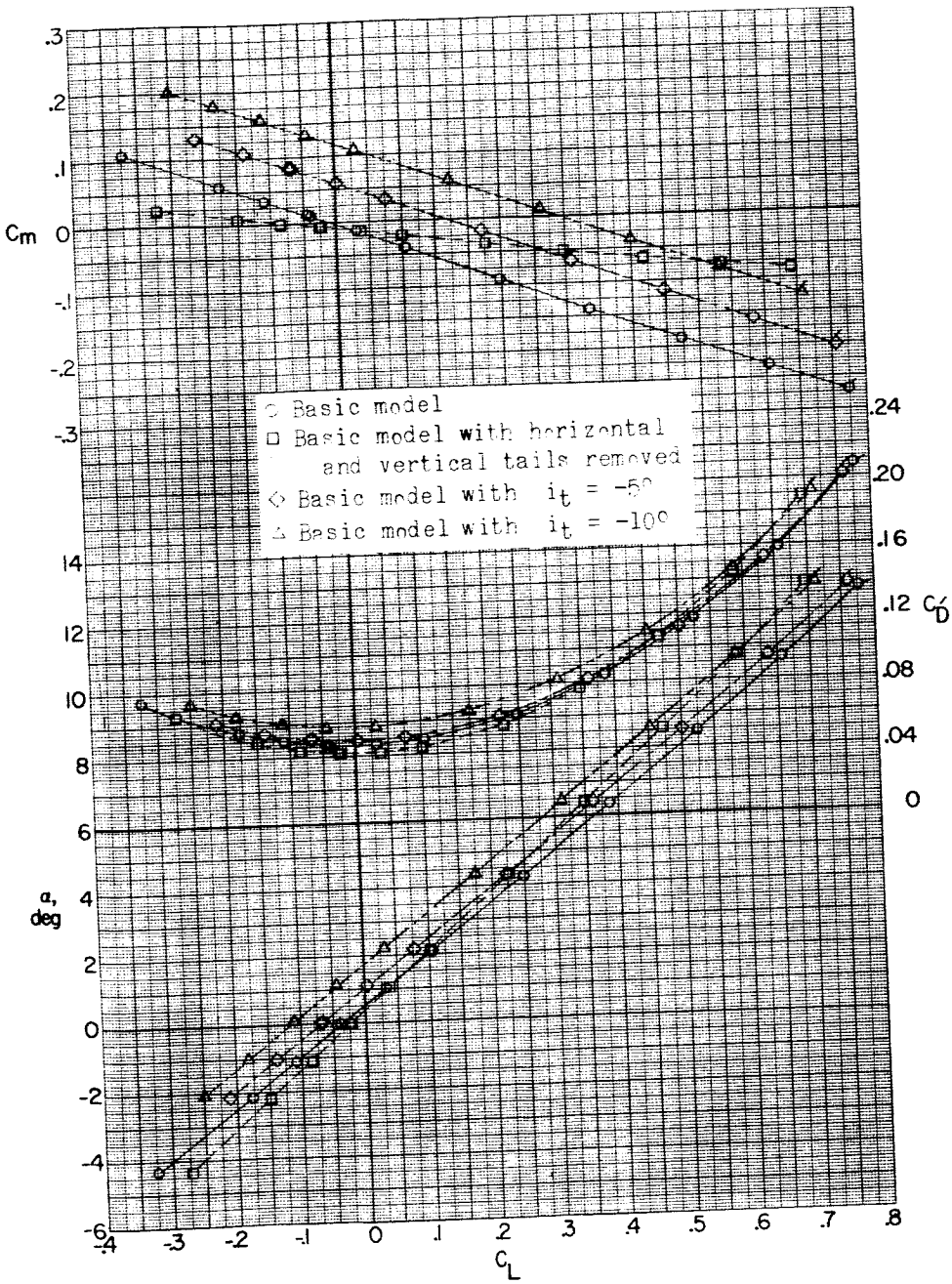

(a) M = 1.56.

Figure 11.- Effect of horizontal and vertical tails on aerodynamic characteristics in pitch. $\beta = 0^{\circ}$. Flagged symbols denote wall-reflected shock waves striking the tail.

[redacted]

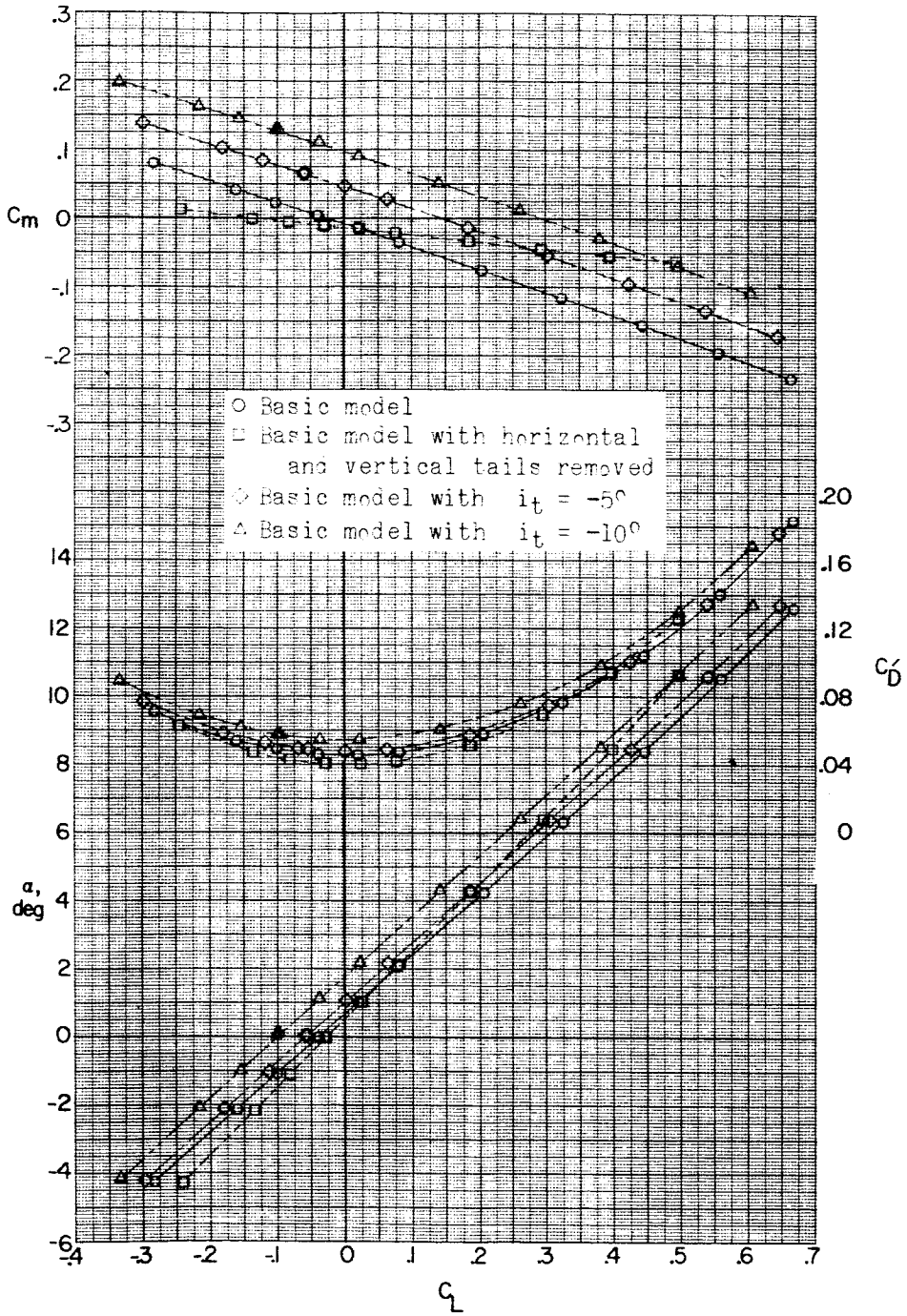

(b) M = 1.76.

Figure 11.- Continued.

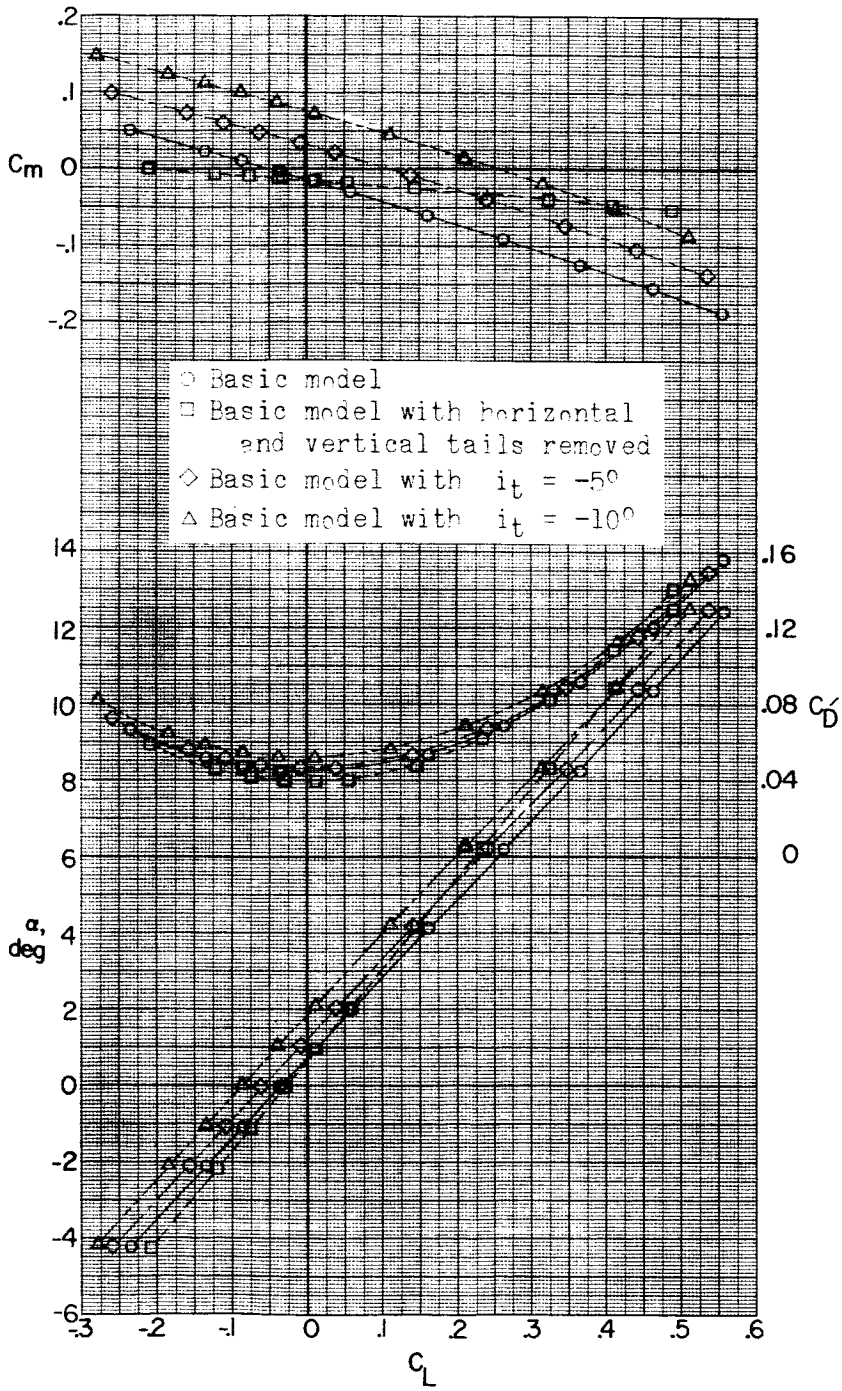

(c) M = 2.06.

Figure 11.- Continued.

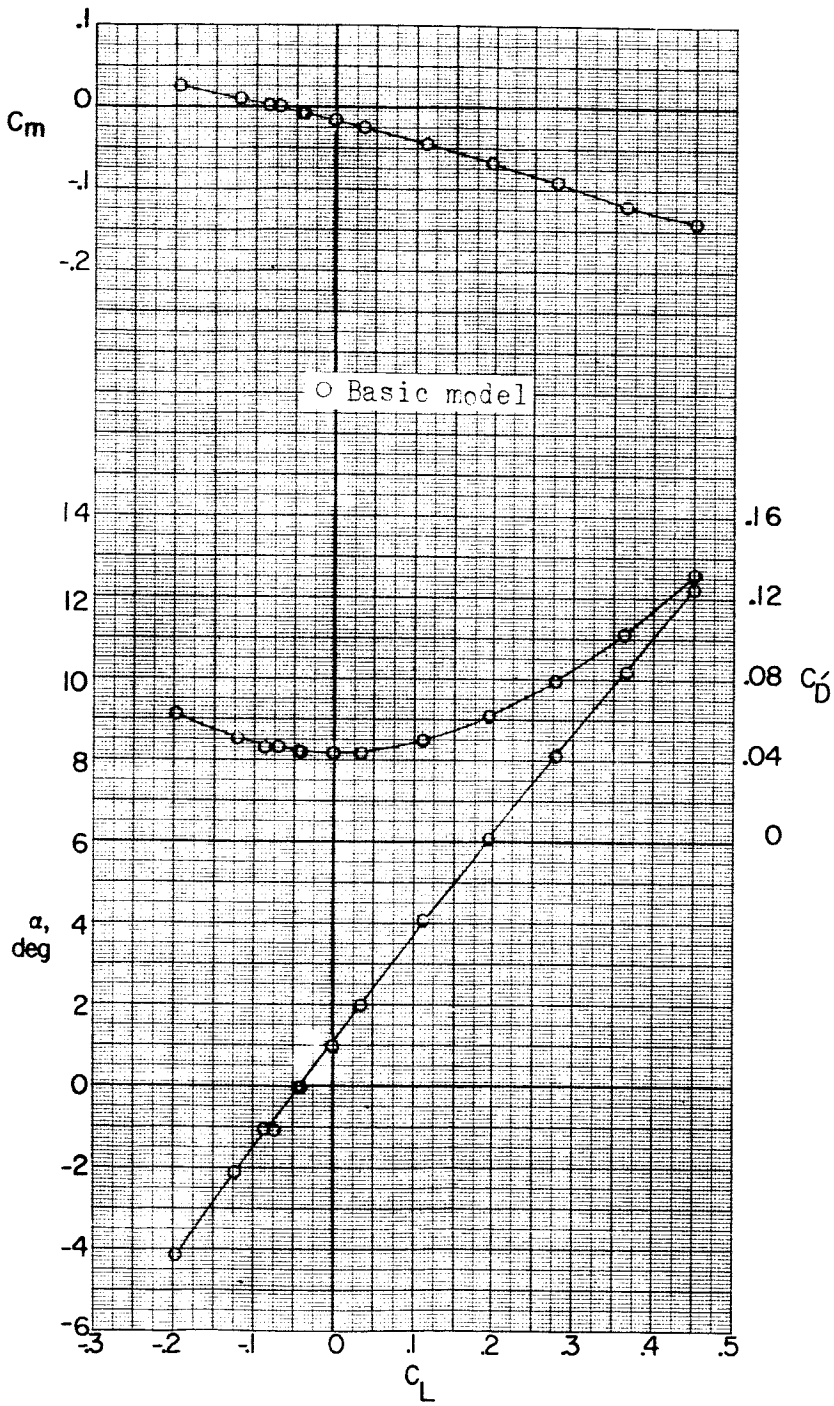

(d) M = 2.53.

Figure 11.- Concluded.

[redacted]

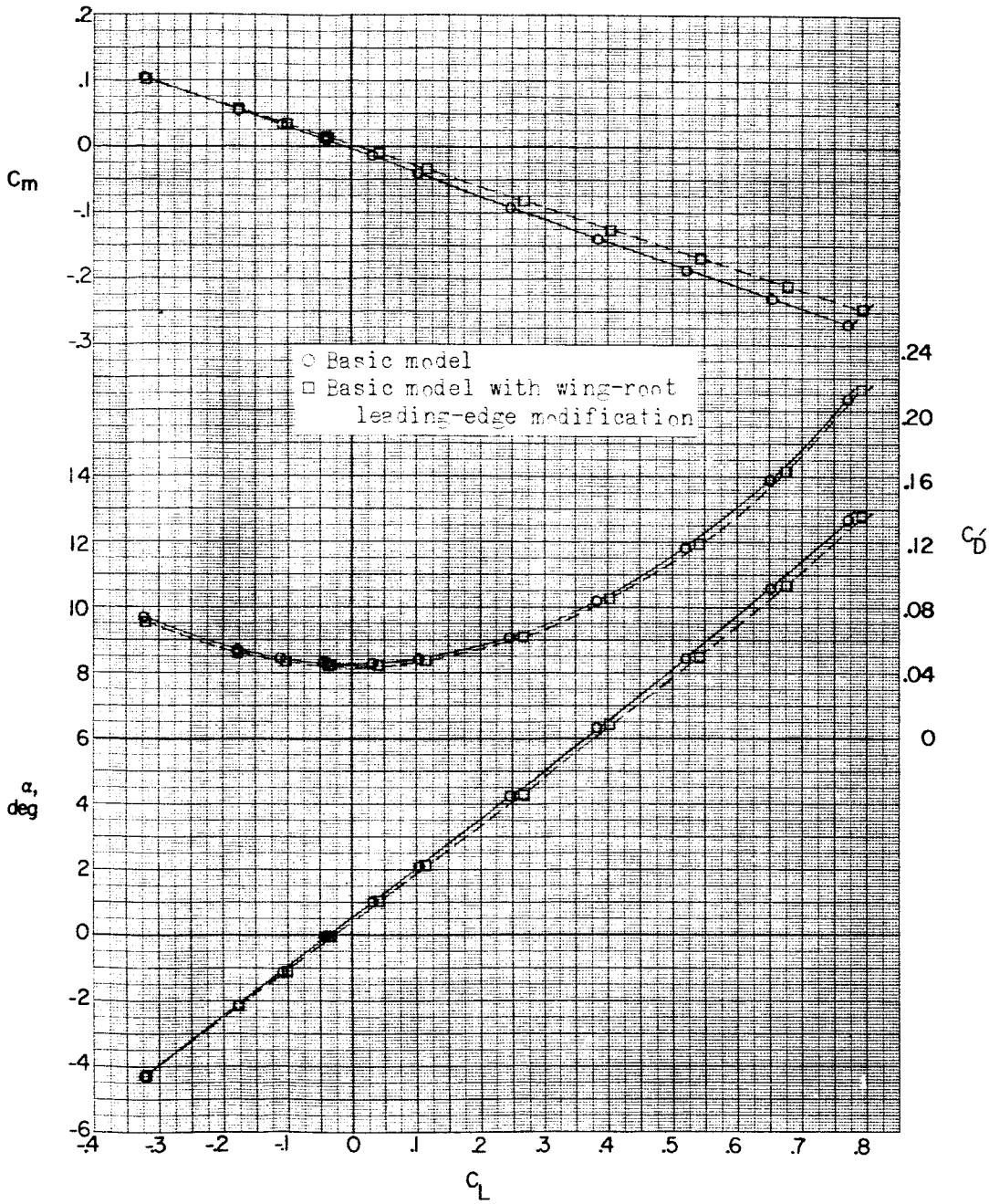

(a) M = 1.56.

Figure 12.- Effect of root leading-edge wing fillets on aerodynamic characteristics in pitch. $\beta = 0^{\circ}$. Flagged symbols denote wall-reflected shock waves striking the tail.

[redacted]

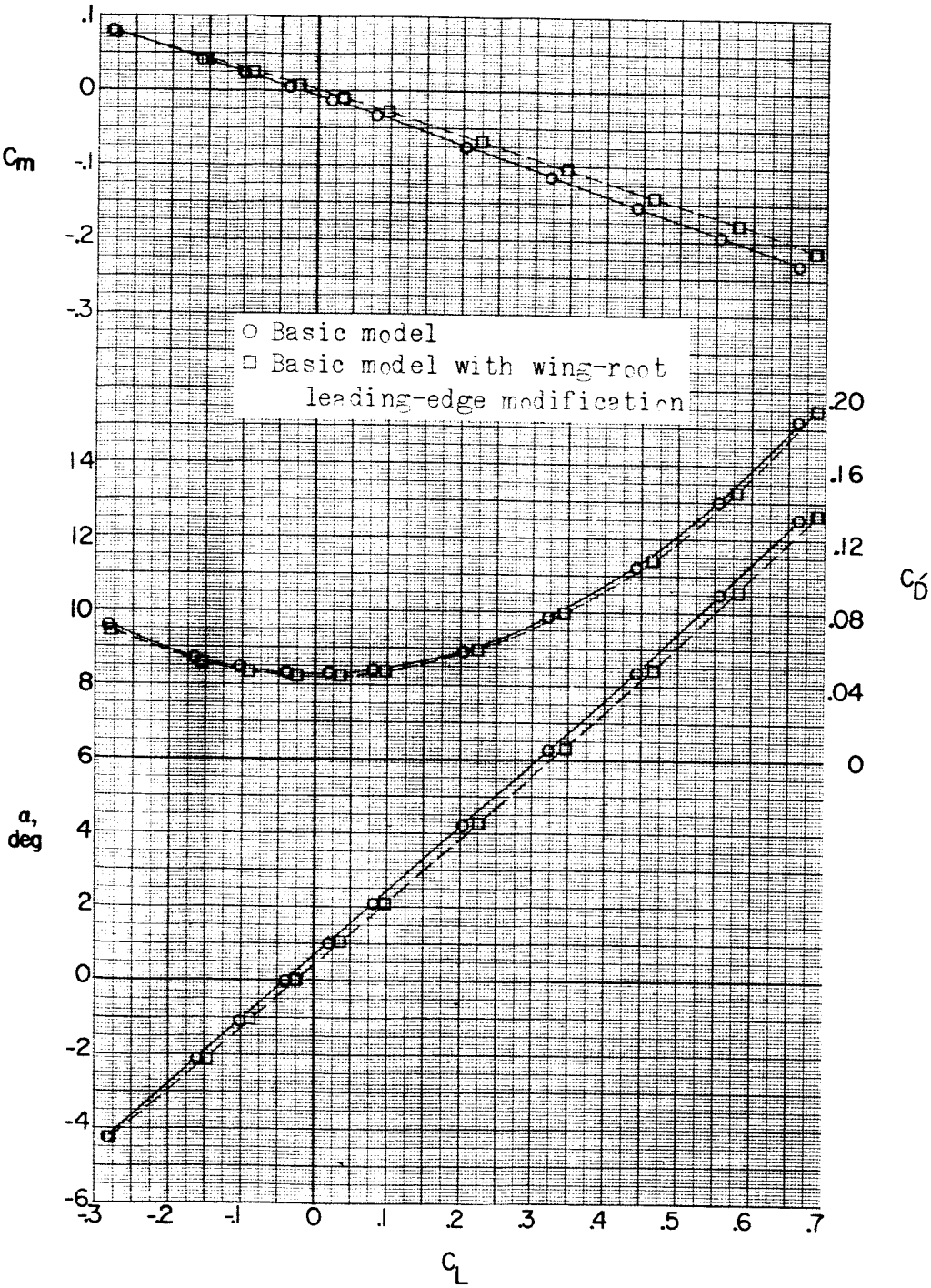

(b) M = 1.76.

Figure 12.- Continued.

DECLASSIFIED

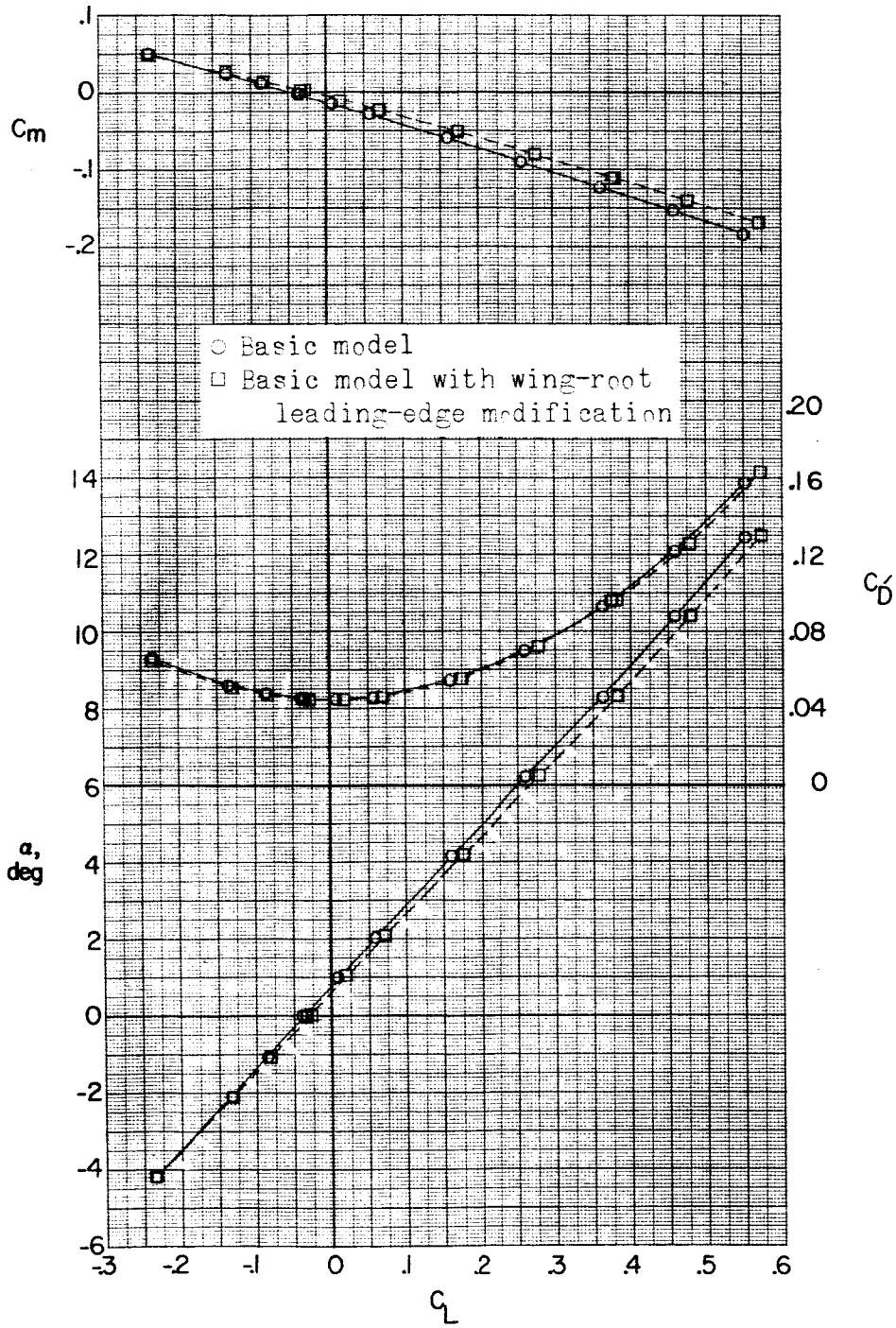

(c) M = 2.06.

Figure 12.- Concluded.

[redacted]

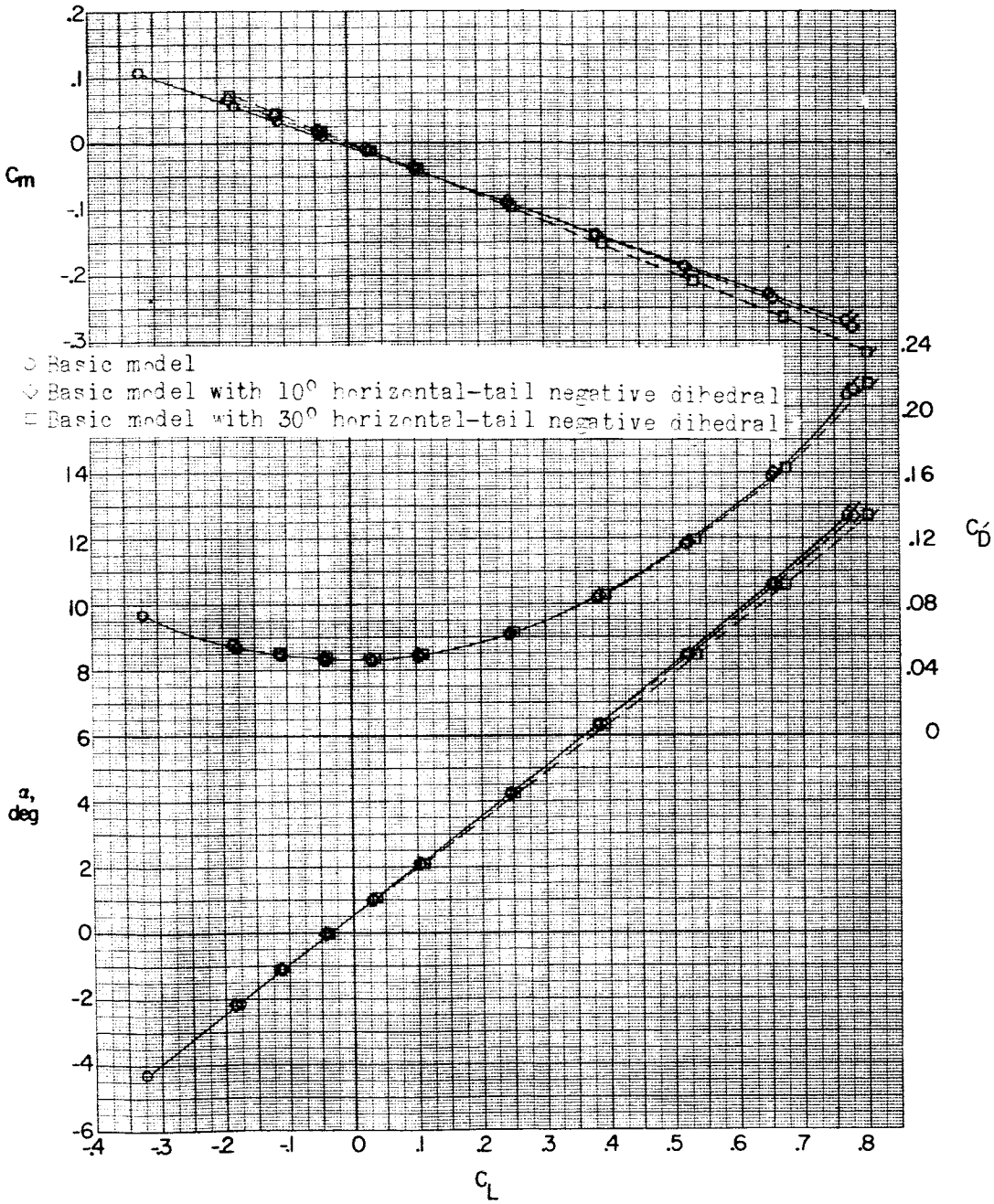

(a) M = 1.56.

Figure 13.- Effect of horizontal-tail negative dihedral on aerodynamic characteristics in pitch. $\beta = 0^{\circ}$. Flagged symbols denote wall-reflected shock waves striking the tail.

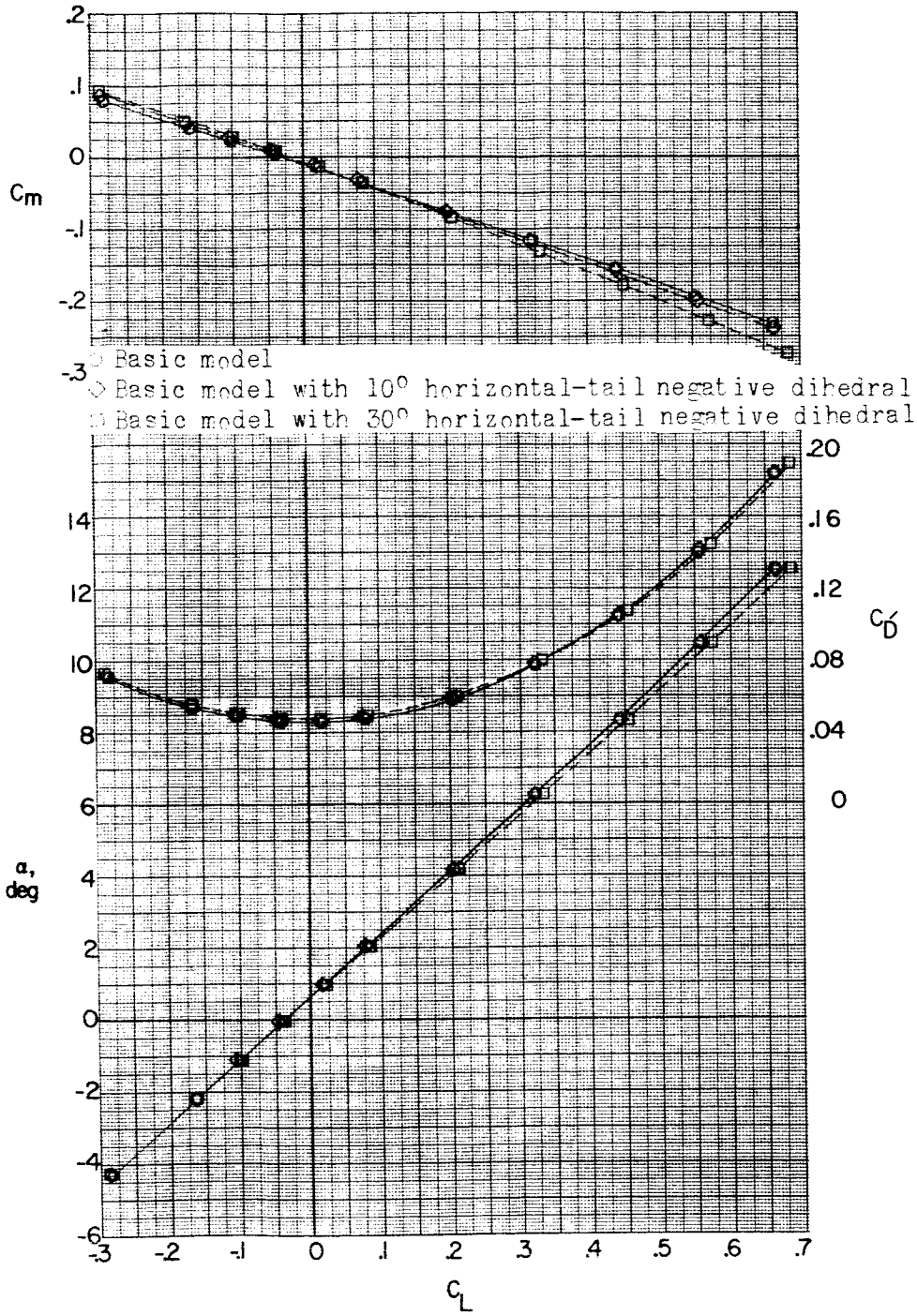

(b) M = 1.76.

Figure 13.- Continued.

[redacted]

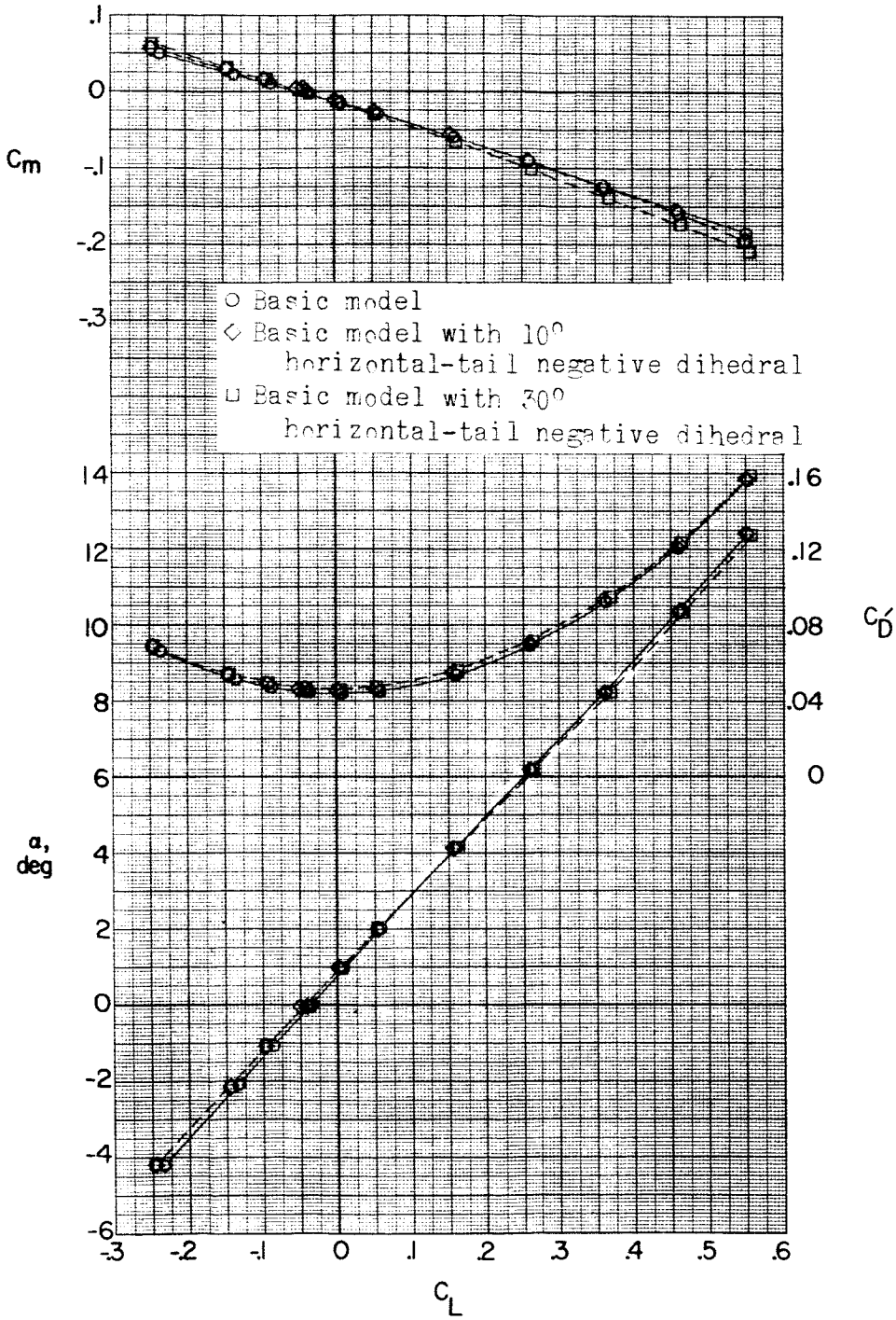

(c) M = 2.06.

Figure 13.- Concluded.

DECLASSIFIED

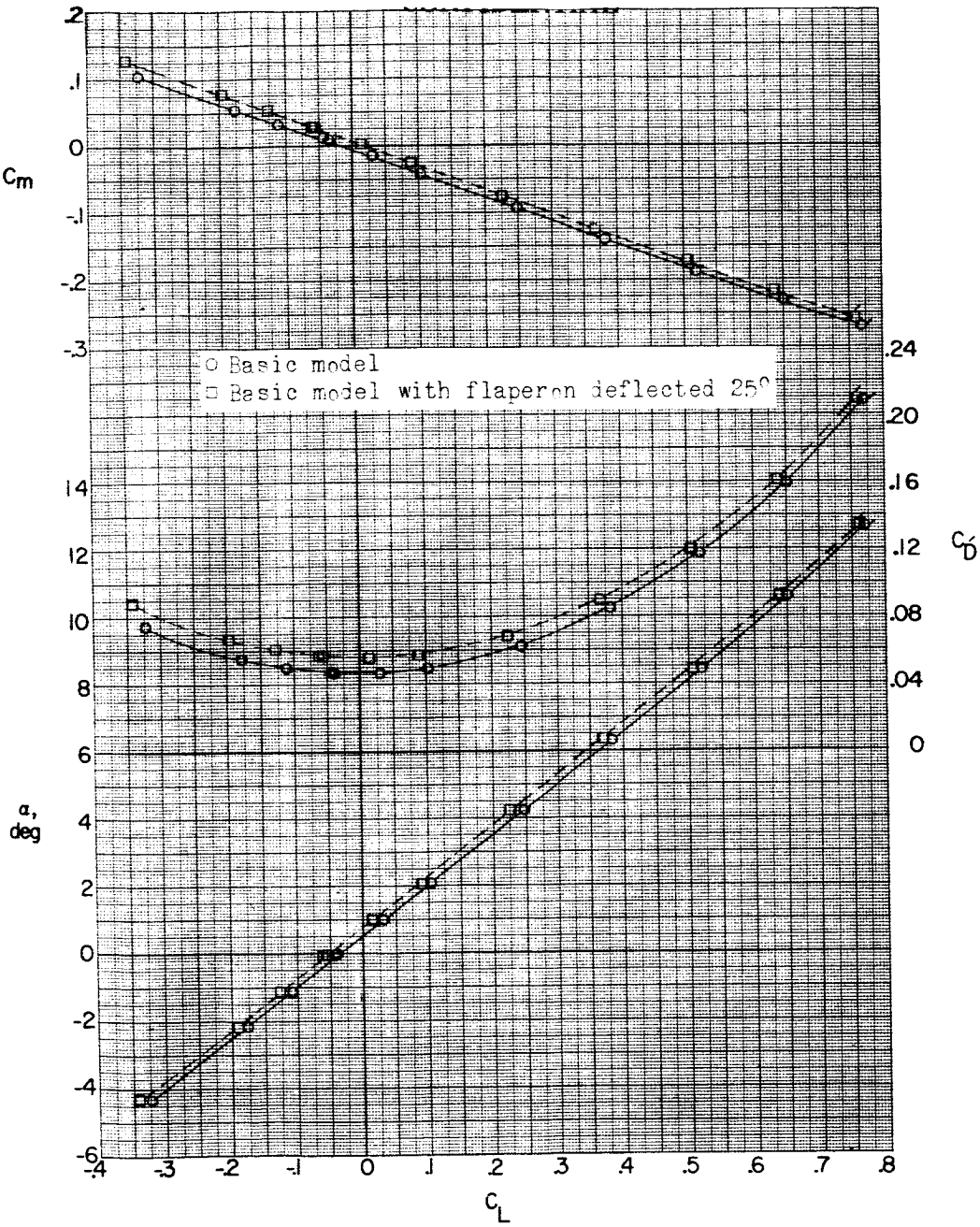

(a) M = 1.56.

Figure 14.- Effect of flaperon on aerodynamic characteristics in pitch. $\beta = 0^{\circ}$. Flagged symbols denote wall-reflected shock waves striking the tail.

[redacted]

DECLASSIFIED

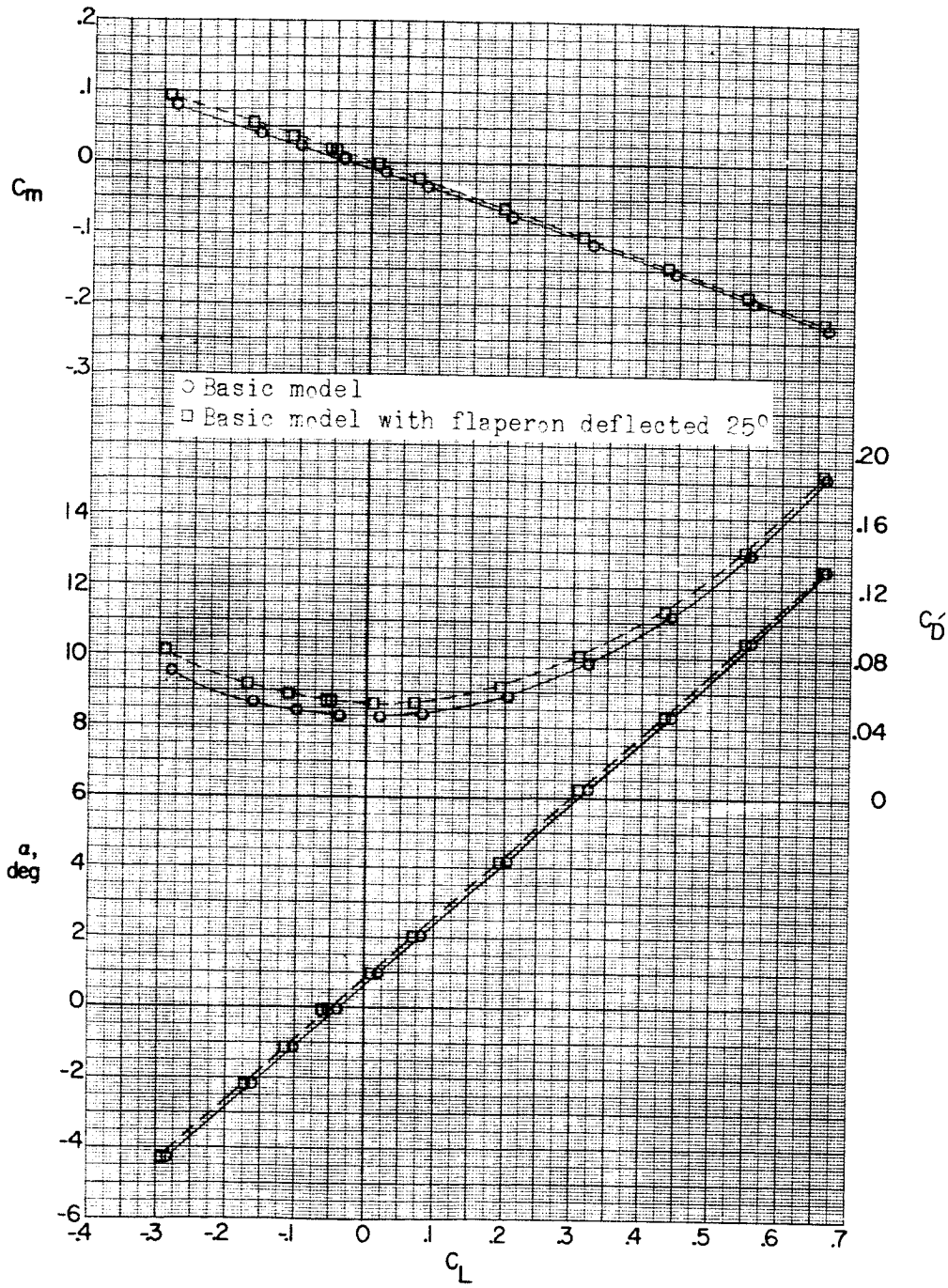

(b) M = 1.76.

Figure 14.- Continued.

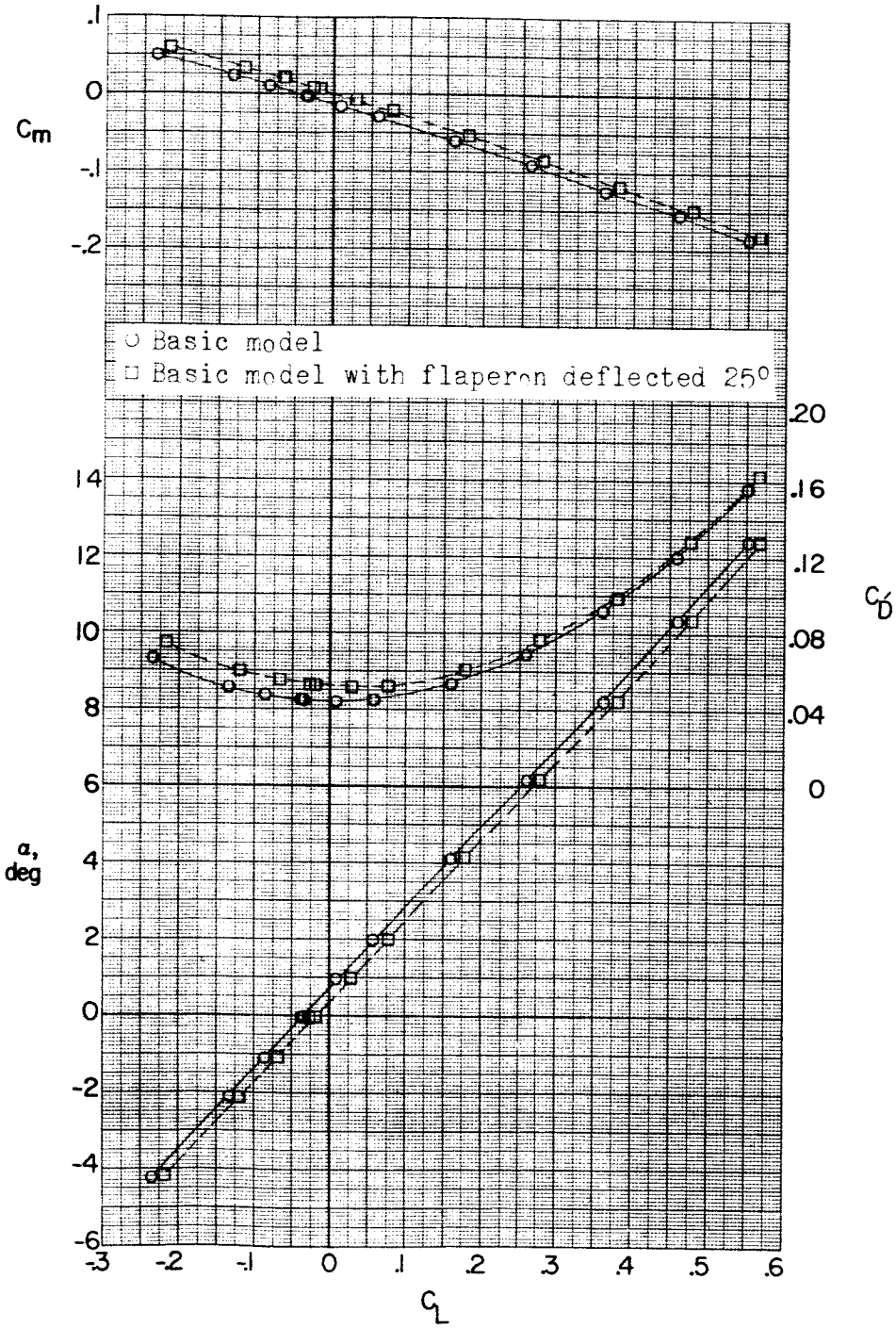

(c) M = 2.06.

Figure 14.- Concluded.

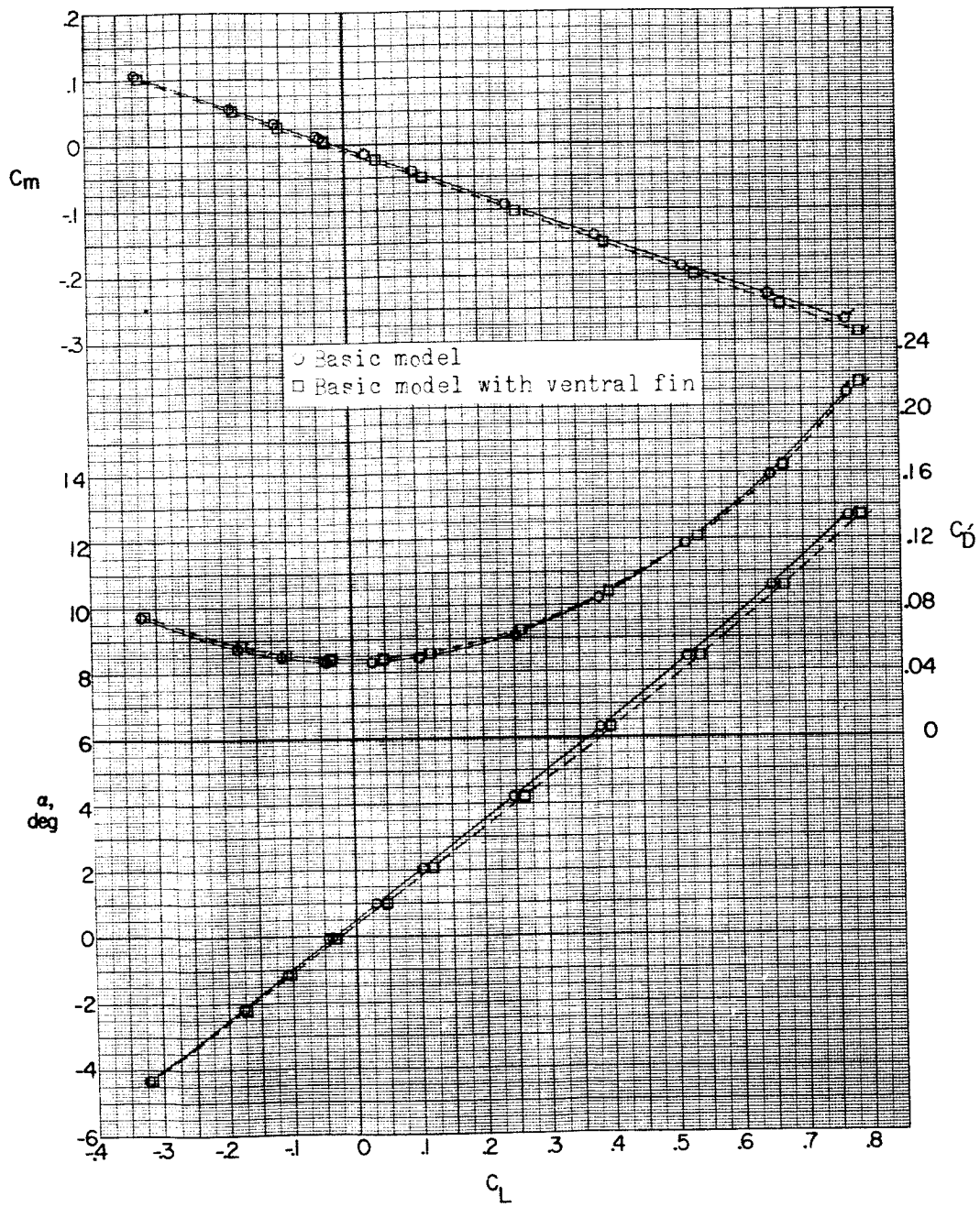

(a) M = 1.56.

Figure 15.- Effect of ventral fins on aerodynamic characteristics in pitch. $\beta = 0^{\circ}$. Flagged symbols denote wall-reflected shock waves striking the tail.

[redacted]

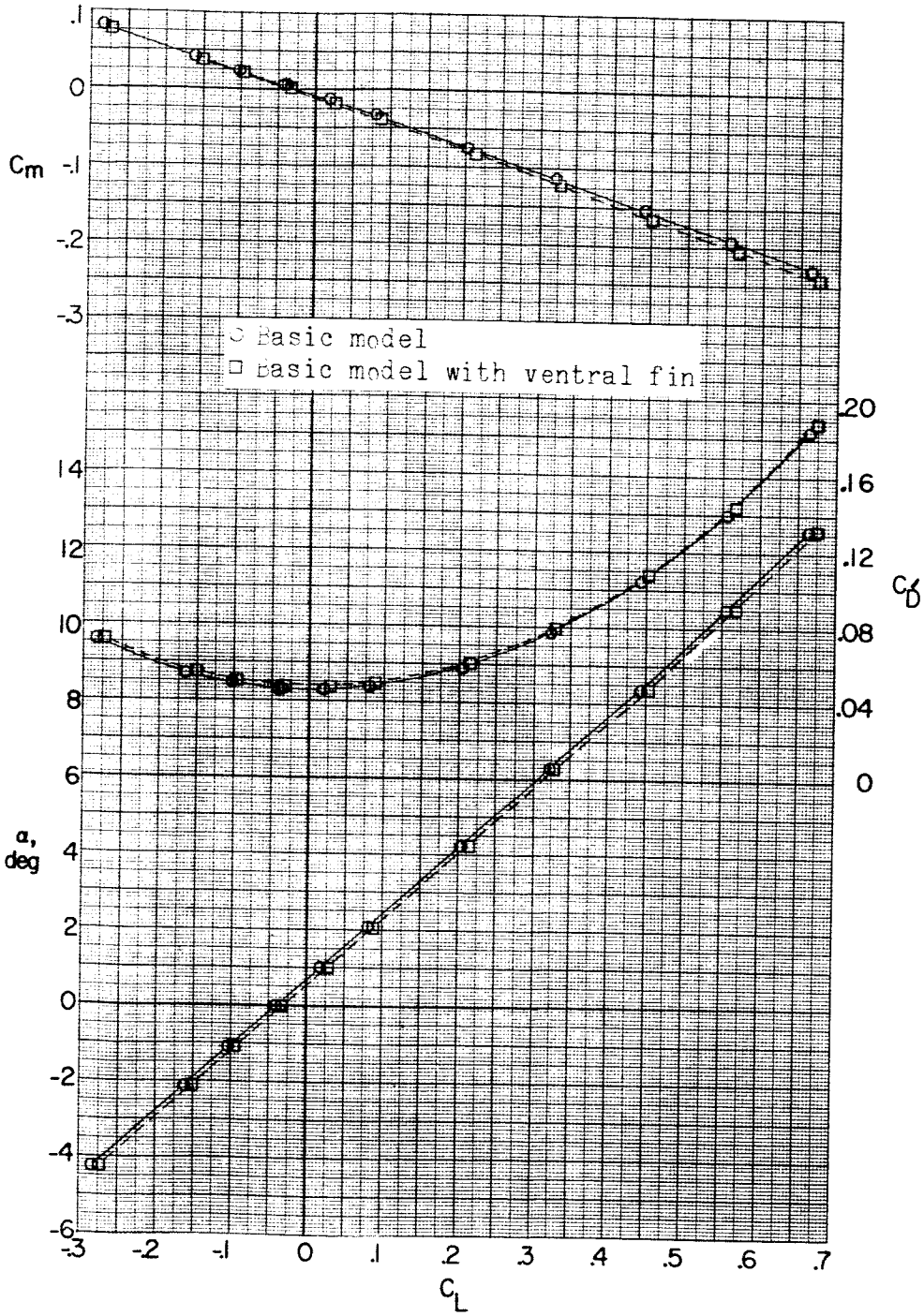

(b) M = 1.76.

Figure 15.- Continued.

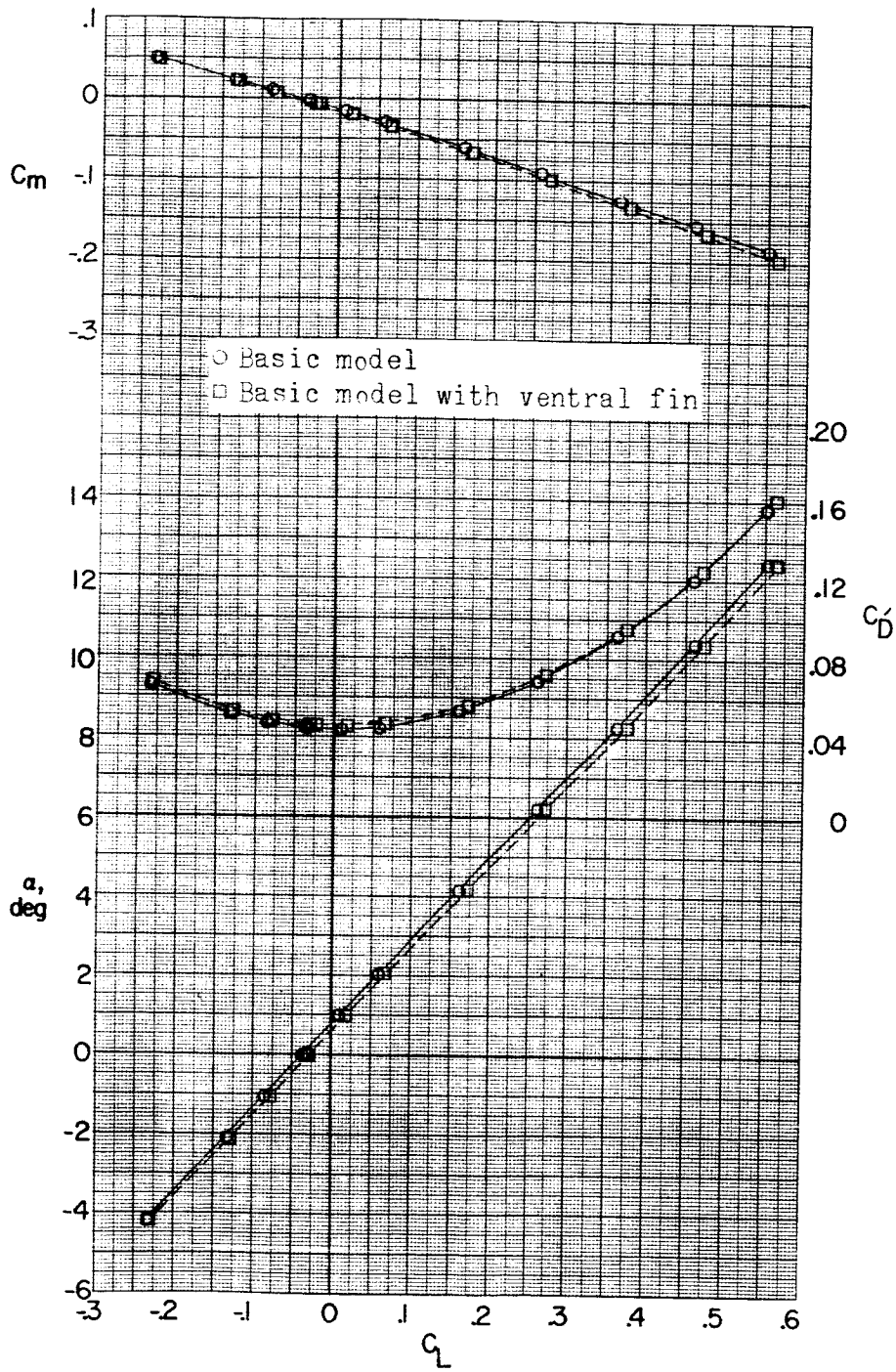

(c) M = 2.06.

Figure 15.- Concluded.

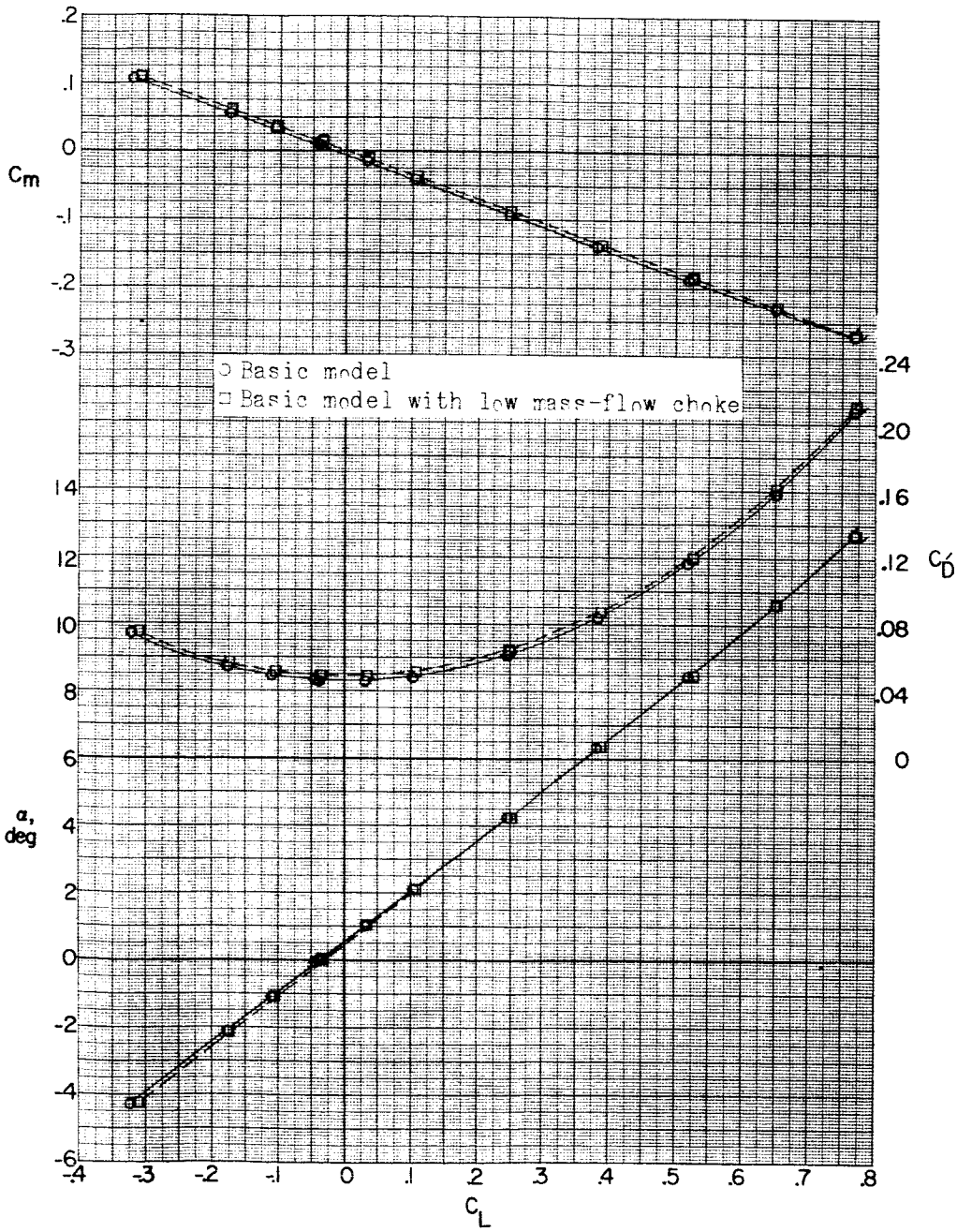

(a) M = 1.56.

Figure 16.- Effect of mass-flow ratio on aerodynamic characteristics in pitch. $\beta = 0^{\circ}$. Flagged symbols denote wall-reflected shock waves striking the tail.

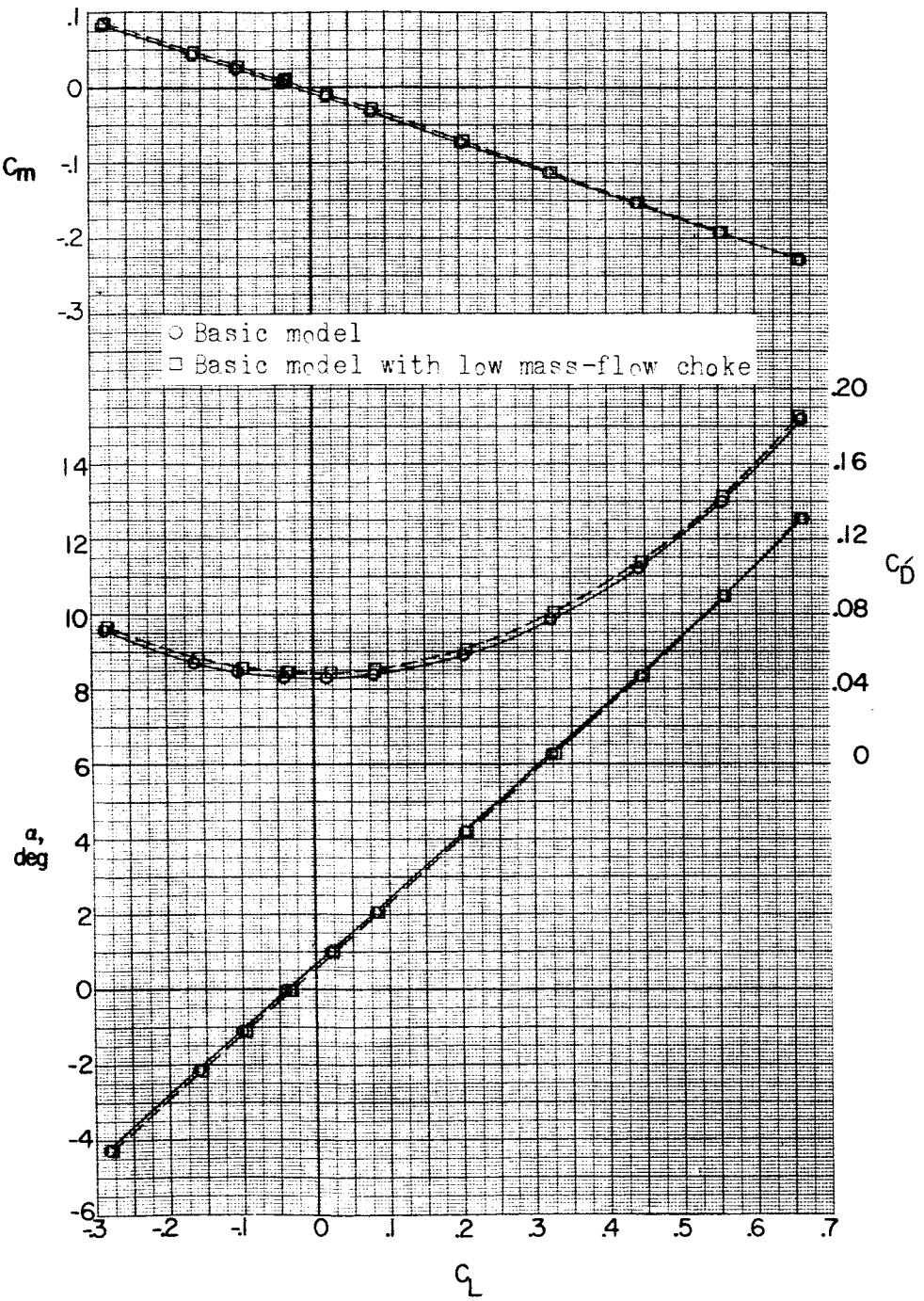

(b) M = 1.76.

Figure 16.- Continued.

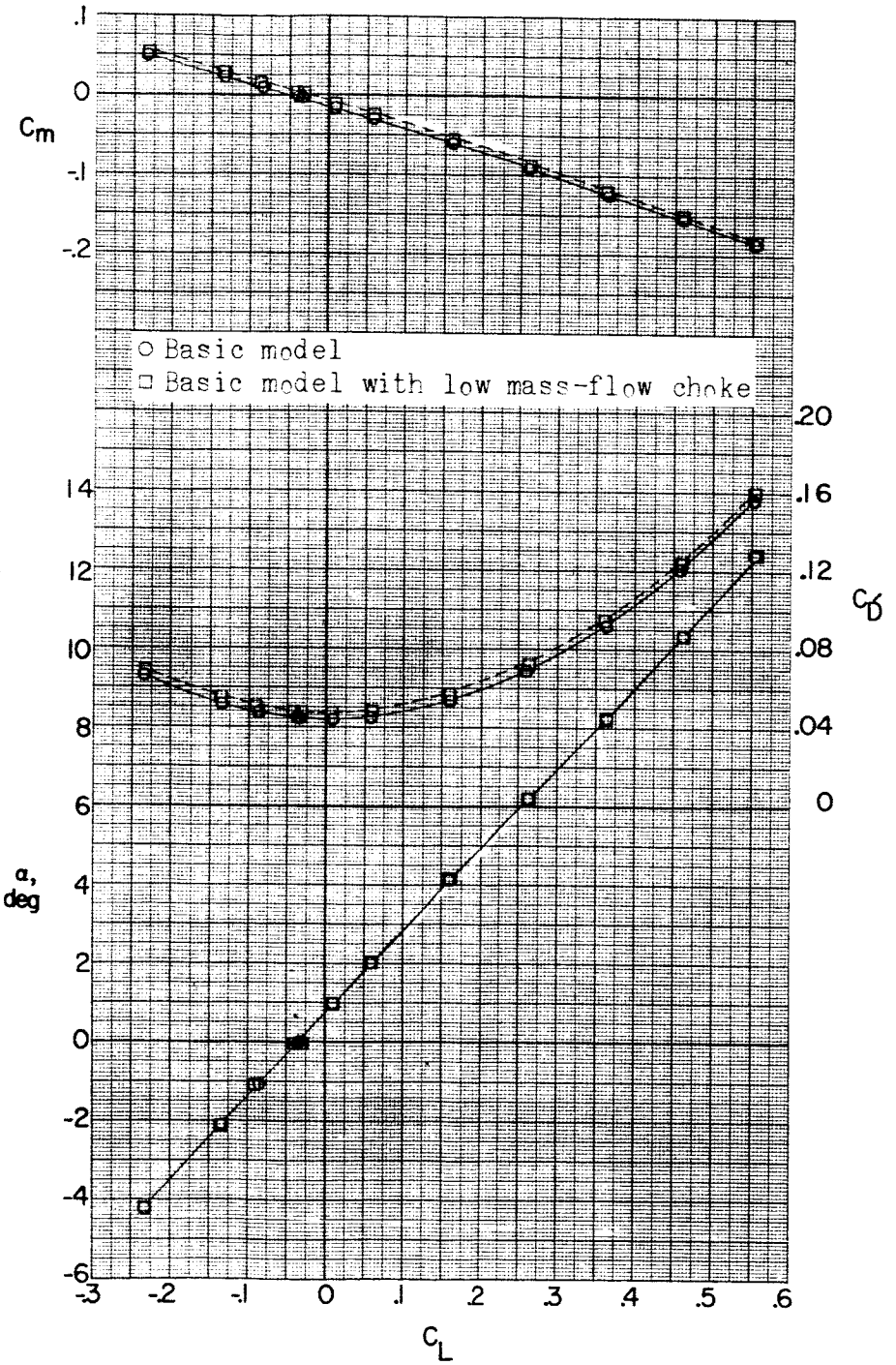

(c) M = 2.06.

Figure 16.- Concluded.

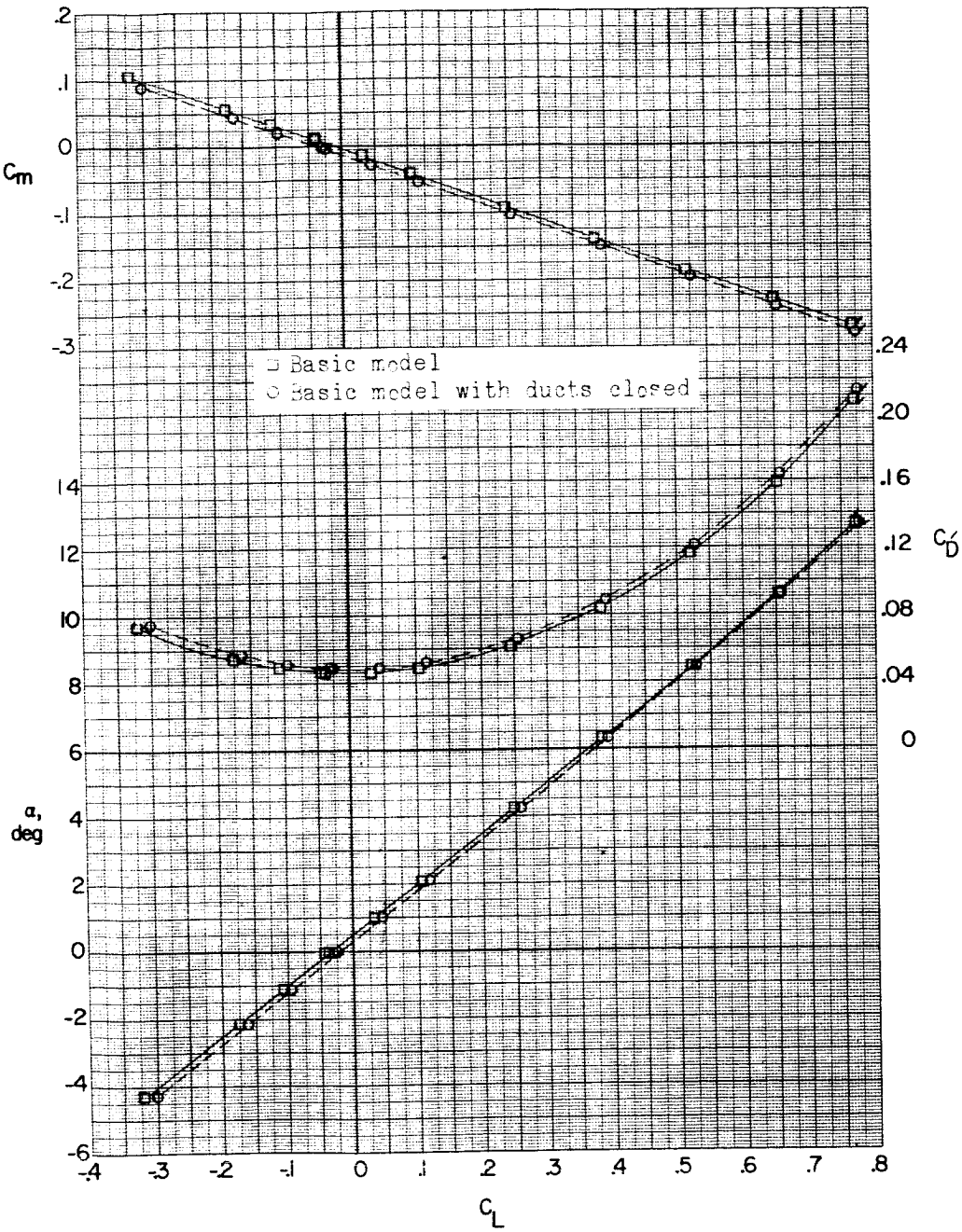

(a) M = 1.56.

Figure 17.- Effect of faired duct inlets on aerodynamic characteristics in pitch. $\beta = 0^{\circ}$. Flagged symbols denote wall-reflected shock waves striking the tail.

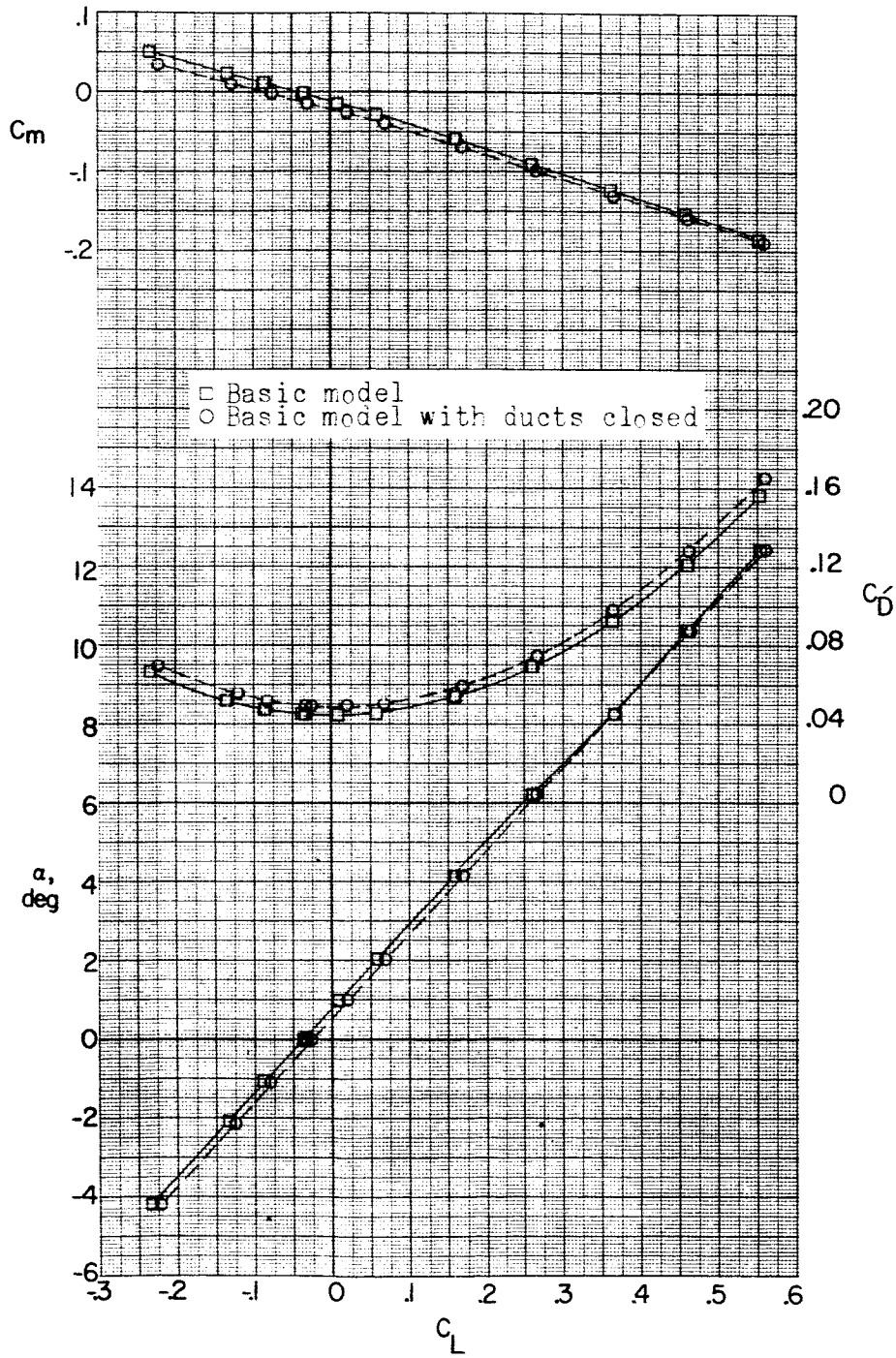

(b) M = 2.06.

Figure 17.- Concluded.

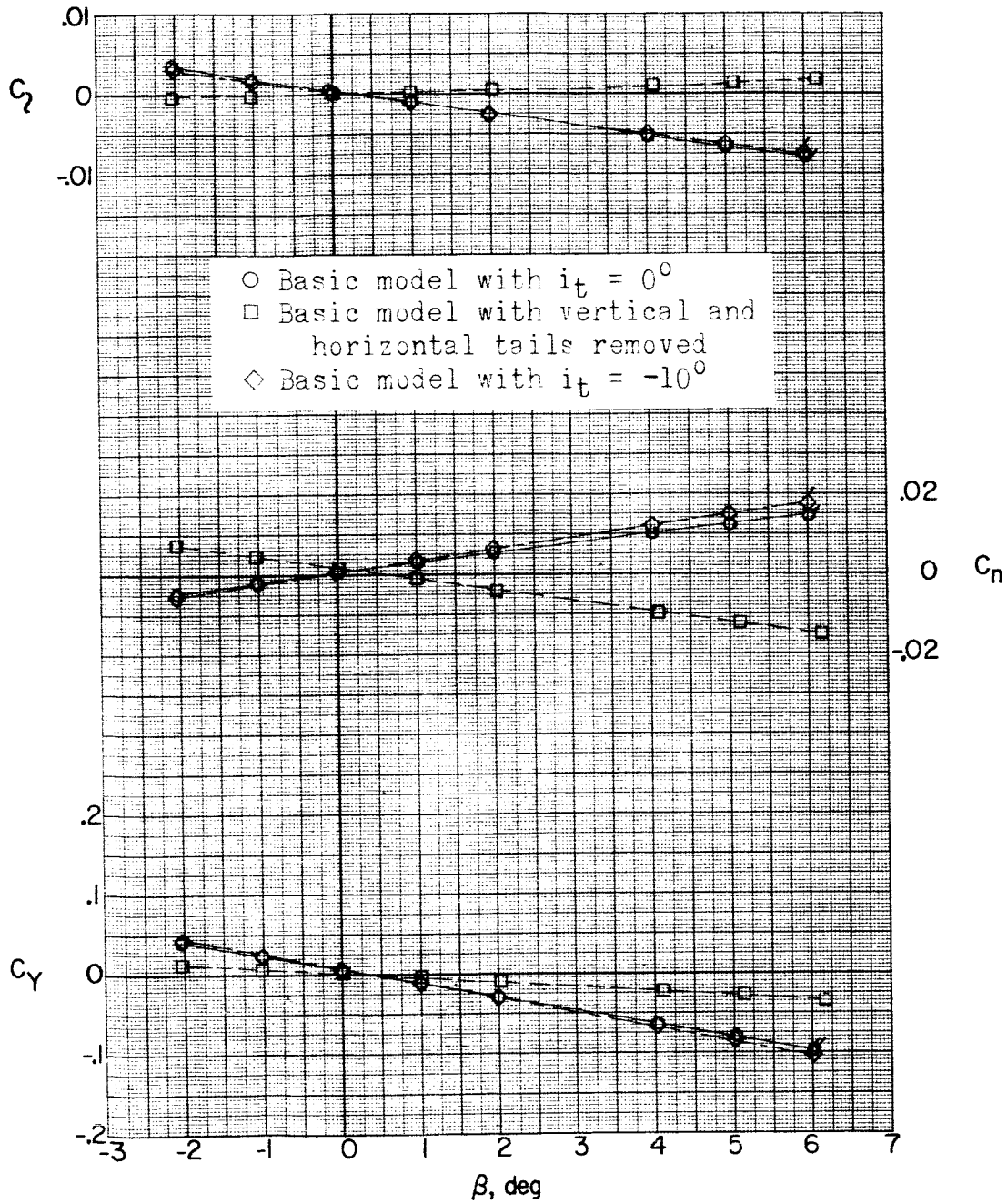

(a) $M = 1.56$; $\alpha = 0^o$.

Figure 18.- Effect of horizontal and vertical tails on aerodynamic characteristics in sideslip. Flagged symbols denote wall-reflected shock waves striking the tail.

[redacted]

DECLASSIFIED
CONFIDENTIAL

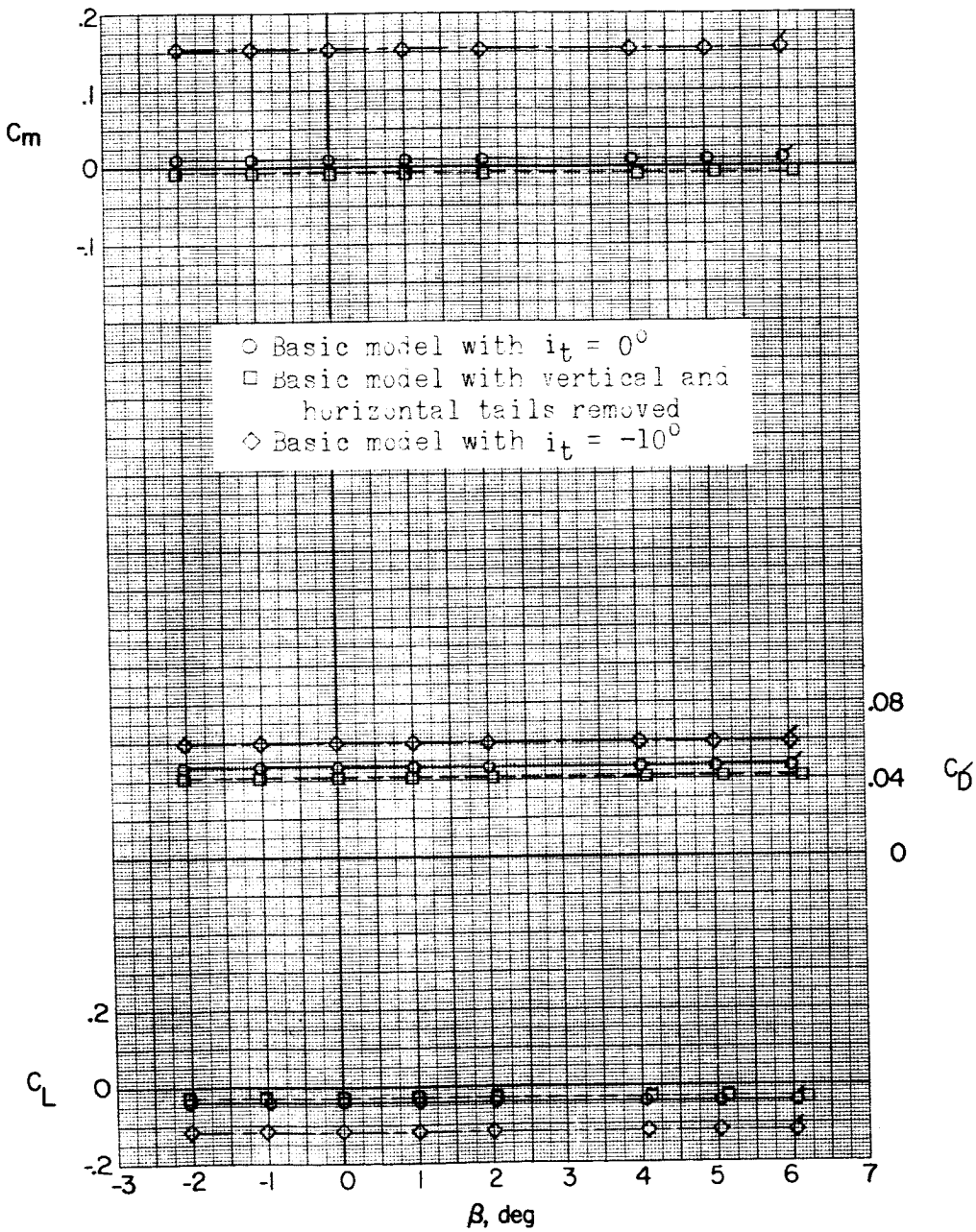

(a) Continued. $\alpha = 0^o$.

Figure 18.- Continued.

[redacted]

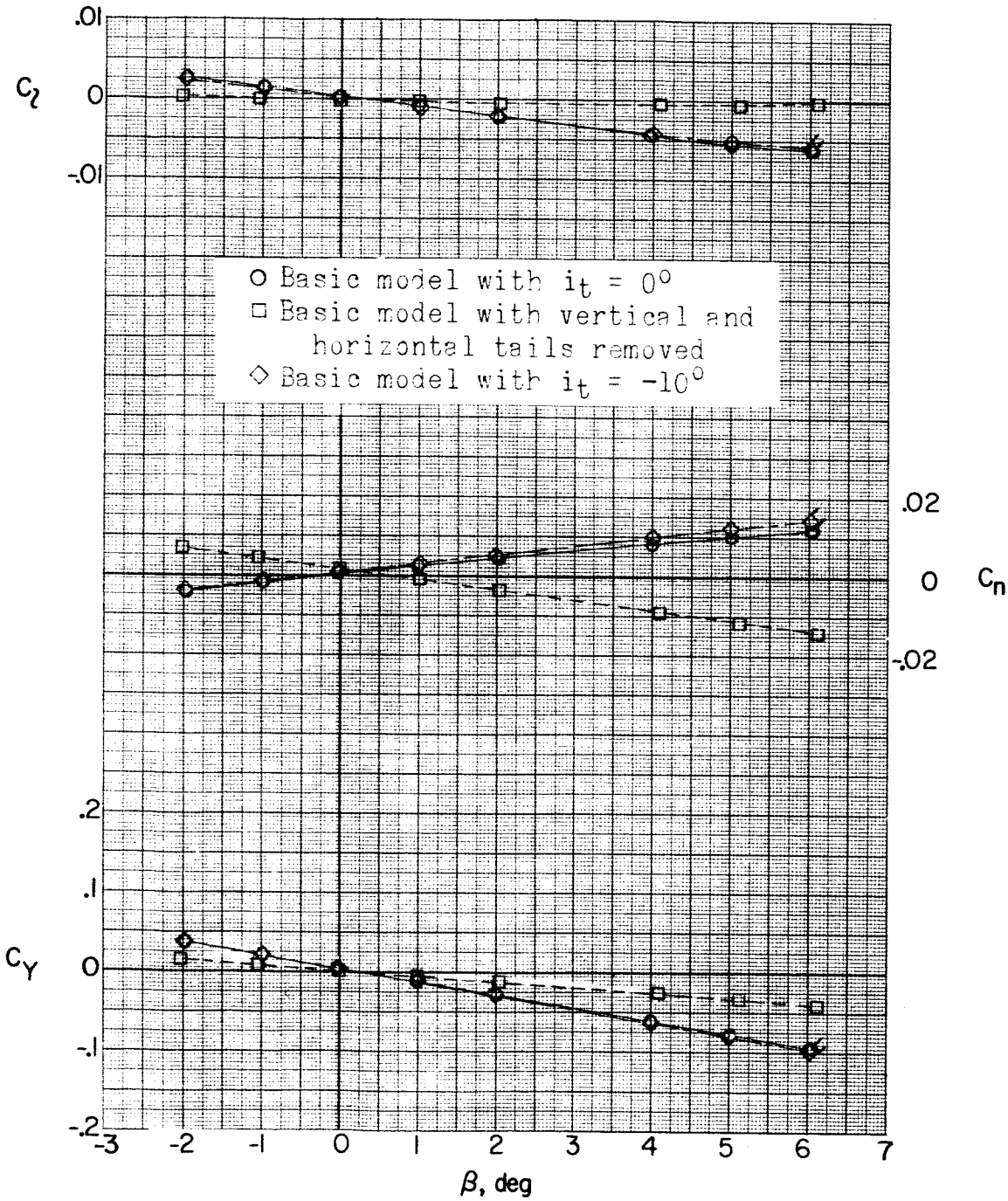

(a) Continued. $\alpha = 5.3^\circ$.

Figure 18.- Continued.

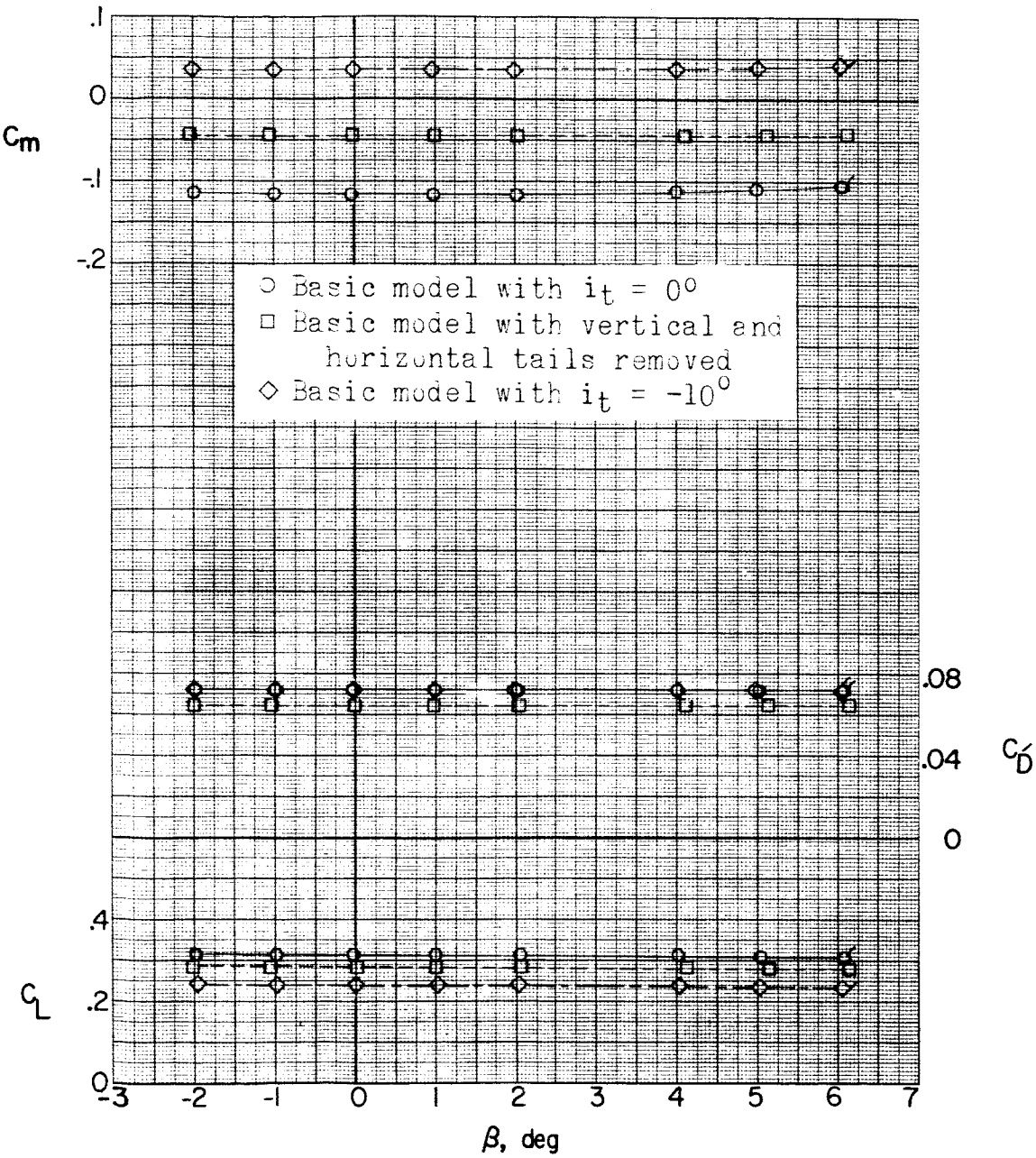

(a) Continued. $\alpha = 5.3^o$.

Figure 18.- Continued.

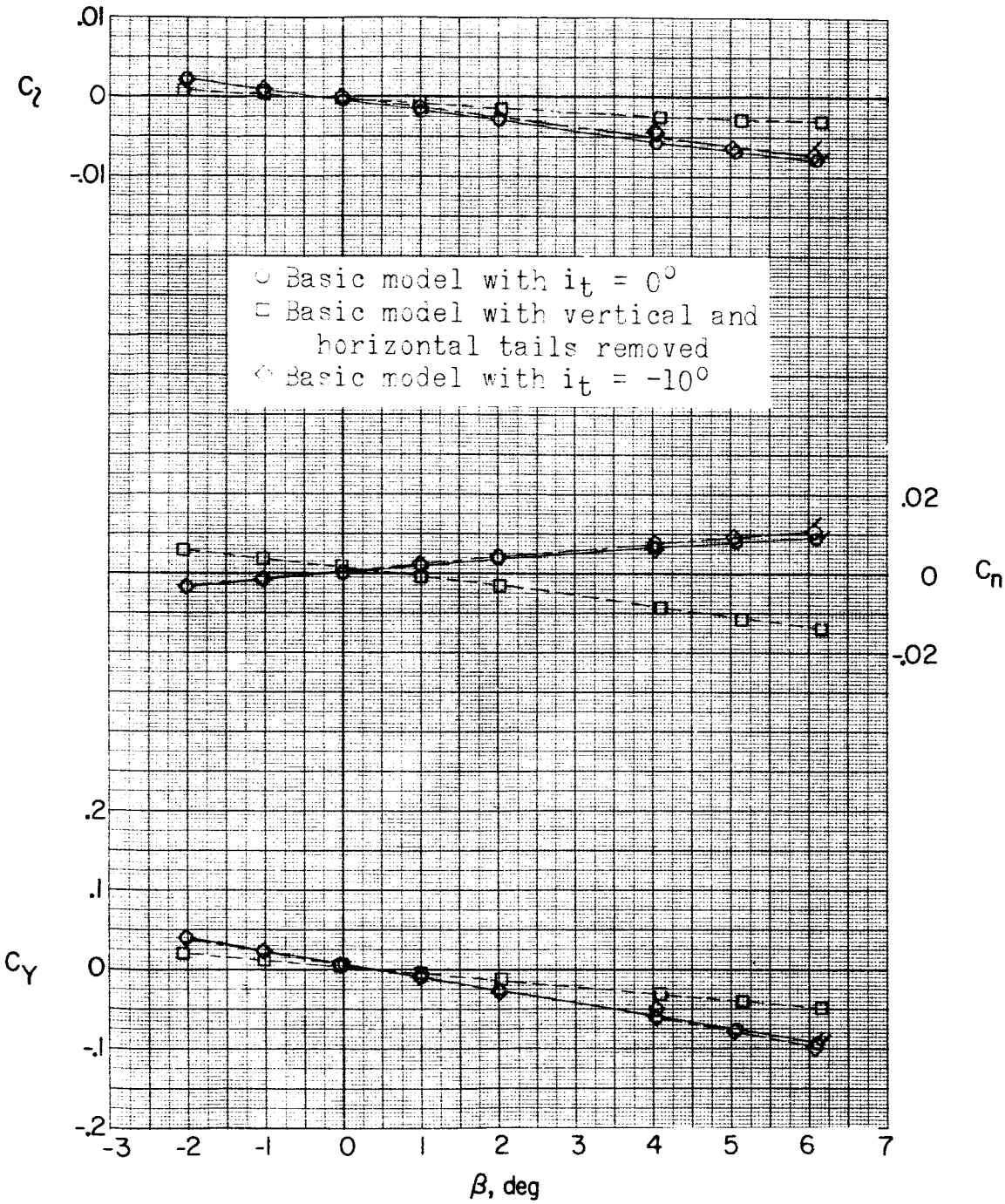

(a) Continued. $\alpha = 10.6^\circ$.

Figure 18.- Continued.

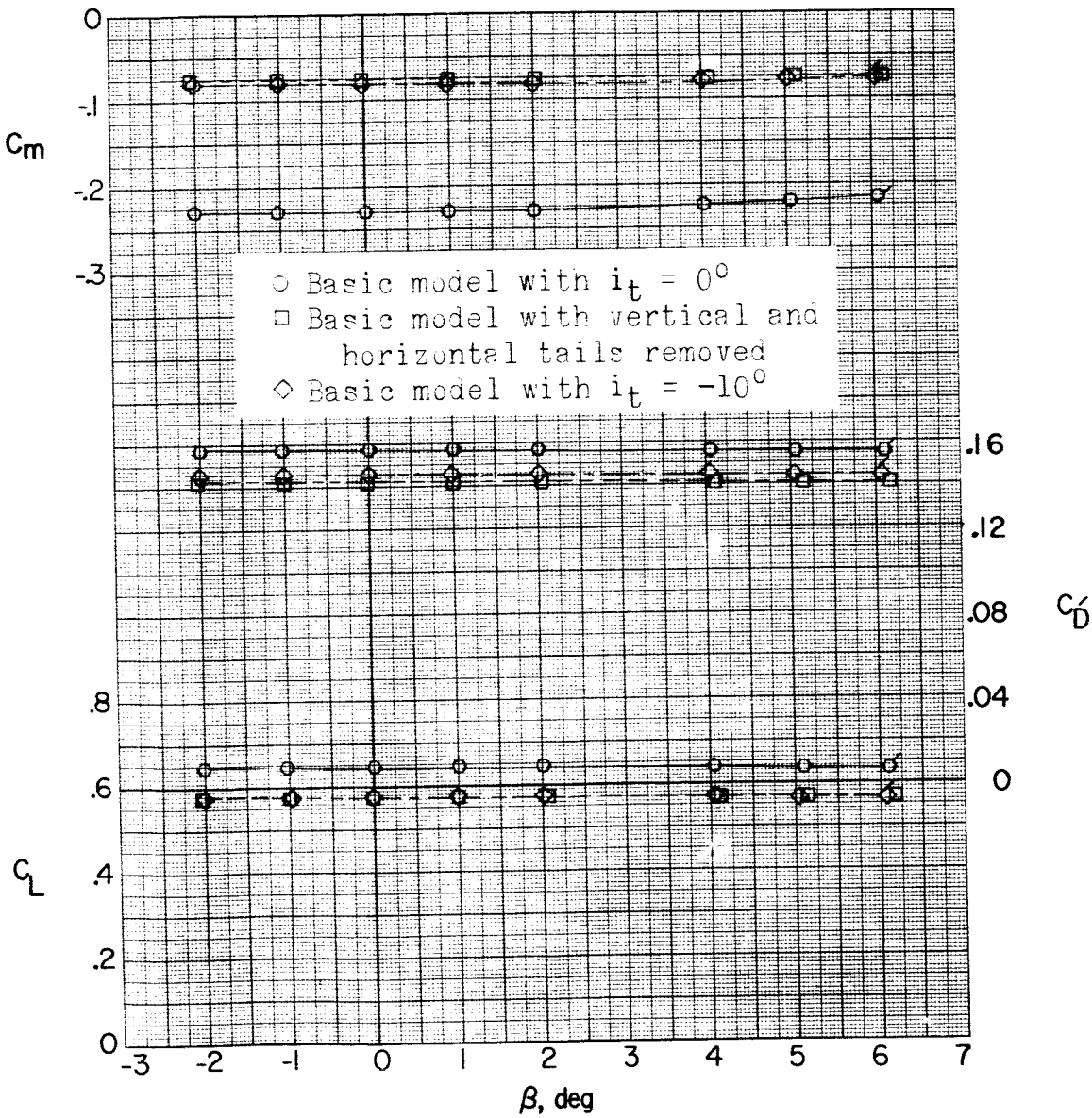

(a) Concluded. $\alpha = 10.6^o$.

Figure 18.- Continued.

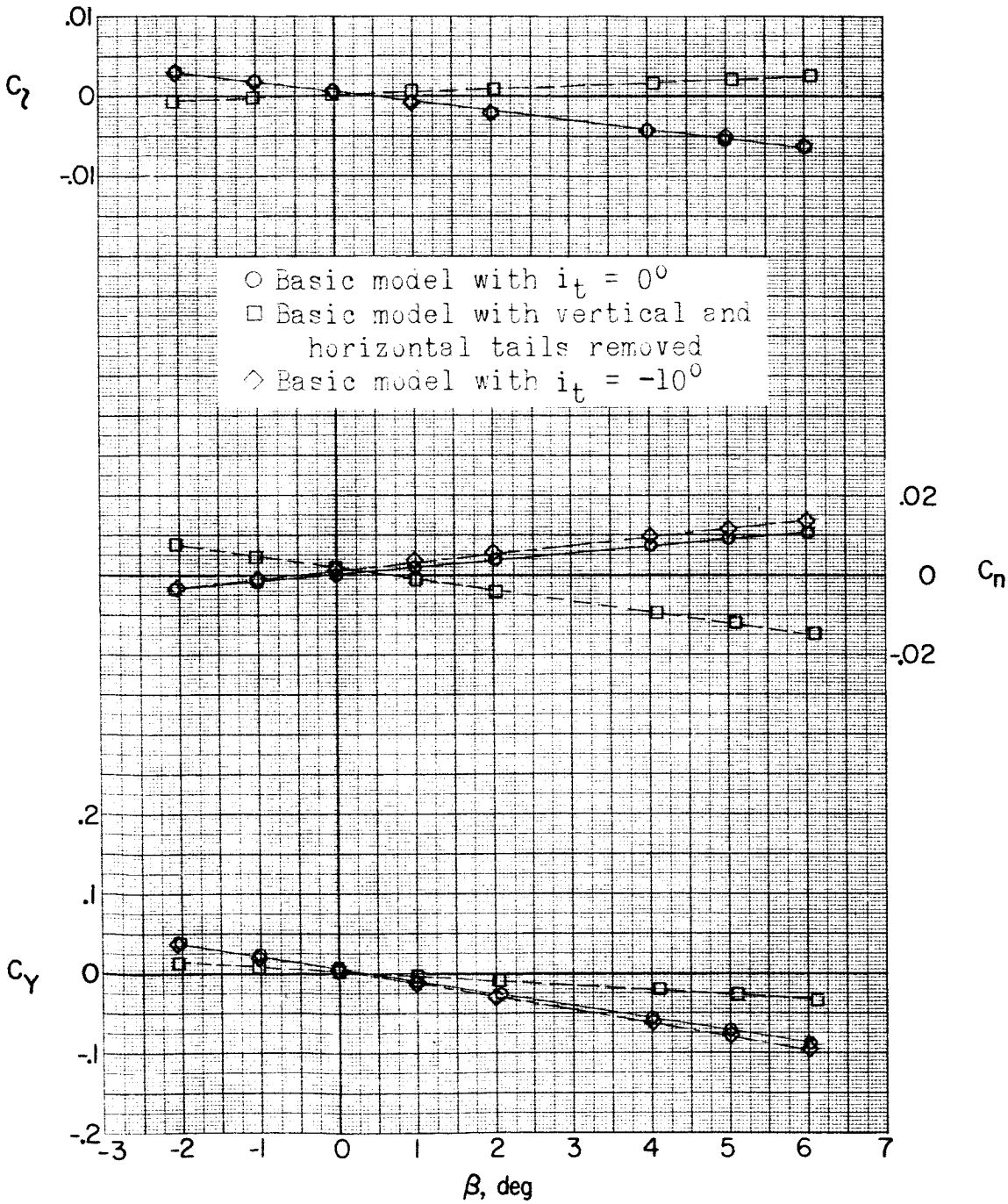

(b) M = 1.76; α = 0°.

Figure 18.- Continued.

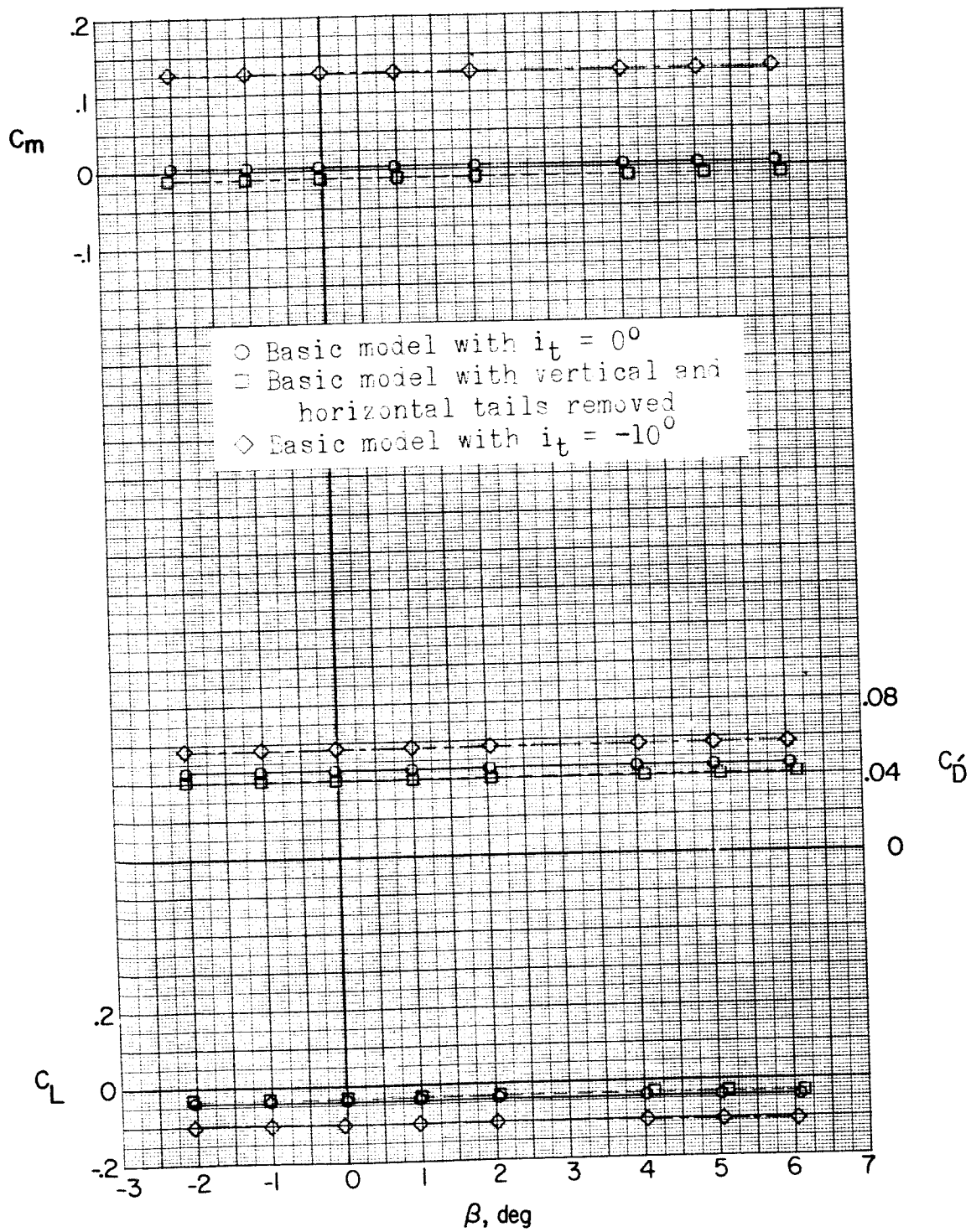

(b) Continued. $\alpha = 0^o$.

Figure 18.- Continued.

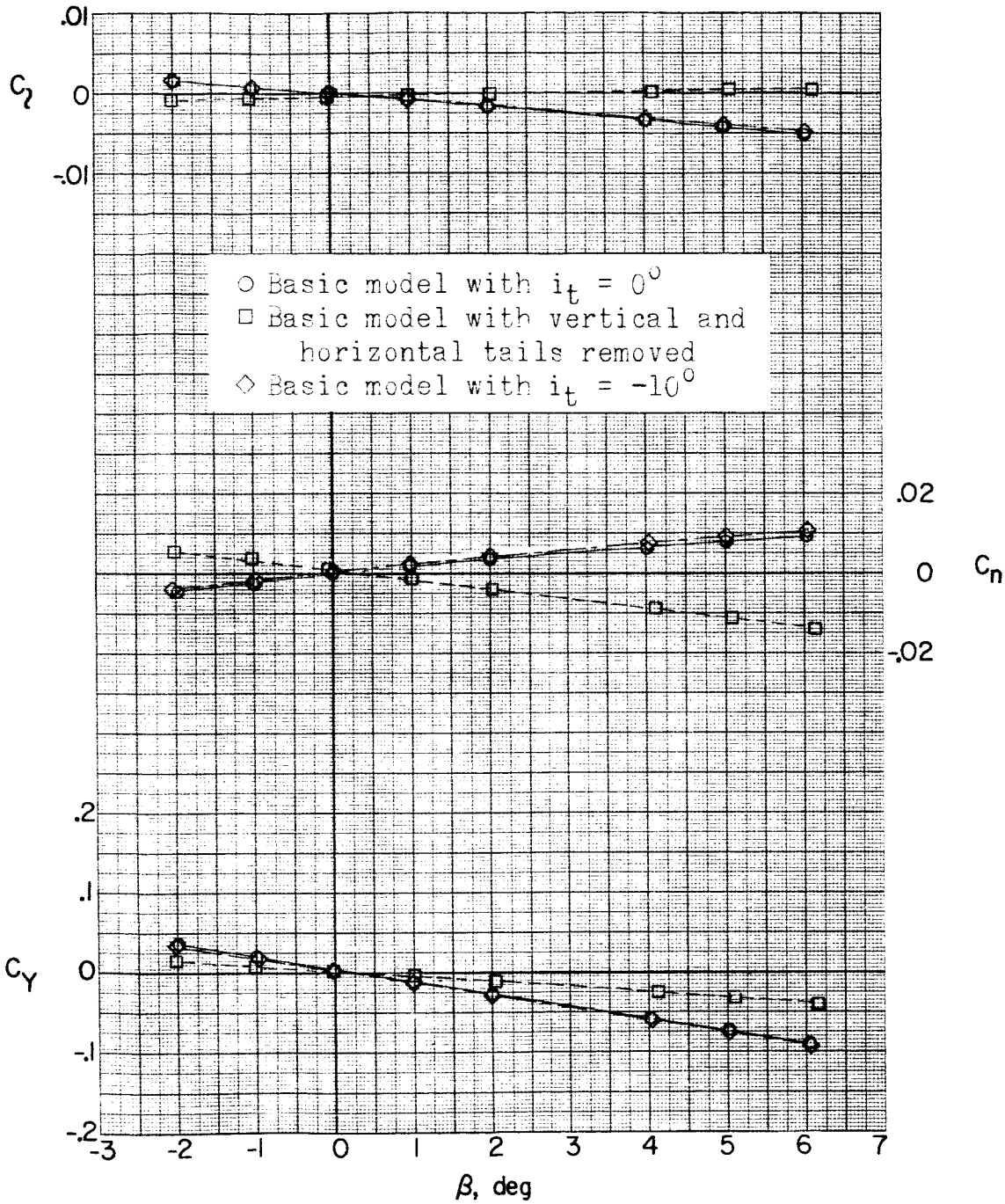

(b) Continued. $\alpha = 5.2^o$.

Figure 18.- Continued.

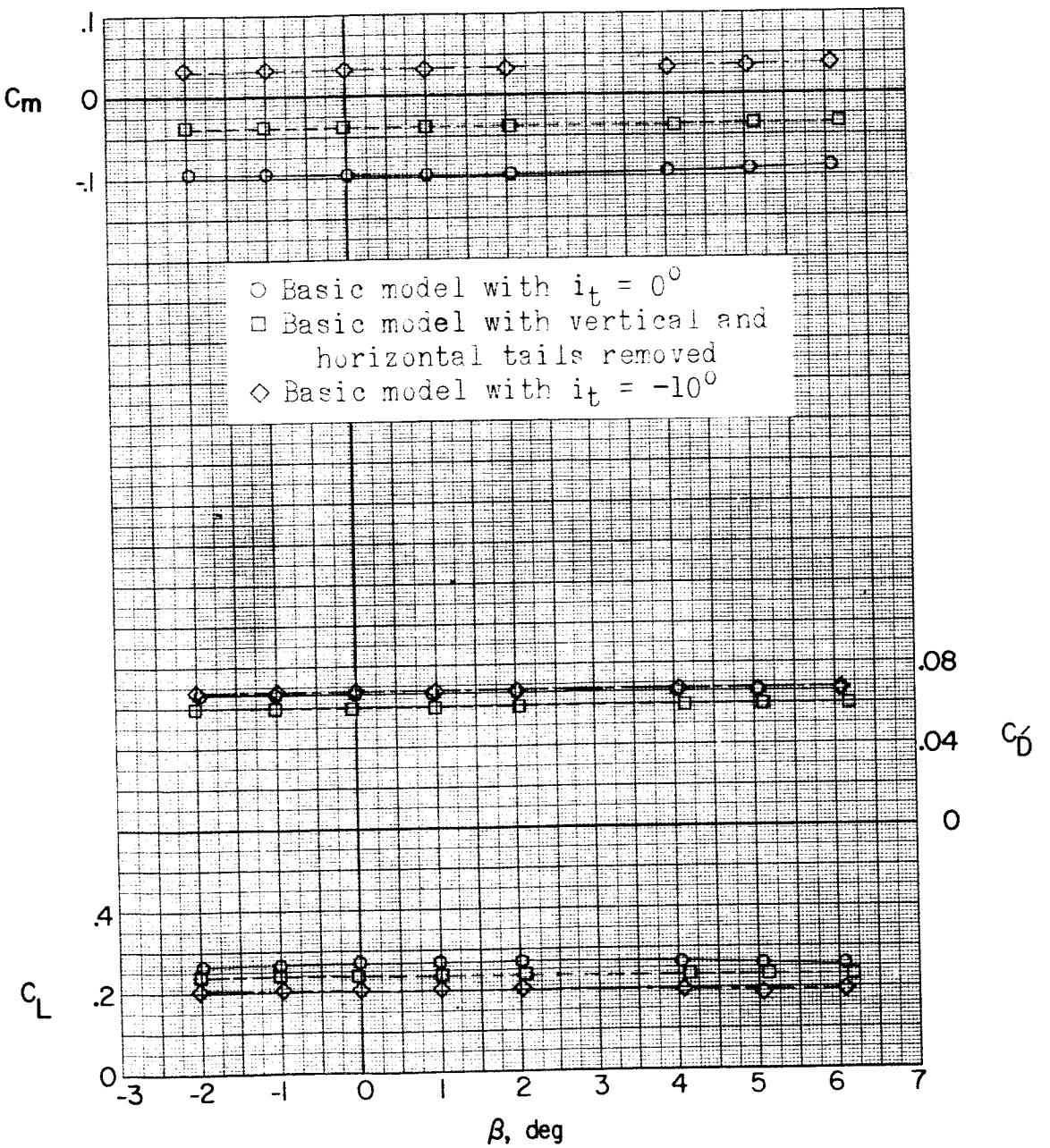

(b) Continued. $\alpha = 5.2^o$.

Figure 18.- Continued.

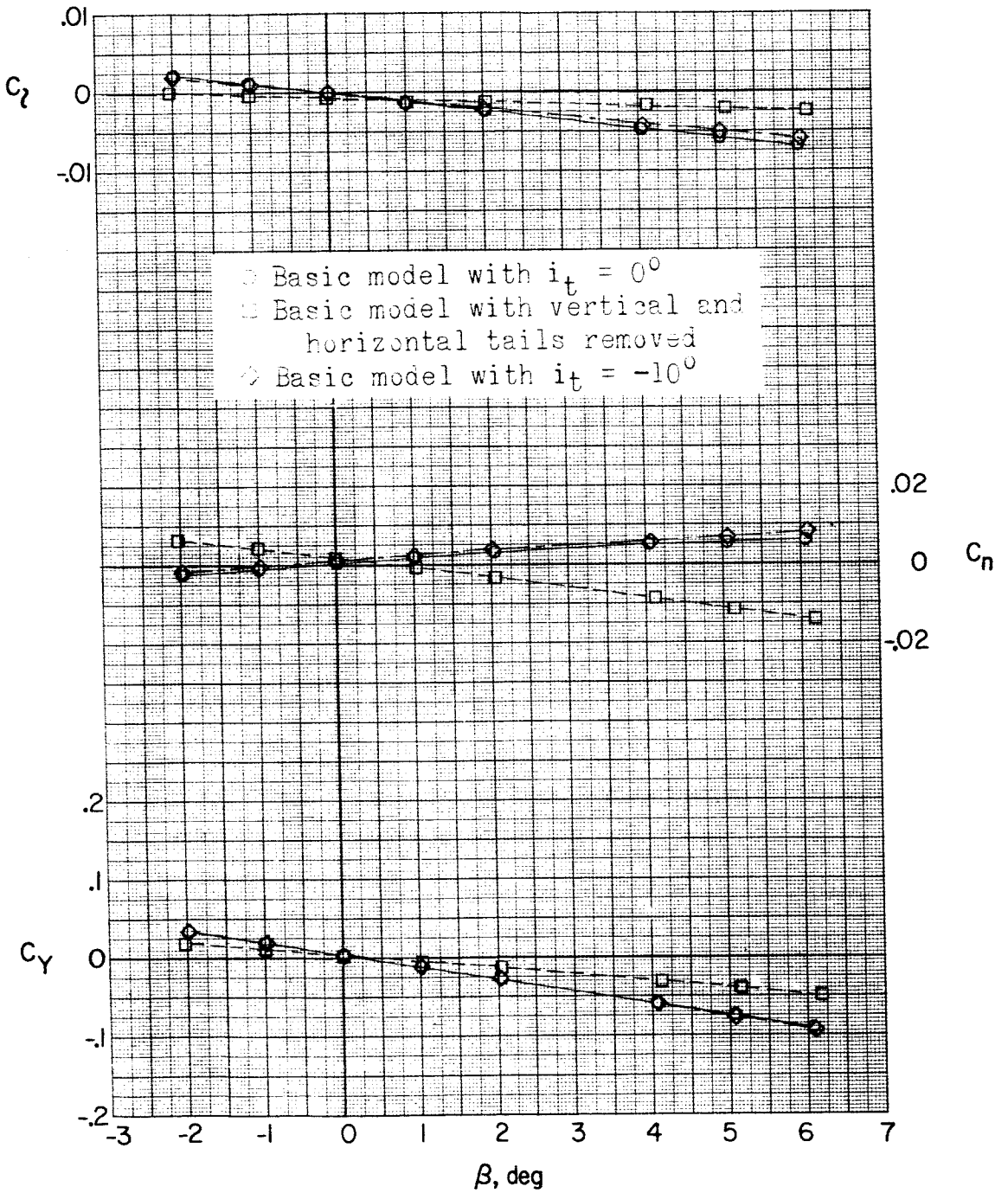

(b) Continued. $\alpha = 10.5^o$.

Figure 18.- Continued.

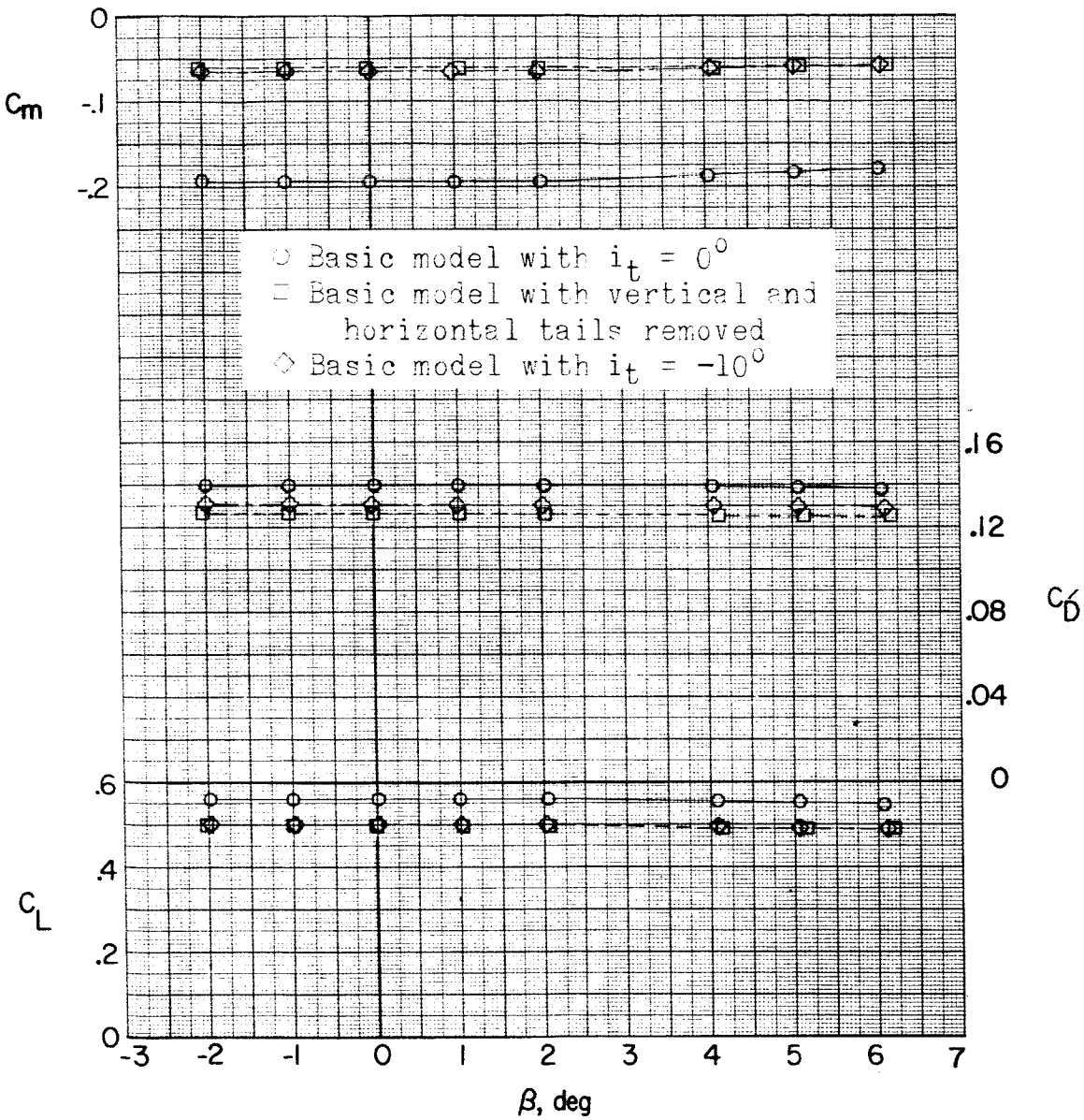

(b) Concluded. $\alpha = 10.5^\circ$.

Figure 18.- Continued.

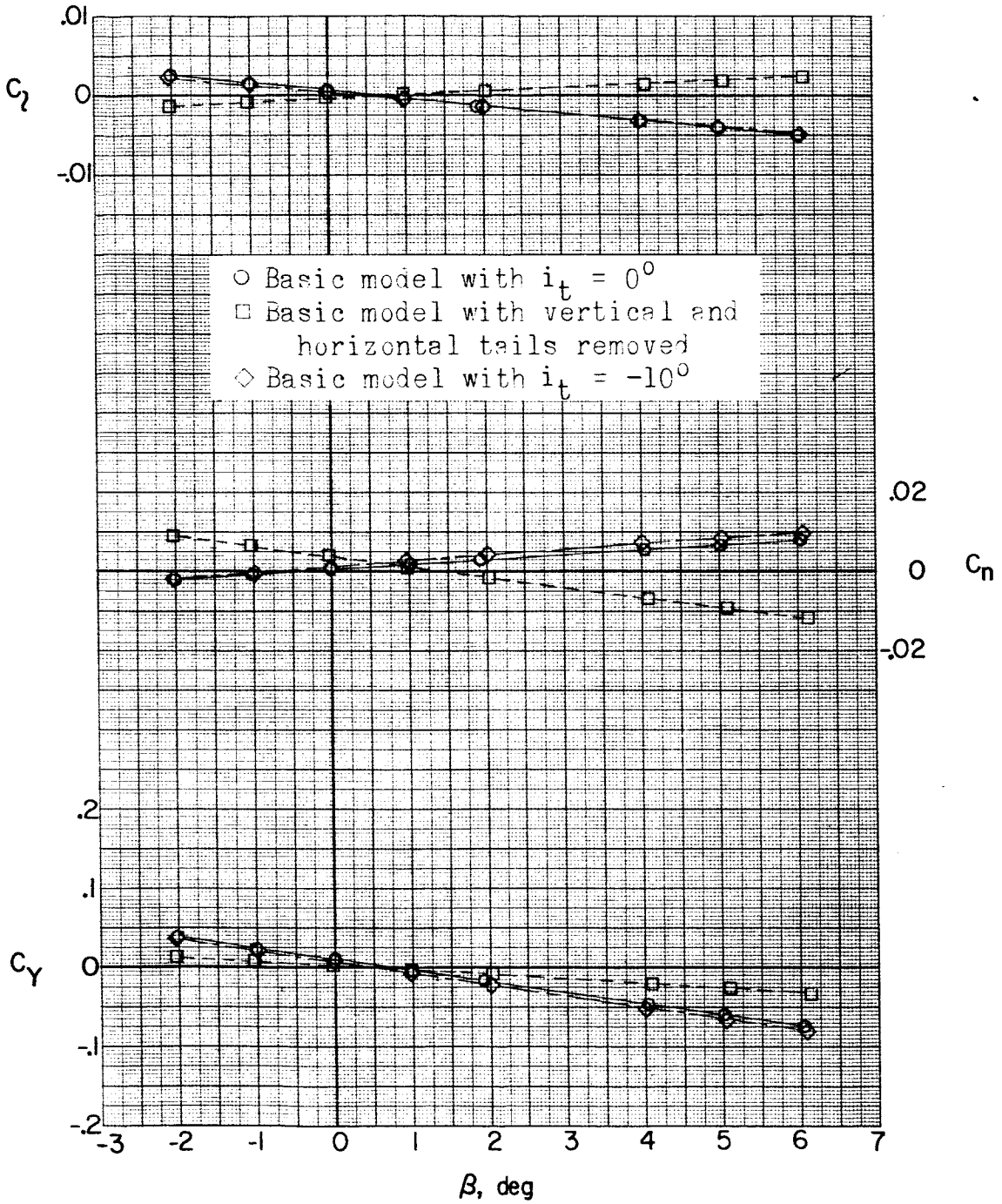

(c) M = 2.06; $\alpha = 0^o$.

Figure 18.- Continued.

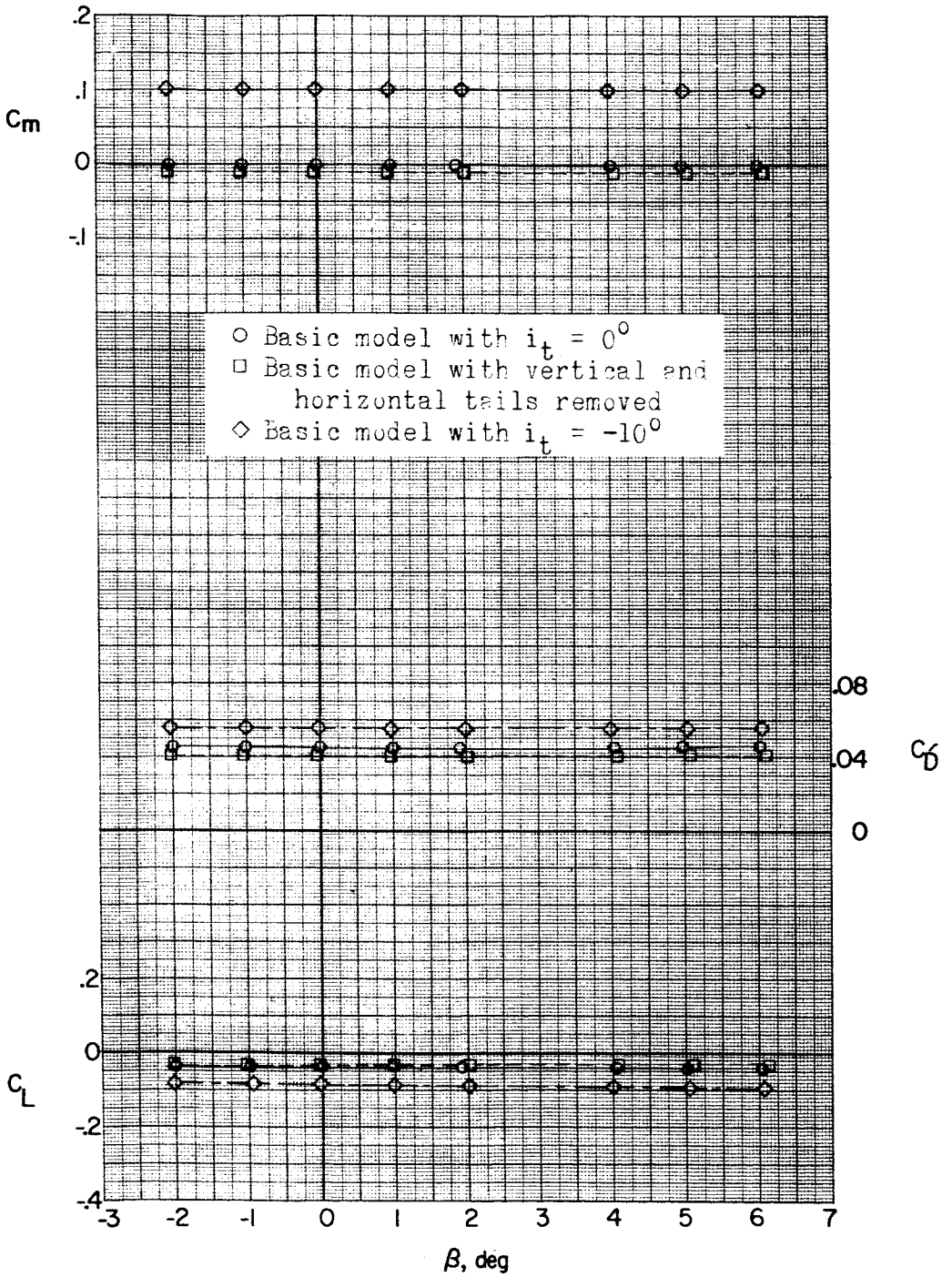

(c) Continued. $\alpha = 0^o$.

Figure 18.- Continued.

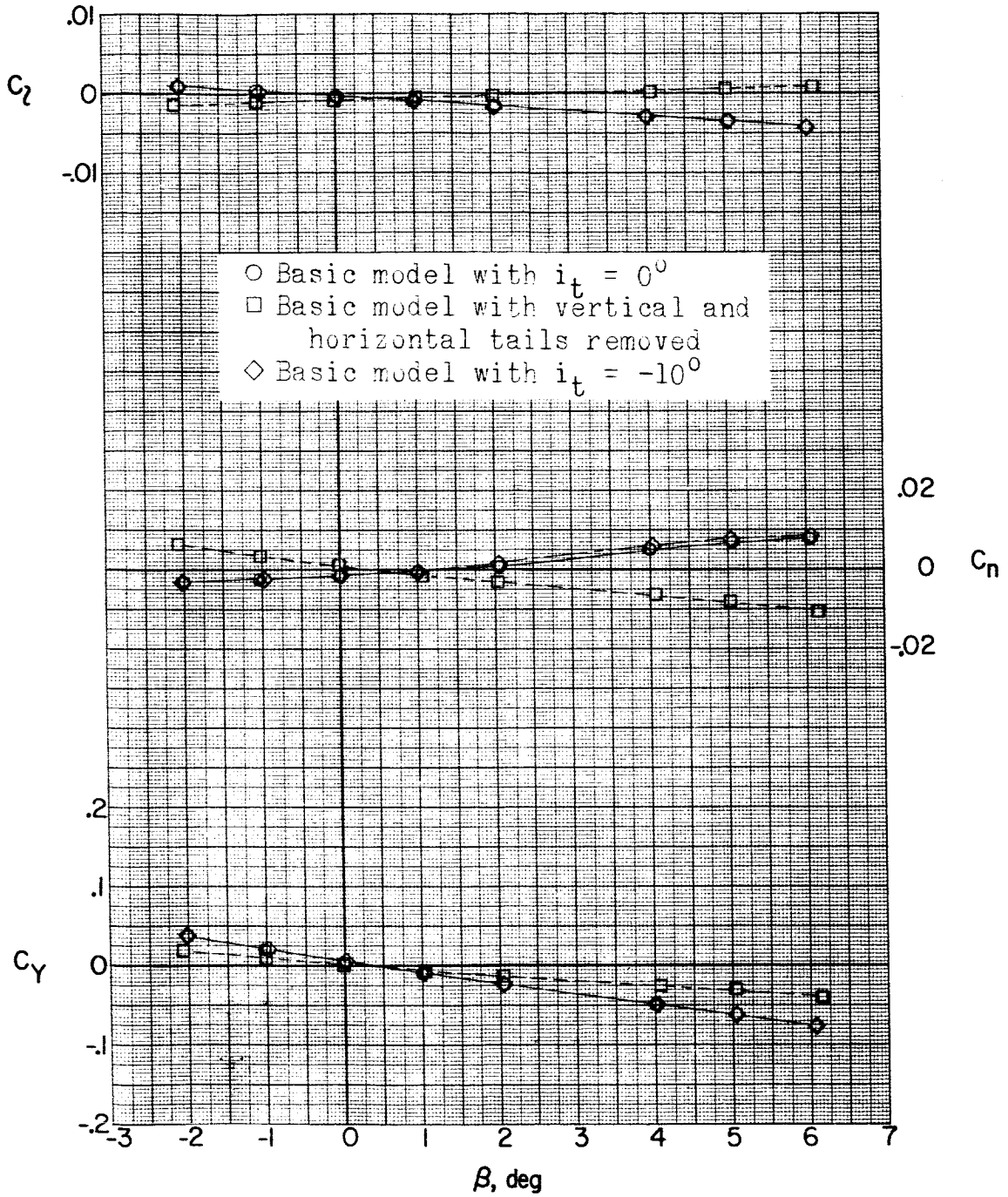

(c) Continued. $\alpha = 5.2^\circ$.

Figure 18.- Continued.

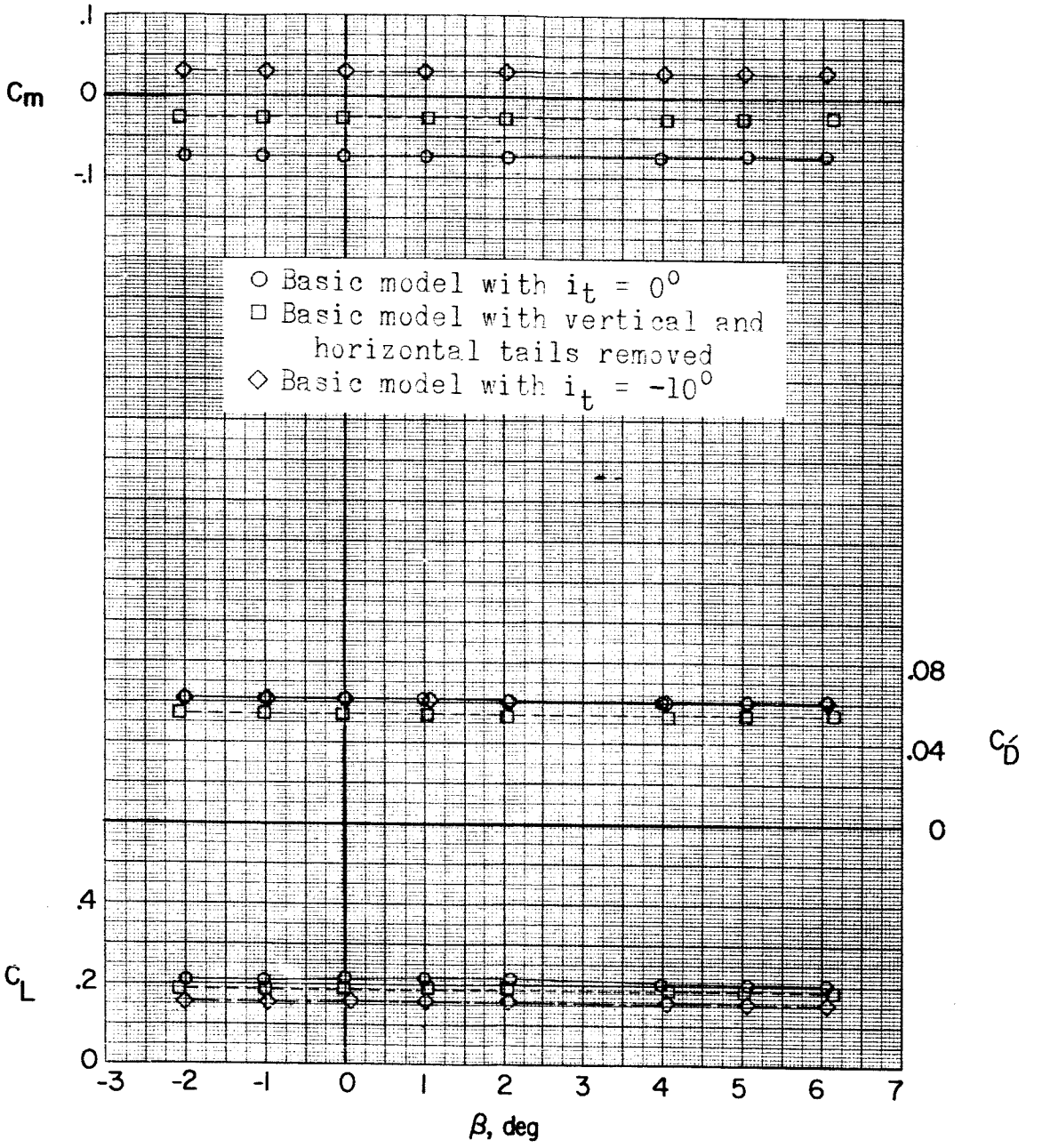

(c) Continued. $\alpha = 5.2^o$.

Figure 18.- Continued.

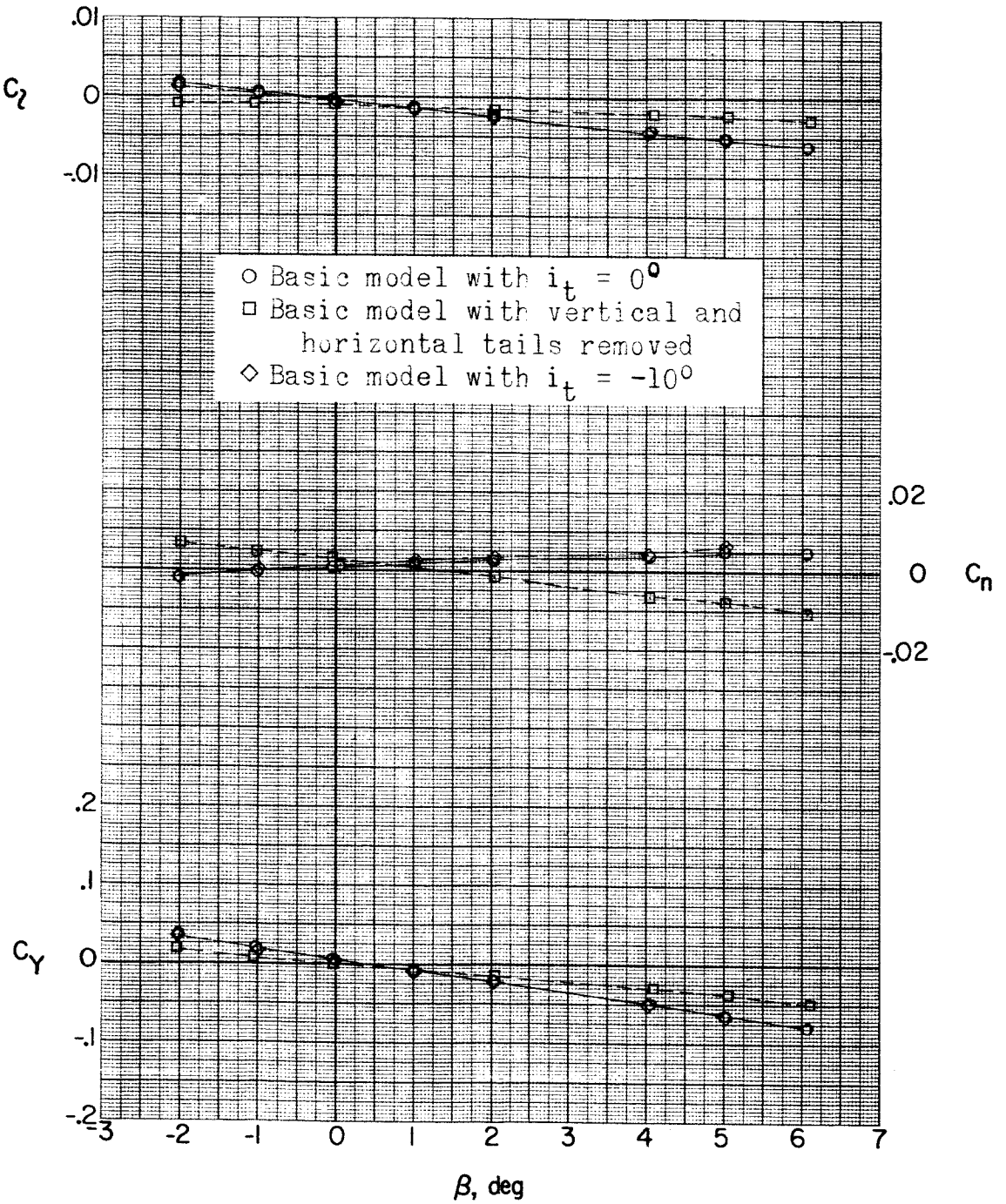

(c) Continued. $\alpha = 10.4^o$.

Figure 18.- Continued.

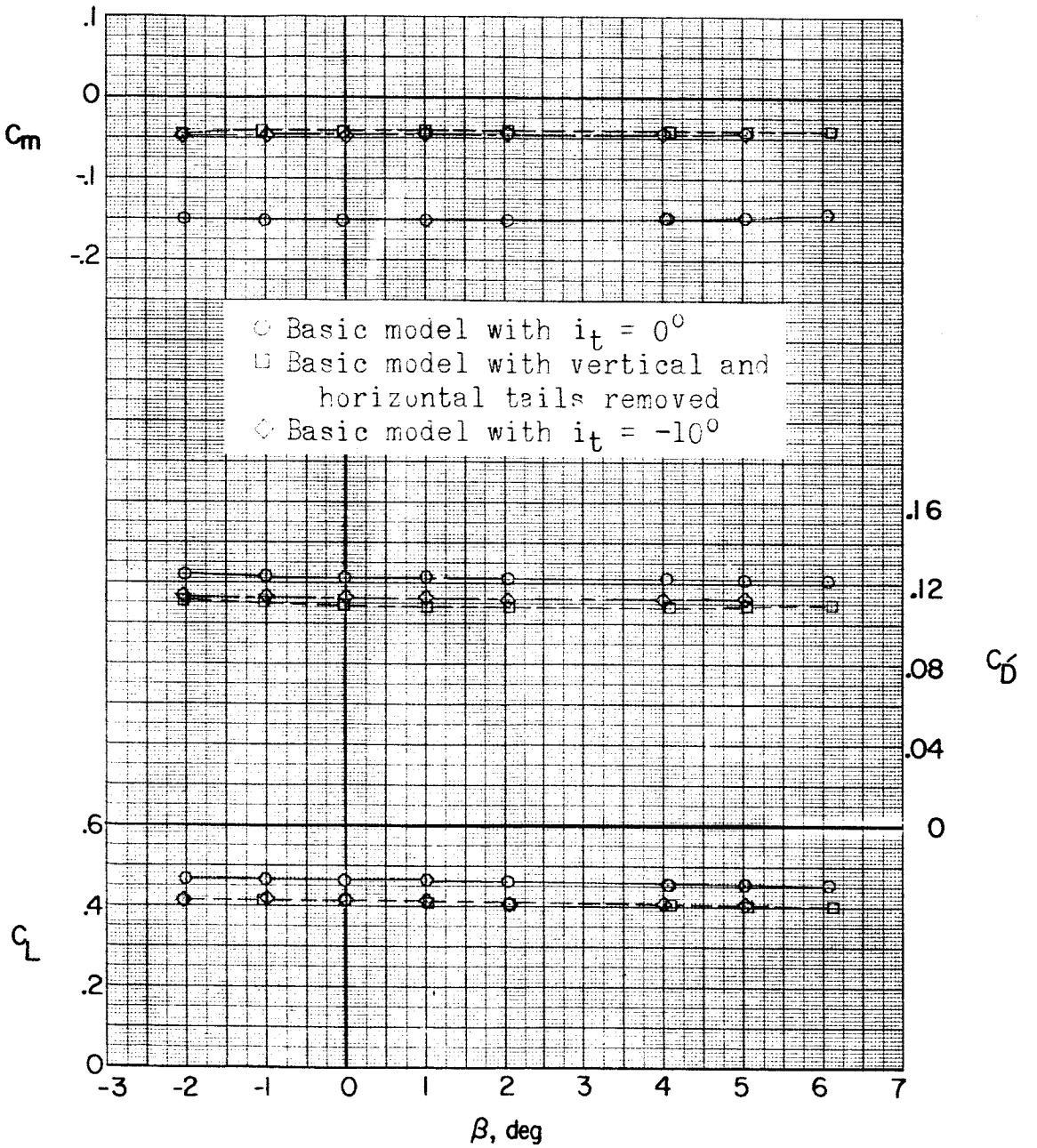

(c) Concluded. $\alpha = 10.4^o$.

Figure 18.- Continued.

[redacted]

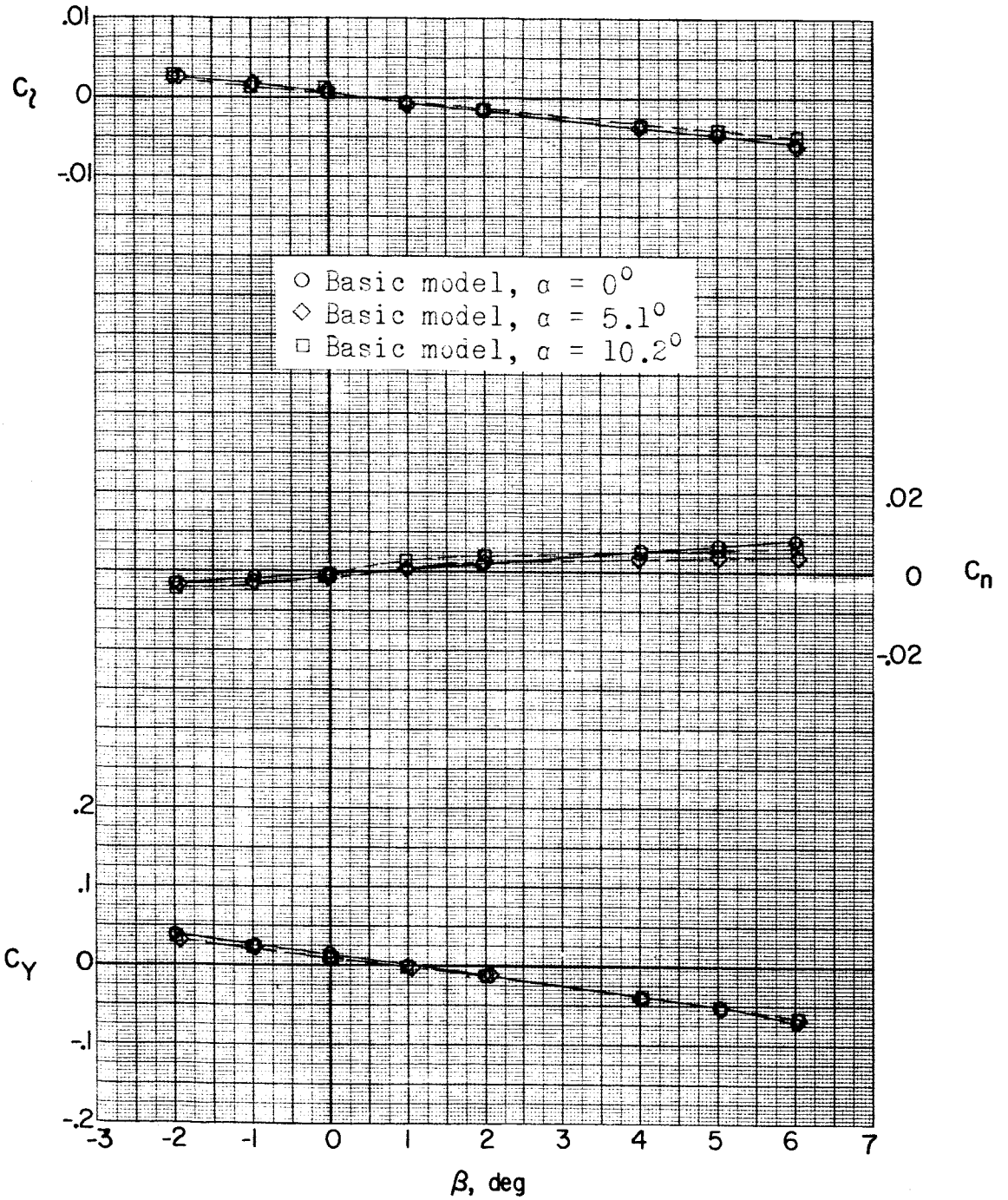

(d) M = 2.53.

Figure 18.- Continued.

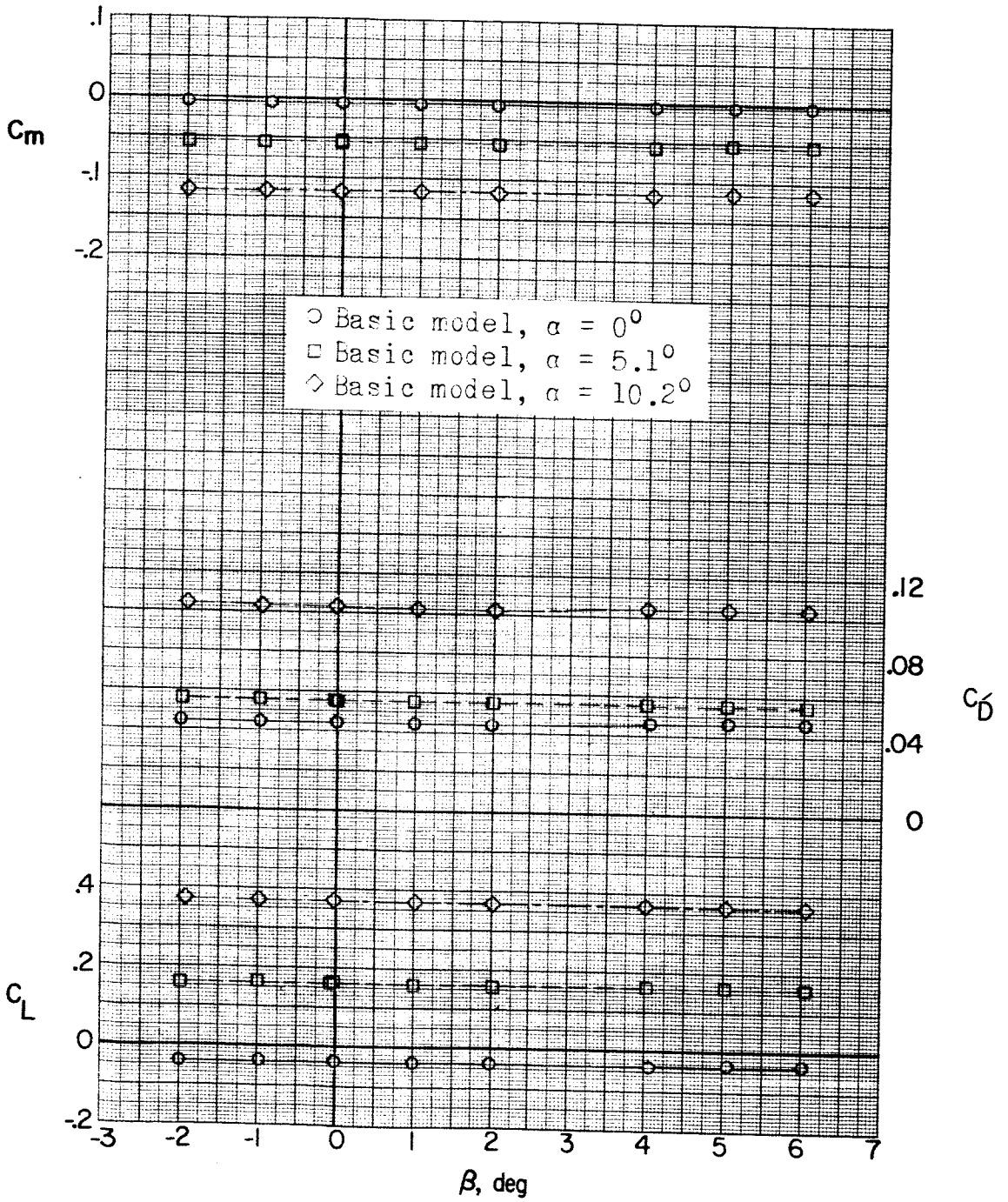

(d) Concluded.

Figure 18.- Concluded.

DECLASSIFIED

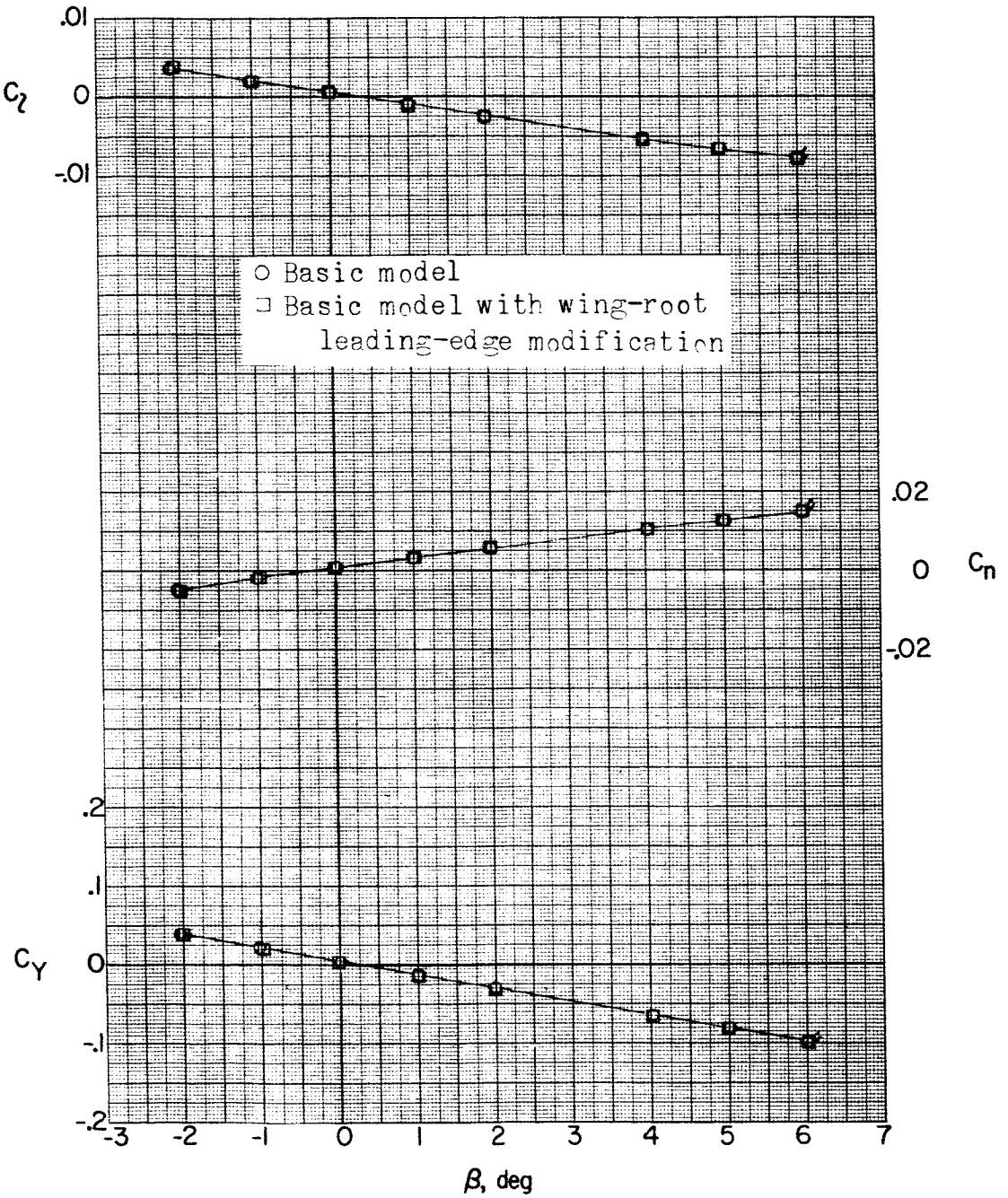

(a) M = 1.56; α = 0°.

Figure 19.- Effect of root leading-edge wing fillets on aerodynamic characteristics in sideslip. Flagged symbols denote wall-reflected shock waves striking the tail.

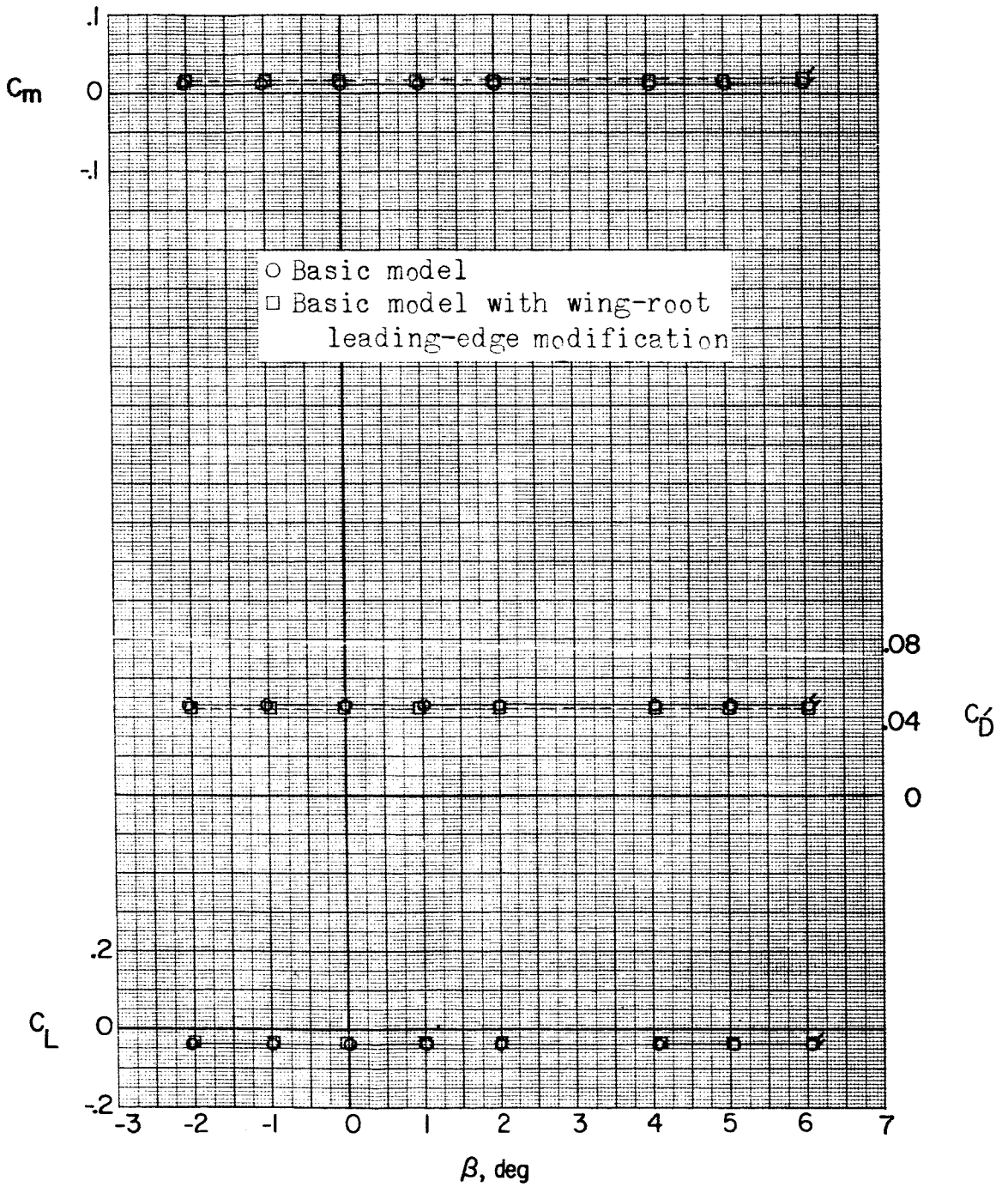

(a) Continued. $\alpha = 0^{\circ}$.

Figure 19.- Continued.

DECLASSIFIED

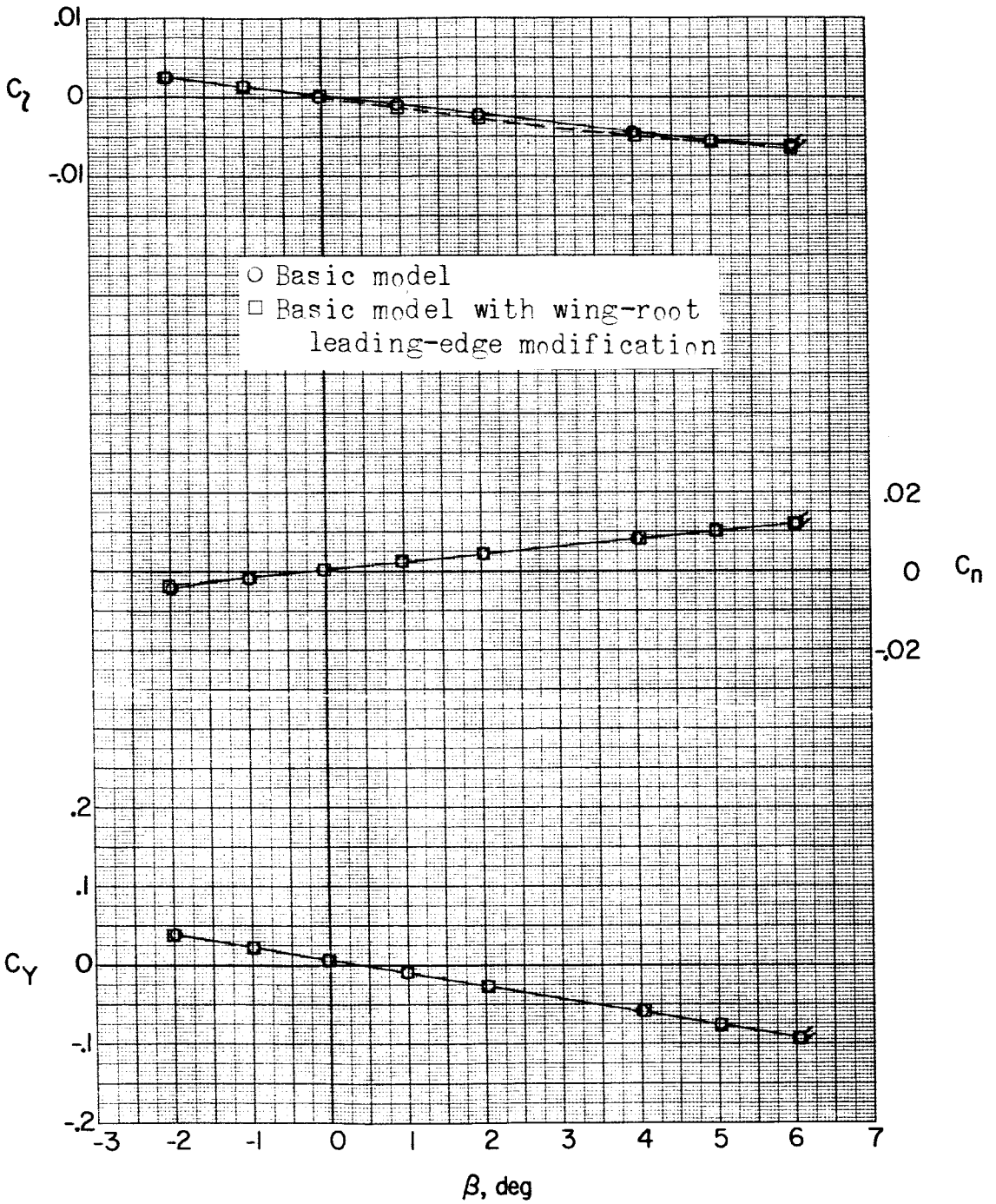

(a) Continued. $\alpha = 5.3^{\circ}$.

Figure 19.- Continued.

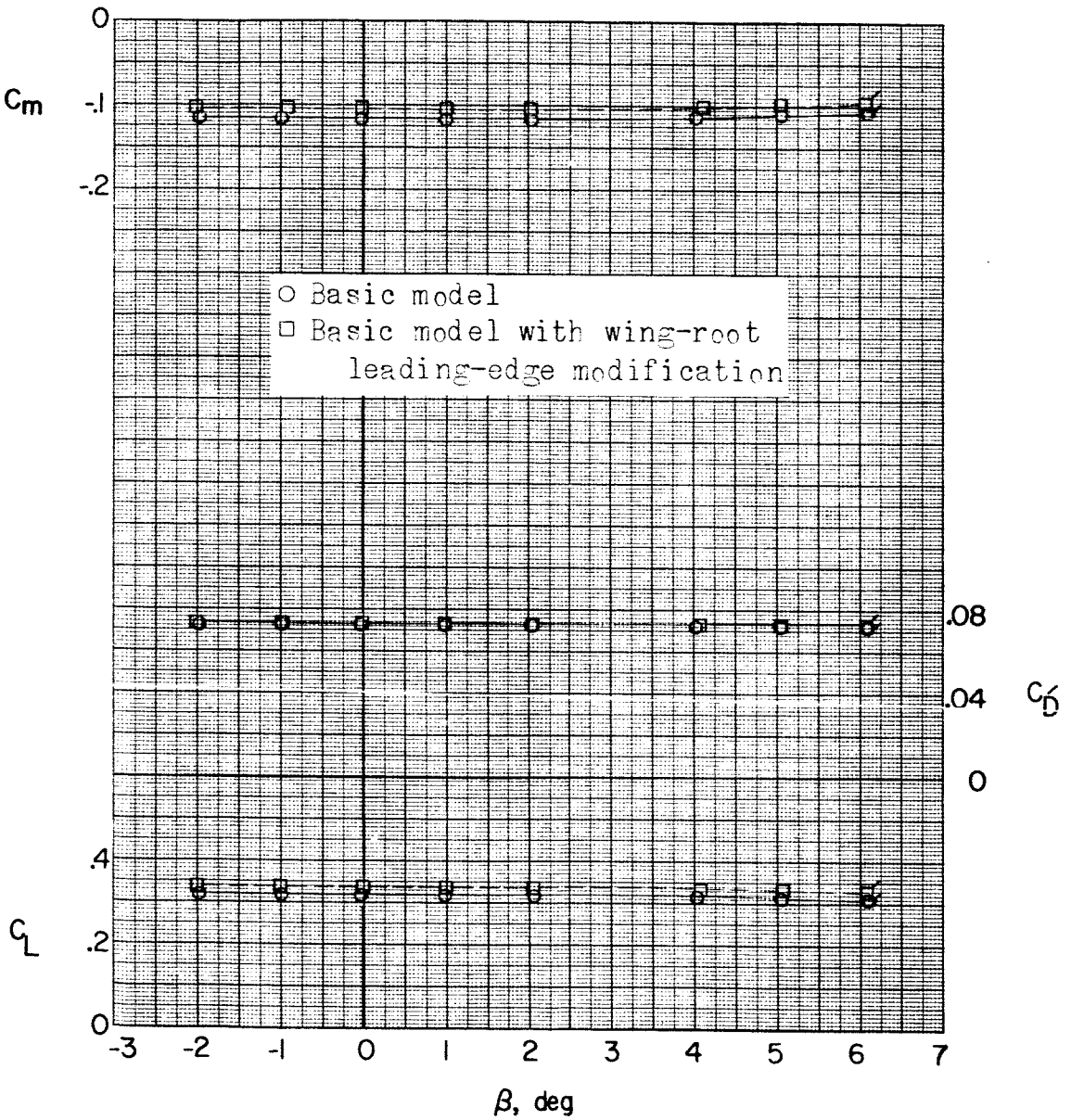

(a) Continued. $\alpha = 5.3^{\circ}$.

Figure 19.- Continued.

DECLASSIFIED

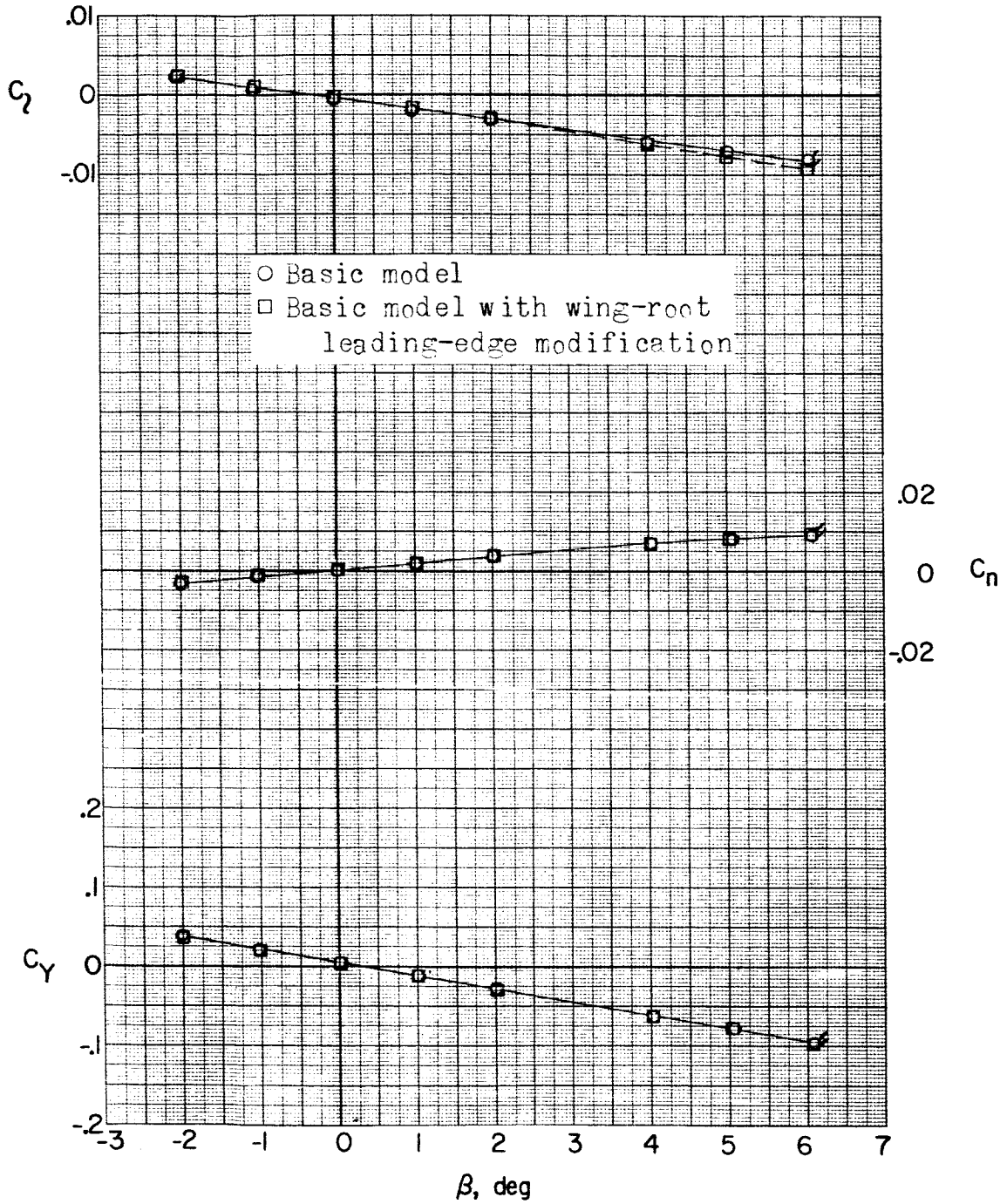

(a) Continued. $\alpha = 10.6^{\circ}$.

Figure 19.- Continued.

[redacted]

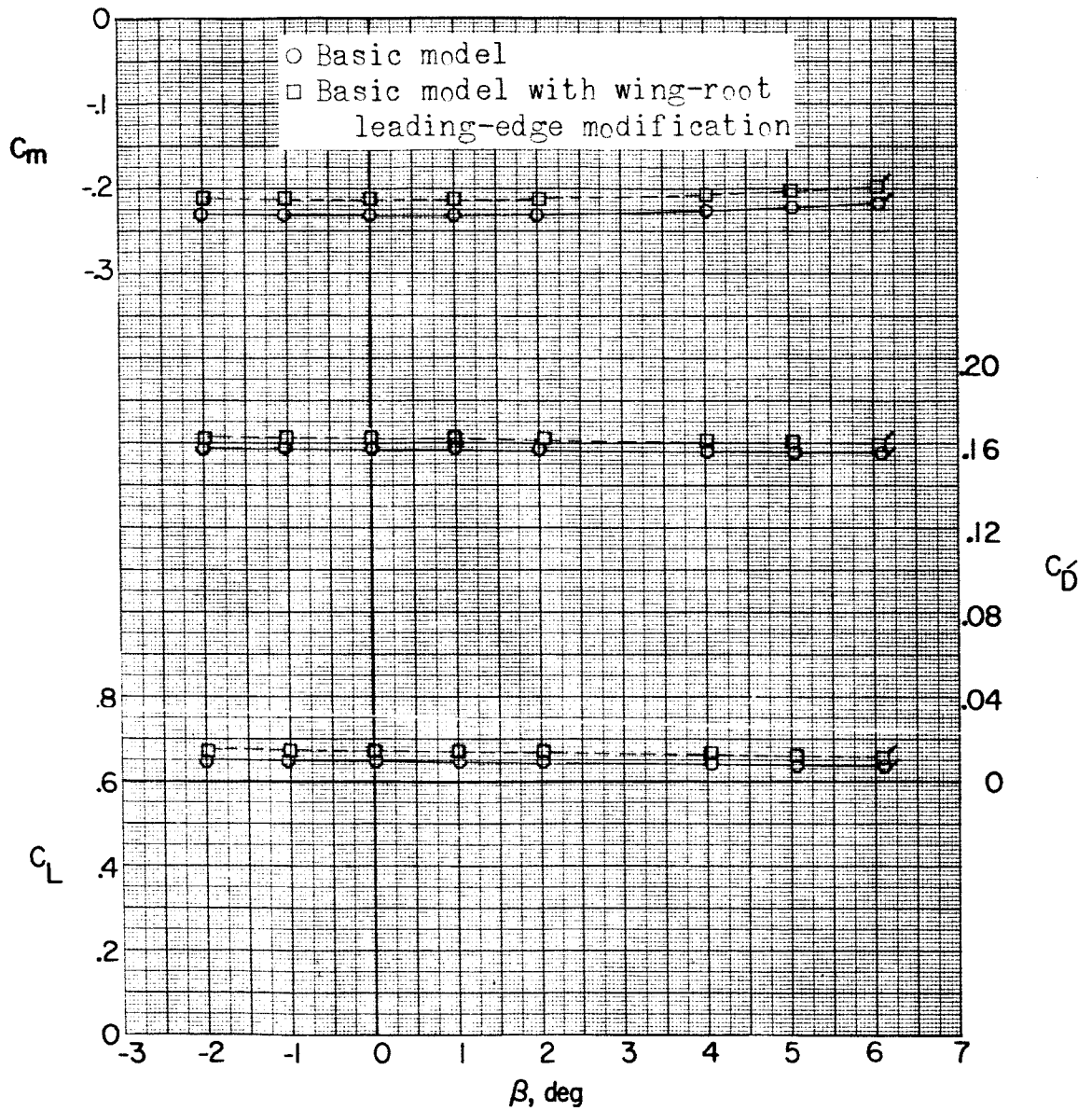

(a) Concluded. $\alpha = 10.6^{\circ}$.

Figure 19.- Continued.

DECLASSIFIED

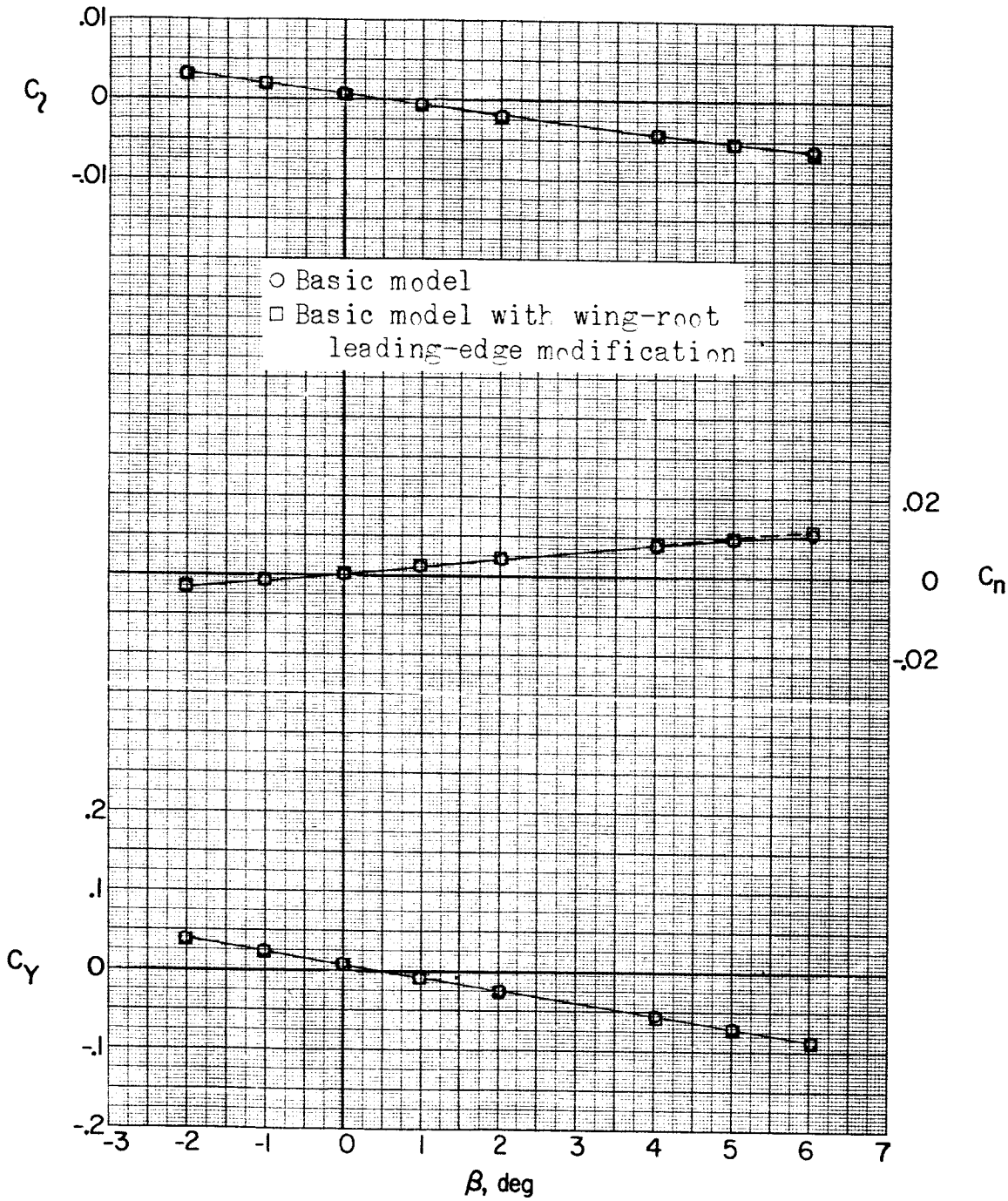

(b) M = 1.76; α = 0°.

Figure 19.- Continued.

[redacted]

DECLASSIFIED

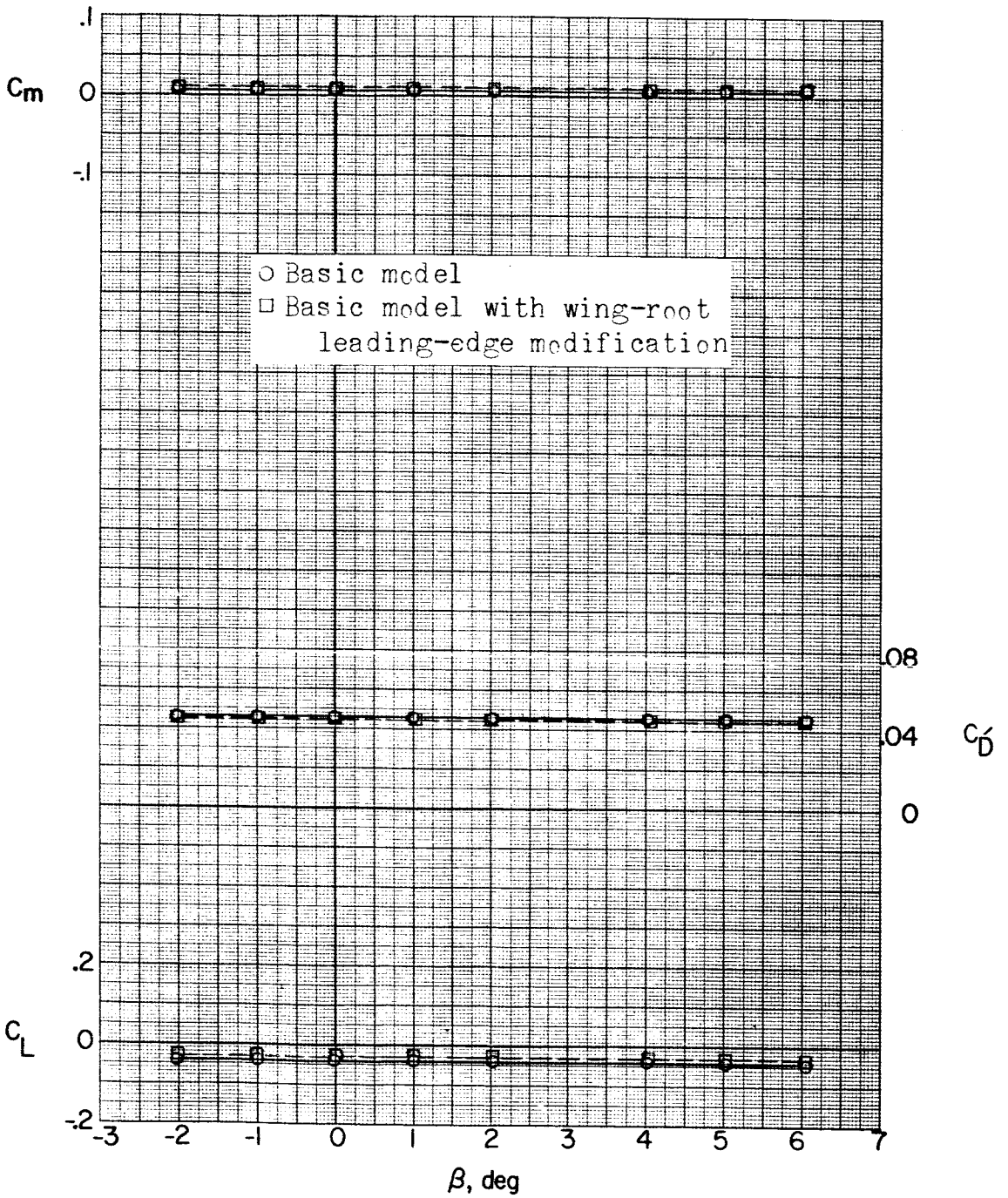

(b) Continued. $\alpha = 0^{\circ}$.

Figure 19.- Continued.

[redacted]

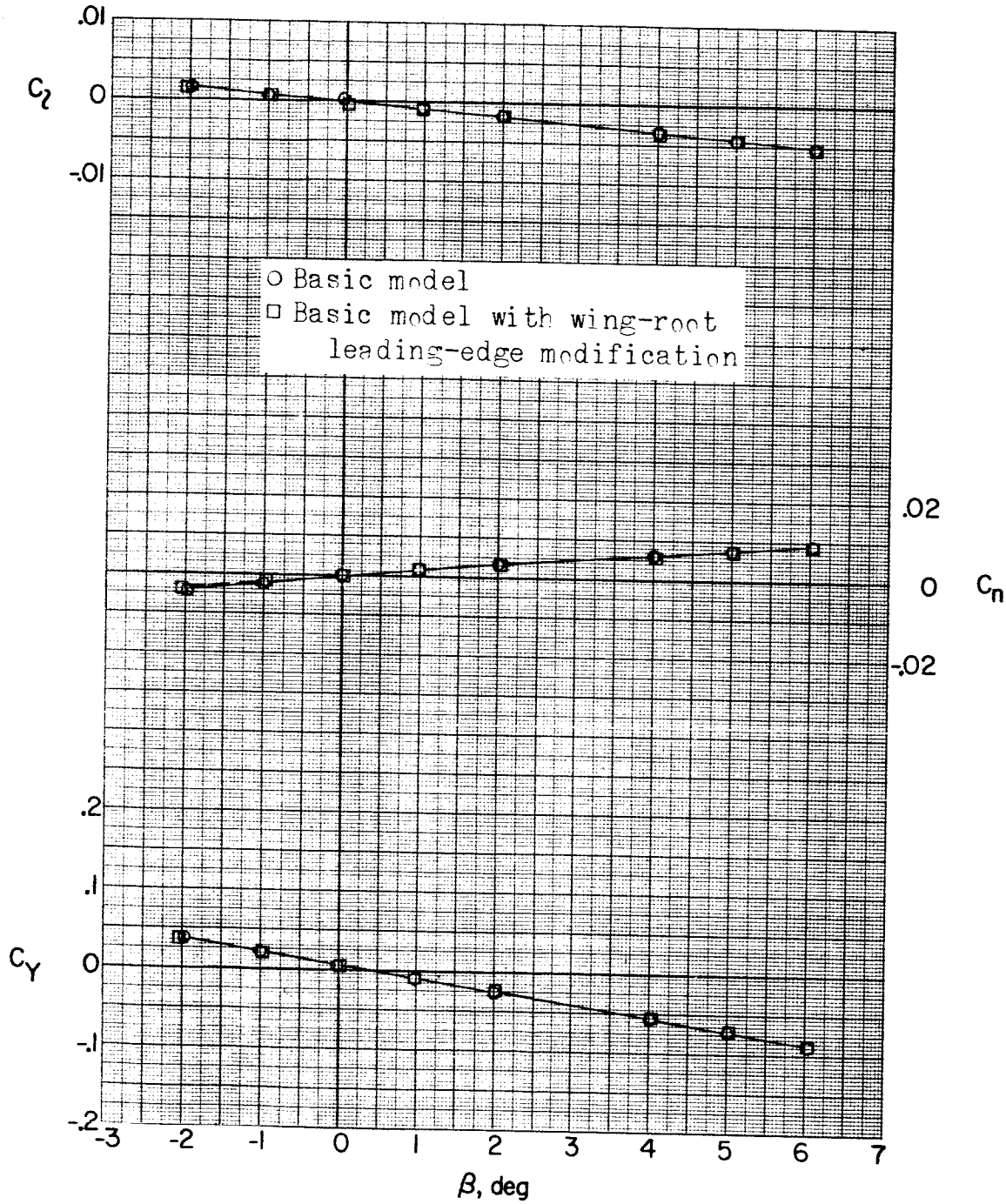

(b) Continued. $\alpha = 5.2^{\circ}$.

Figure 19.- Continued.

DECLASSIFIED

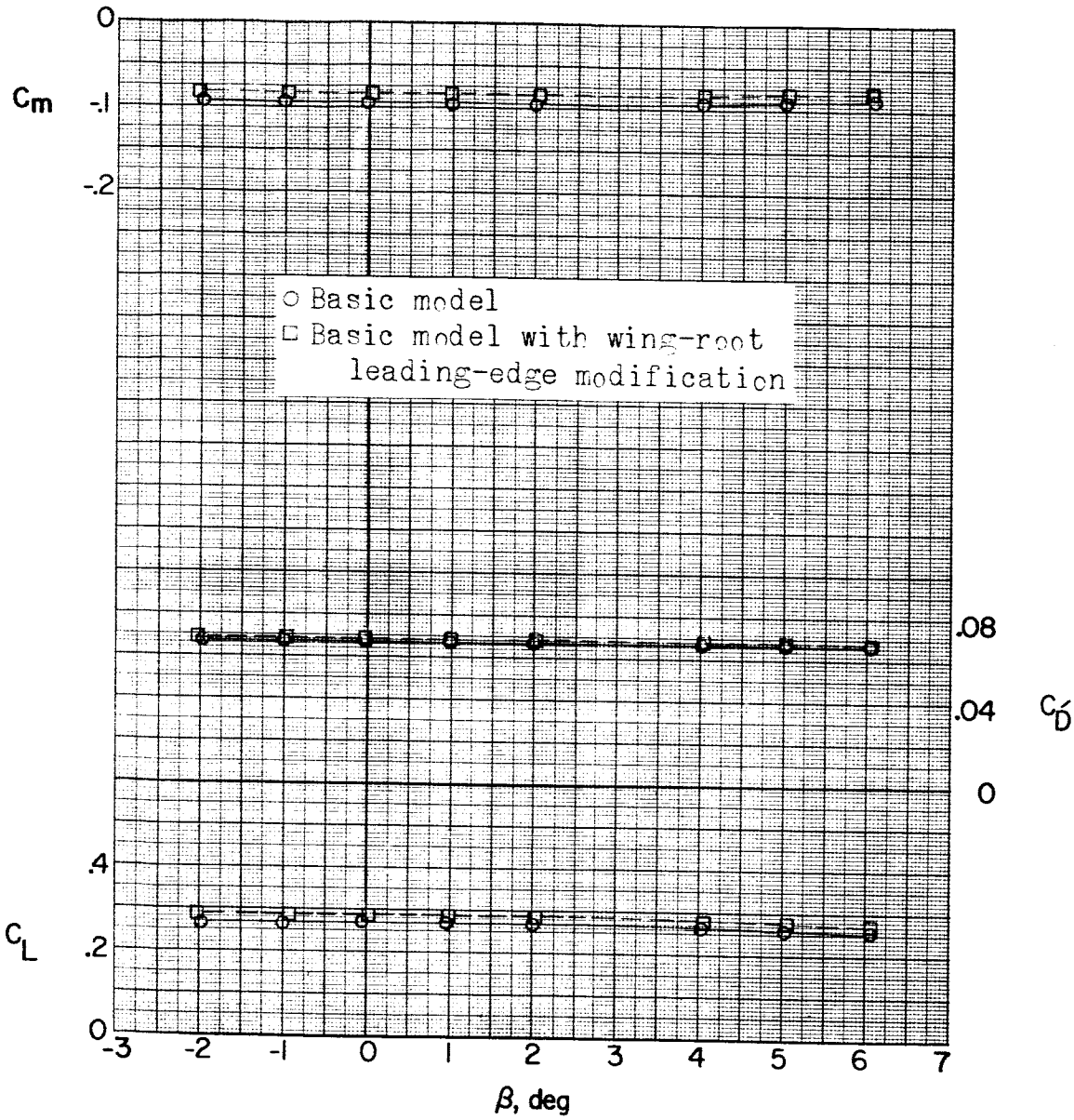

(b) Continued. $\alpha = 5.2^{\circ}$.

Figure 19.- Continued.

[redacted]

DECLASSIFIED

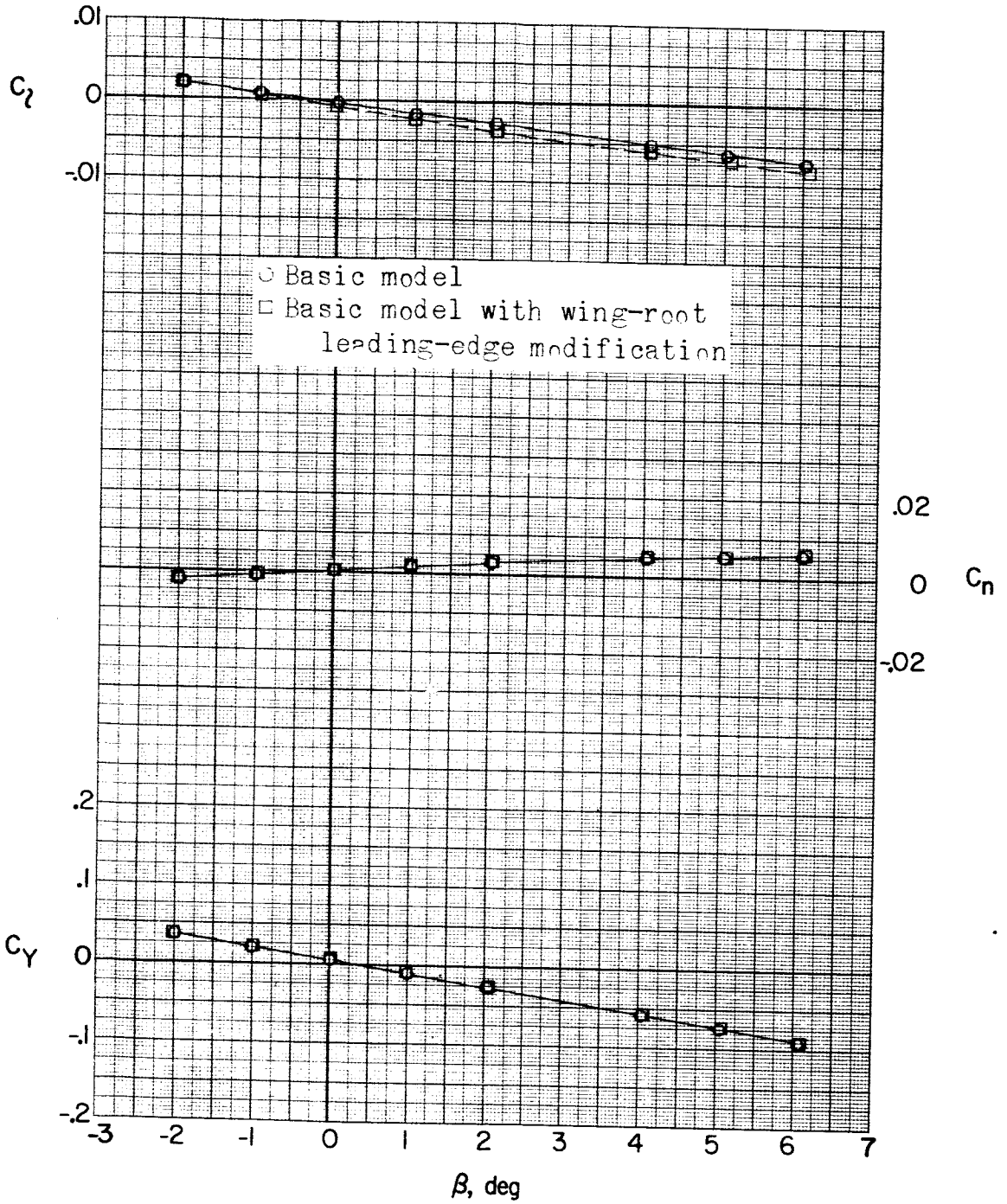

(b) Continued. $\alpha = 10.5^{\circ}$.

Figure 19.- Continued.

[redacted]

DECLASSIFIED

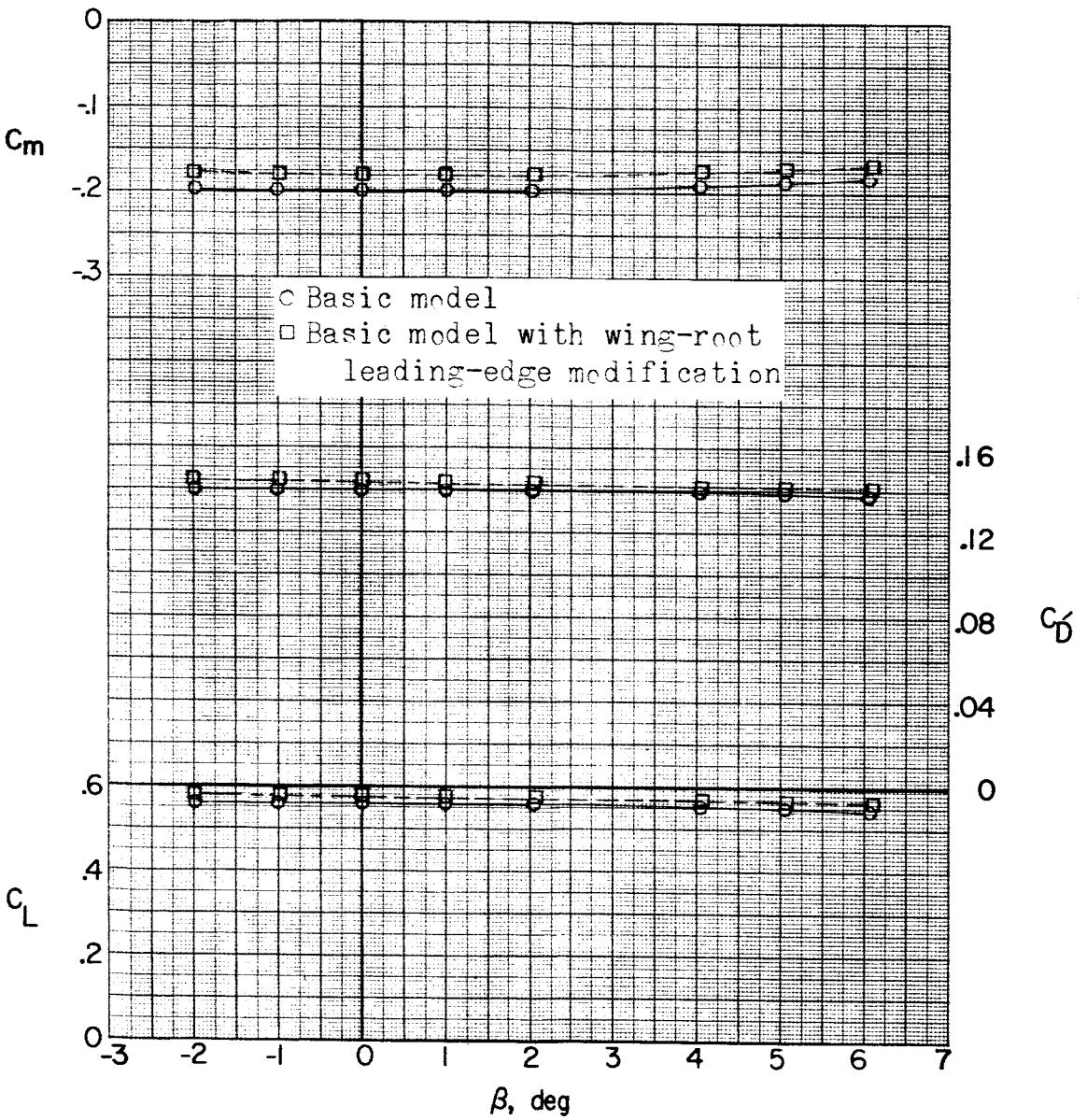

(b) Concluded. $\alpha = 10.5^{\circ}$.

Figure 19.- Continued.

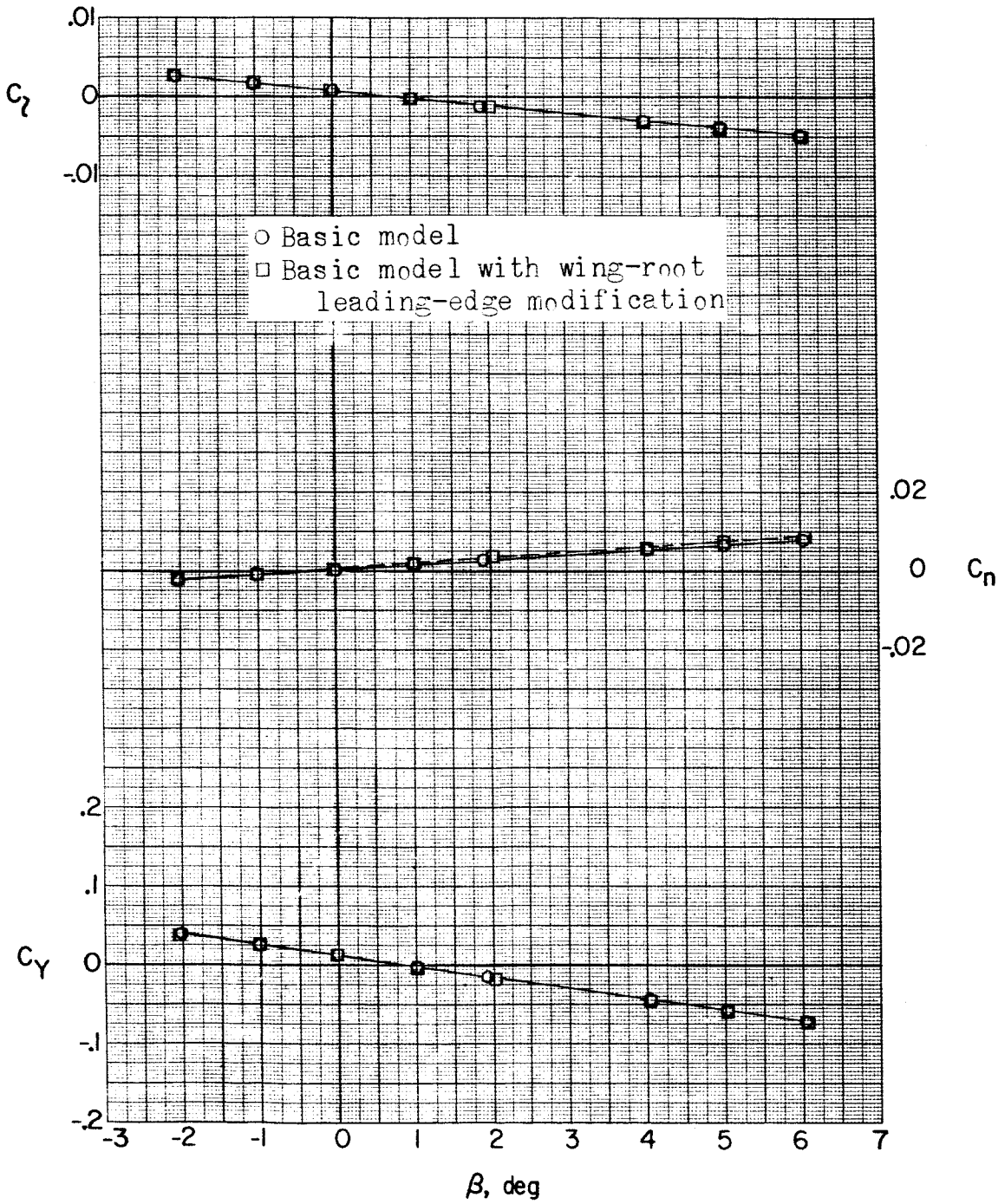

(c) M = 2.06; α = 0°.

Figure 19.- Continued.

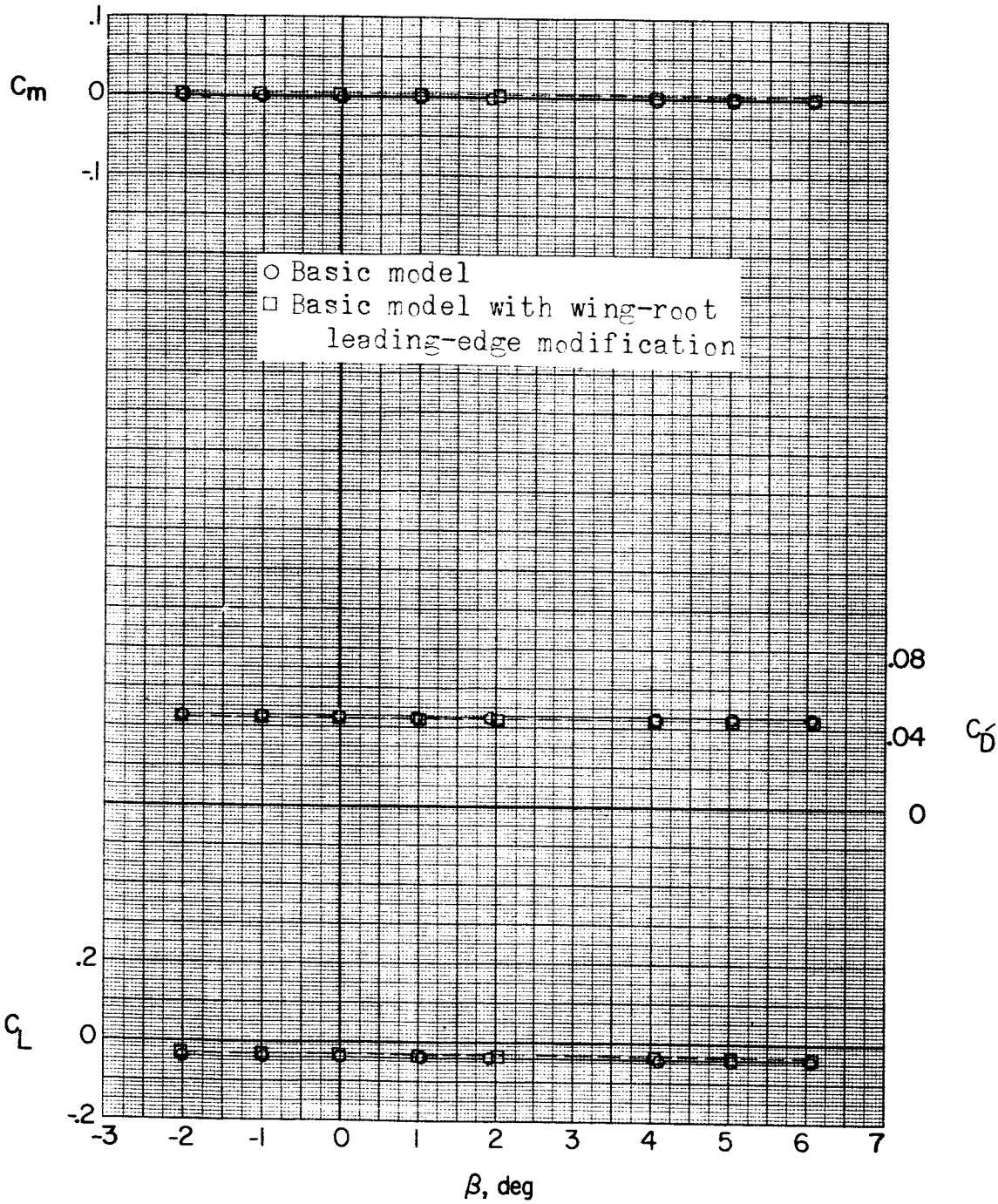

(c) Continued. $\alpha = 0^{\circ}$.

Figure 19.- Continued.

[redacted]

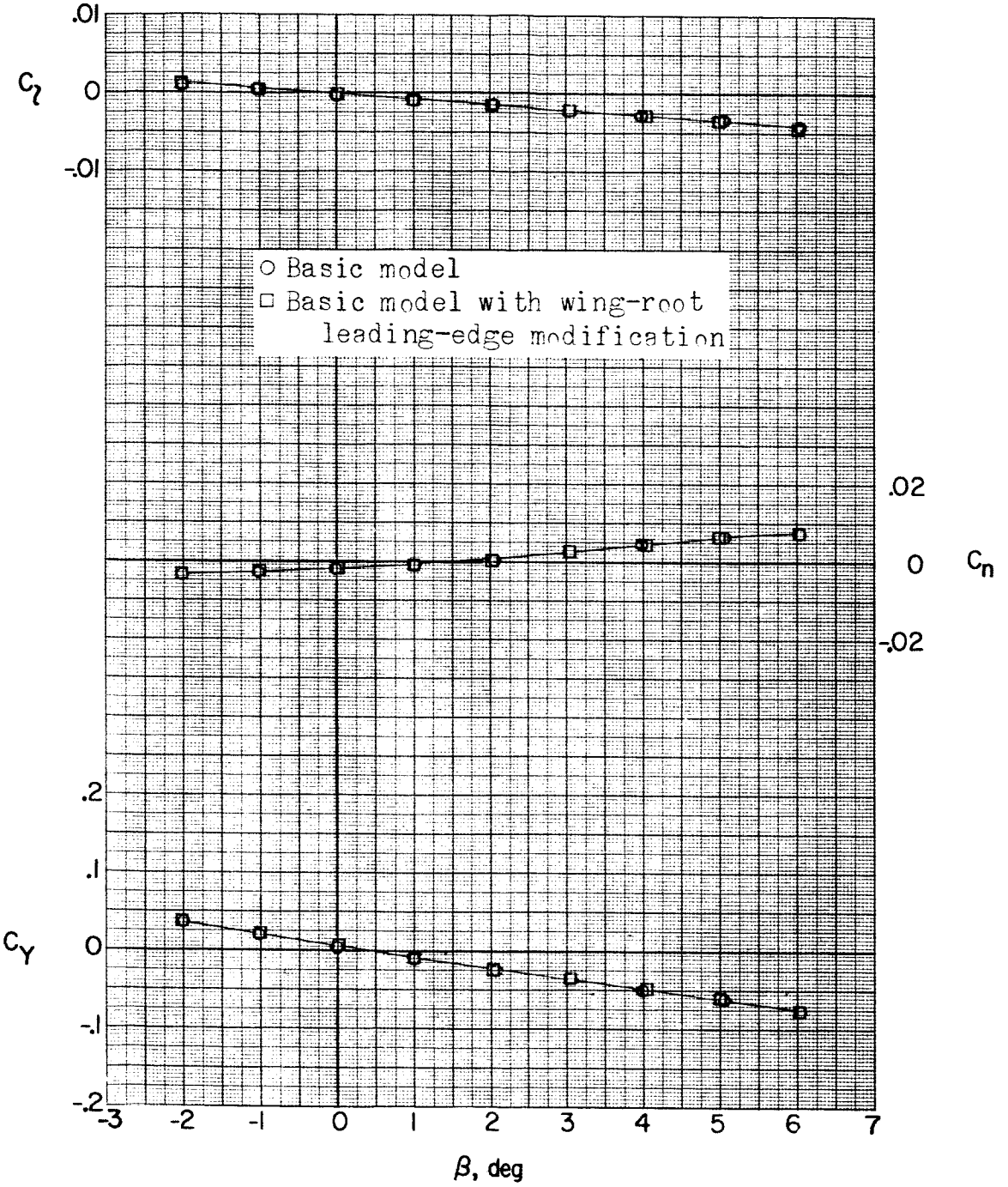

(c) Continued. $\alpha = 5.2^{\circ}$.

Figure 19.- Continued.

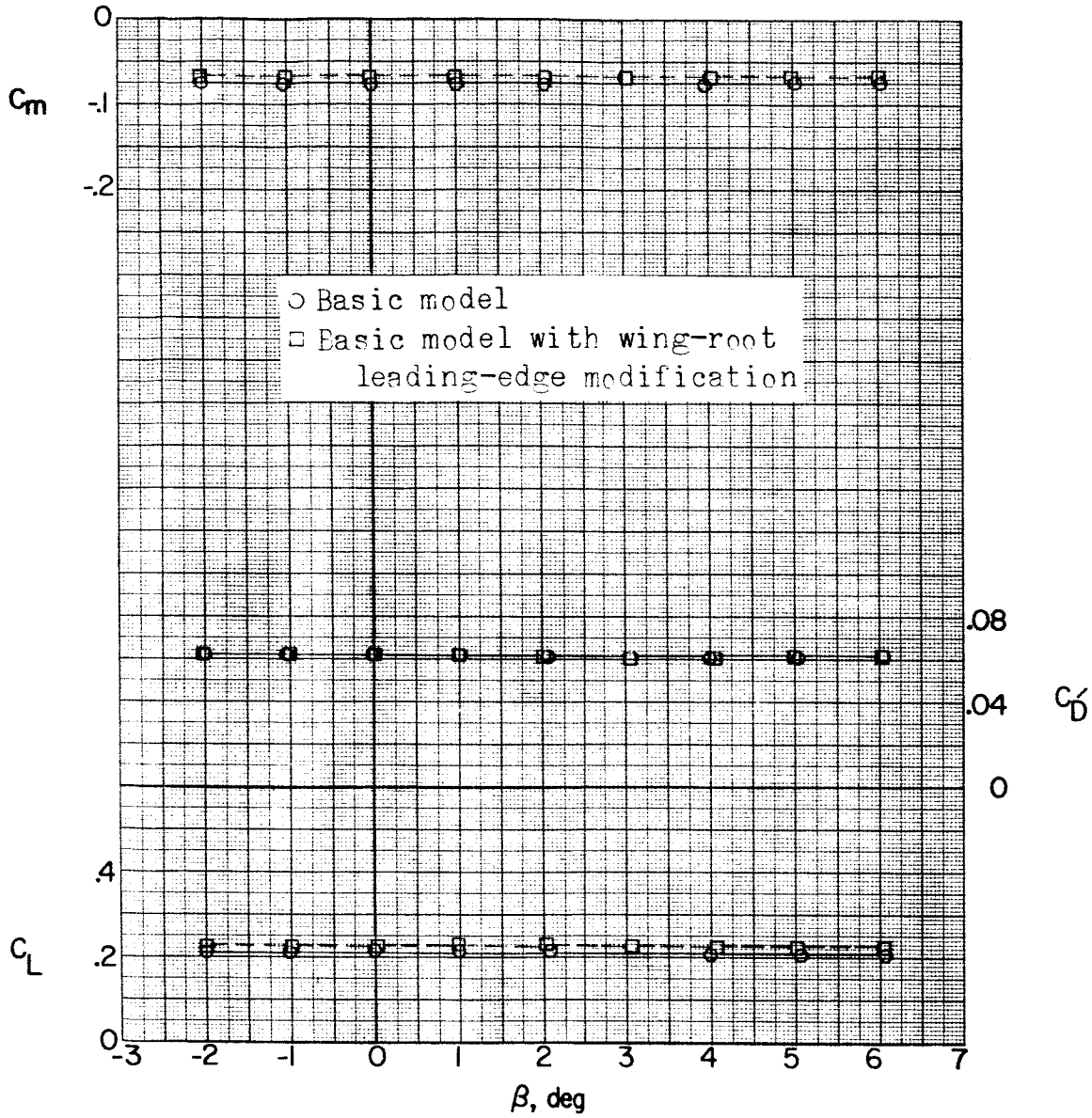

(c) Continued. $\alpha = 5.2^{\circ}$.

Figure 19.- Continued.

DECLASSIFIED

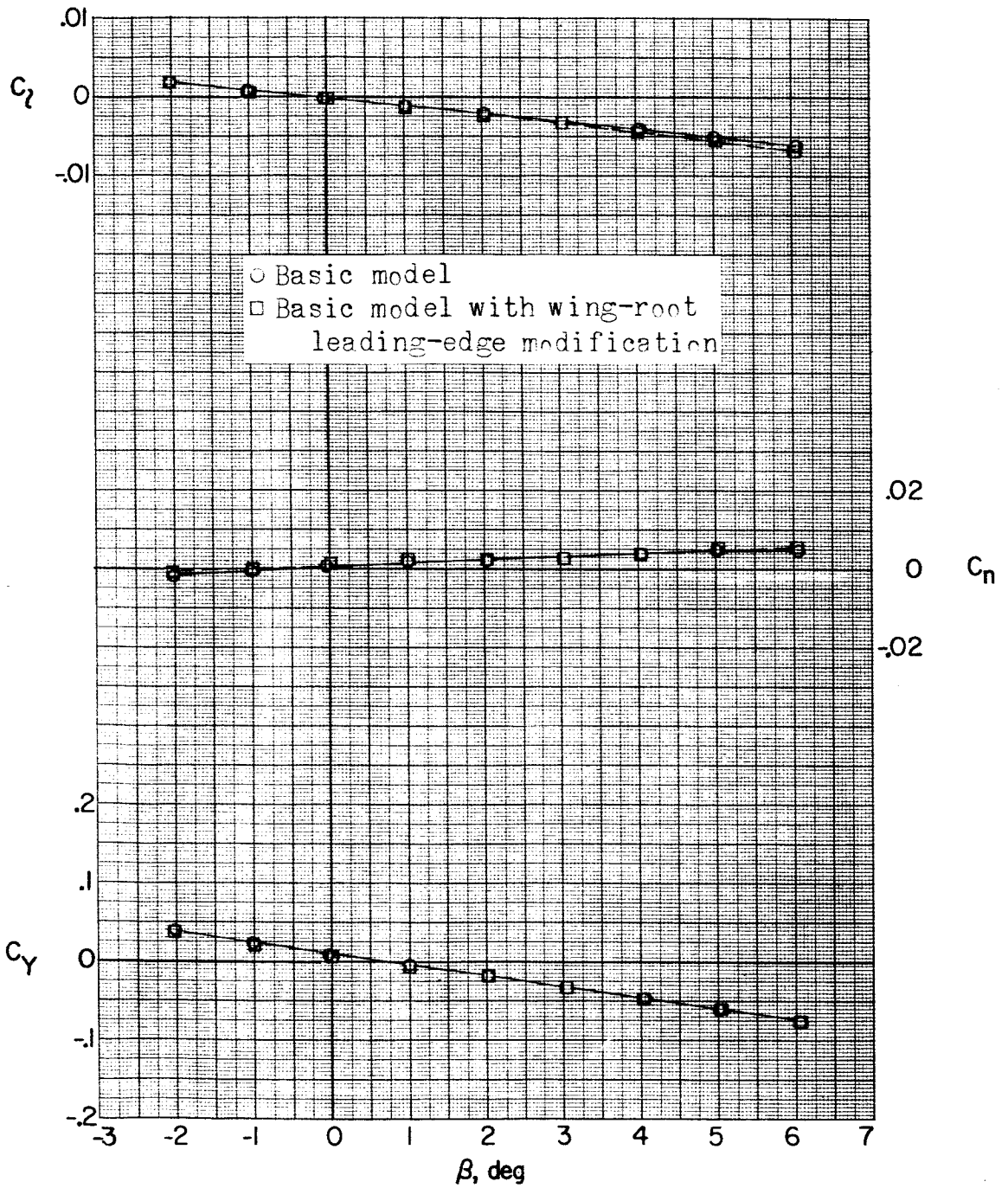

(c) Continued. $\alpha = 10.4^{\circ}$.

Figure 19.- Continued.

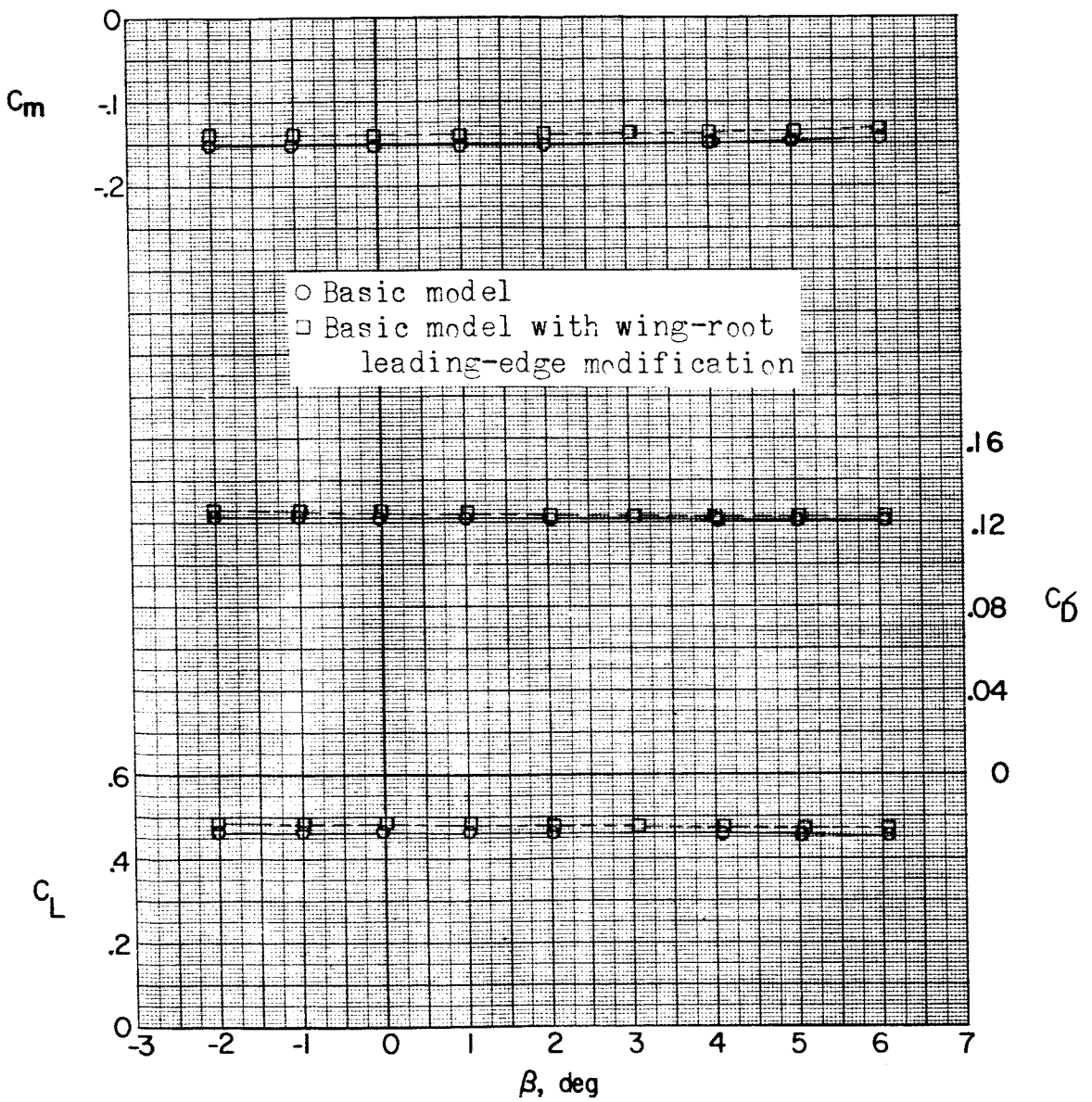

(c) Concluded. $\alpha = 10.4^{\circ}$.

Figure 19.- Concluded.

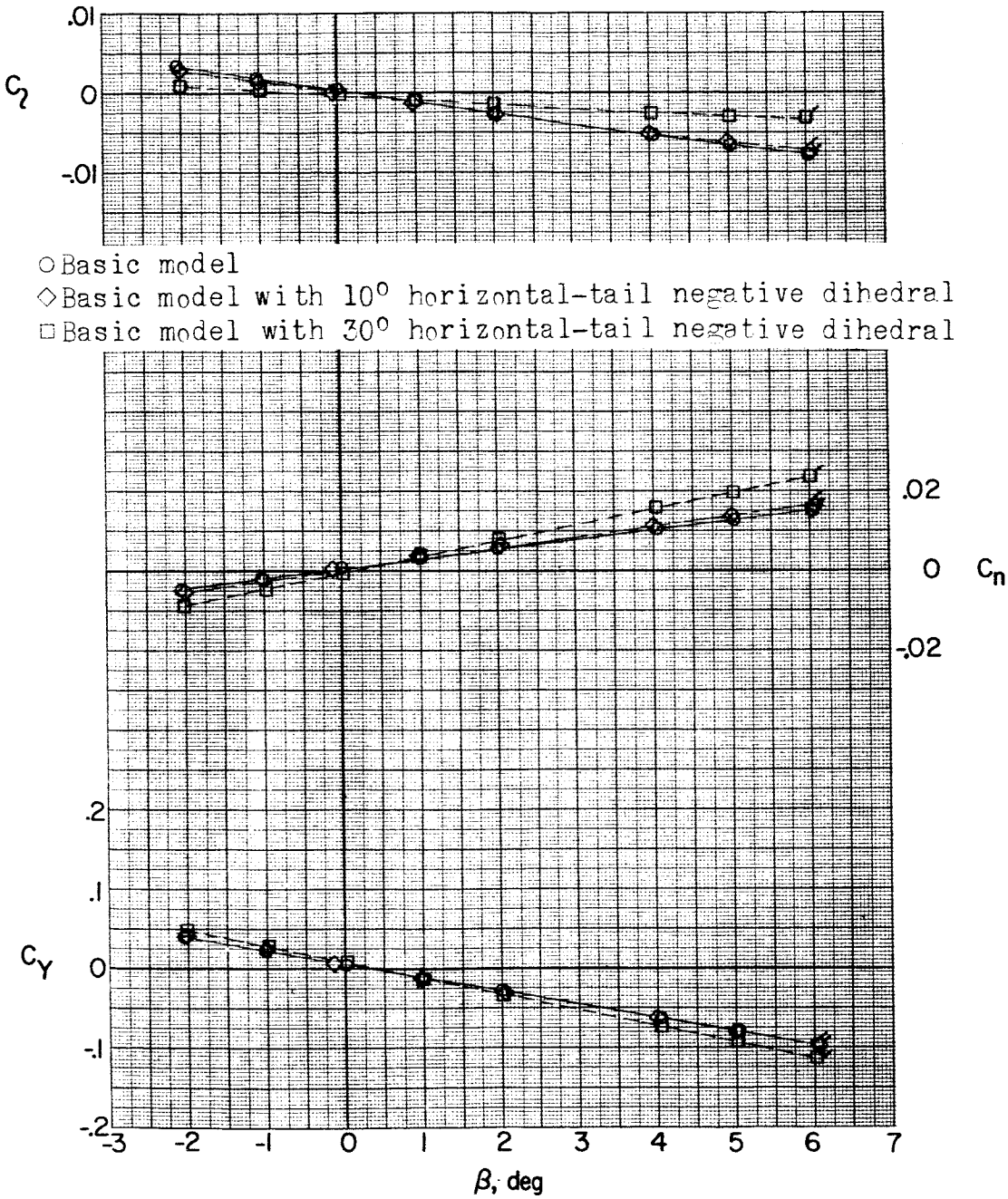

(a) M = 1.56; α = 0°.

Figure 20.- Effect of horizontal-tail negative dihedral on aerodynamic characteristics in sideslip. Flagged symbols denote wall-reflected shock waves striking the tail.

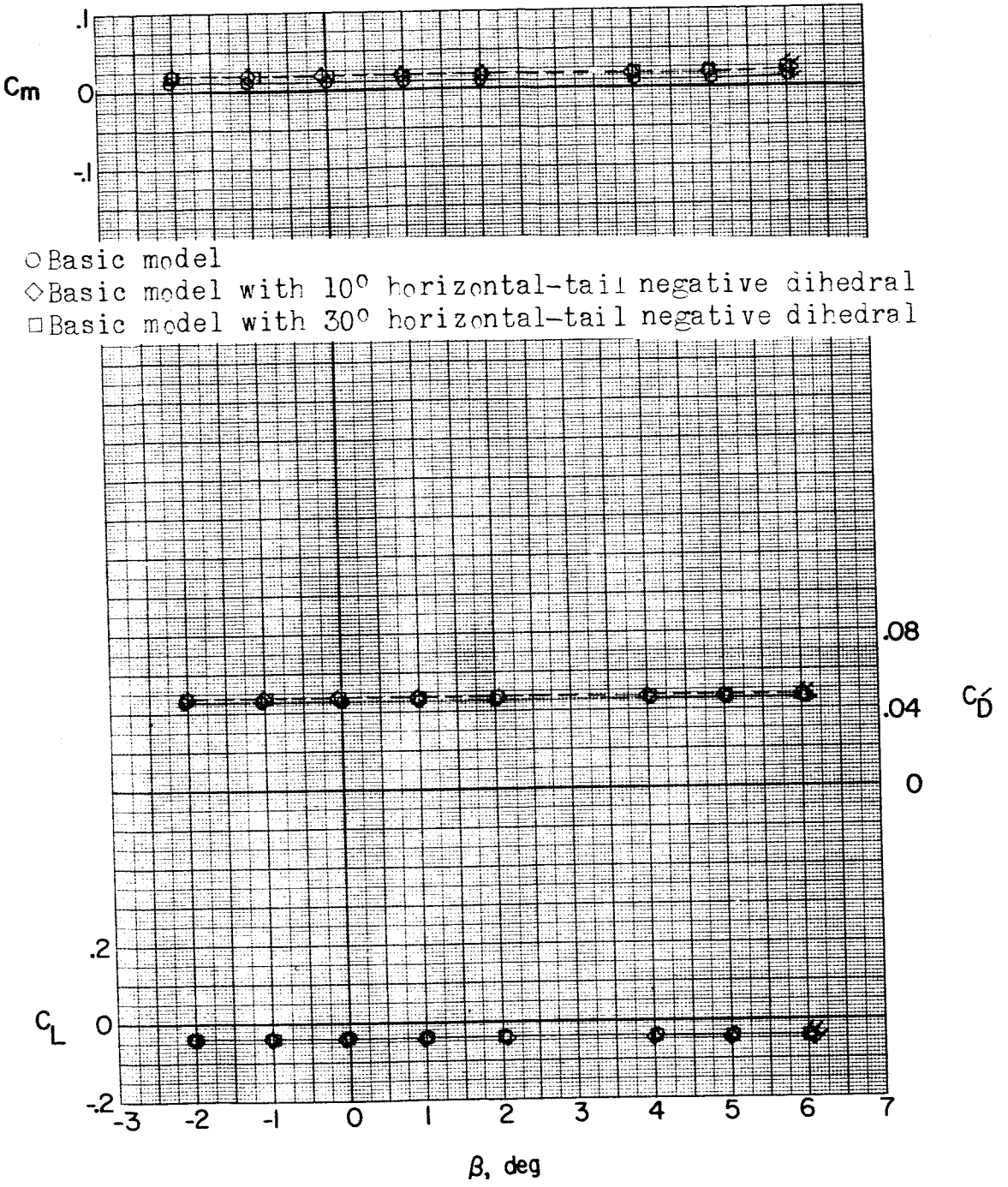

(a) Continued. $\alpha = 0^{\circ}$.

Figure 20.- Continued.

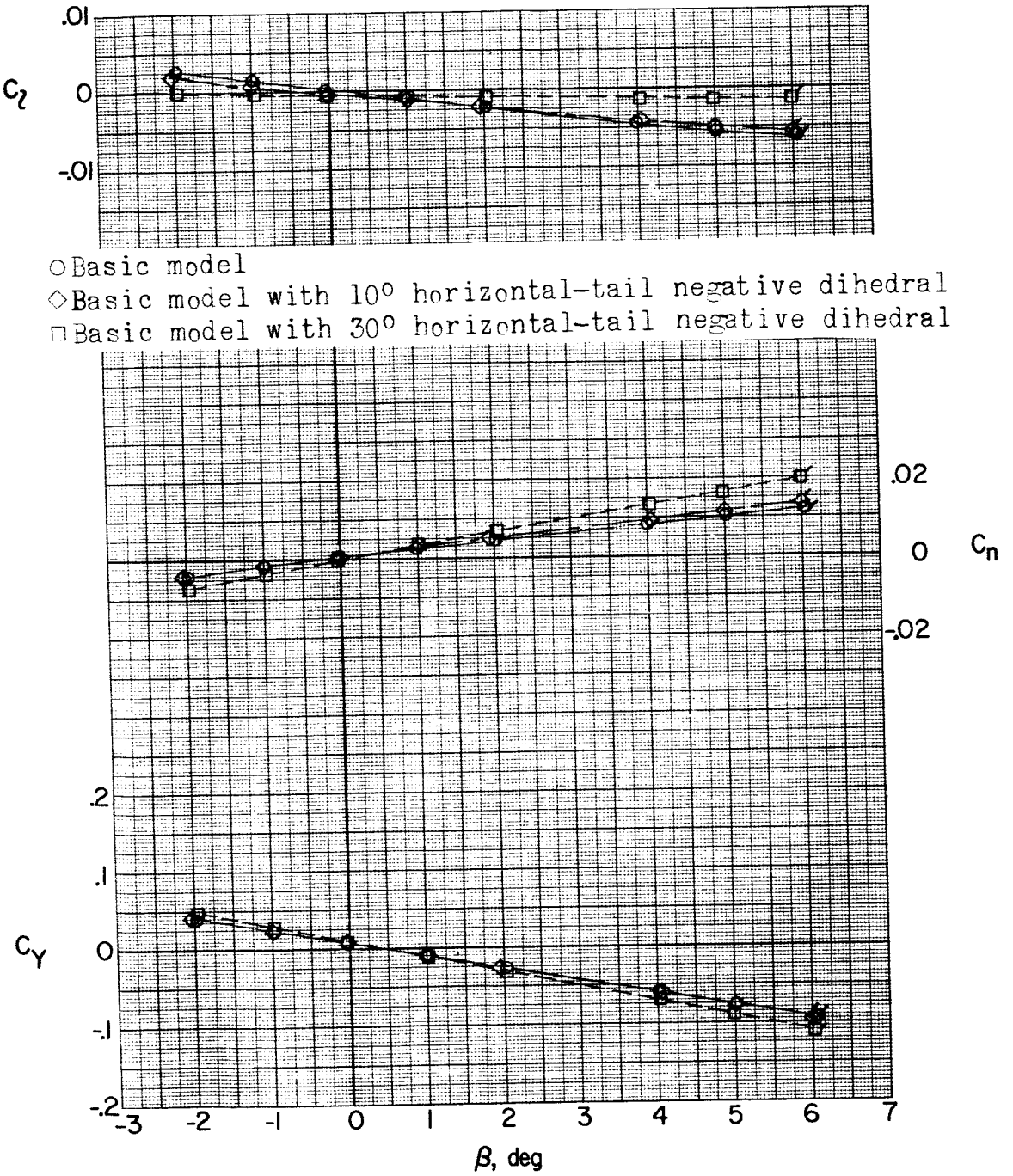

(a) Continued. $\alpha = 5.3^{\circ}$.

Figure 20.- Continued.

[redacted]

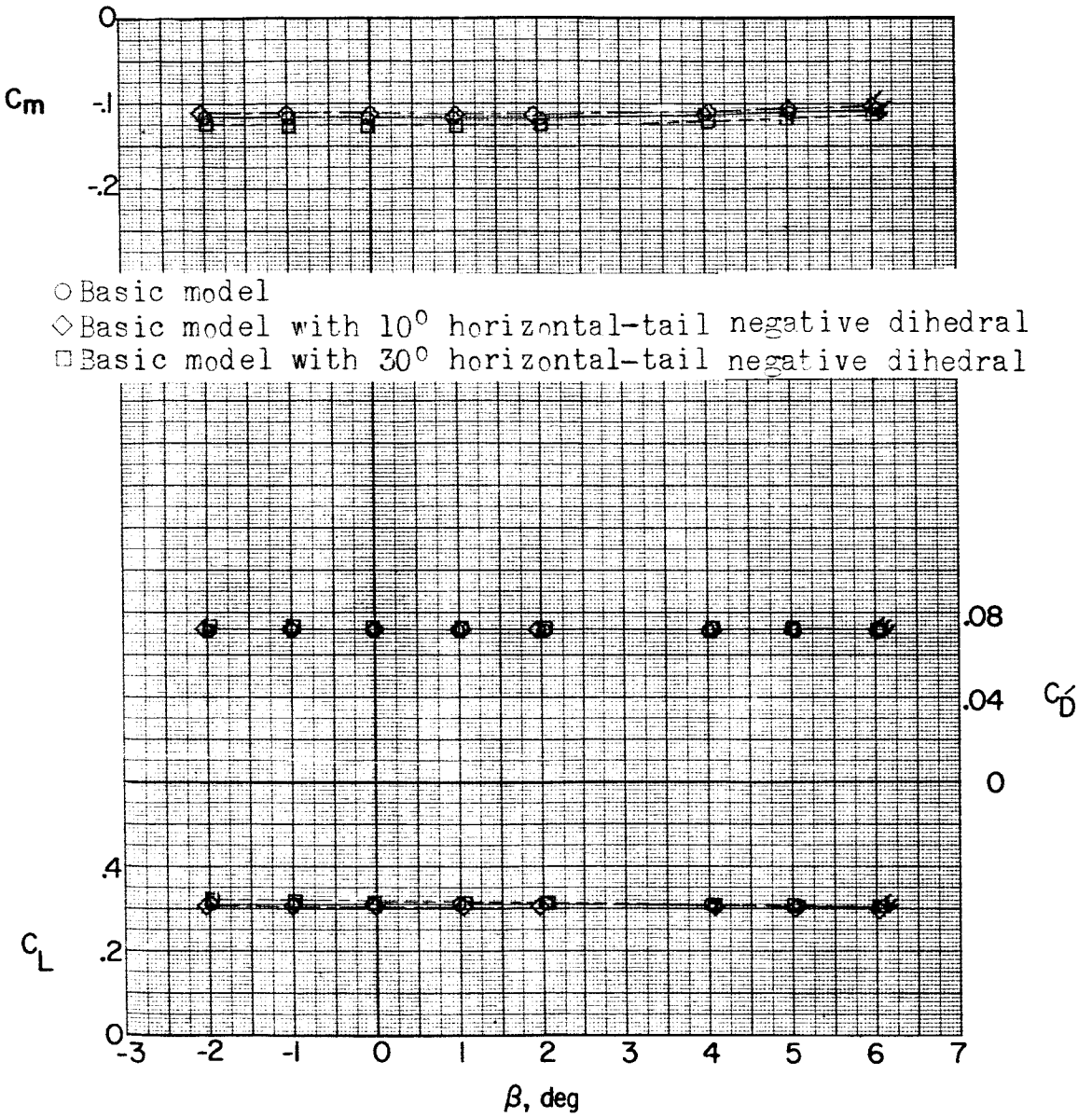

(a) Continued. $\alpha = 5.3^{\circ}$.

Figure 20.- Continued.

[redacted]

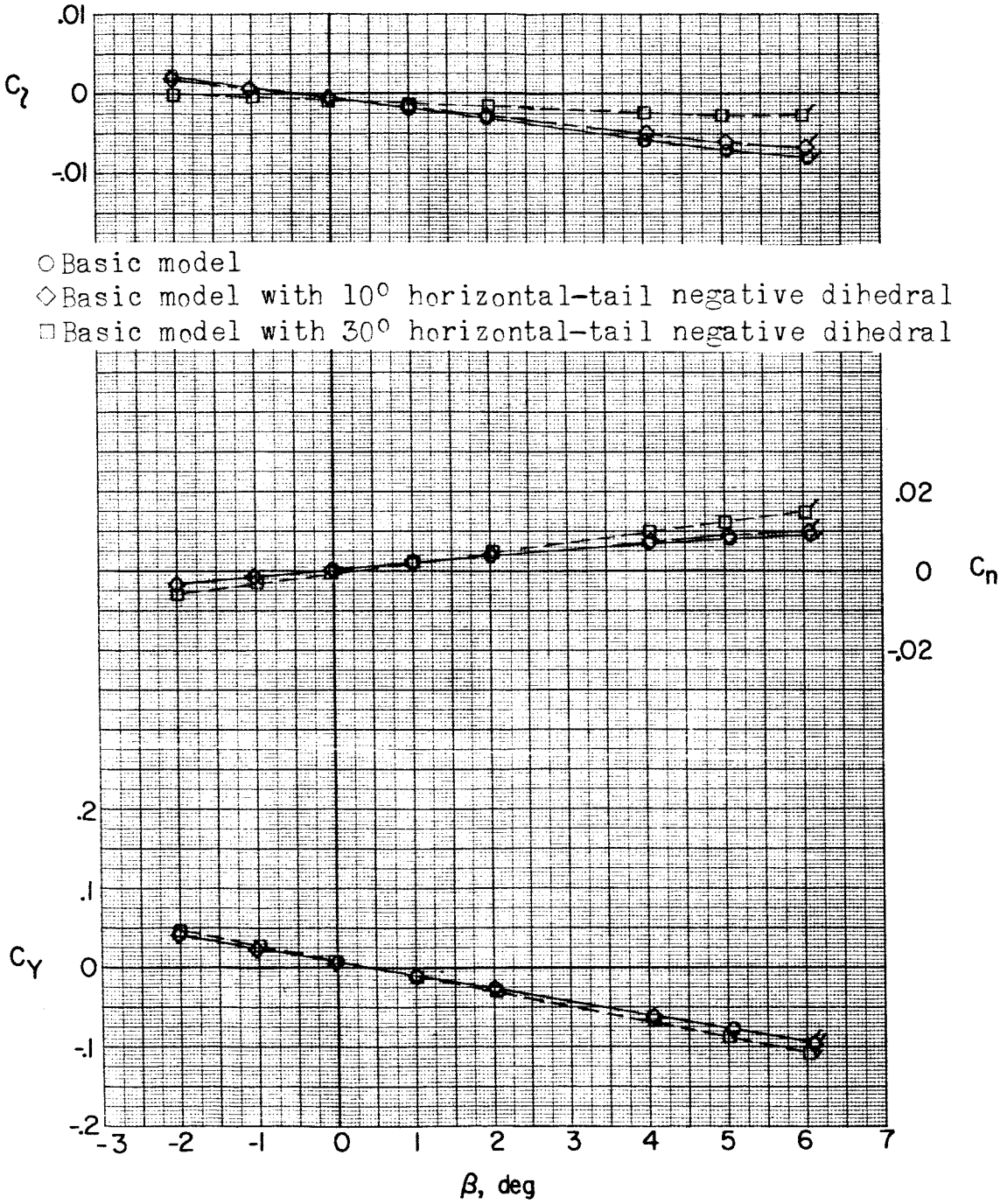

(a) Continued. $\alpha = 10.6^{\circ}$.

Figure 20.- Continued.

[redacted]

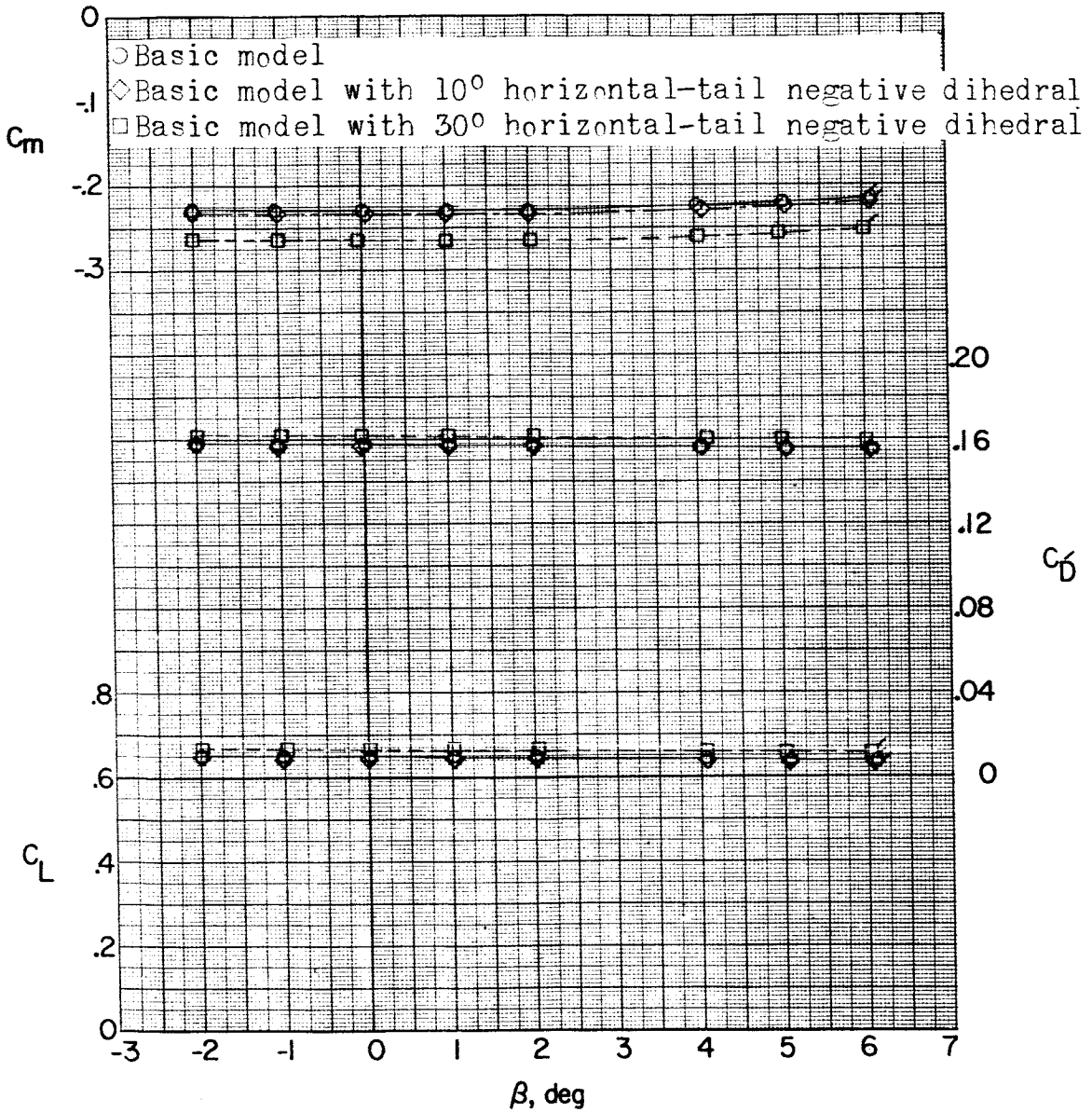

(a) Concluded. $\alpha = 10.6^{\circ}$.

Figure 20.- Continued.

[redacted]

DECLASSIFIED

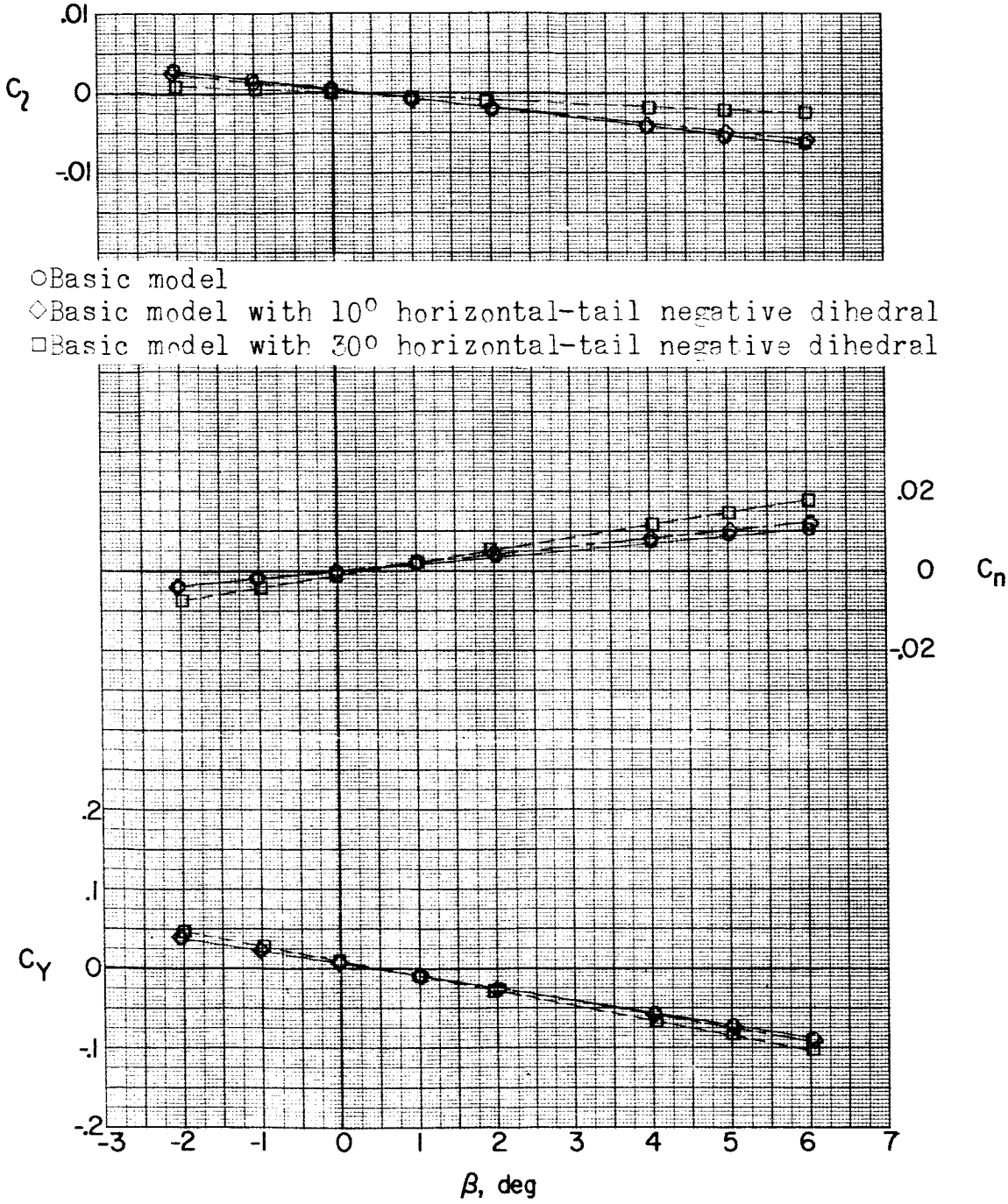

(b) M = 1.76. α = 0°.

Figure 20.- Continued.

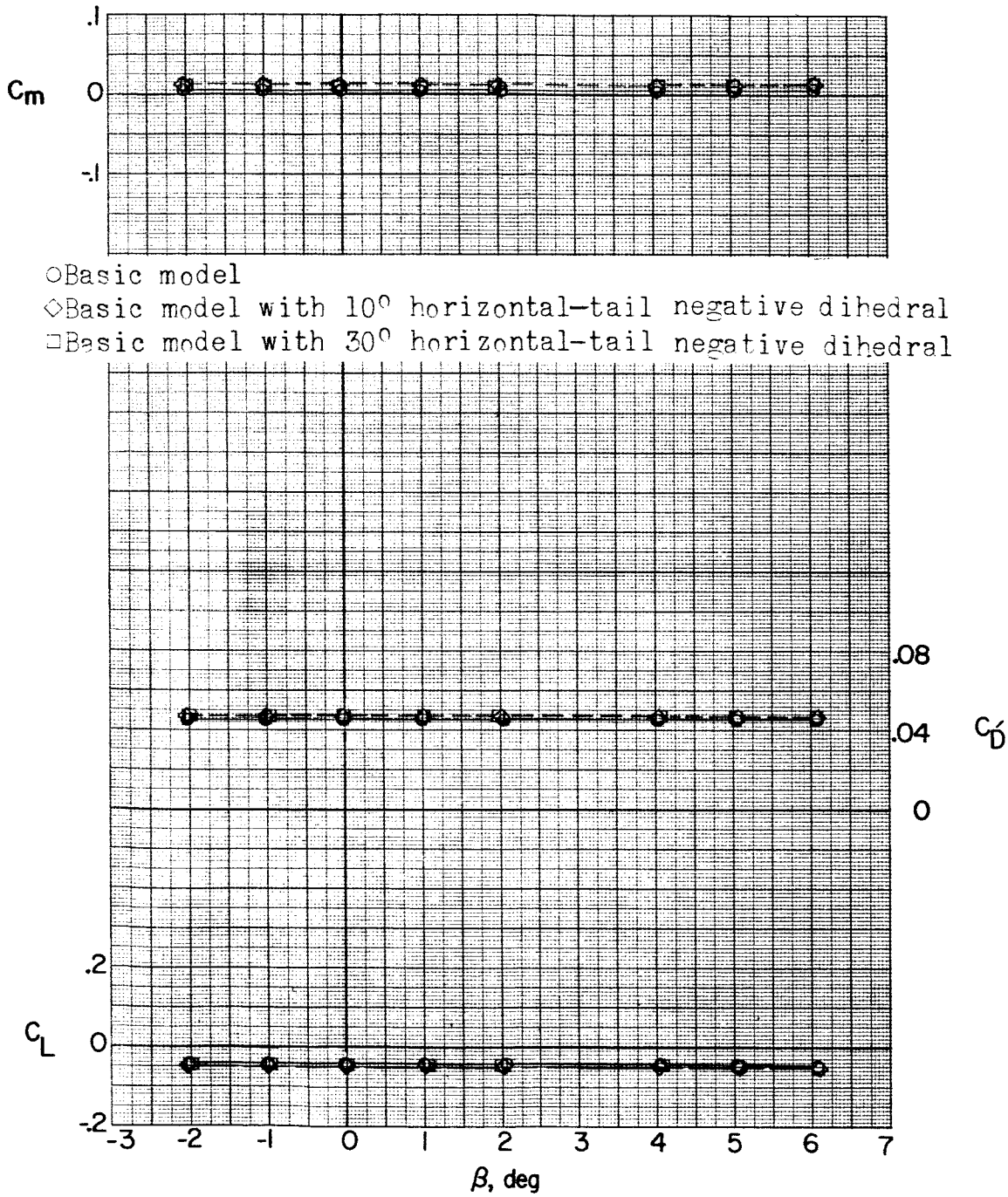

(b) Continued. $\alpha = 0^{\circ}$.

Figure 20.- Continued.

[redacted]

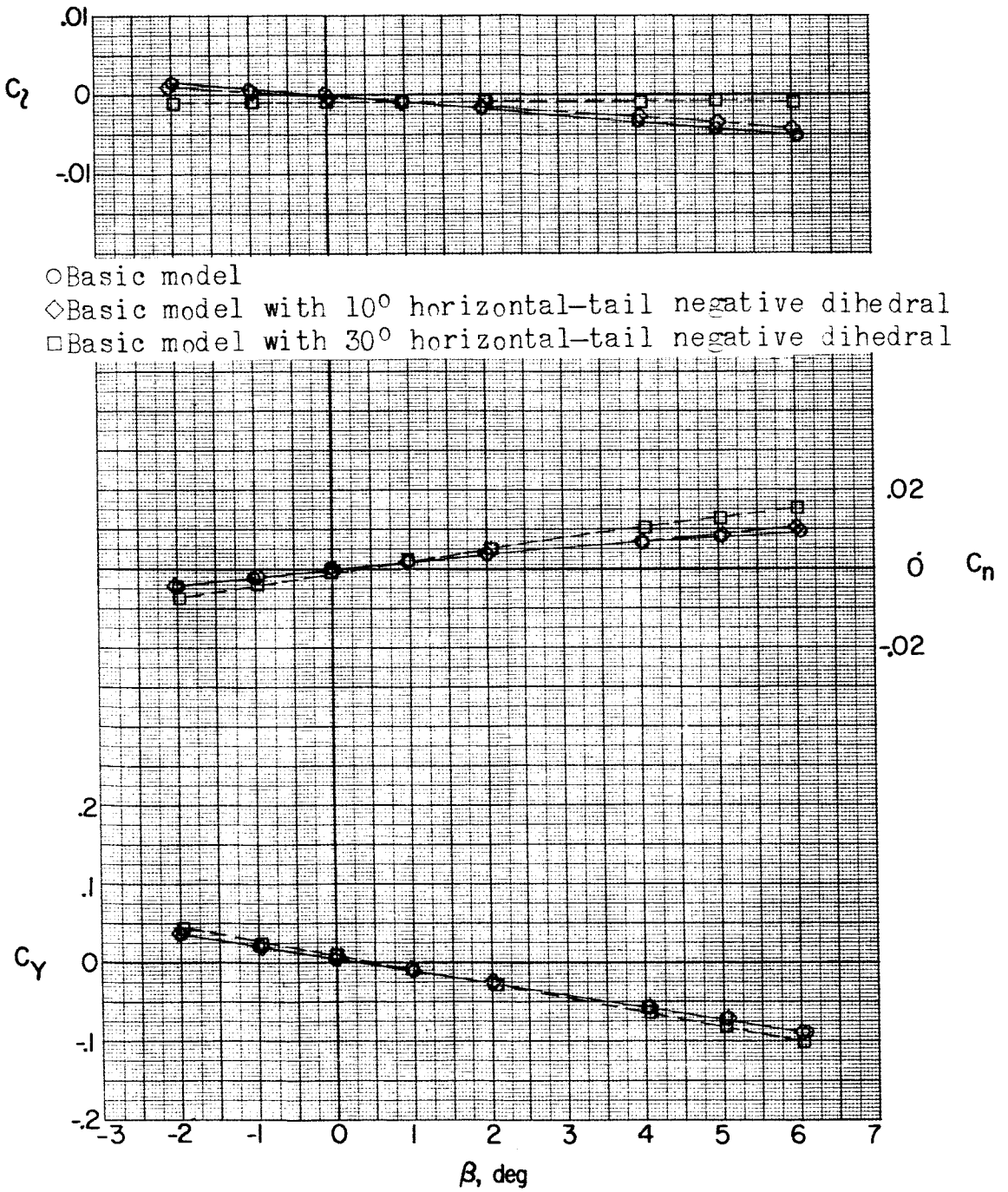

(b) Continued. $\alpha = 5.2^{\circ}$.

Figure 20.- Continued.

[redacted]

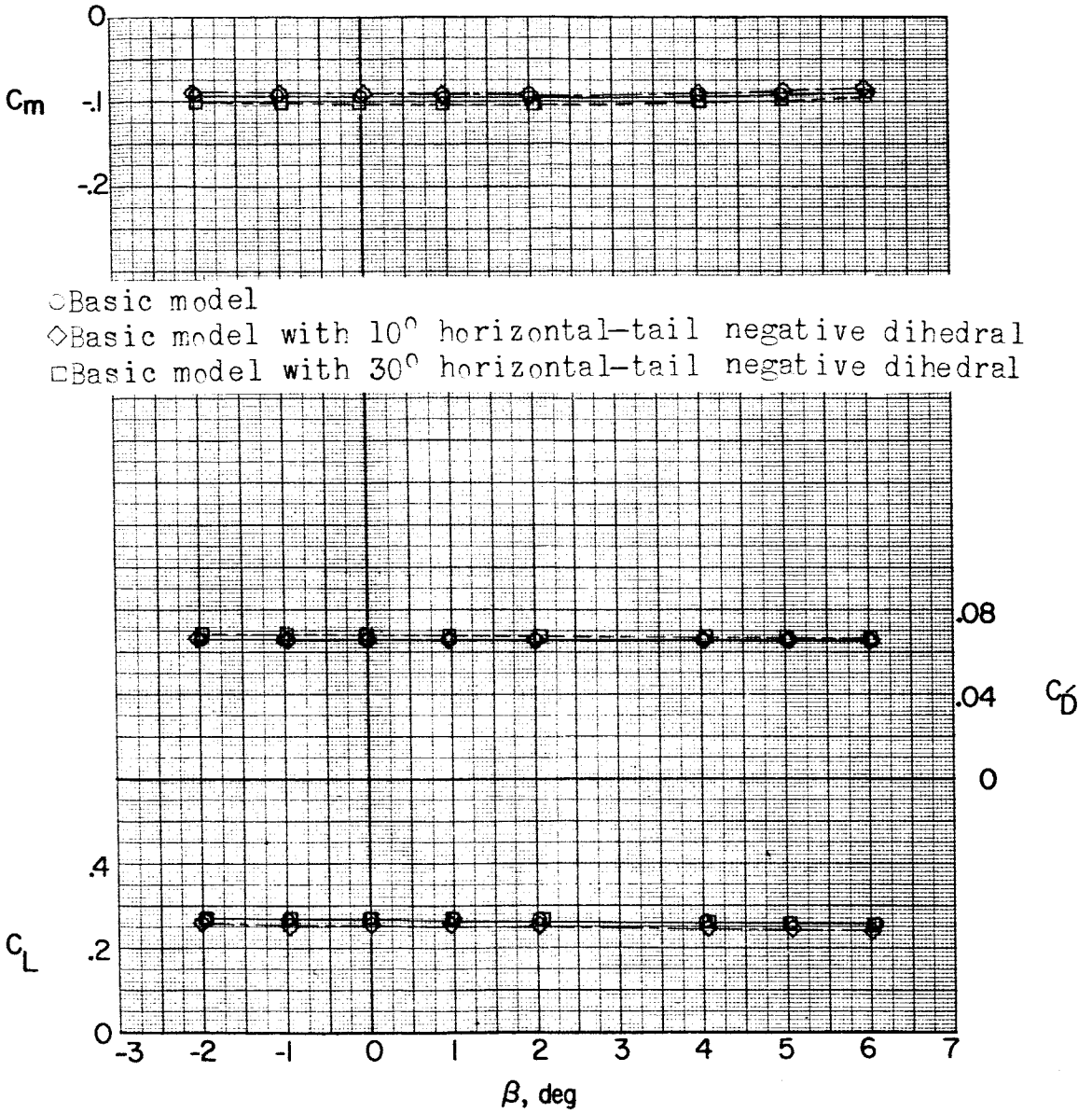

(b) Continued. $\alpha = 5.2^{\circ}$.

Figure 20.- Continued.

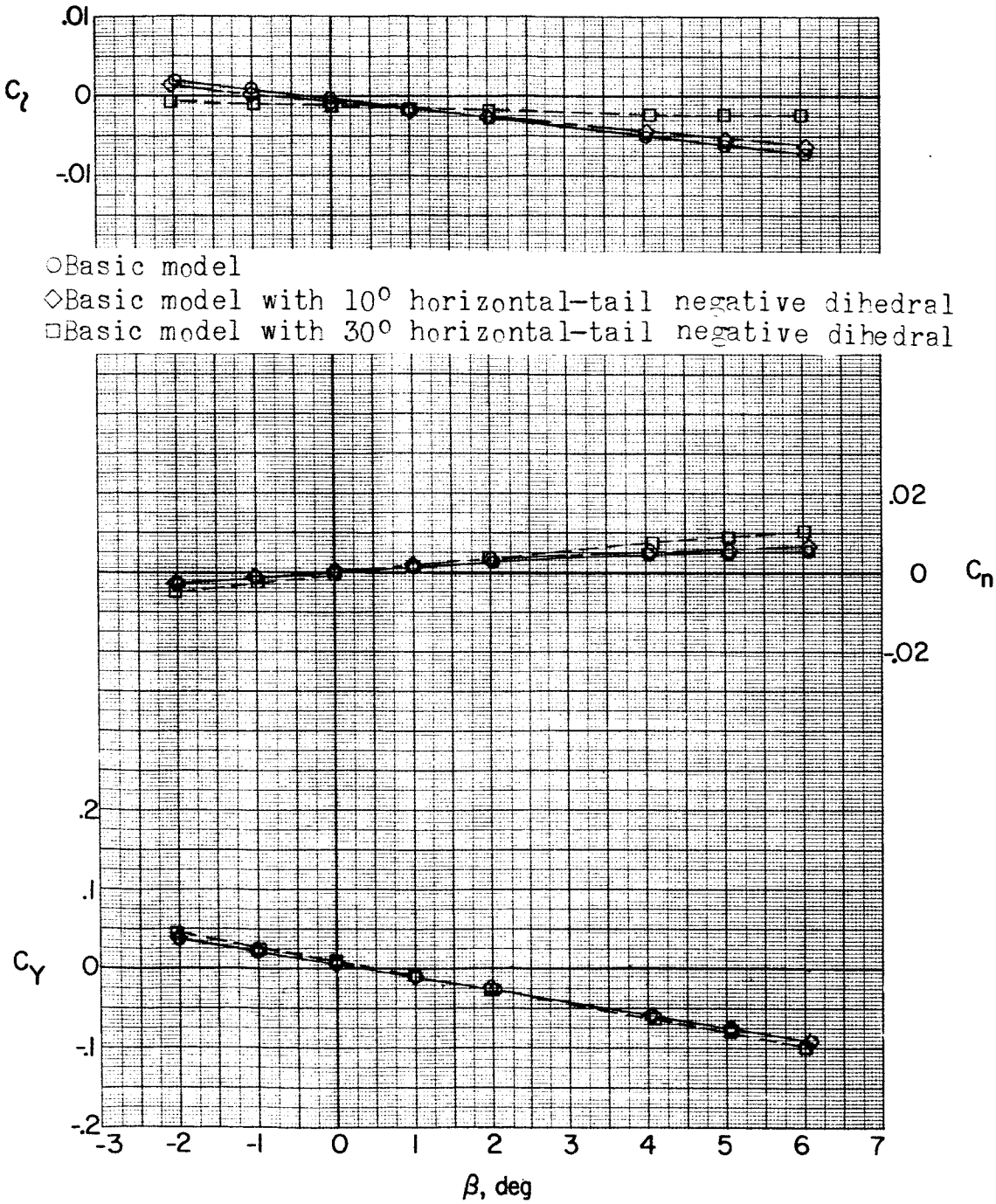

(b) Continued. $\alpha = 10.5^{\circ}$.

Figure 20.- Continued.

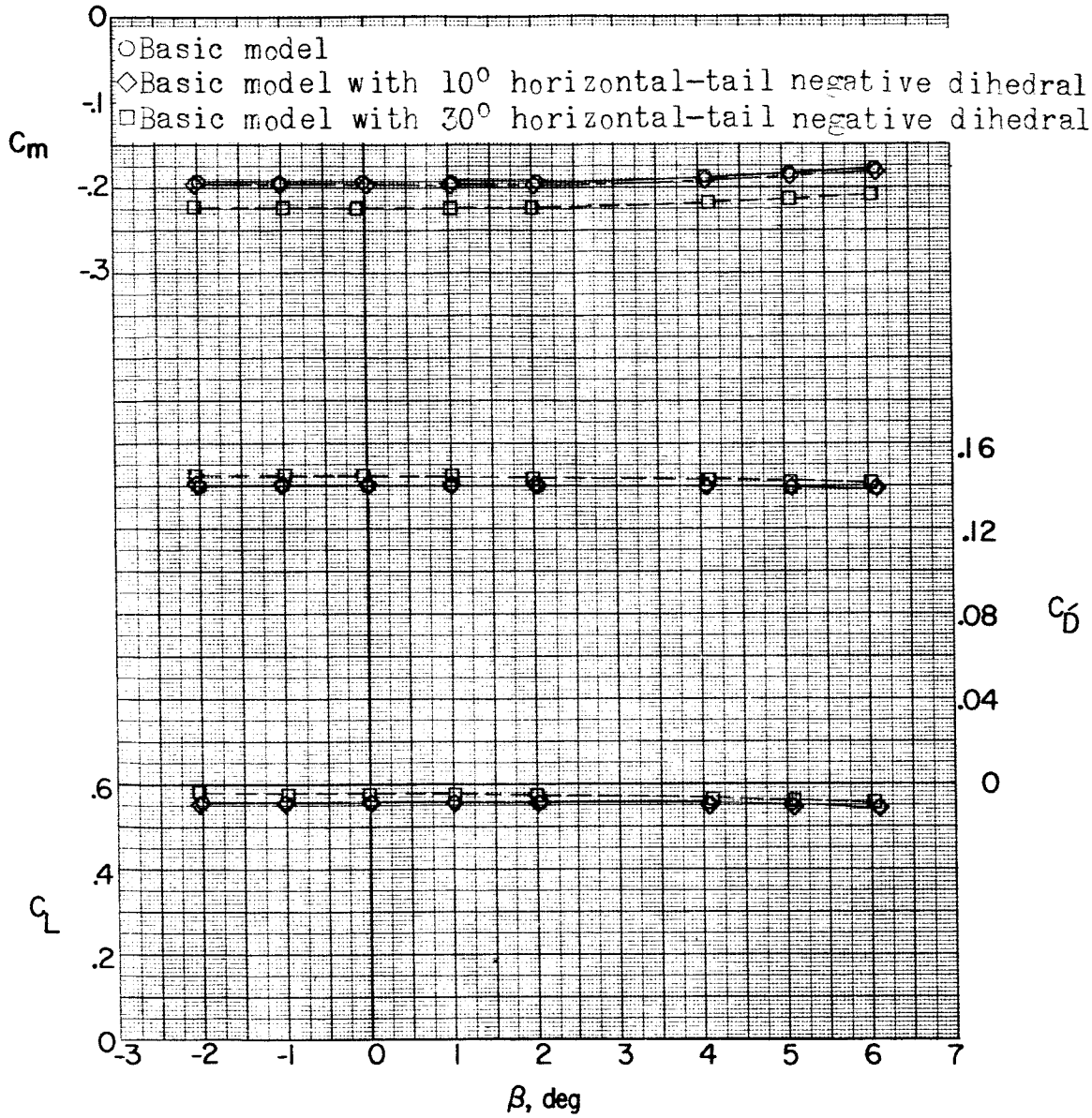

(b) Concluded. $\alpha = 10.5^{\circ}$.

Figure 20.- Continued.

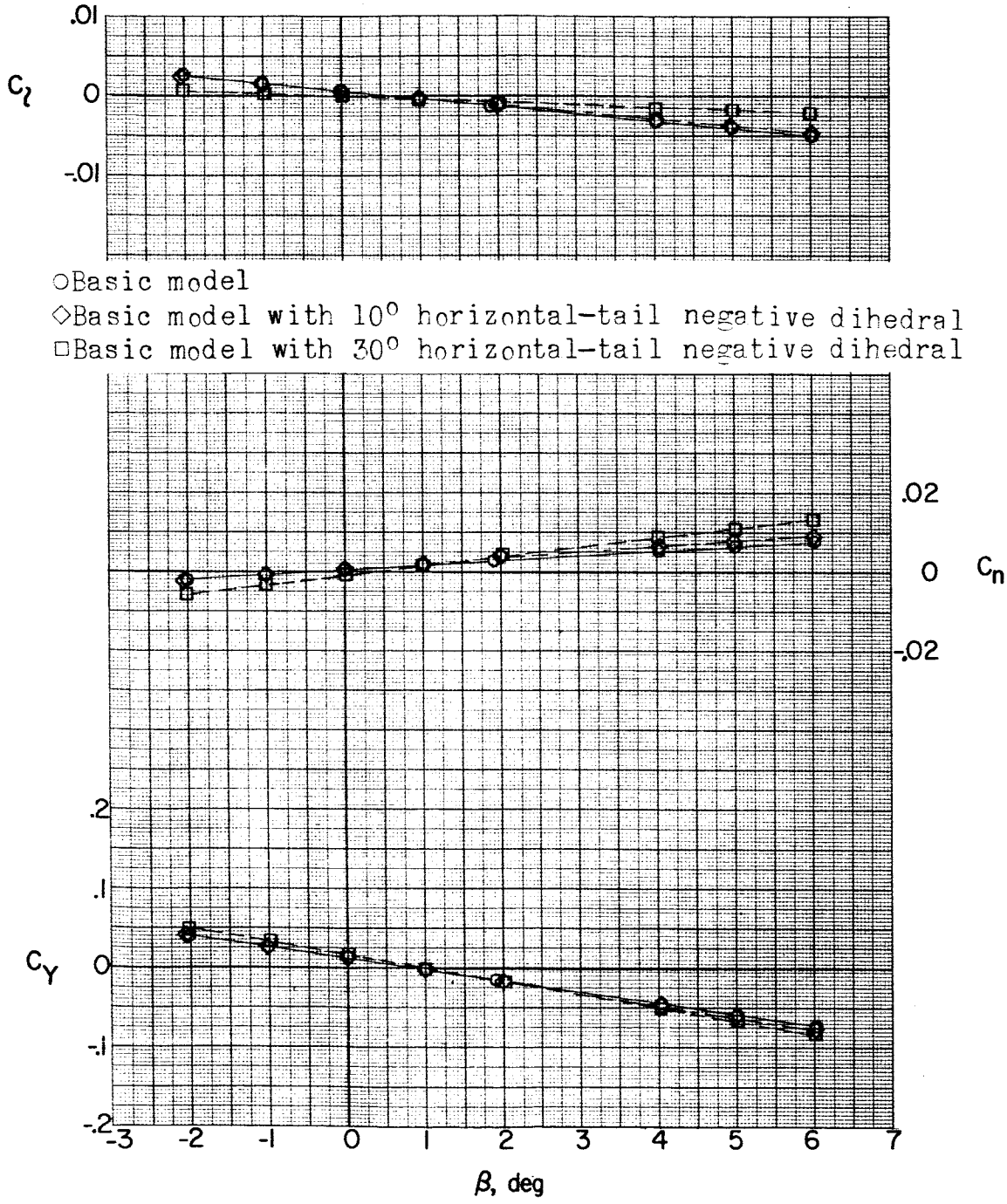

(c) M = 2.06. α = 0°.

Figure 20.- Continued.

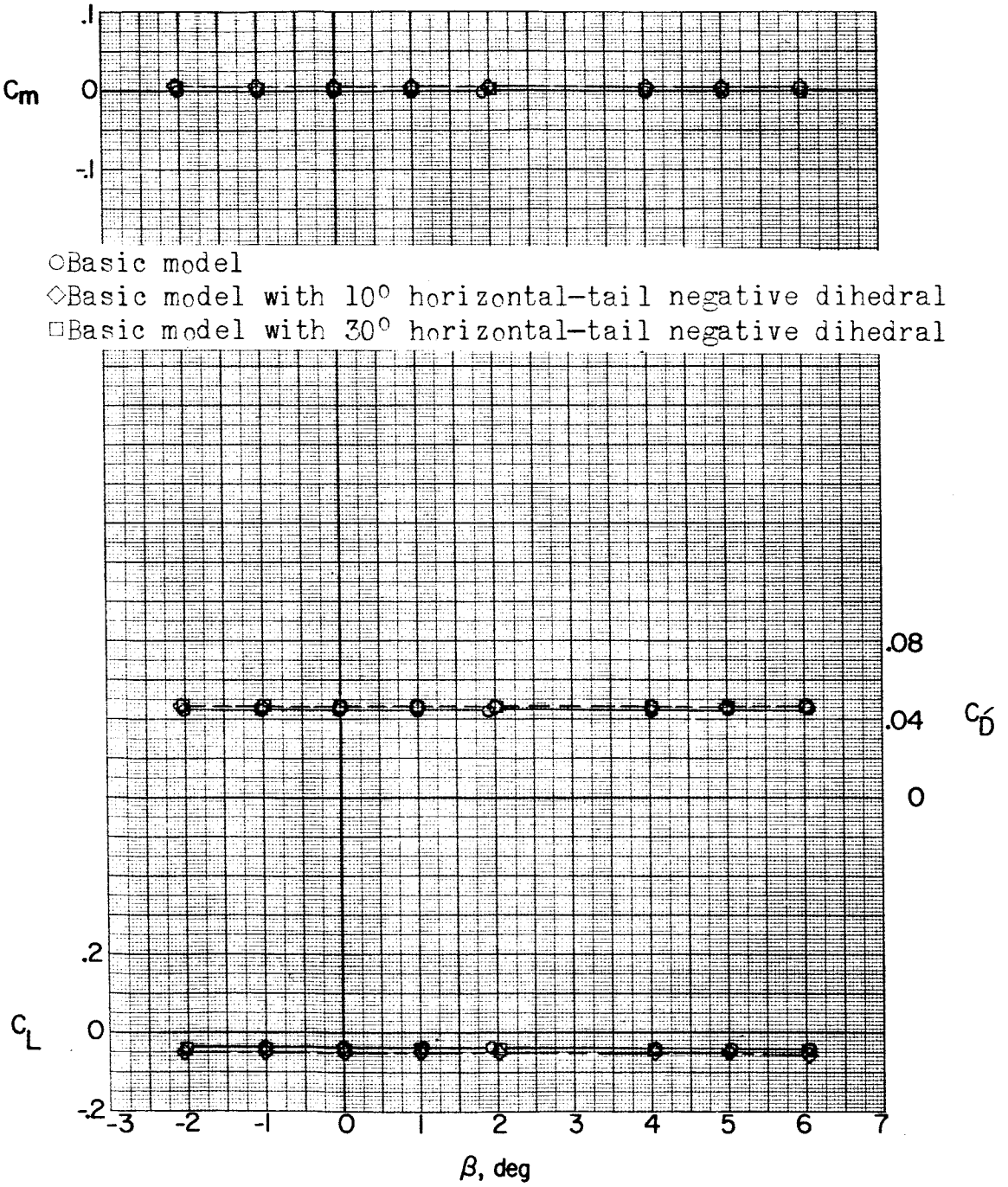

(c) Continued. $\alpha = 0^{\circ}$.

Figure 20.- Continued.

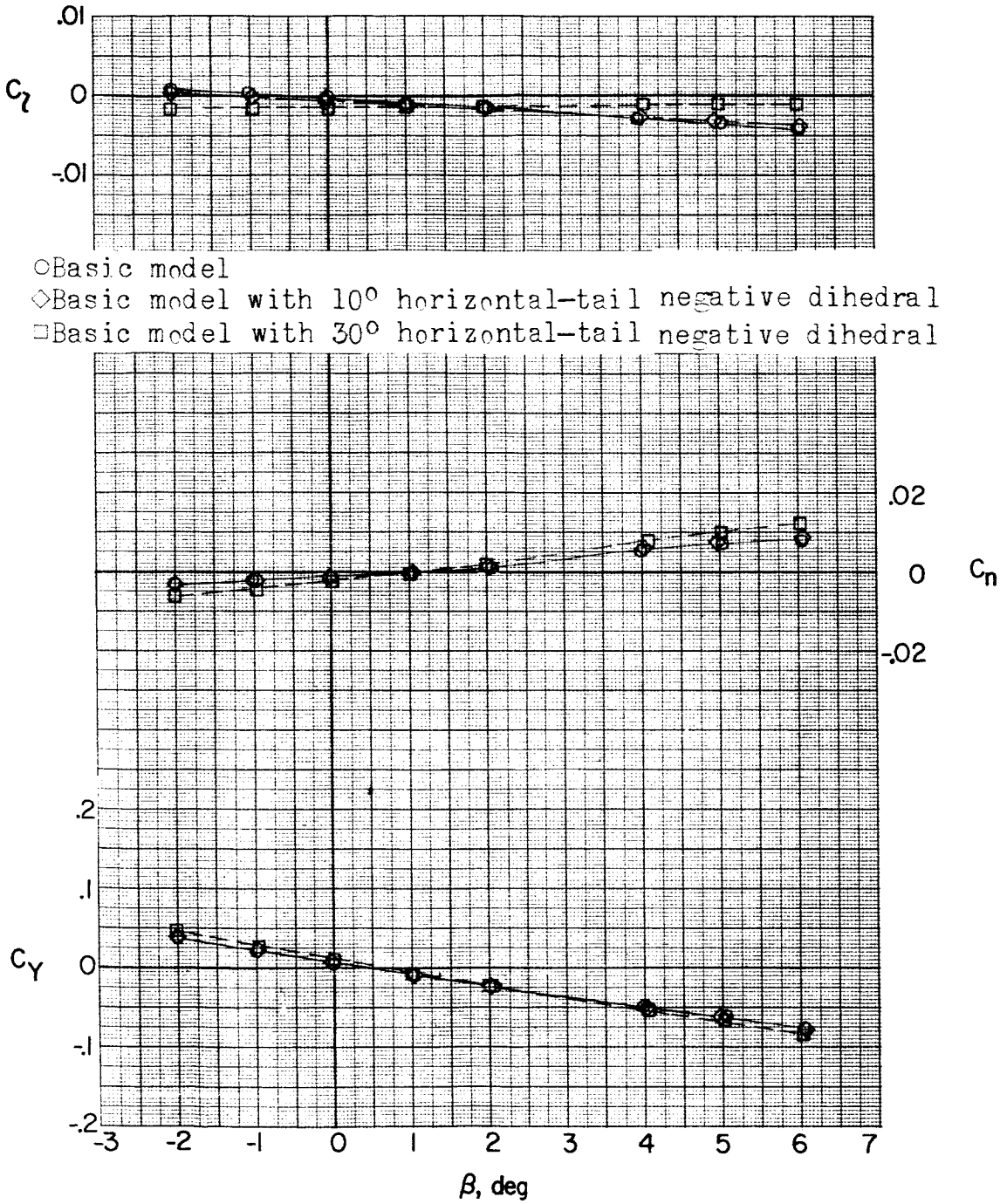

(c) Continued. $\alpha = 5.2^{\circ}$.

Figure 20.- Continued.

[redacted]

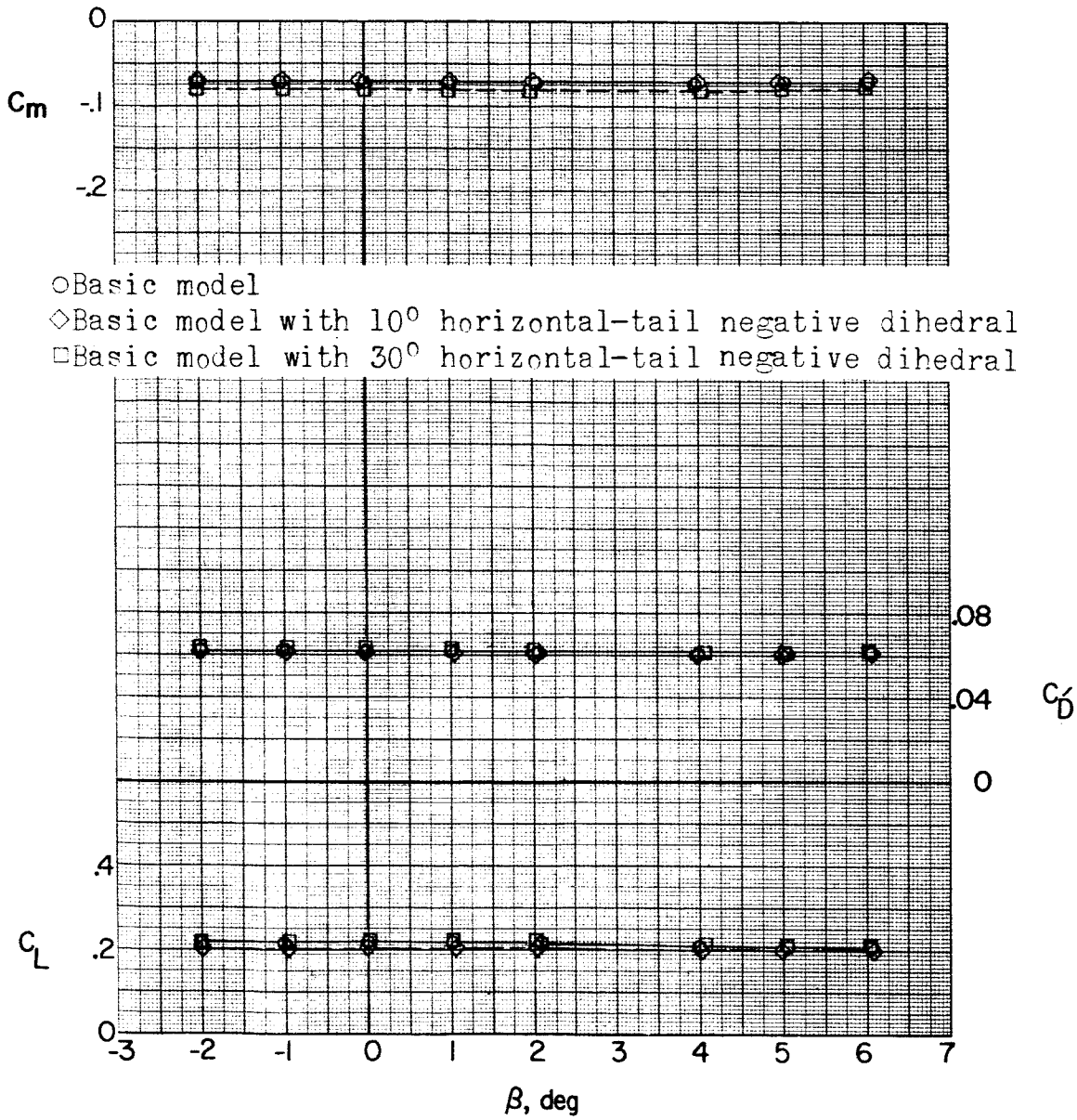

(c) Continued. $\alpha = 5.2^{\circ}$.

Figure 20.- Continued.

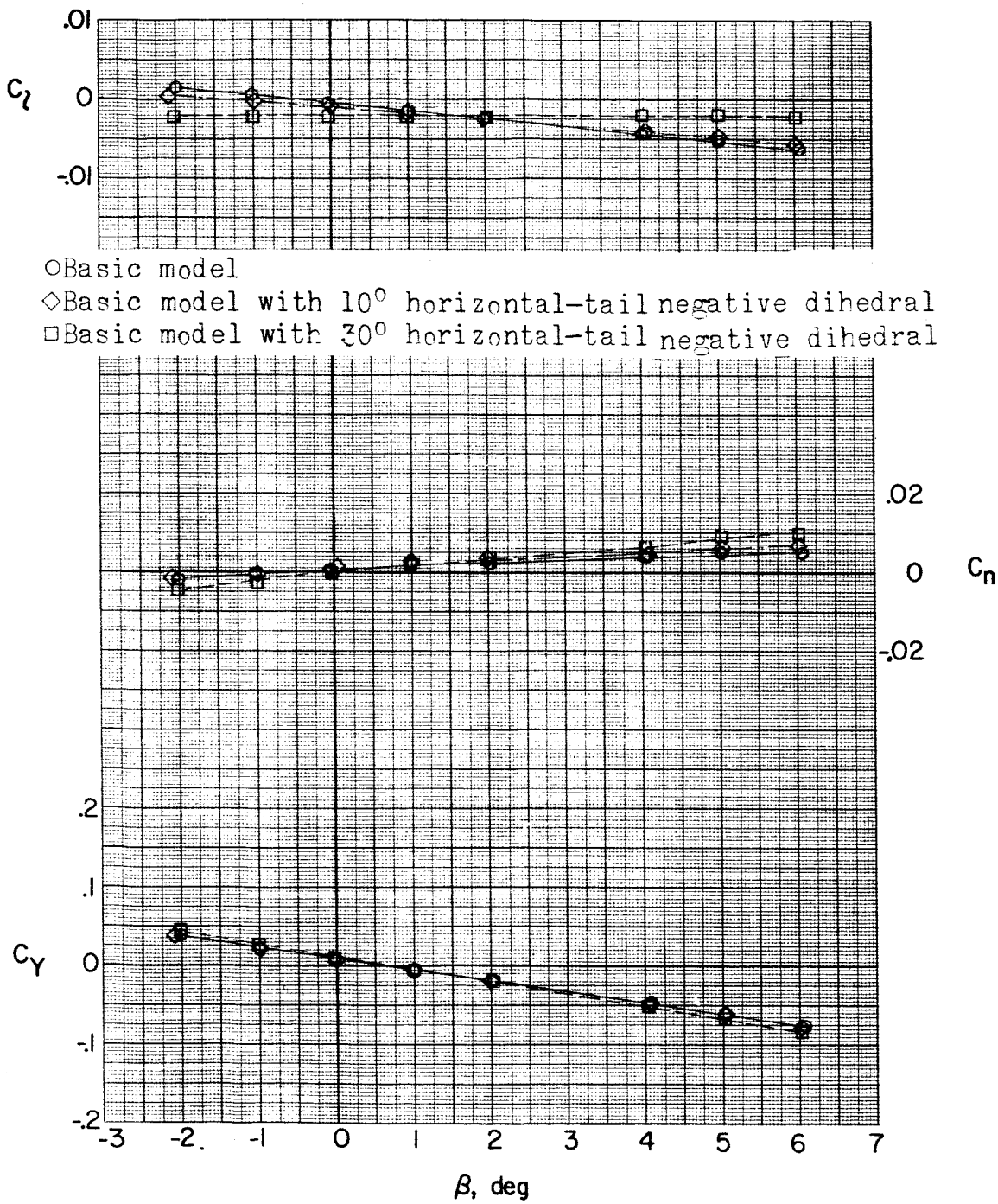

(c) Continued. $\alpha = 10.4^{\circ}$.

Figure 20.- Continued.

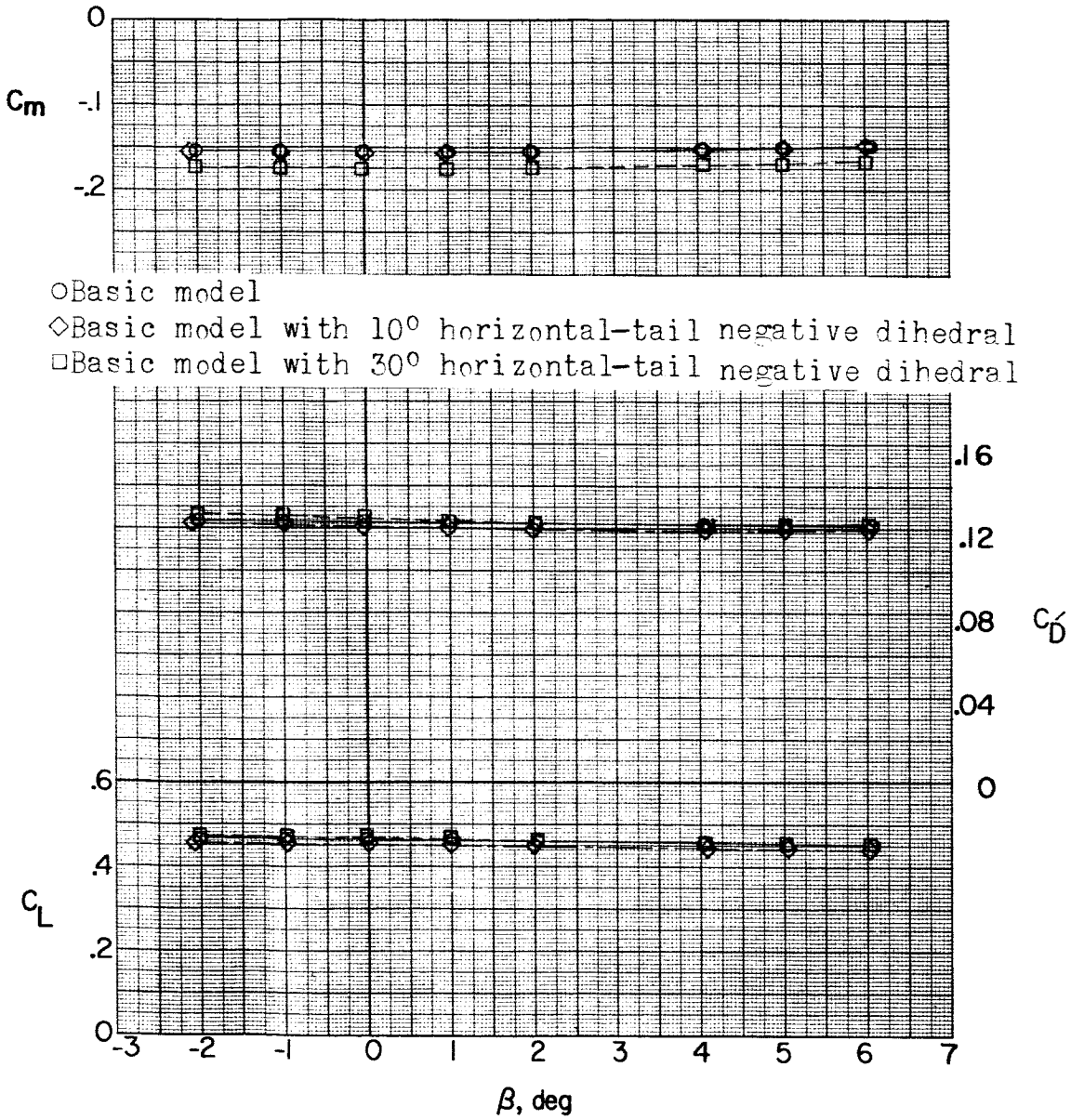

(c) Concluded. $\alpha = 10.4^{\circ}$.

Figure 20.- Concluded.

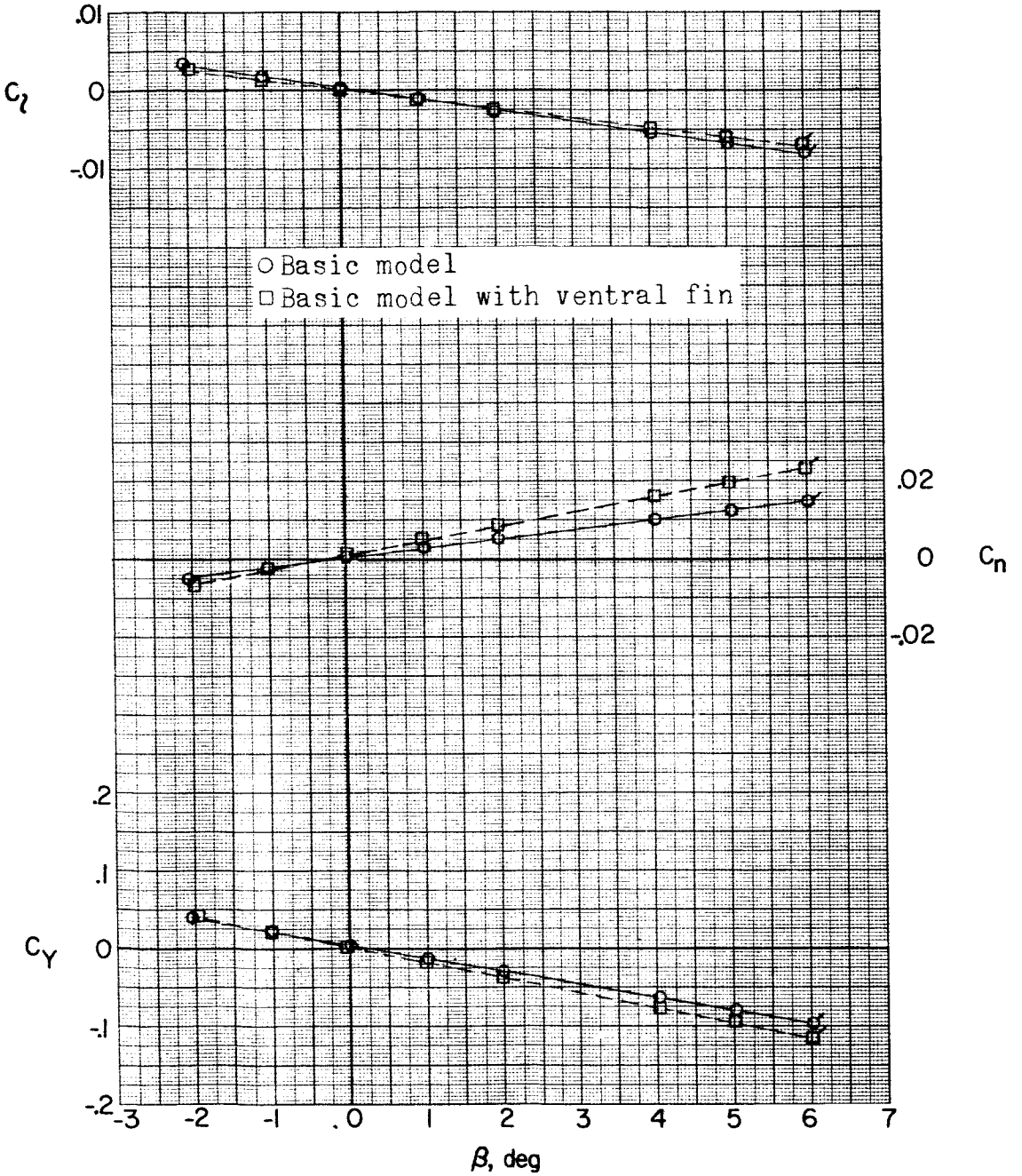

(a) M = 1.56; α = 0°.

Figure 21.- Effect of ventral fins on aerodynamic characteristics in sideslip. Flagged symbols denote wall-reflected shock waves striking the tail.

DECLASSIFIED

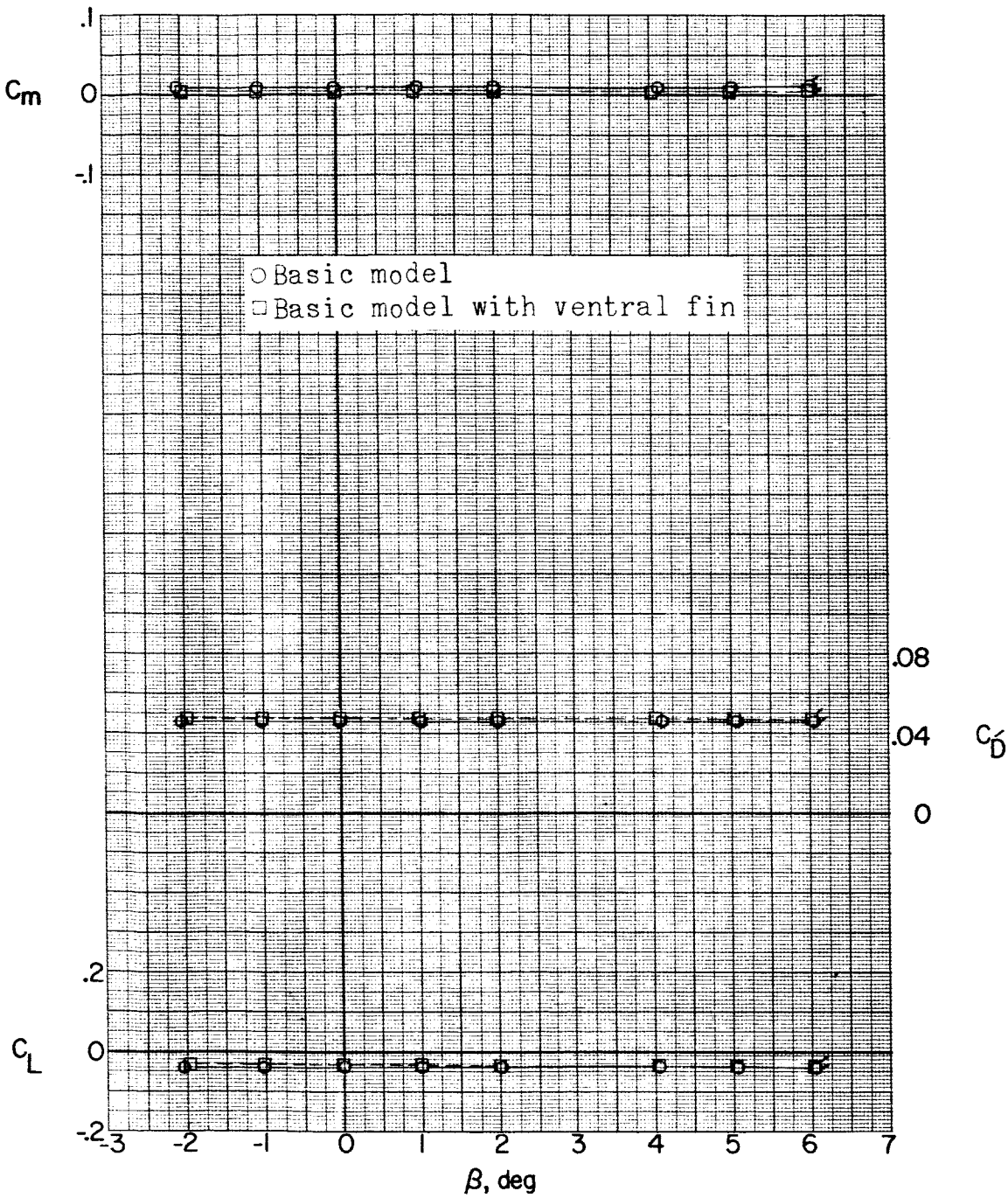

(a) Continued. $\alpha = 0^{\circ}$.

Figure 21.- Continued.

[redacted]

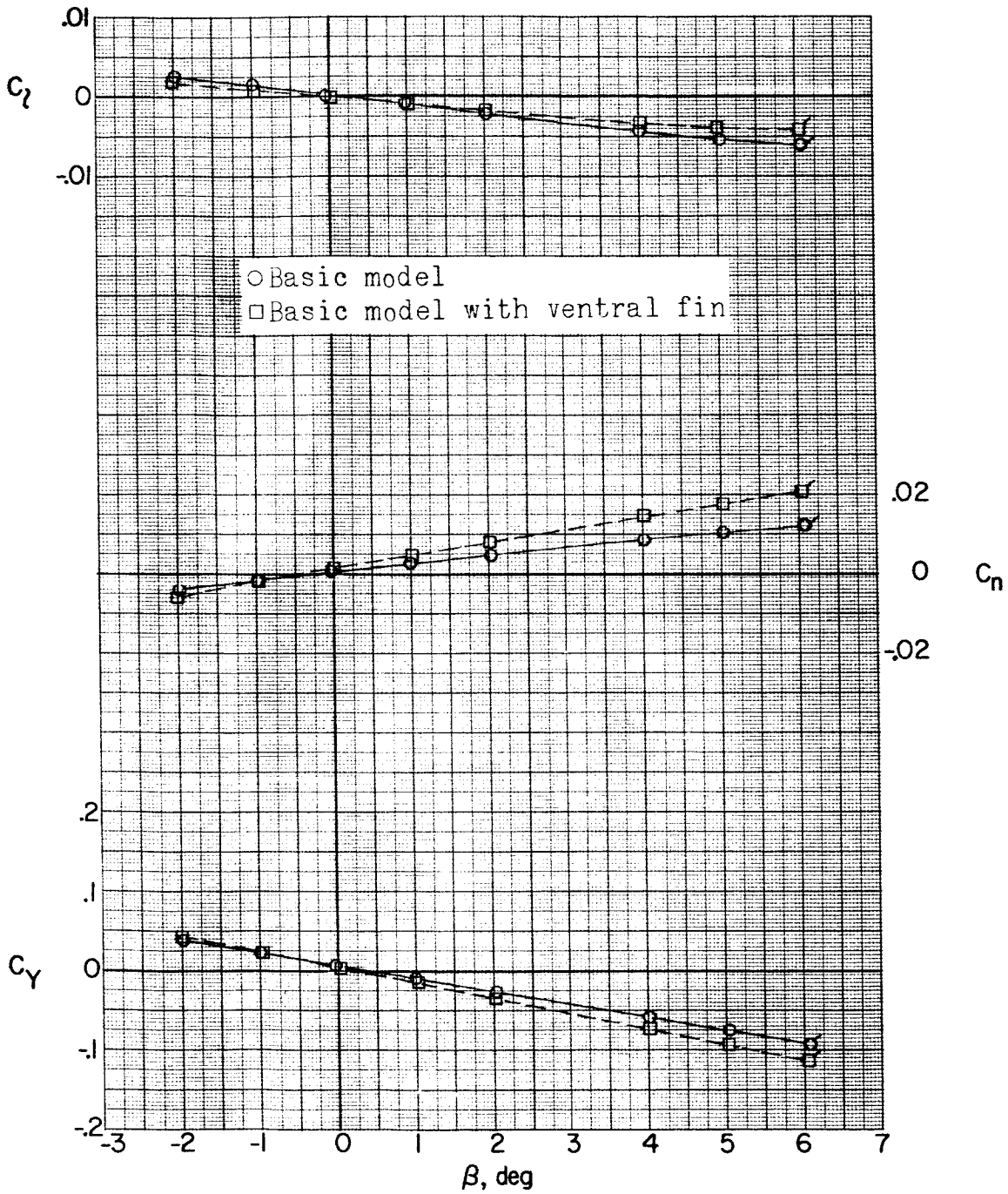

(a) Continued. $\alpha = 5.3^{\circ}$.

Figure 21.- Continued.

DECLASSIFIED

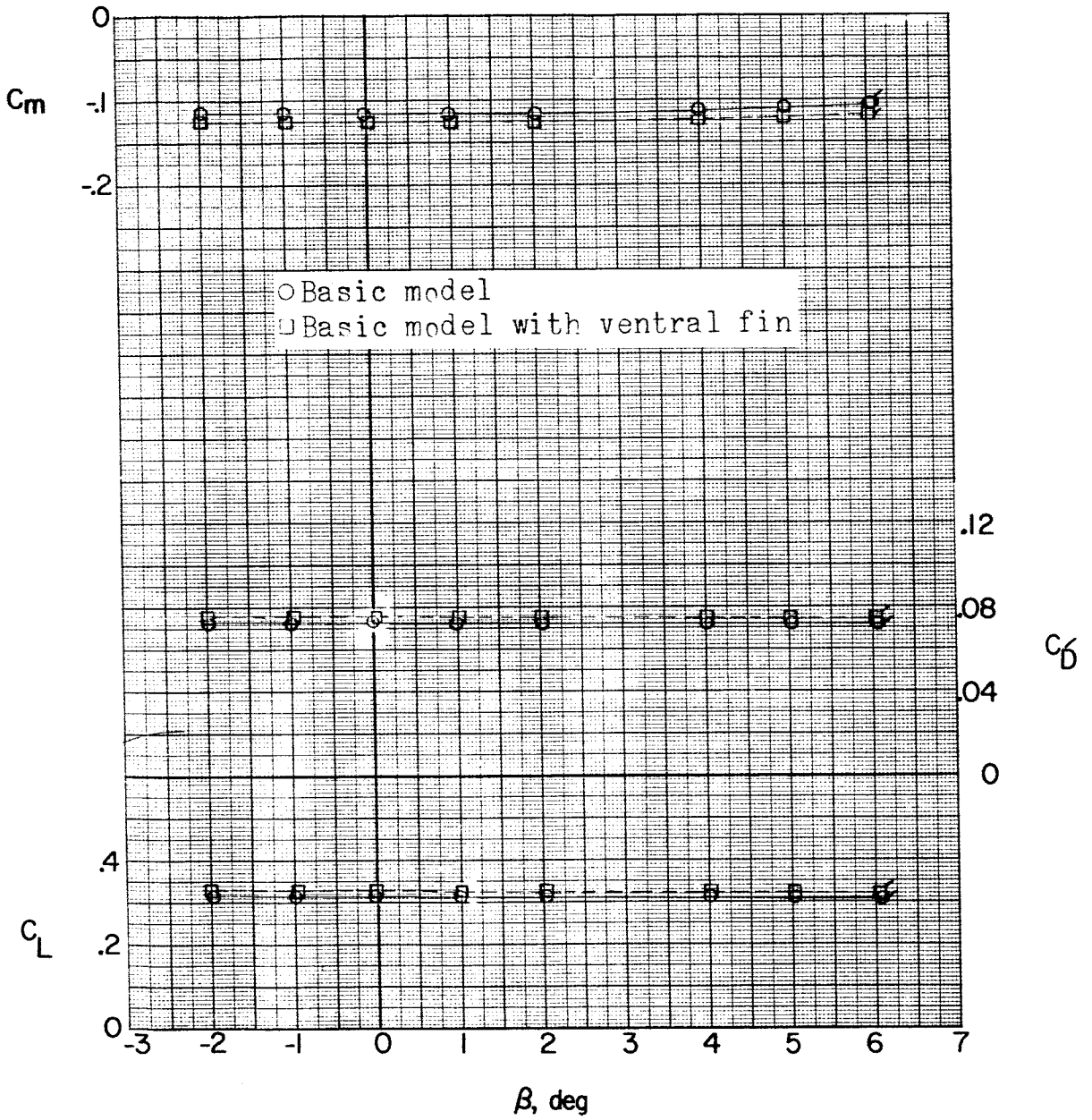

(a) Continued. $\alpha = 5.3^{\circ}$.

Figure 21.- Continued.

[redacted]

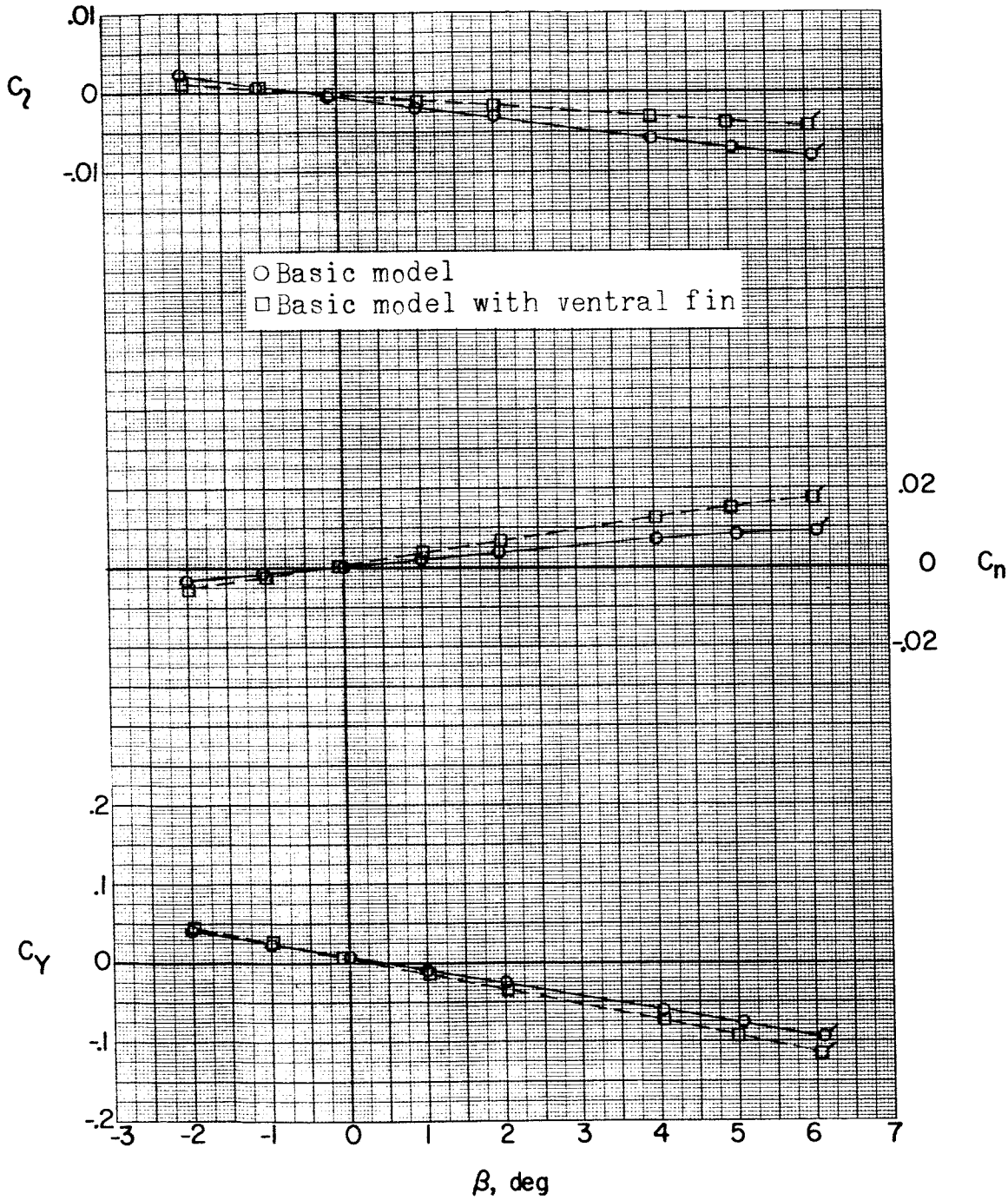

(a) Continued. $\alpha = 10.6^{\circ}$.

Figure 21.- Continued.

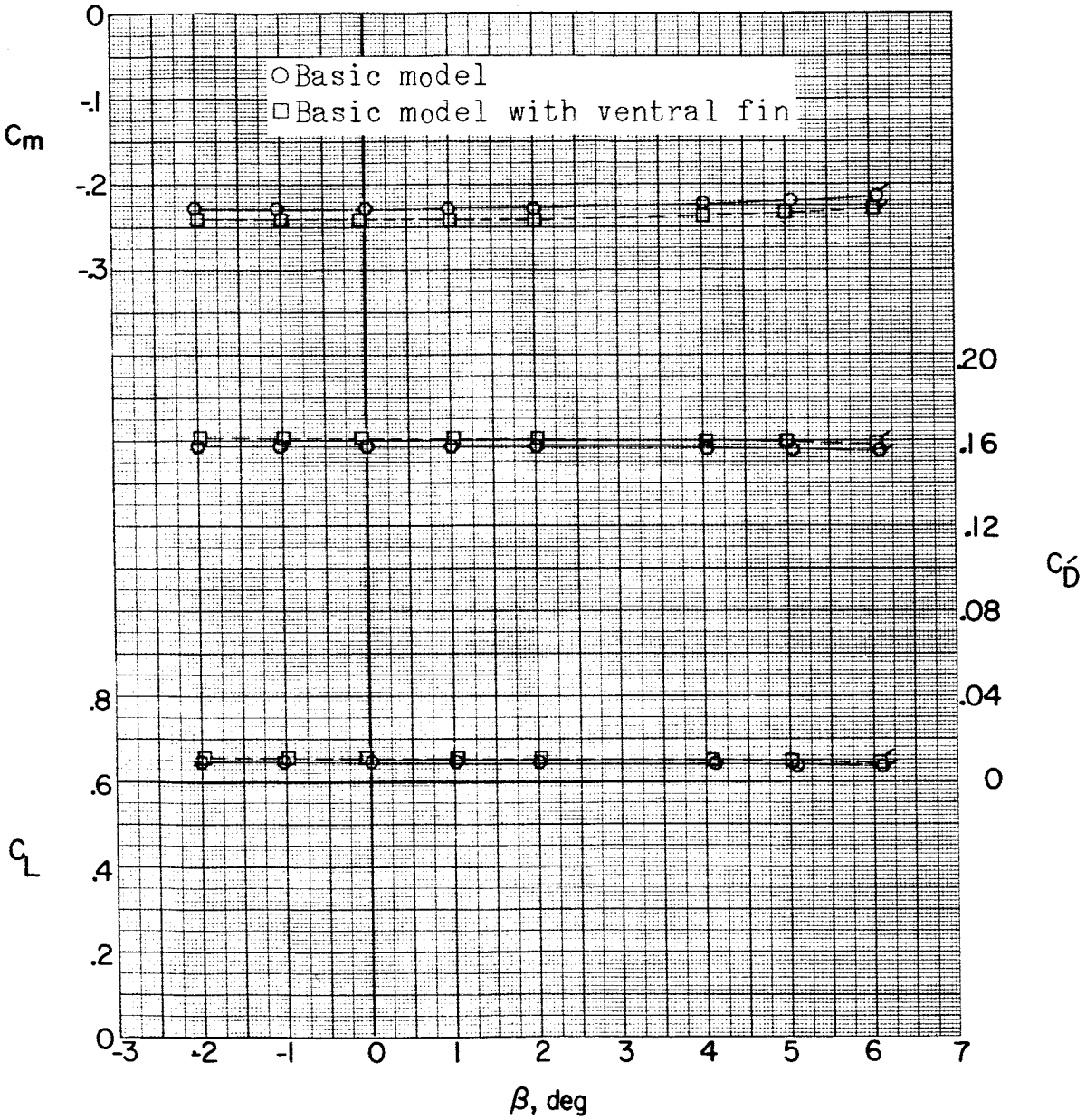

(a) Concluded. $\alpha = 10.6^{\circ}$.

Figure 21.- Continued.

DECLASSIFIED

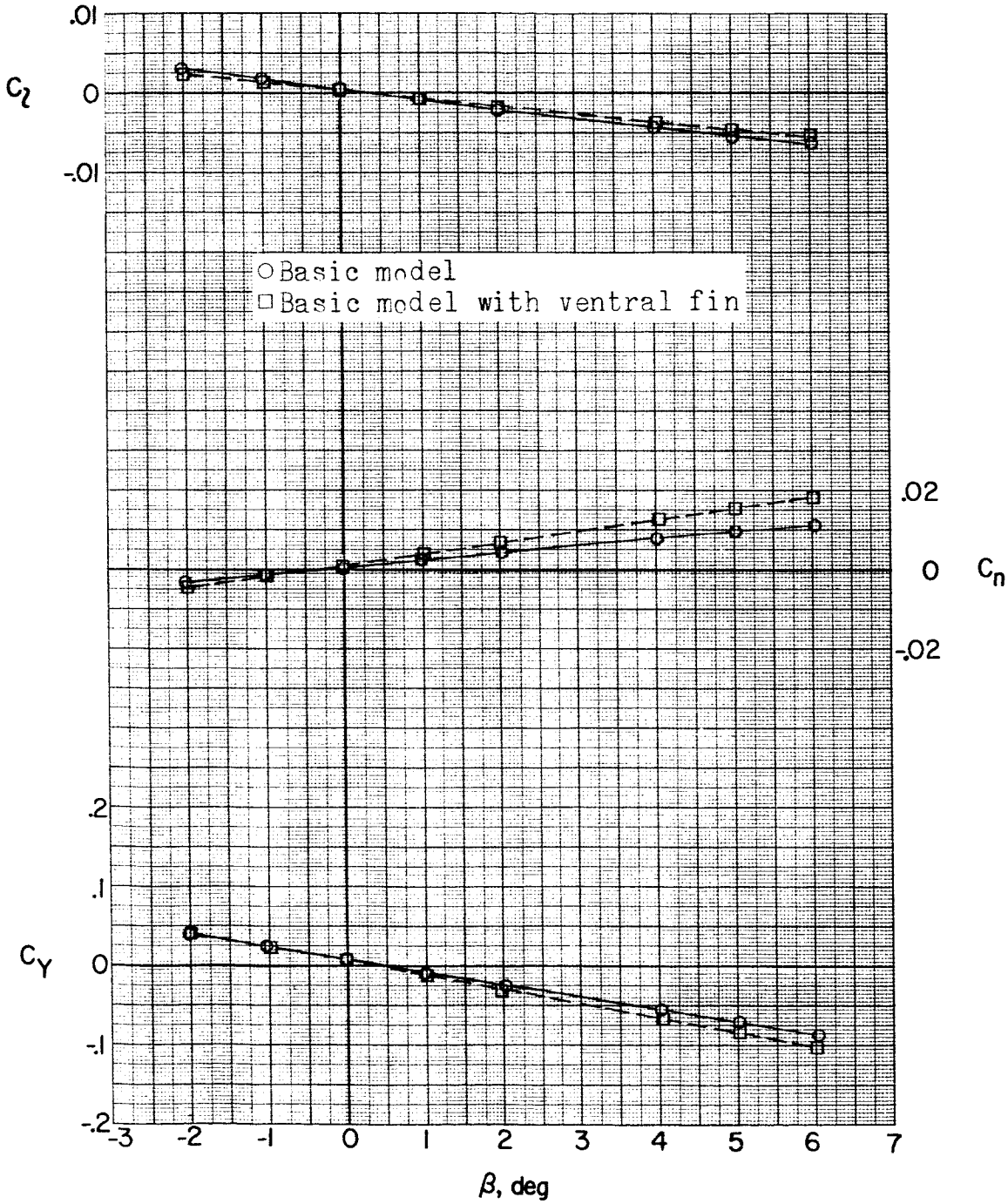

(b) M = 1.76. α = 0°.

Figure 21.- Continued.

[redacted]

DECLASSIFIED

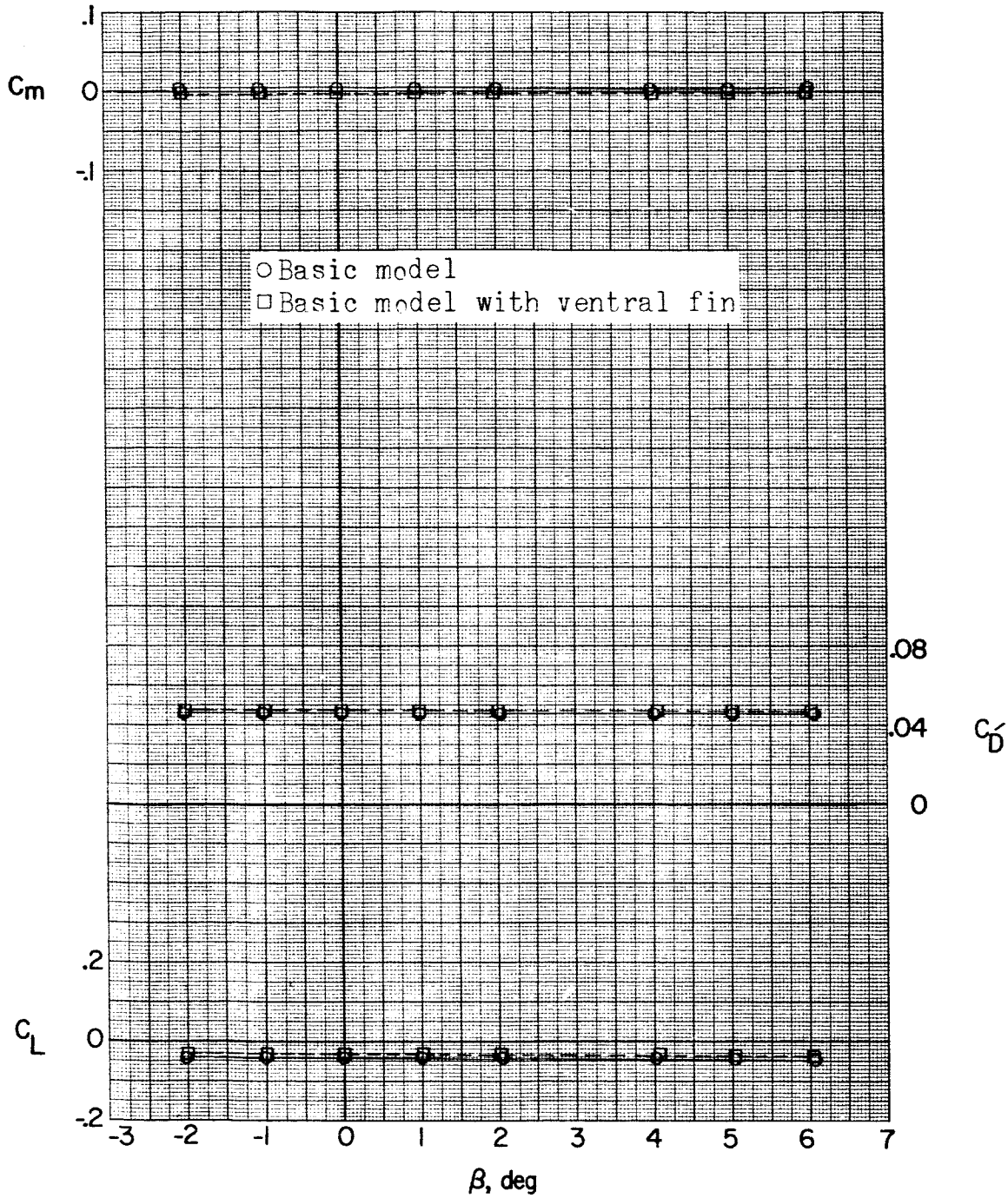

(b) Continued. $\alpha = 0^{\circ}$.

Figure 21.- Continued.

[redacted]

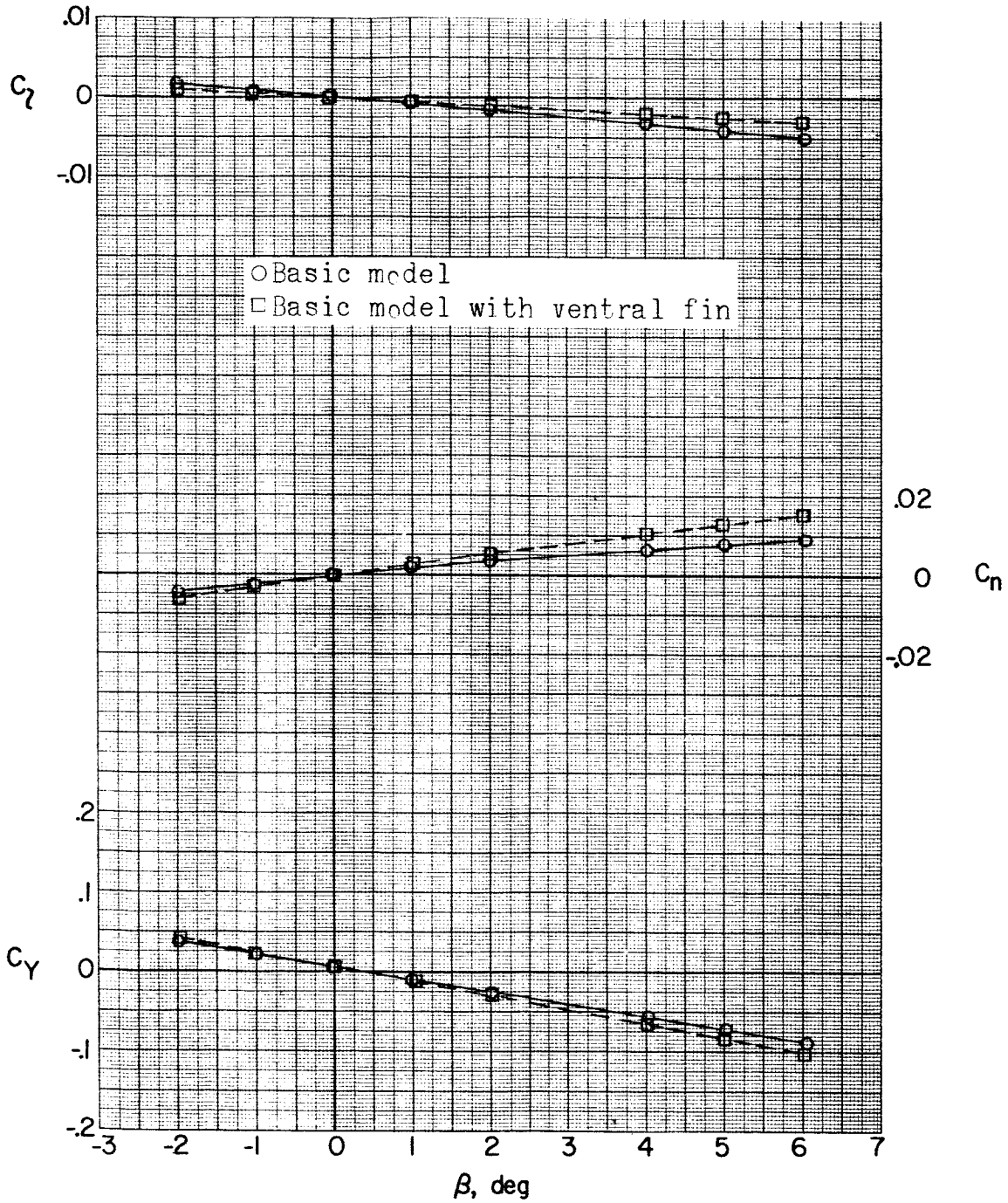

(b) Continued. $\alpha = 5.2^{\circ}$.

Figure 21.- Continued.

[redacted]

DECLASSIFIED

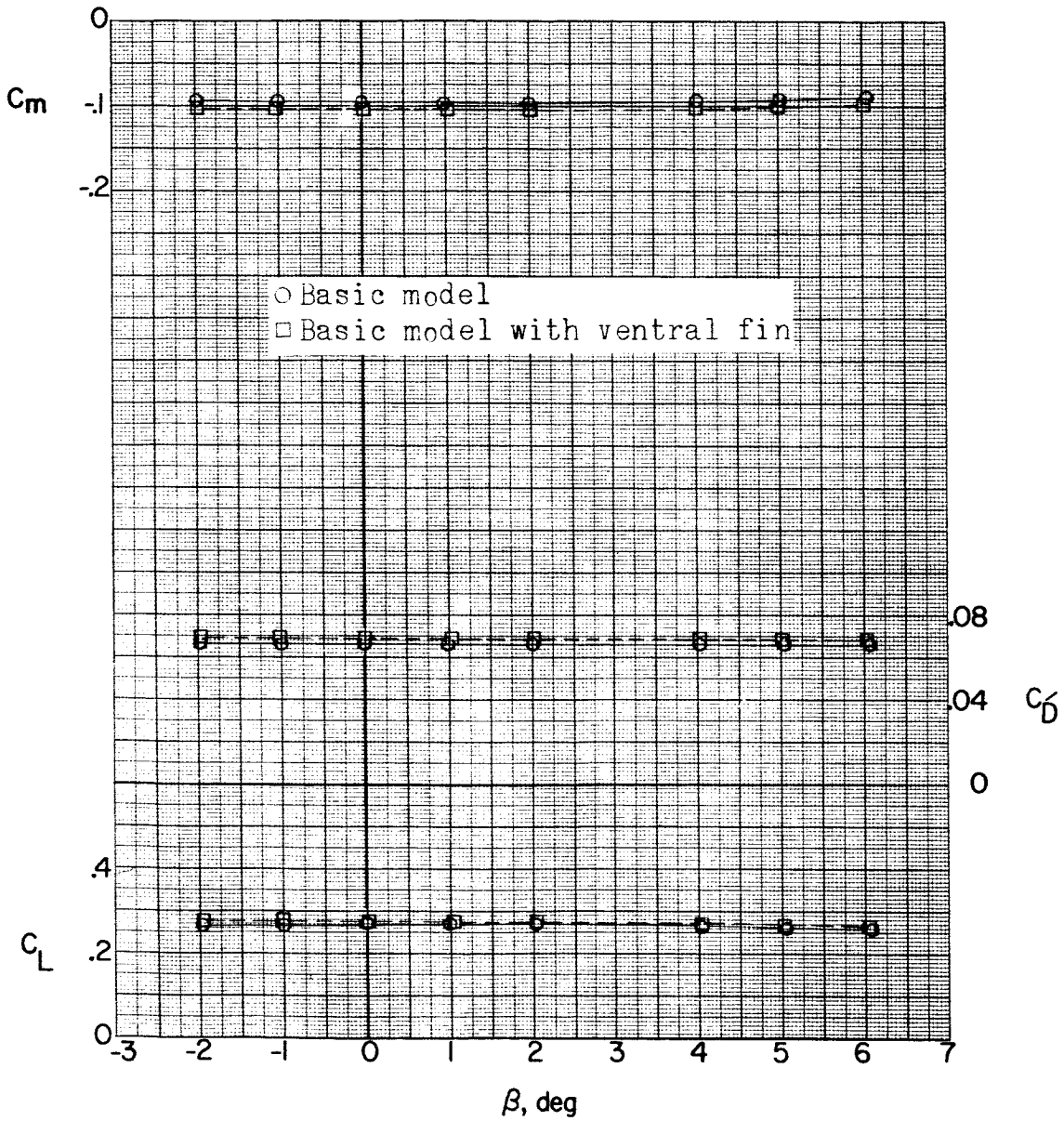

(b) Continued. $\alpha = 5.2^{\circ}$.

Figure 21.- Continued.

[redacted]

DECLASSIFIED

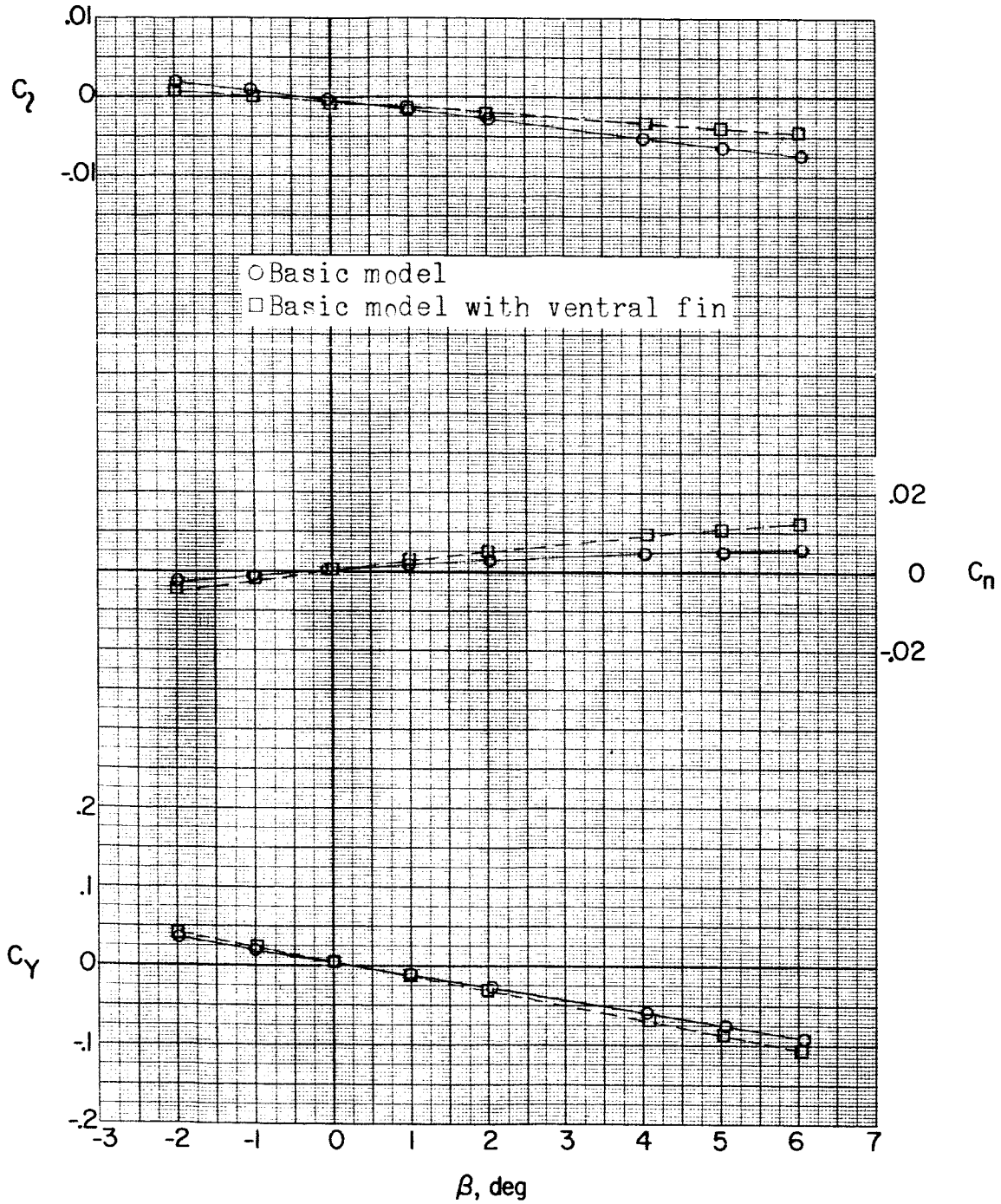

(b) Continued. $\alpha = 10.5^{\circ}$.

Figure 21.- Continued.

[redacted]

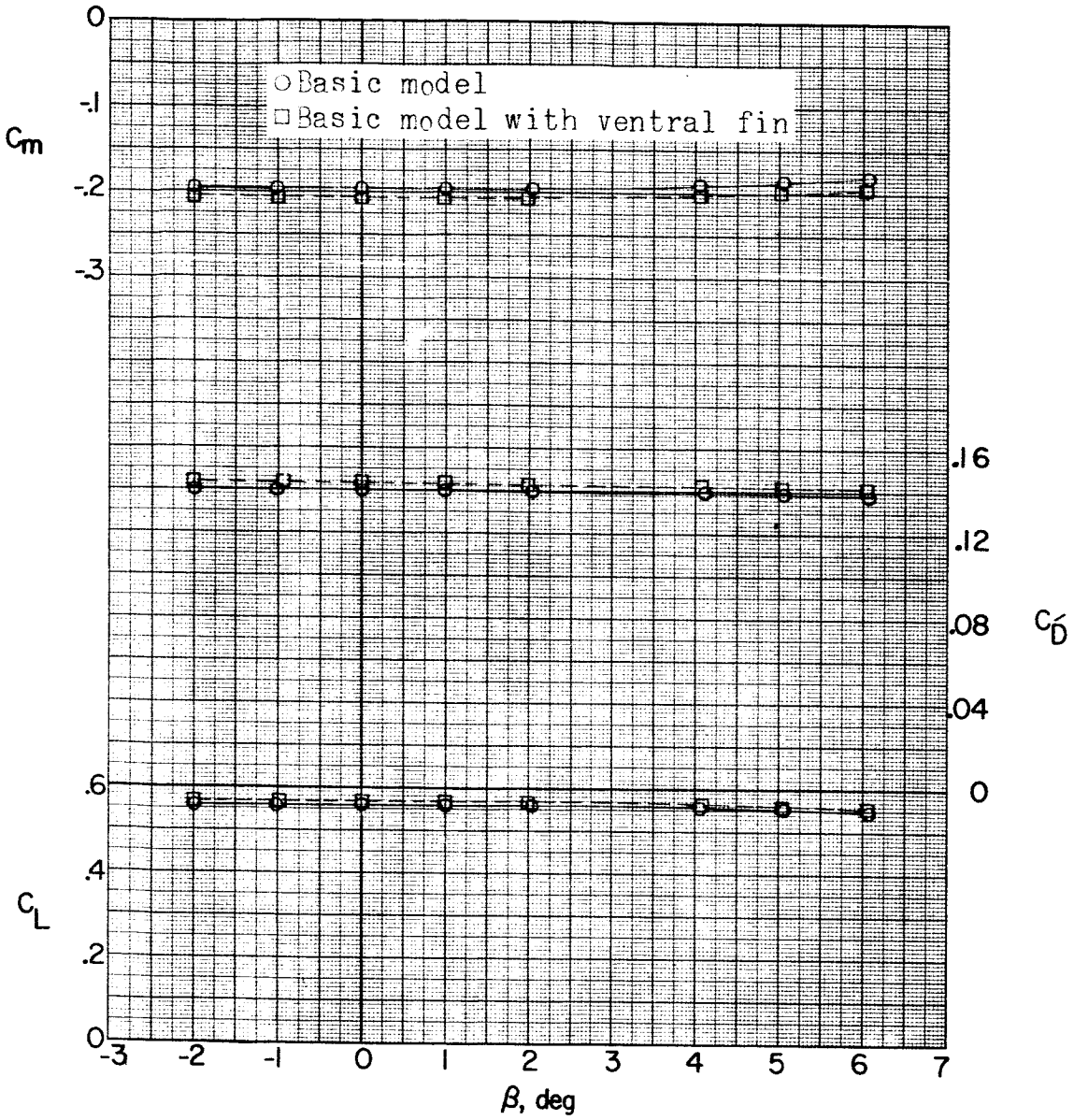

(b) Concluded. $\alpha = 10.5^{\circ}$.

Figure 21.- Continued.

DECLASSIFIED

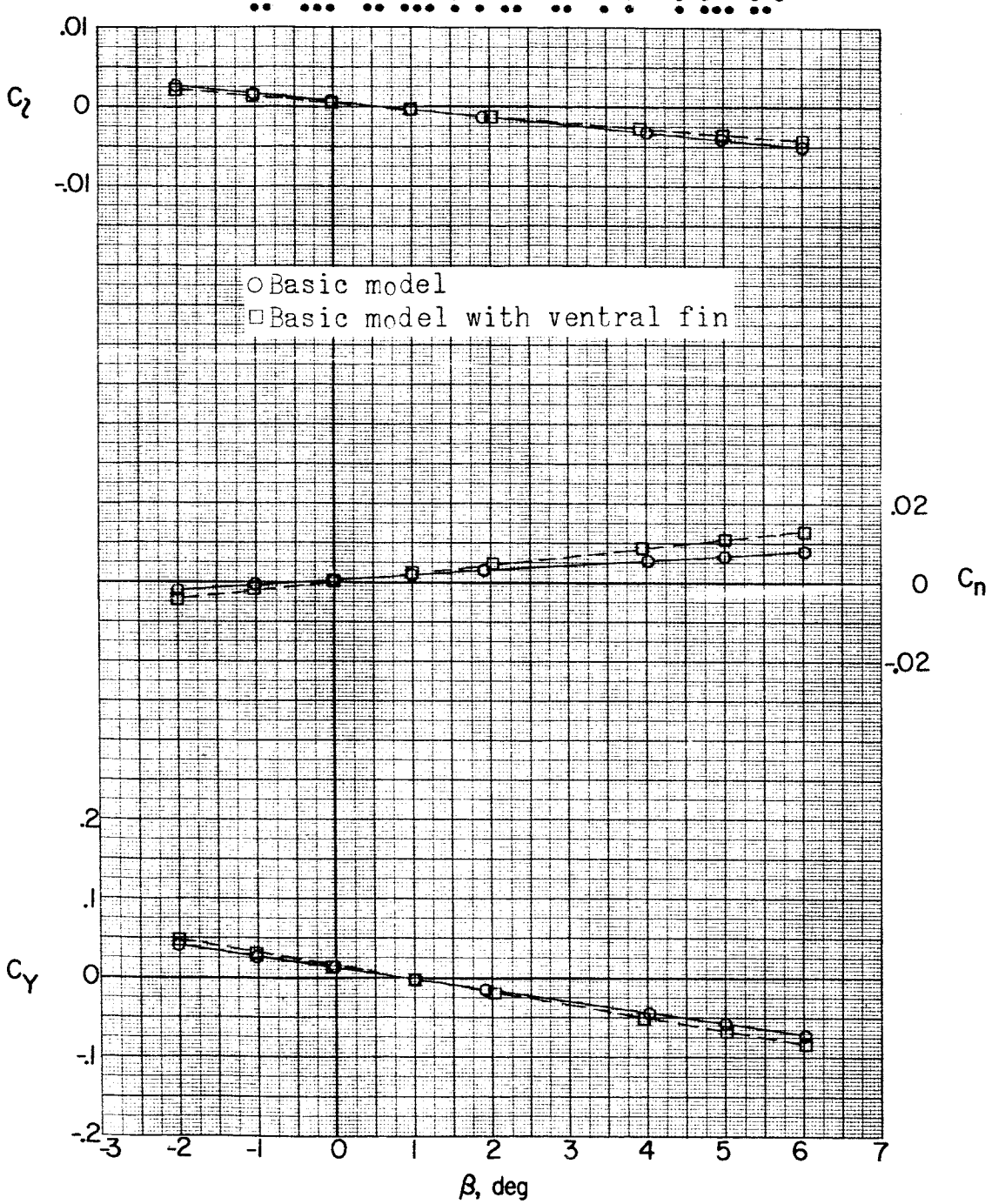

(c) M = 2.06. $\alpha = 0^{\circ}$.

Figure 21.- Continued.

[redacted]

DECLASSIFIED

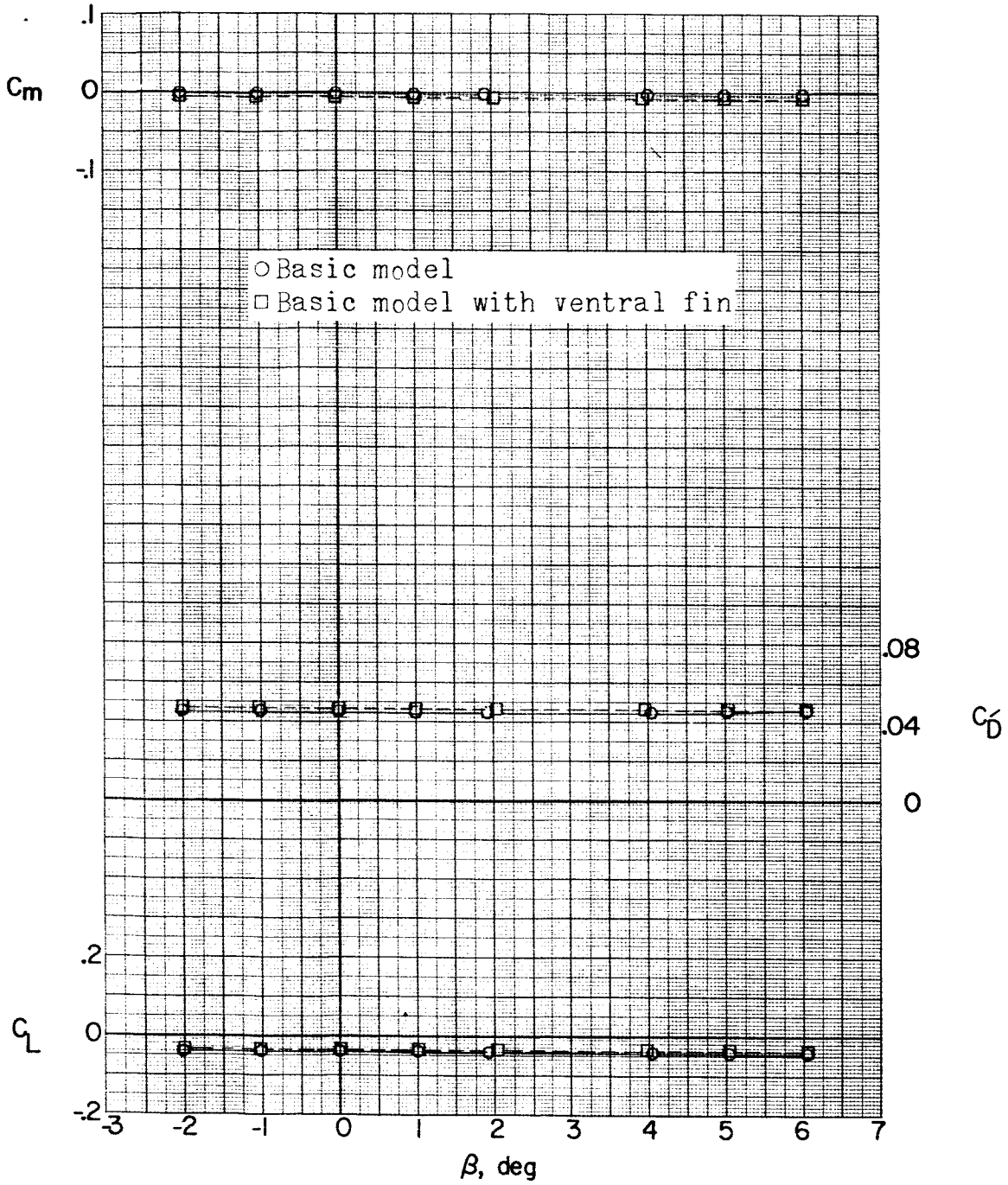

(c) Continued. $\alpha = 0^{\circ}$.

Figure 21.- Continued.

[redacted]

DECLASSIFIED

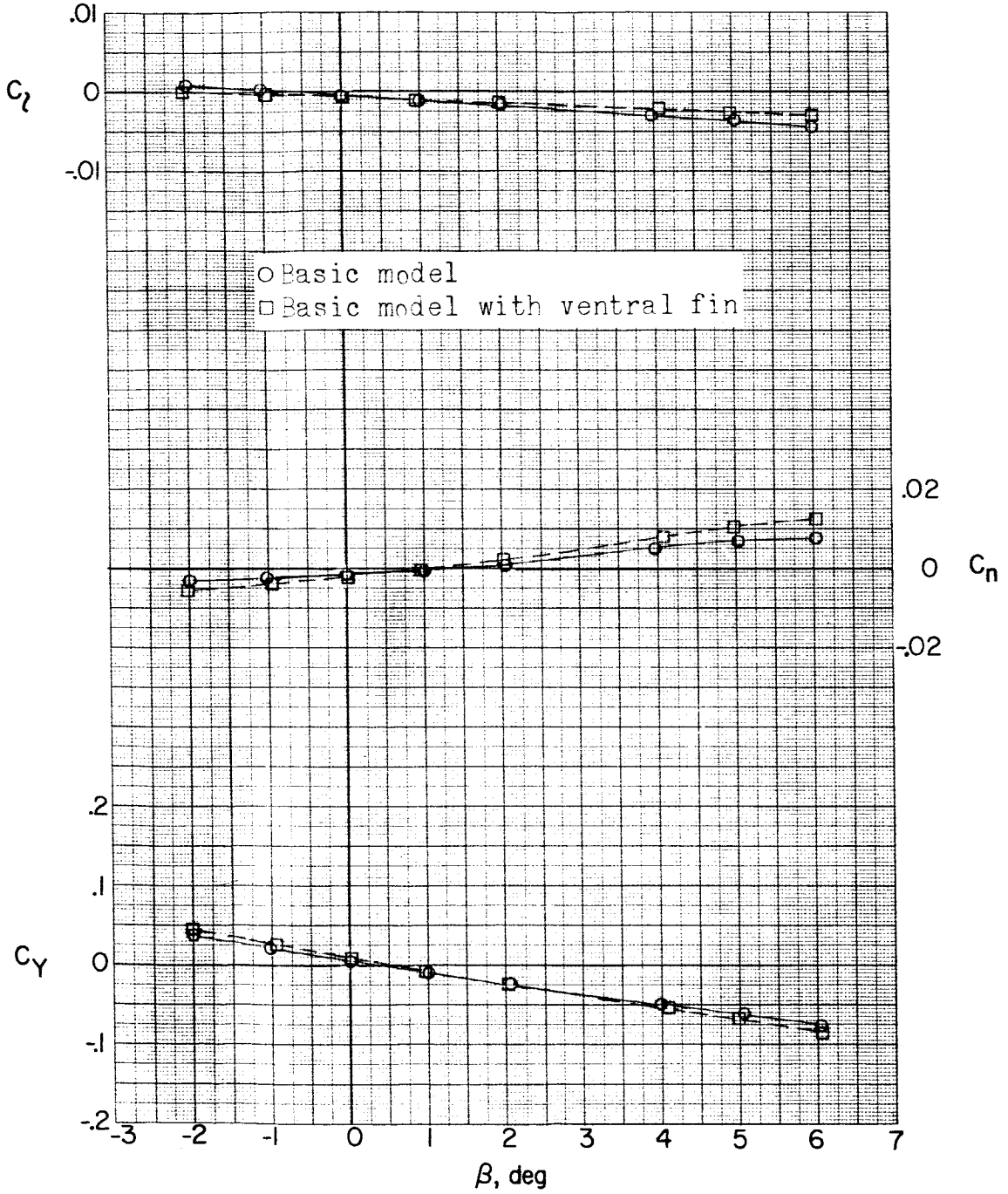

(c) Continued. $\alpha = 5.2^{\circ}$.

Figure 21.- Continued.

[redacted]

DECLASSIFIED

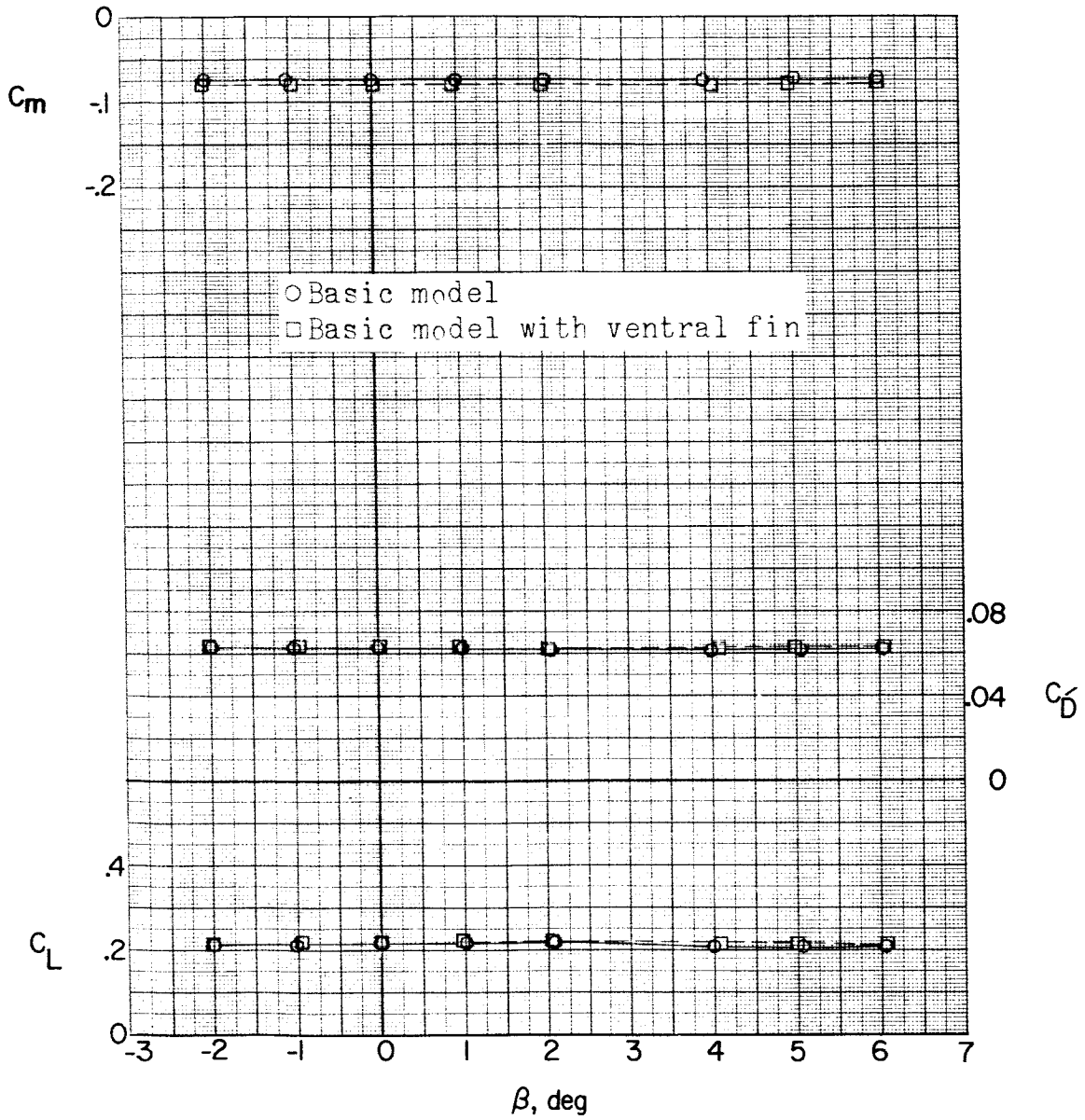

(c) Continued. $\alpha = 5.2^{\circ}$.

Figure 21.- Continued.

DECLASSIFIED

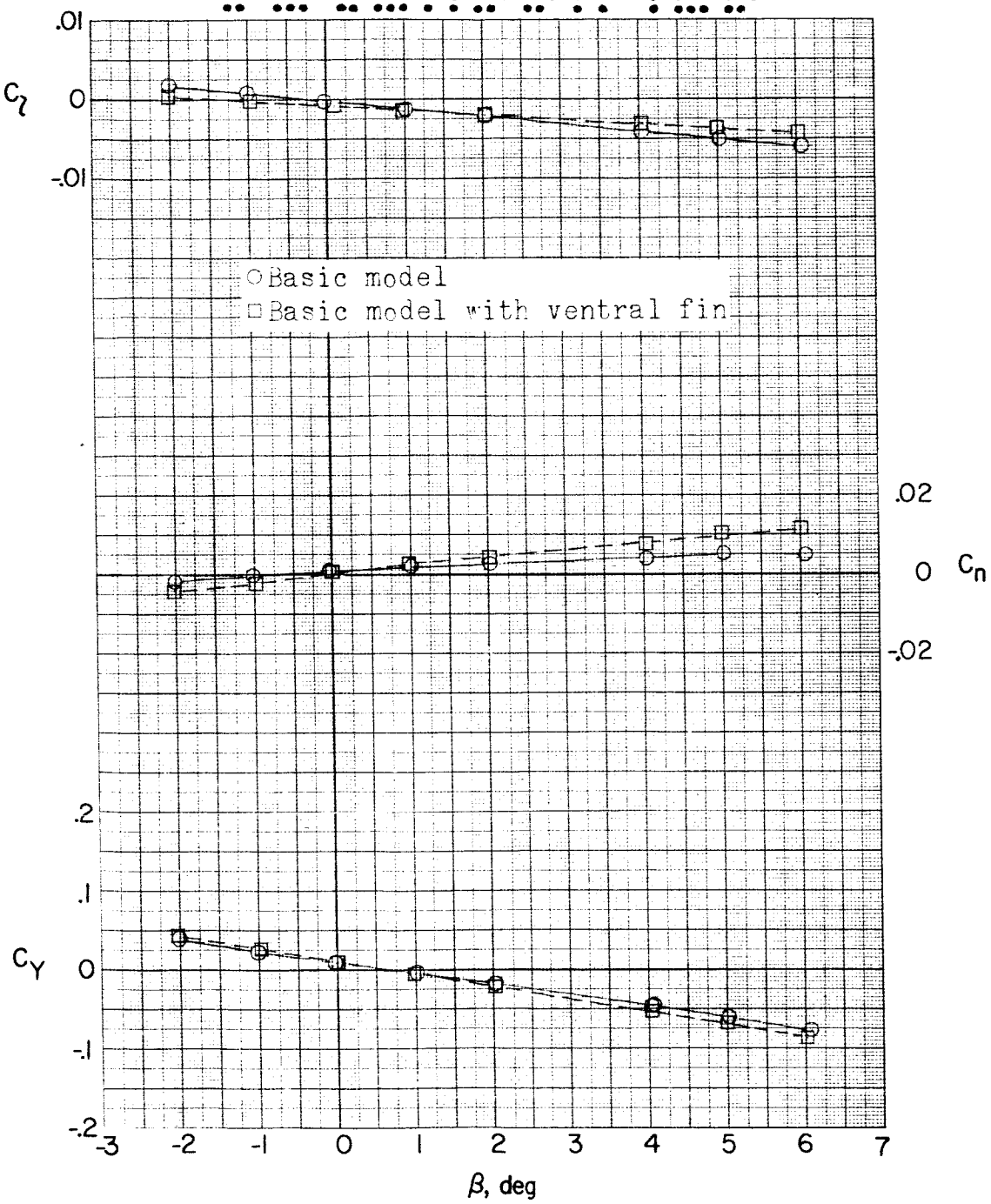

(c) Continued. $\alpha = 10.4^{\circ}$.

Figure 21.- Continued.

[redacted]

DECLASSIFIED

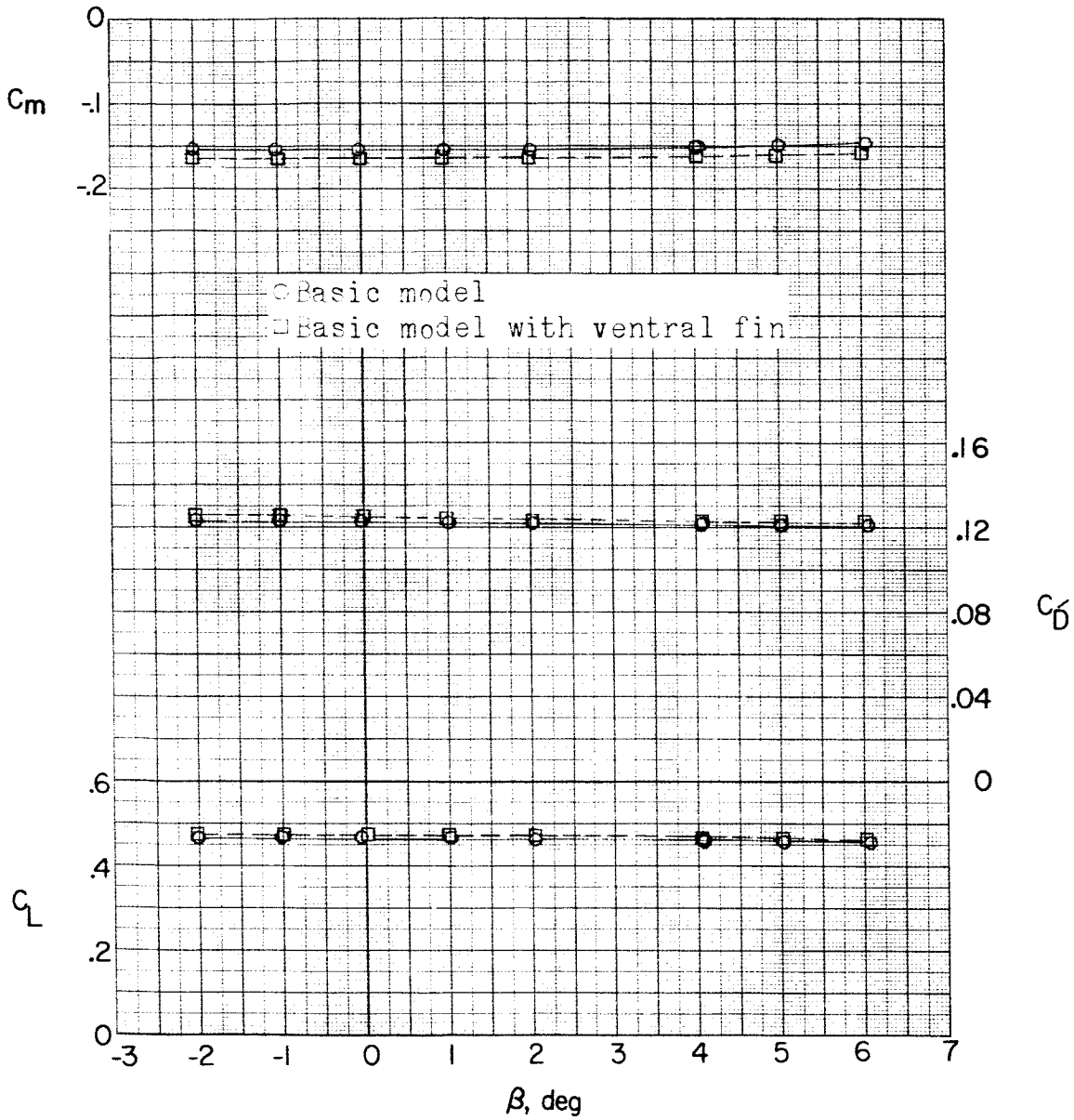

(c) Concluded. $\alpha = 10.4^{\circ}$.

Figure 21.- Concluded.

[redacted]

DECLASSIFIED

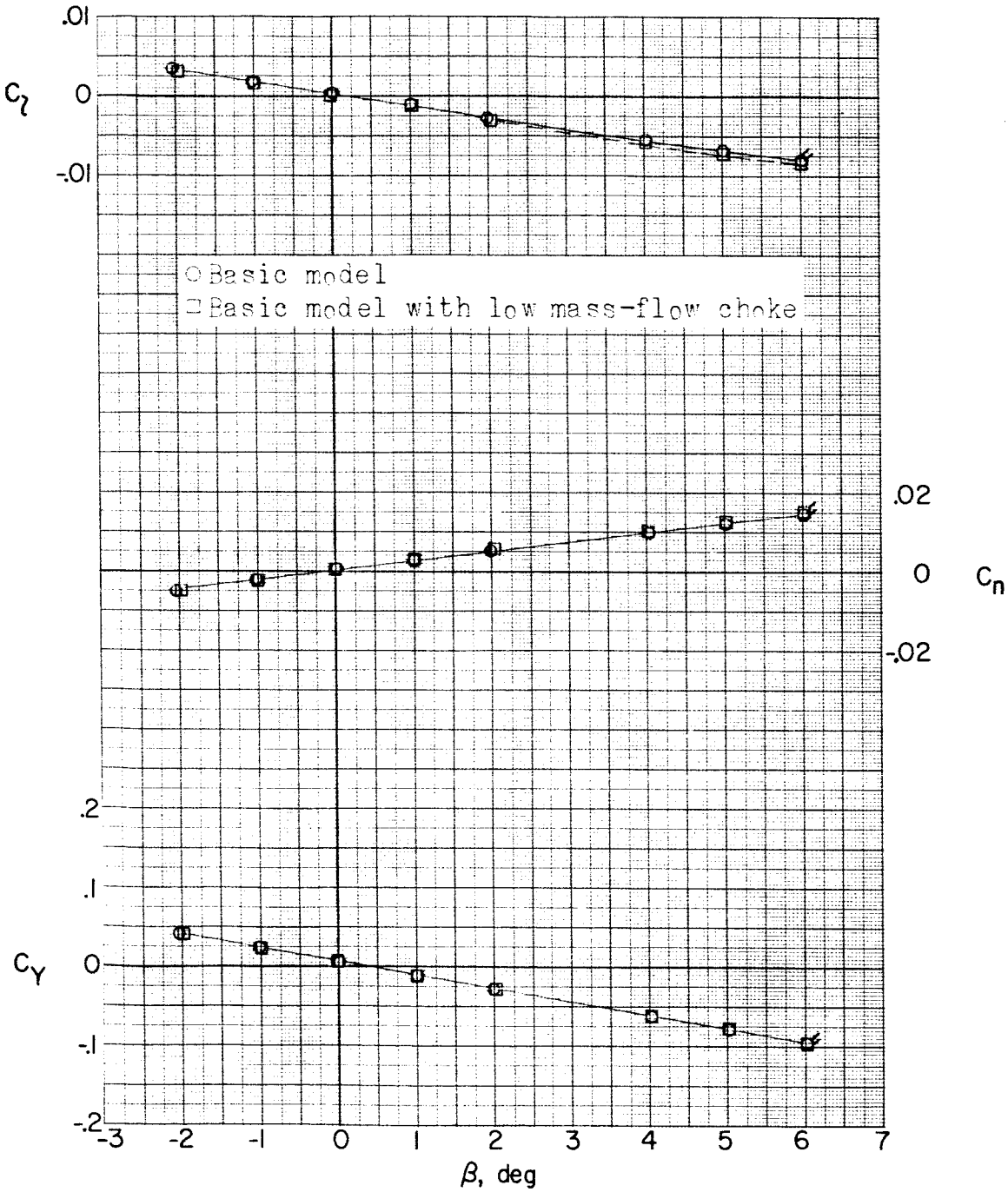

(a) M = 1.56; α = 0°.

Figure 22.- Effect of mass-flow ratio on aerodynamic characteristics in sideslip. Flagged symbols denote wall-reflected shock waves striking the tail.

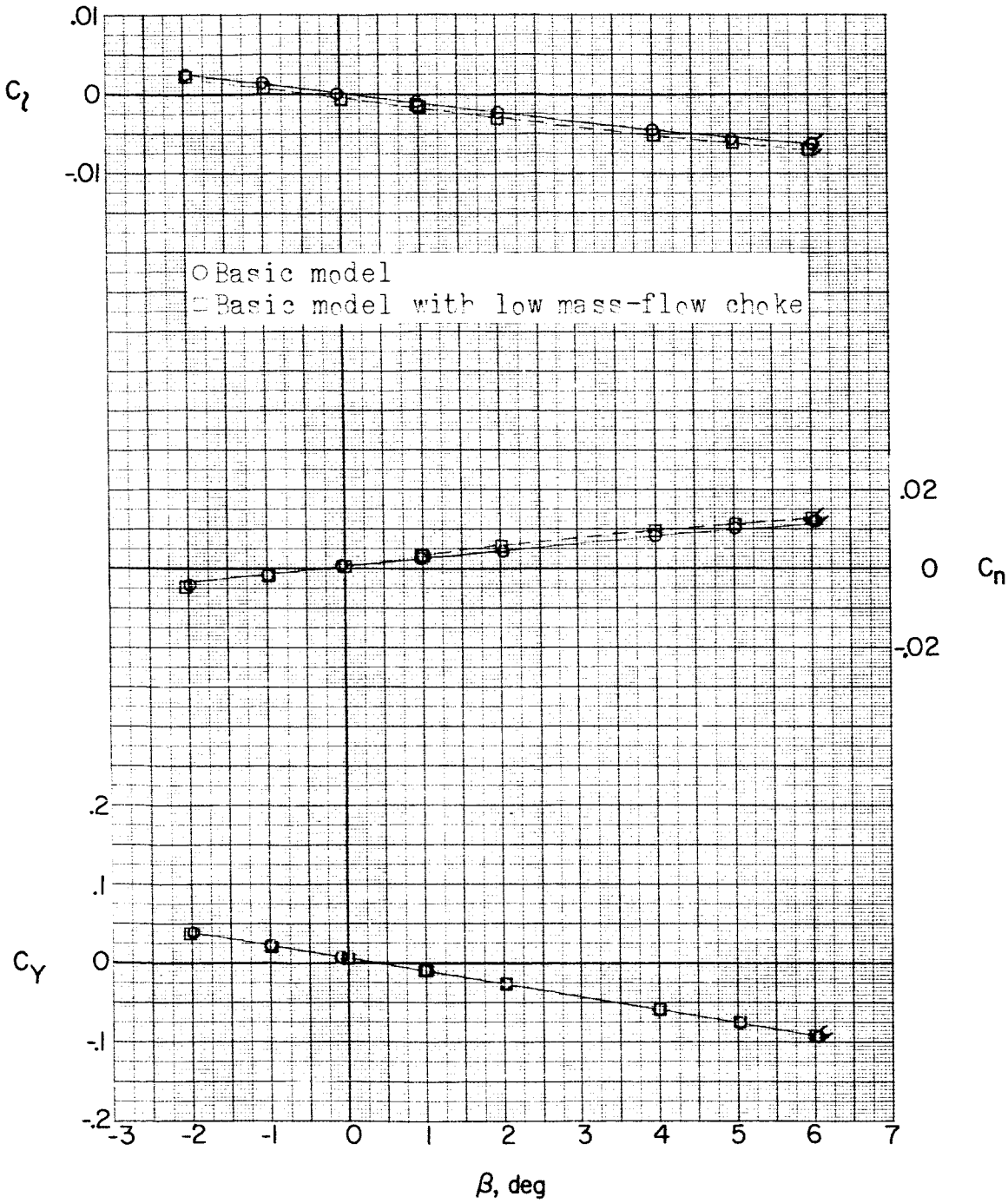

(a) Continued. $\alpha = 5.3^{\circ}$.

Figure 22.- Continued.

[redacted]

DECLASSIFIED

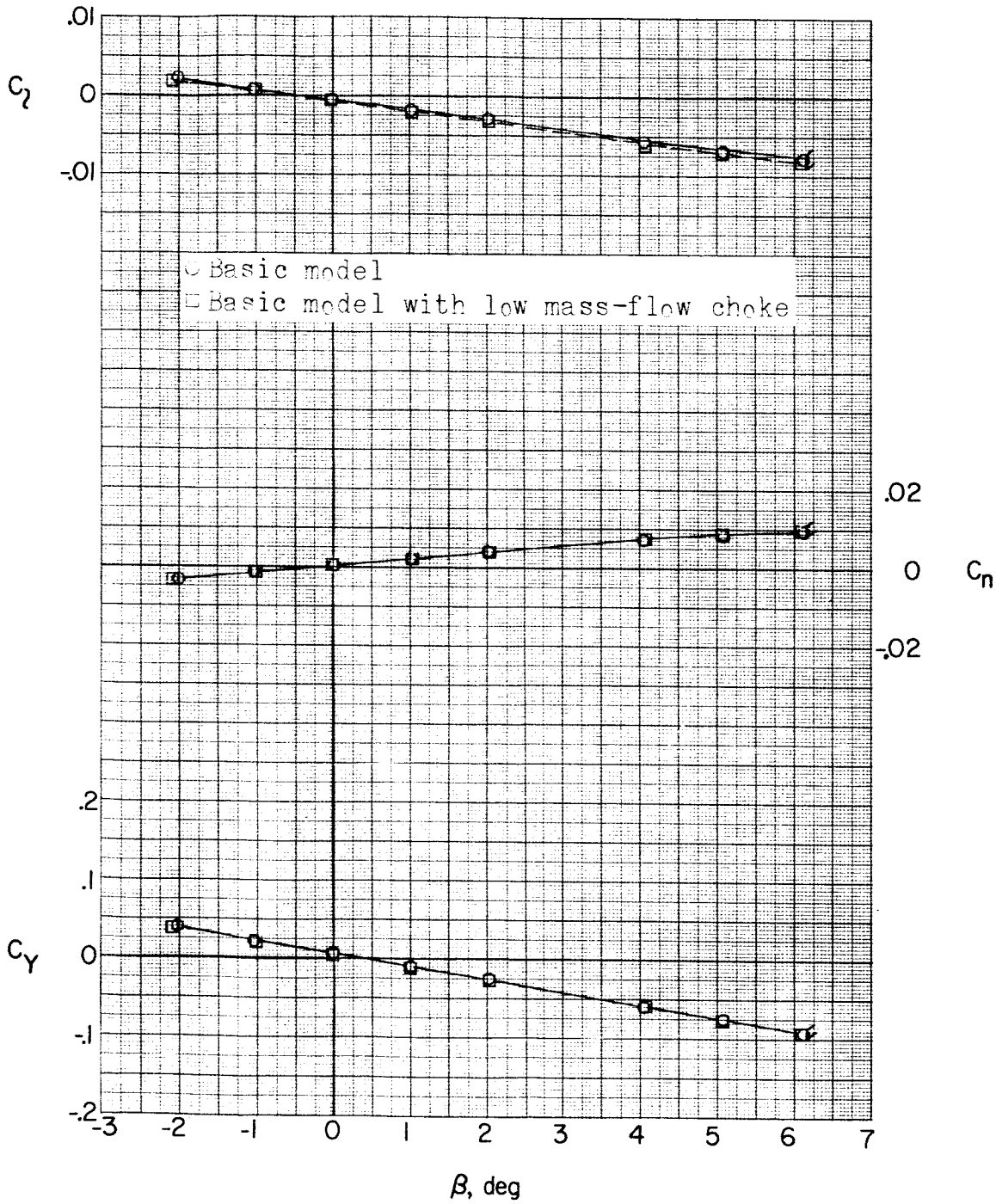

(a) Concluded. $\alpha = 10.6^{\circ}$.

Figure 22.- Continued.

DECLASSIFIED

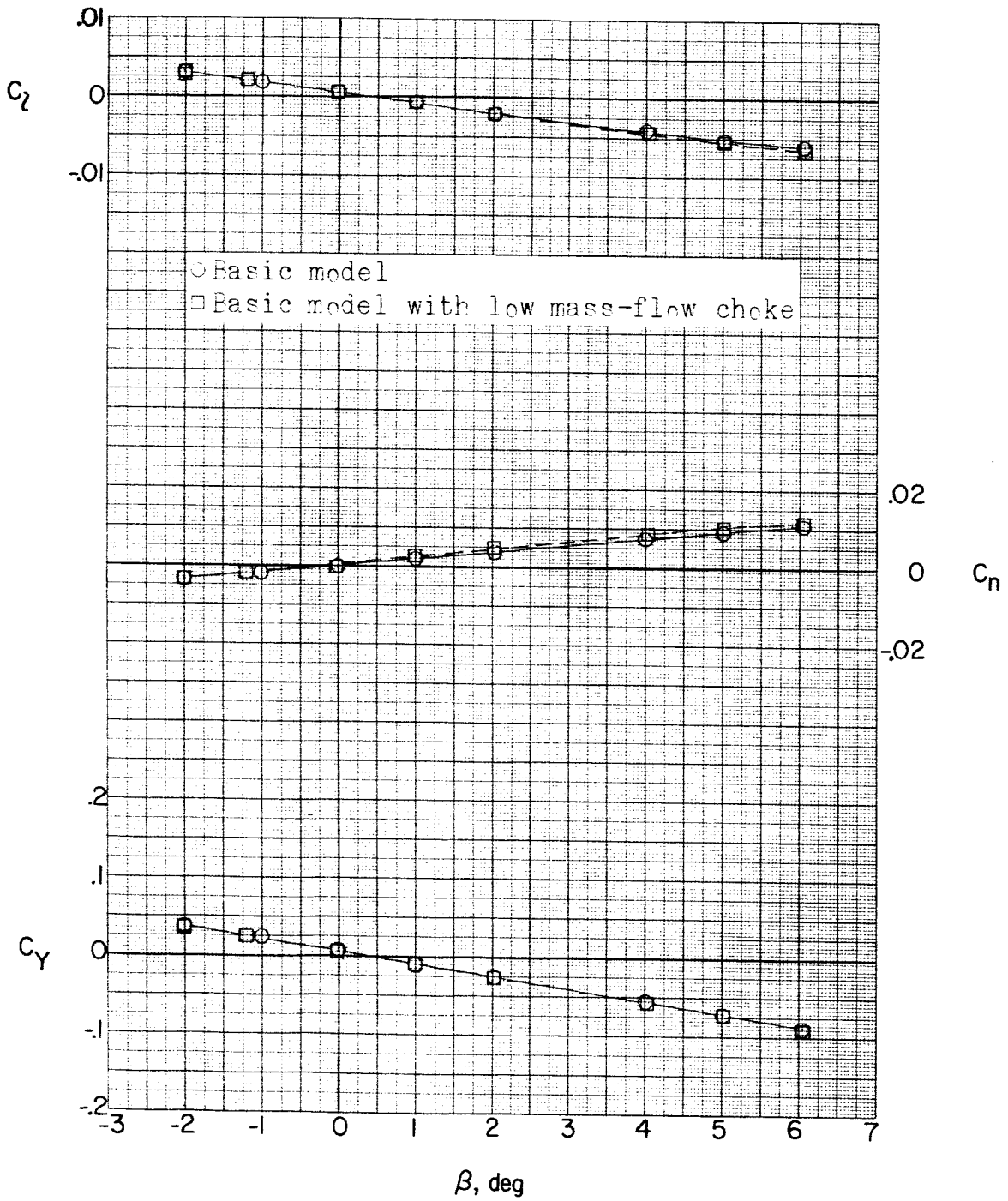

(b) M = 1.76. α = 0°.

Figure 22.- Continued.

[redacted]

DECLASSIFIED

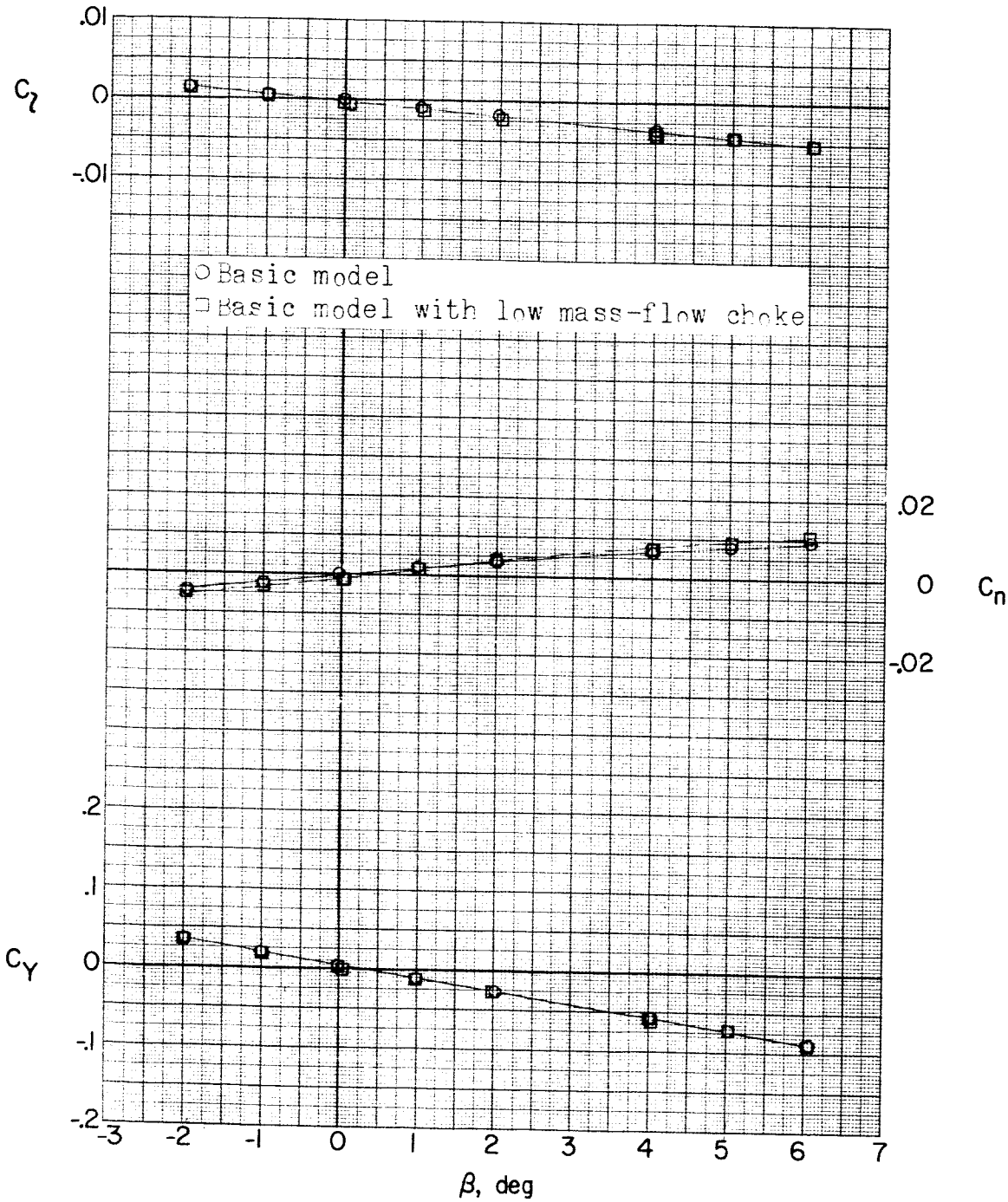

(b) Continued. $\alpha = 5.2^{\circ}$.

Figure 22.- Continued.

[redacted]

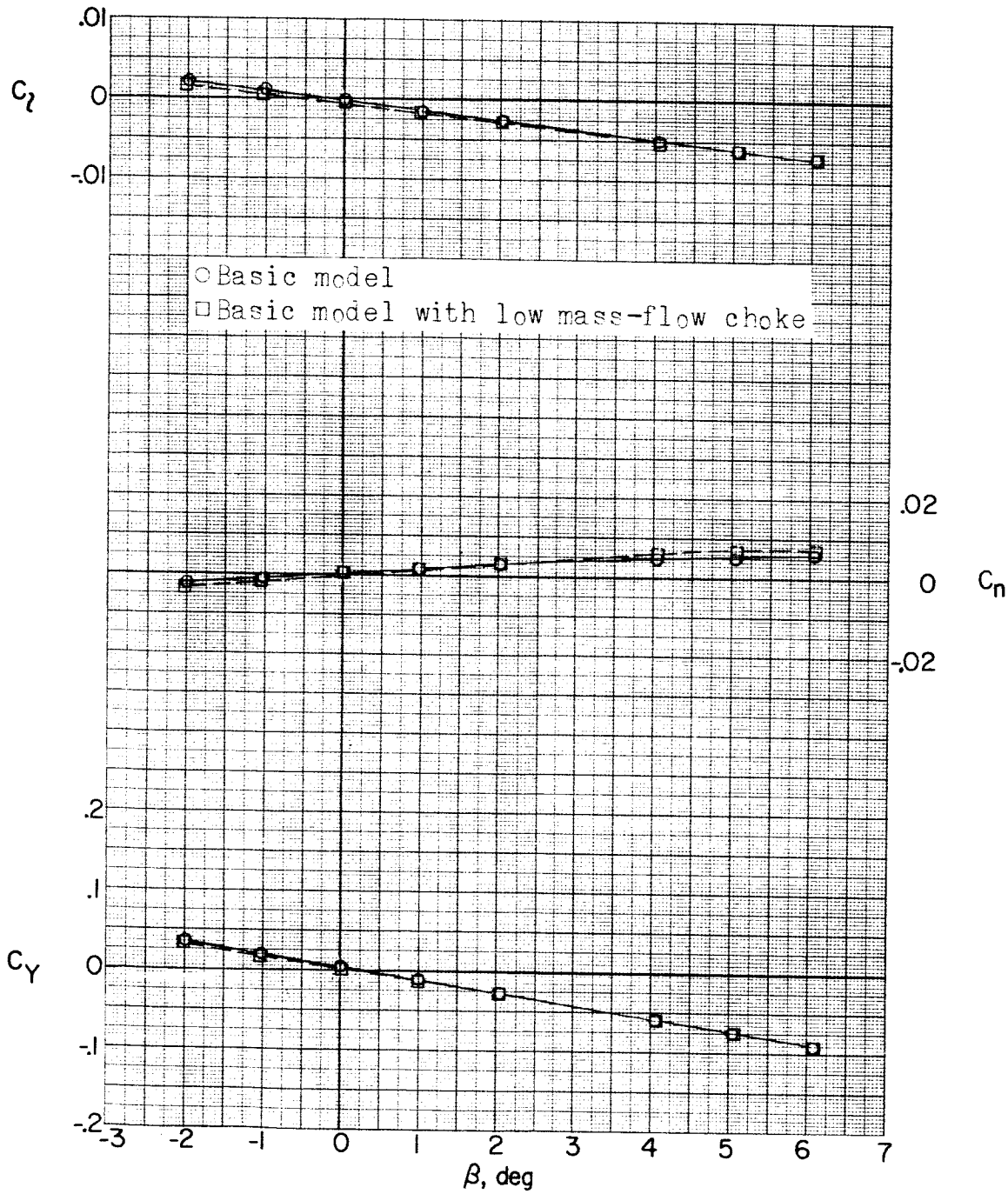

(b) Concluded. $\alpha = 10.5^{\circ}$.

Figure 22.- Continued.

[redacted]

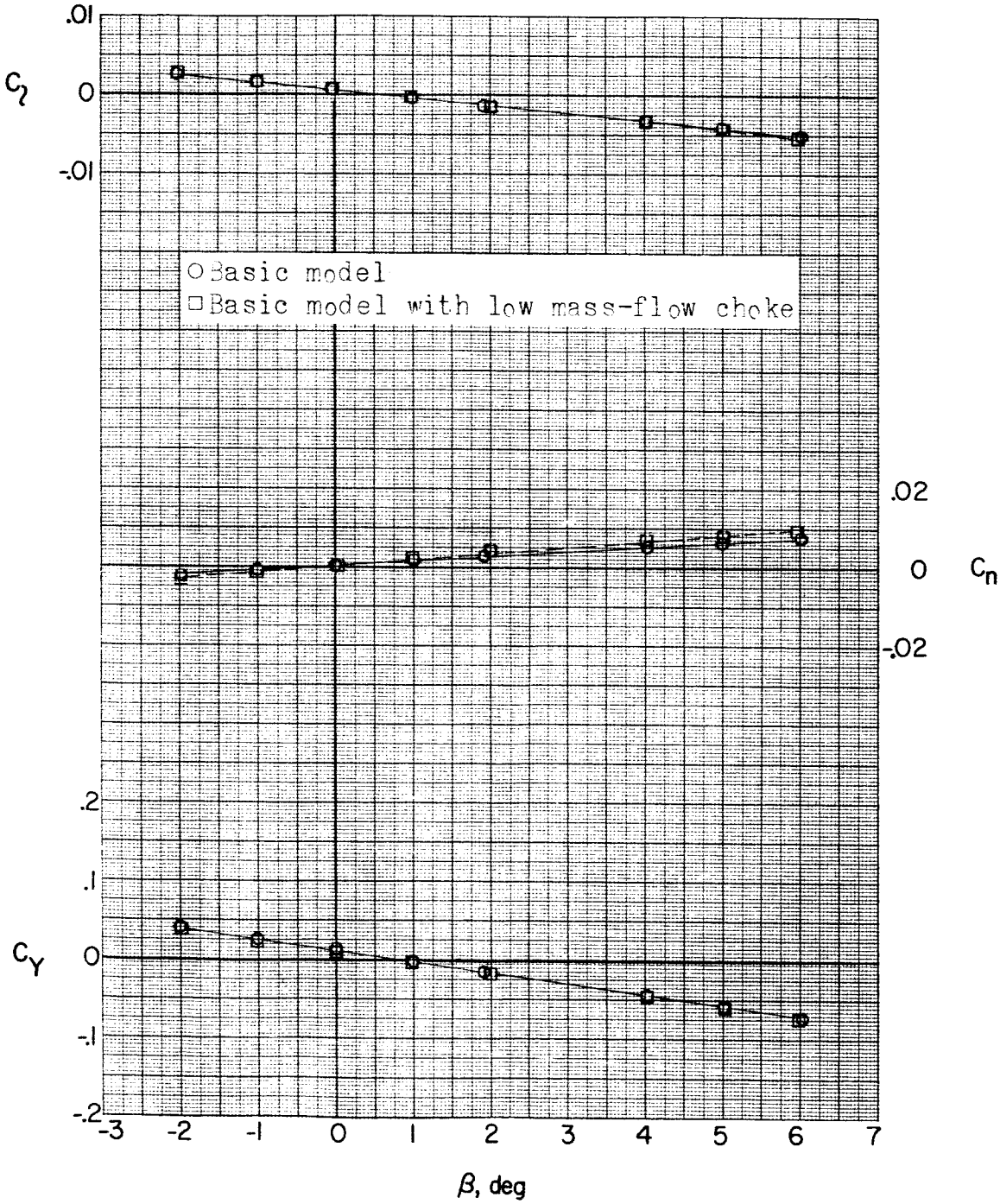

(c) M = 2.06. α = 0°.

Figure 22.- Continued.

[redacted]

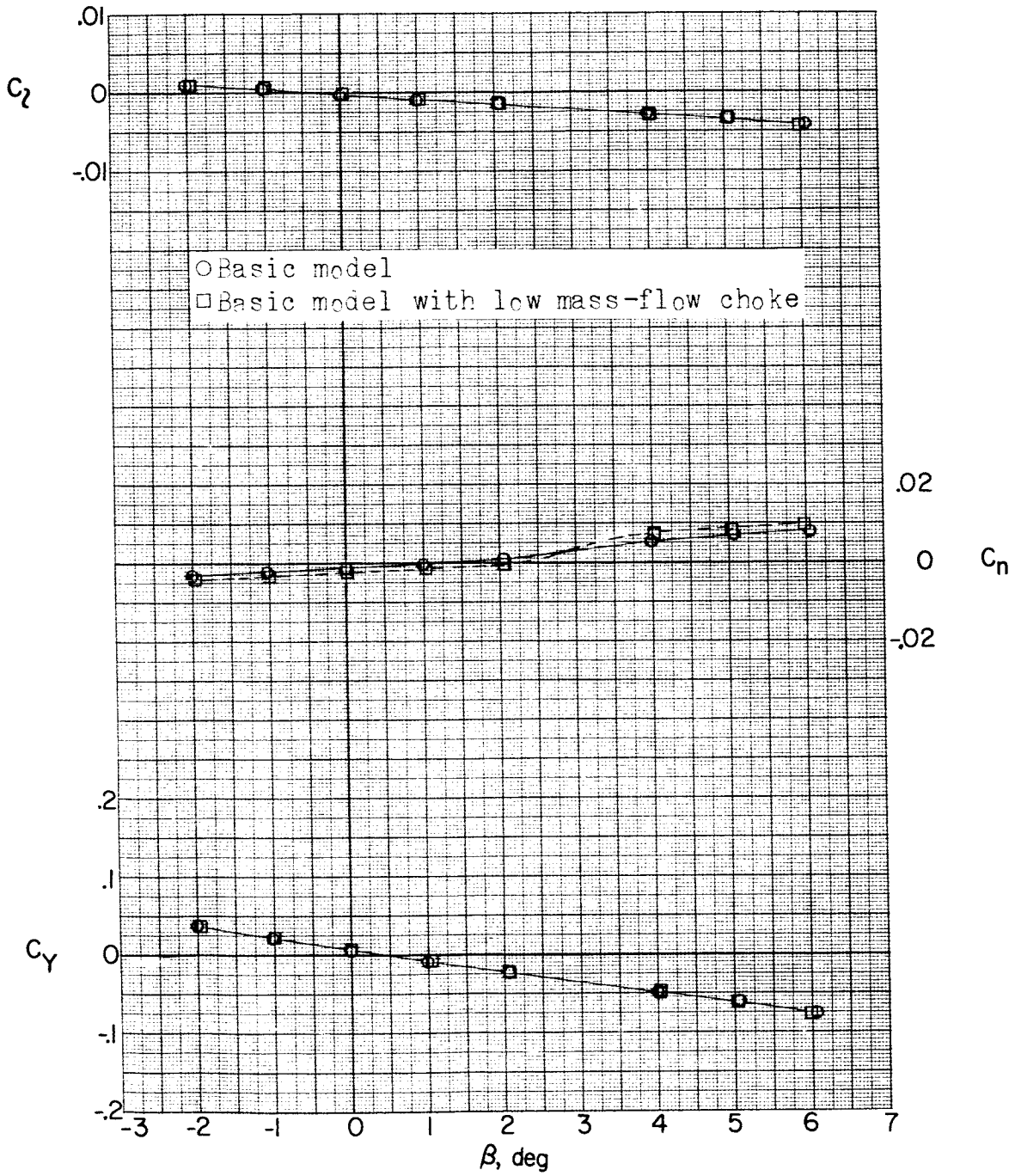

(c) Continued. $\alpha = 5.2^{\circ}$.

Figure 22.- Continued.

[redacted]

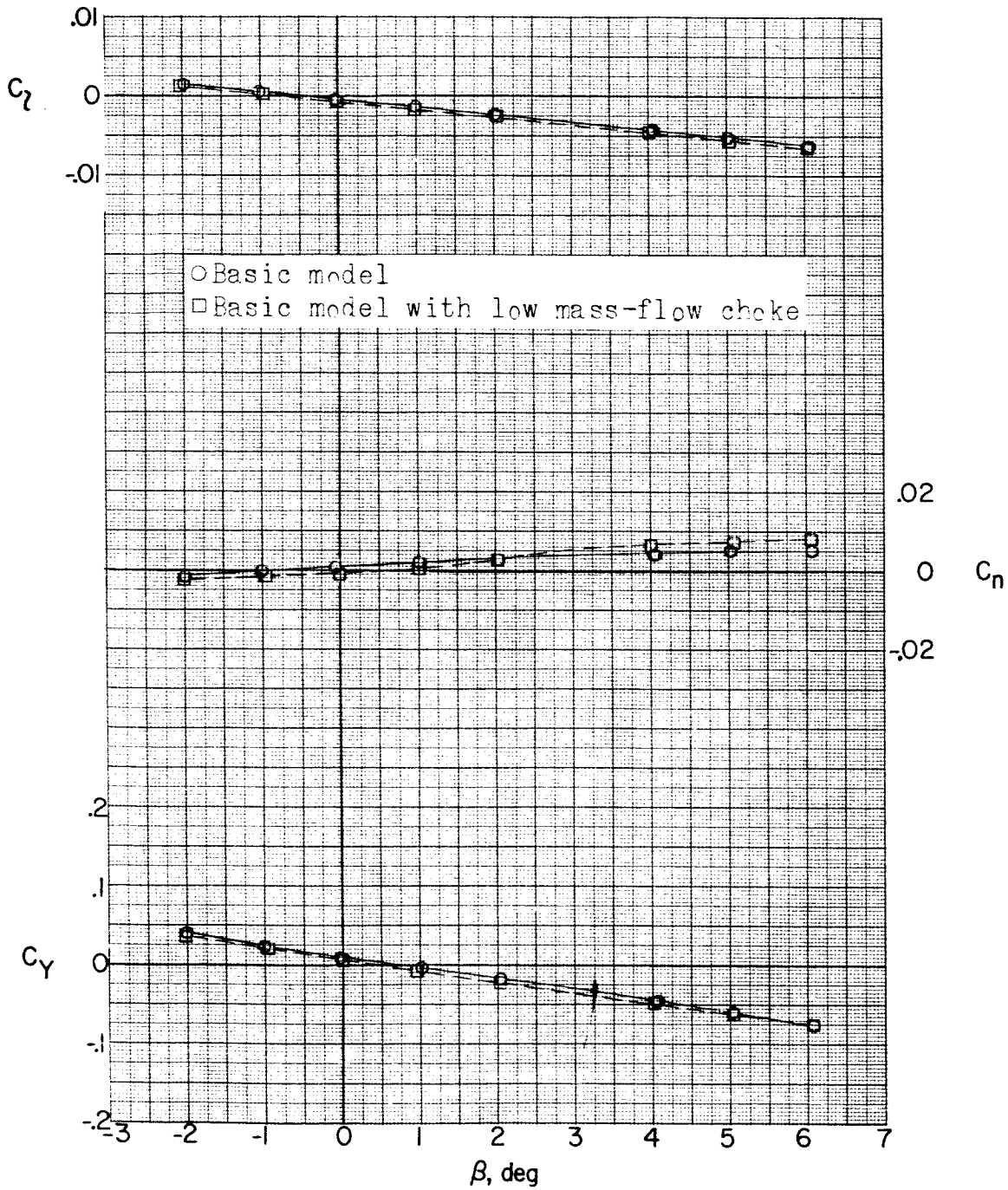

(c) Concluded. $\alpha = 10.4^{\circ}$.

Figure 22.- Concluded.

[redacted]

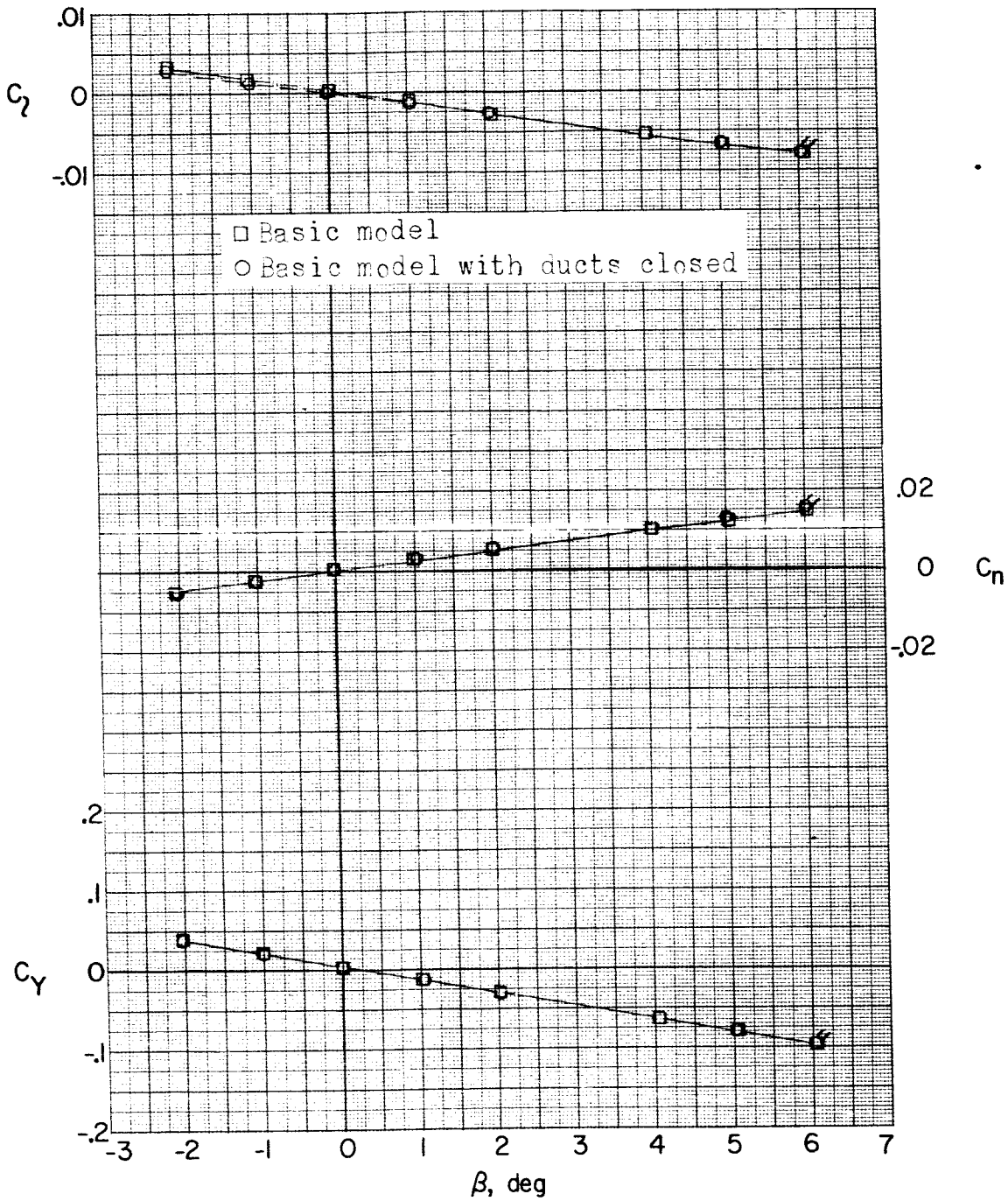

(a) M = 1.56; α = 0°.

Figure 23.- Effect of faired duct inlets on aerodynamic characteristics in sideslip. Flagged symbols denote wall-reflected shock waves striking the tail.

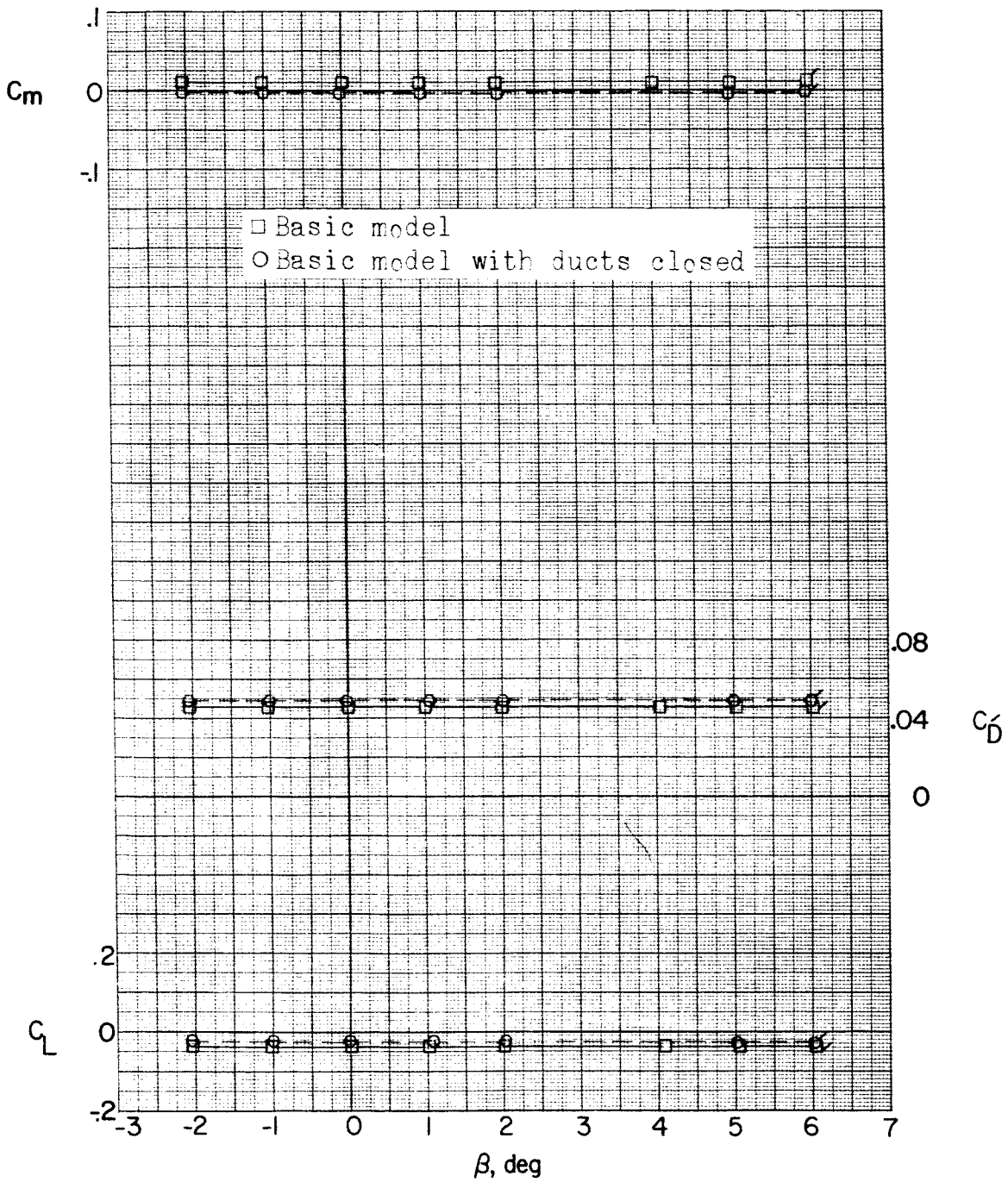

(a) Continued. $\alpha = 0^{\circ}$.

Figure 23.- Continued.

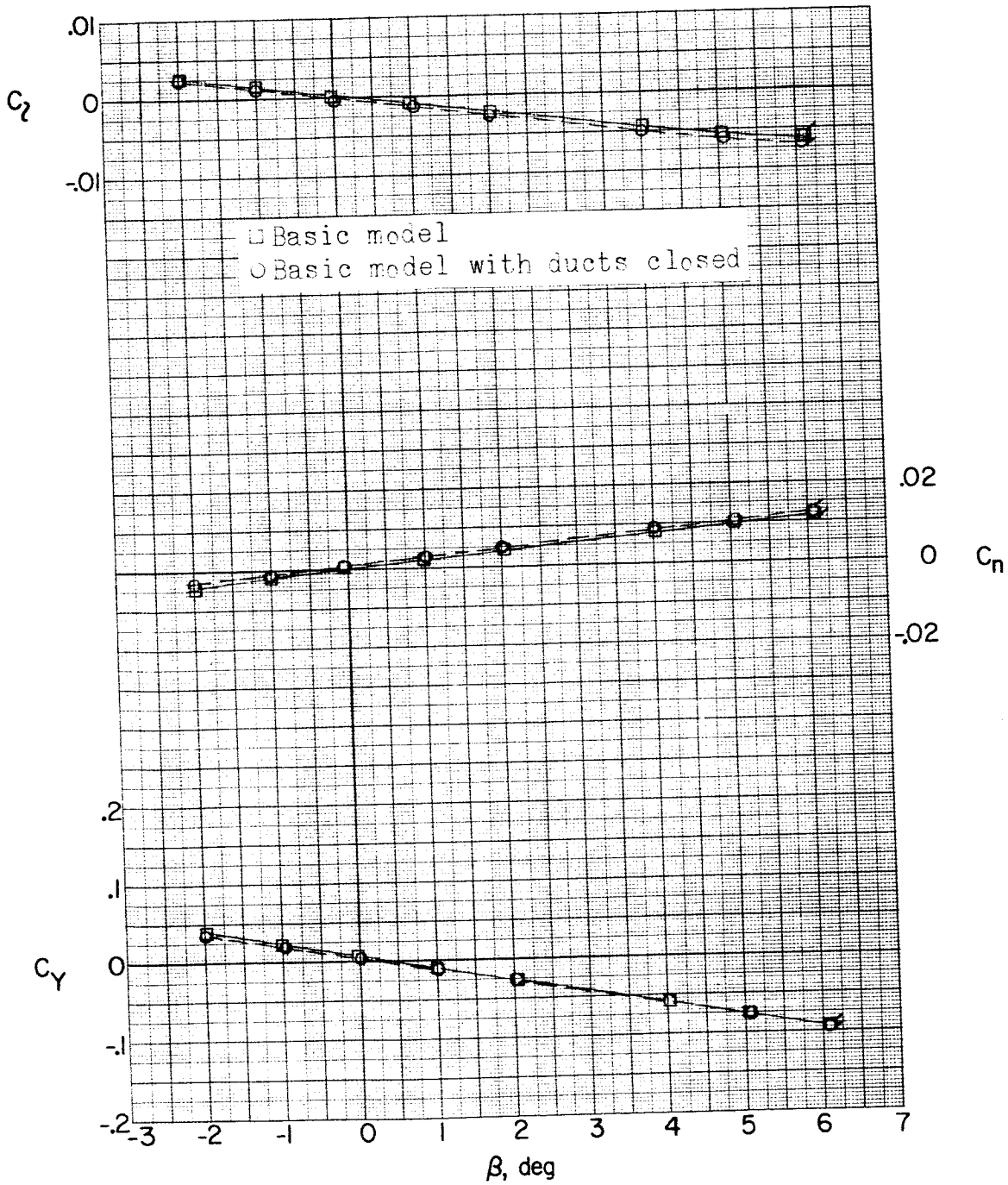

(a) Continued. $\alpha = 5.3^{\circ}$.

Figure 23.- Continued.

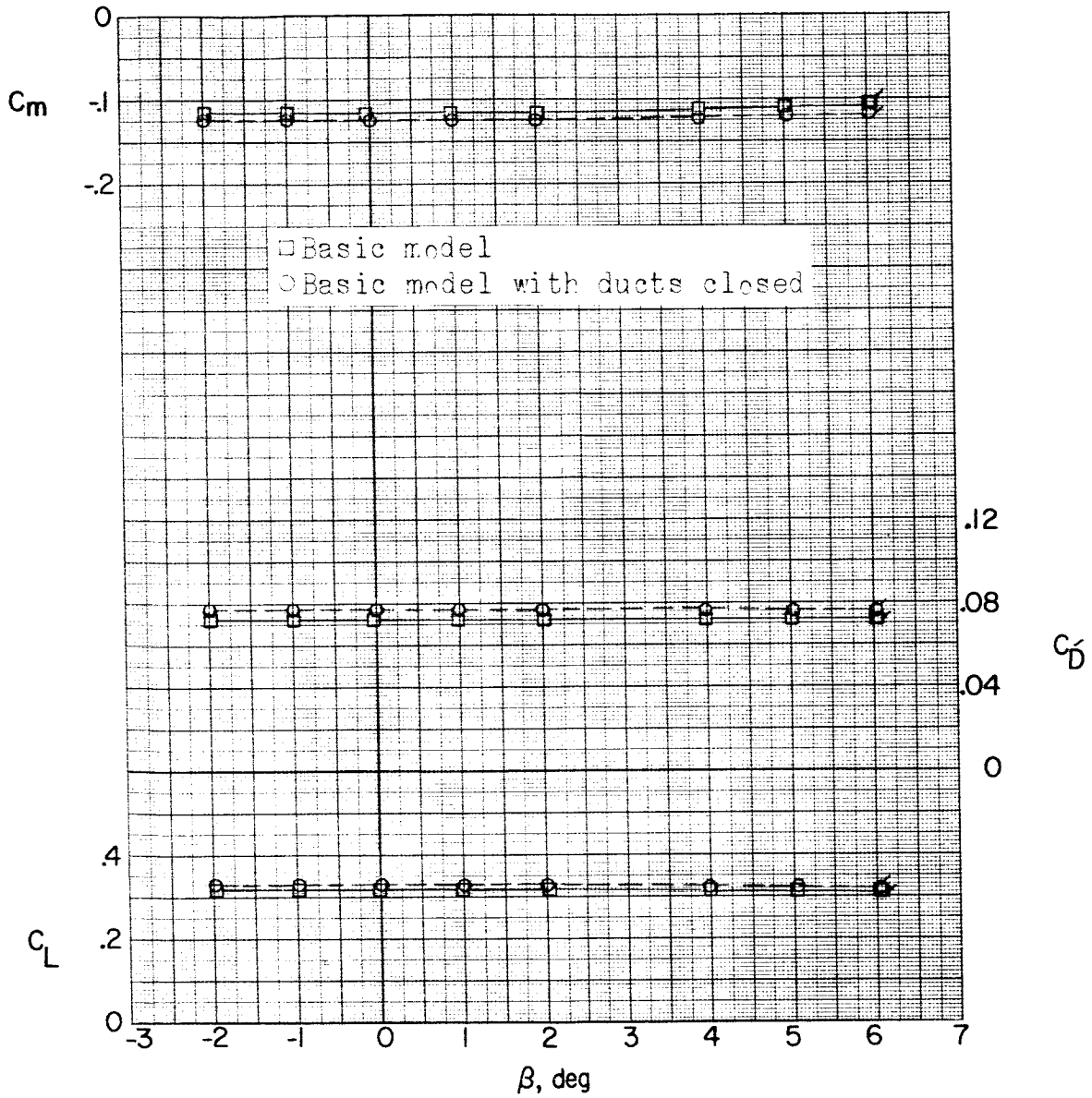

(a) Continued. $\alpha = 5.3^{\circ}$.

Figure 23.- Continued.

[redacted]

DECLASSIFIED

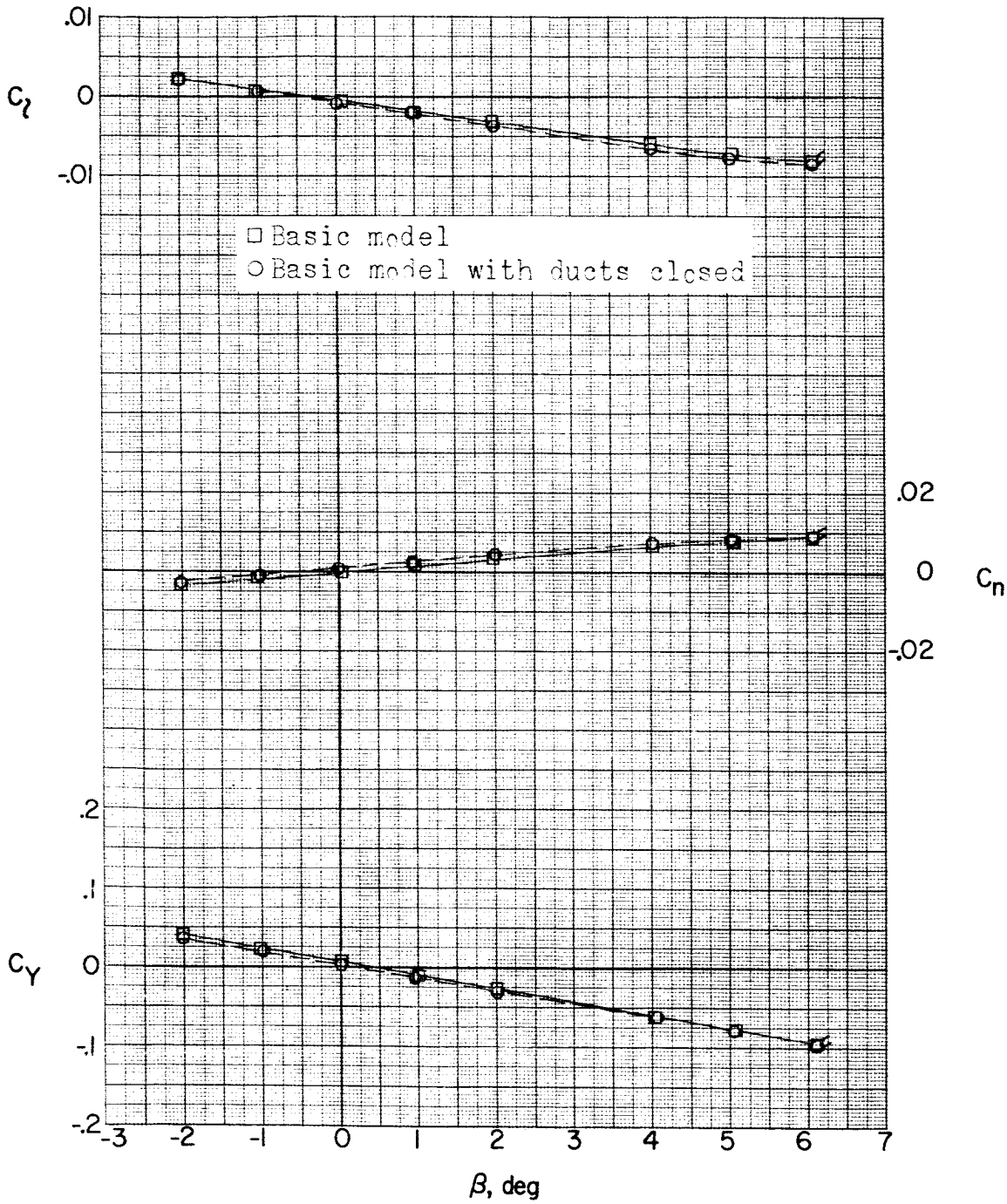

(a) Continued. $\alpha = 10.6^{\circ}$.

Figure 23.- Continued.

DECLASSIFIED

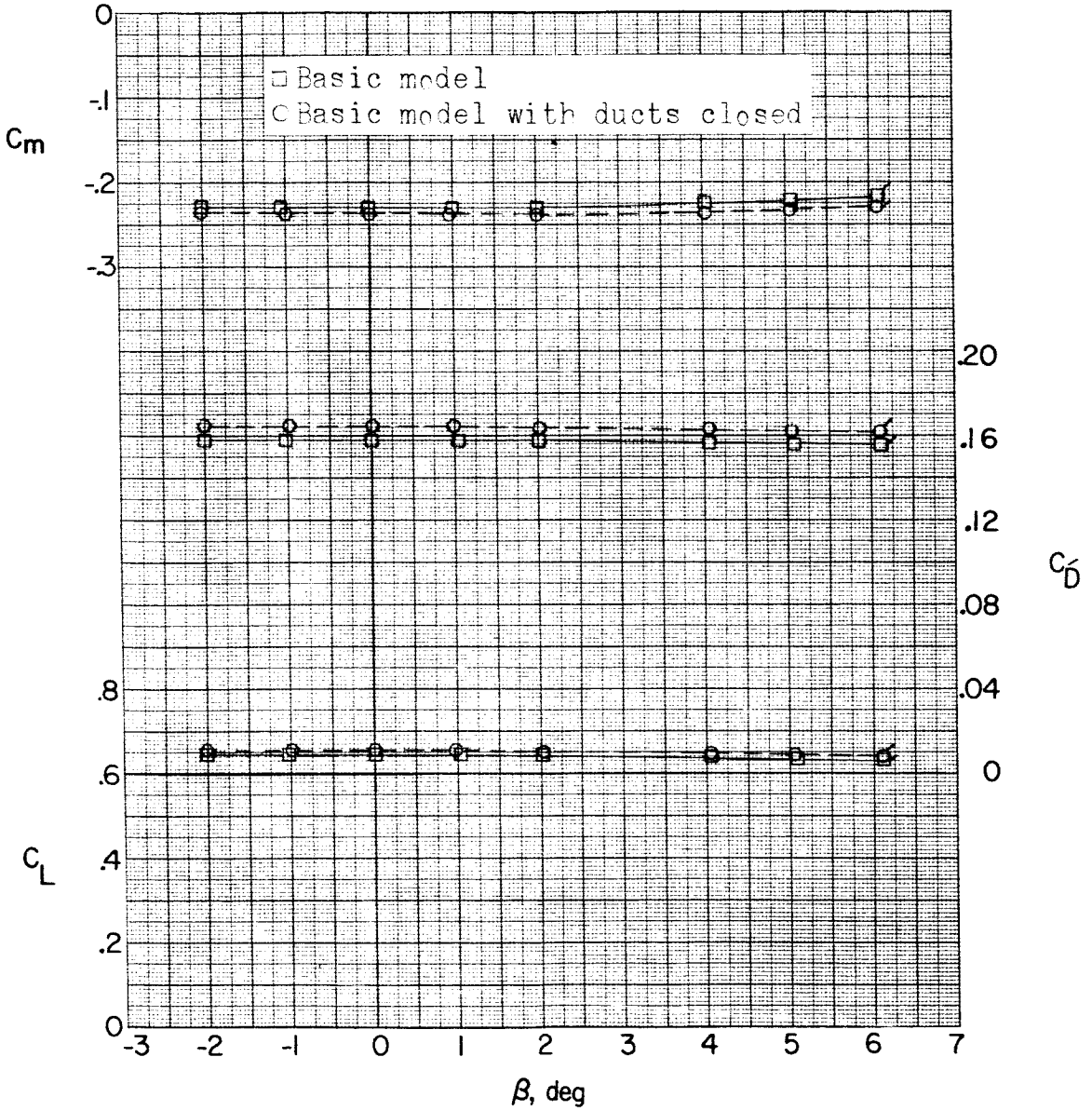

(a) Concluded. $\alpha = 10.6^{\circ}$.

Figure 23.- Continued.

[redacted]

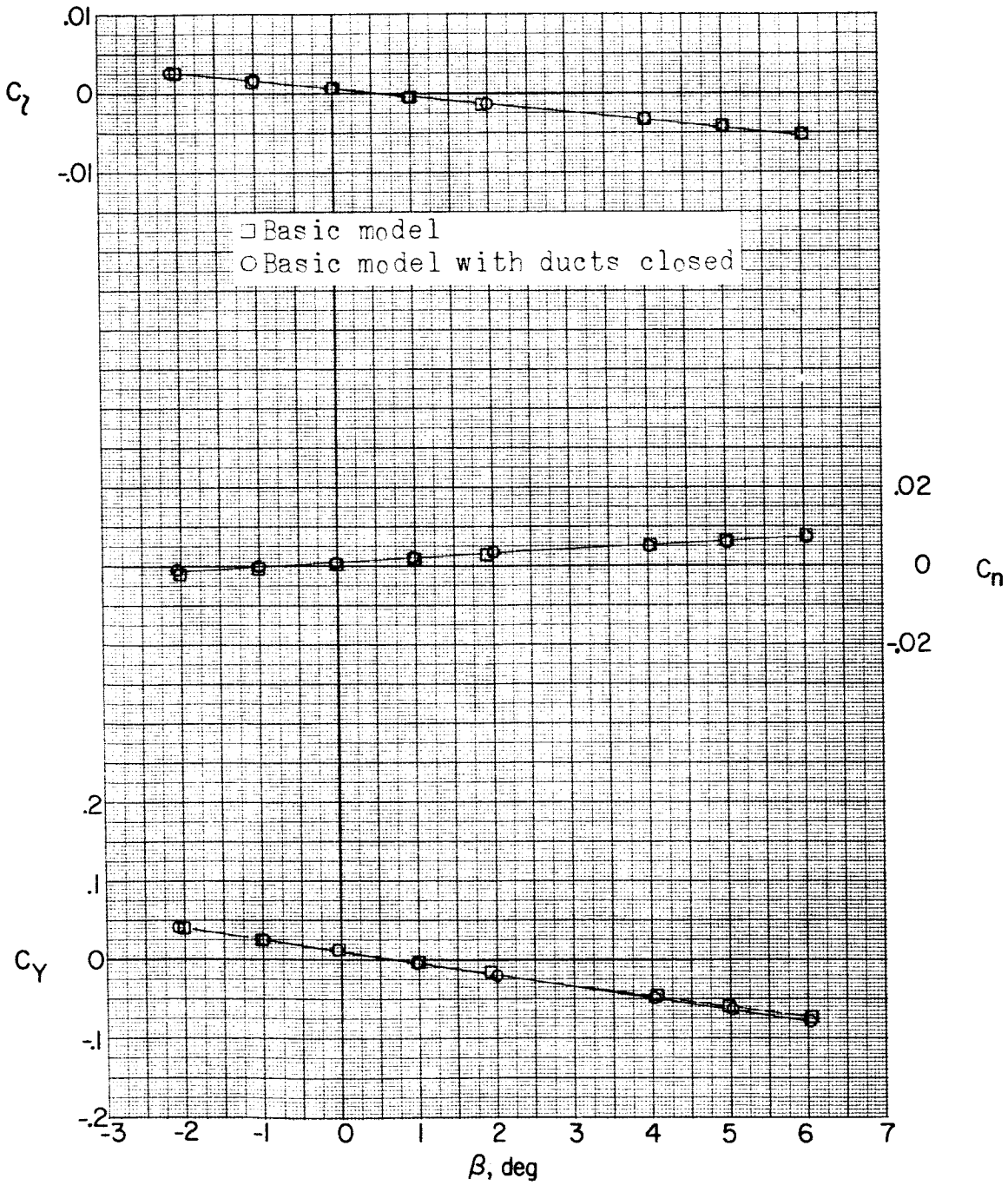

(b) M = 2.06; $\alpha = 0^{\circ}$.

Figure 23.- Continued.

[redacted]

DECLASSIFIED

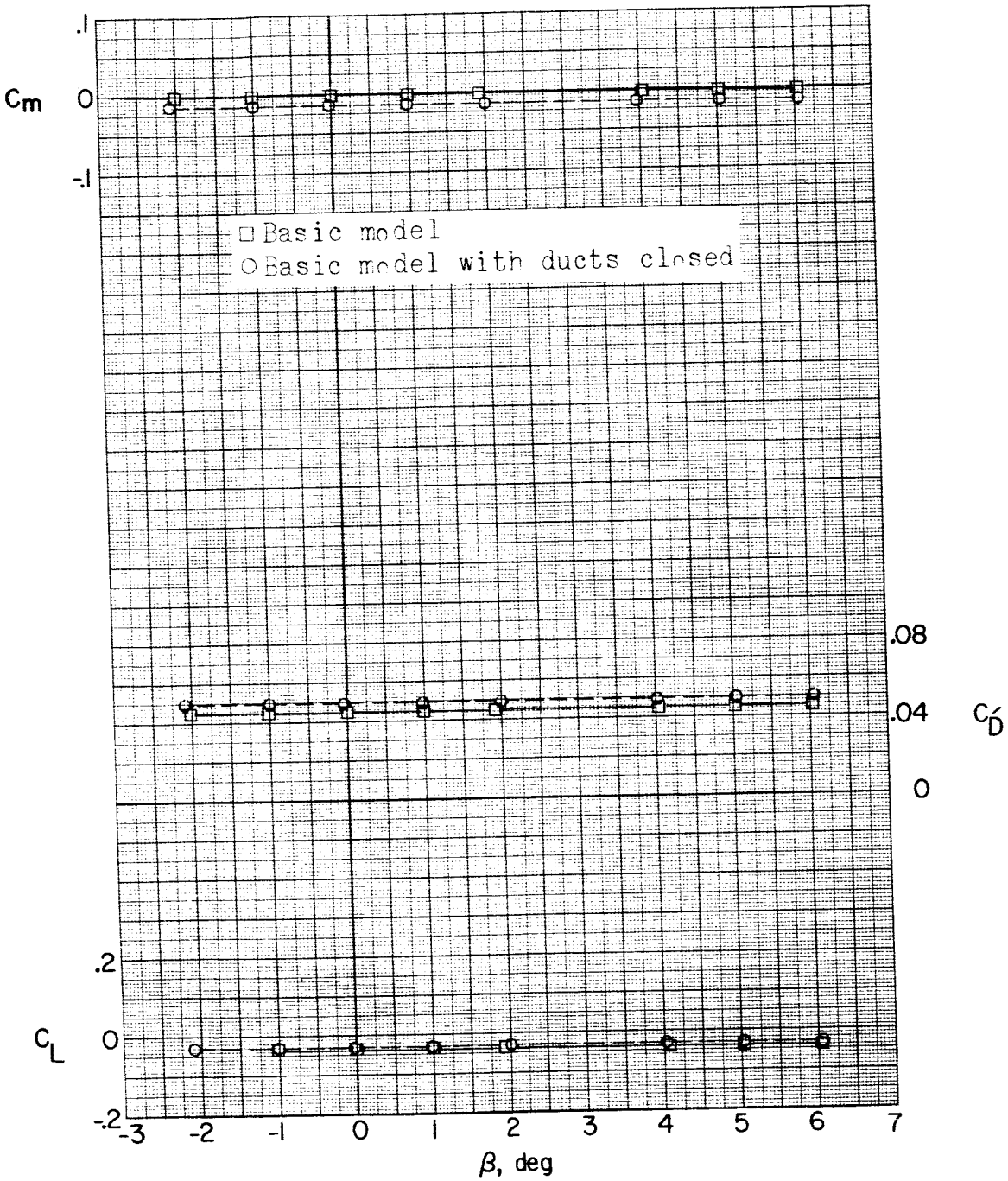

(b) Continued. $\alpha = 0^{\circ}$.

Figure 23.- Continued.

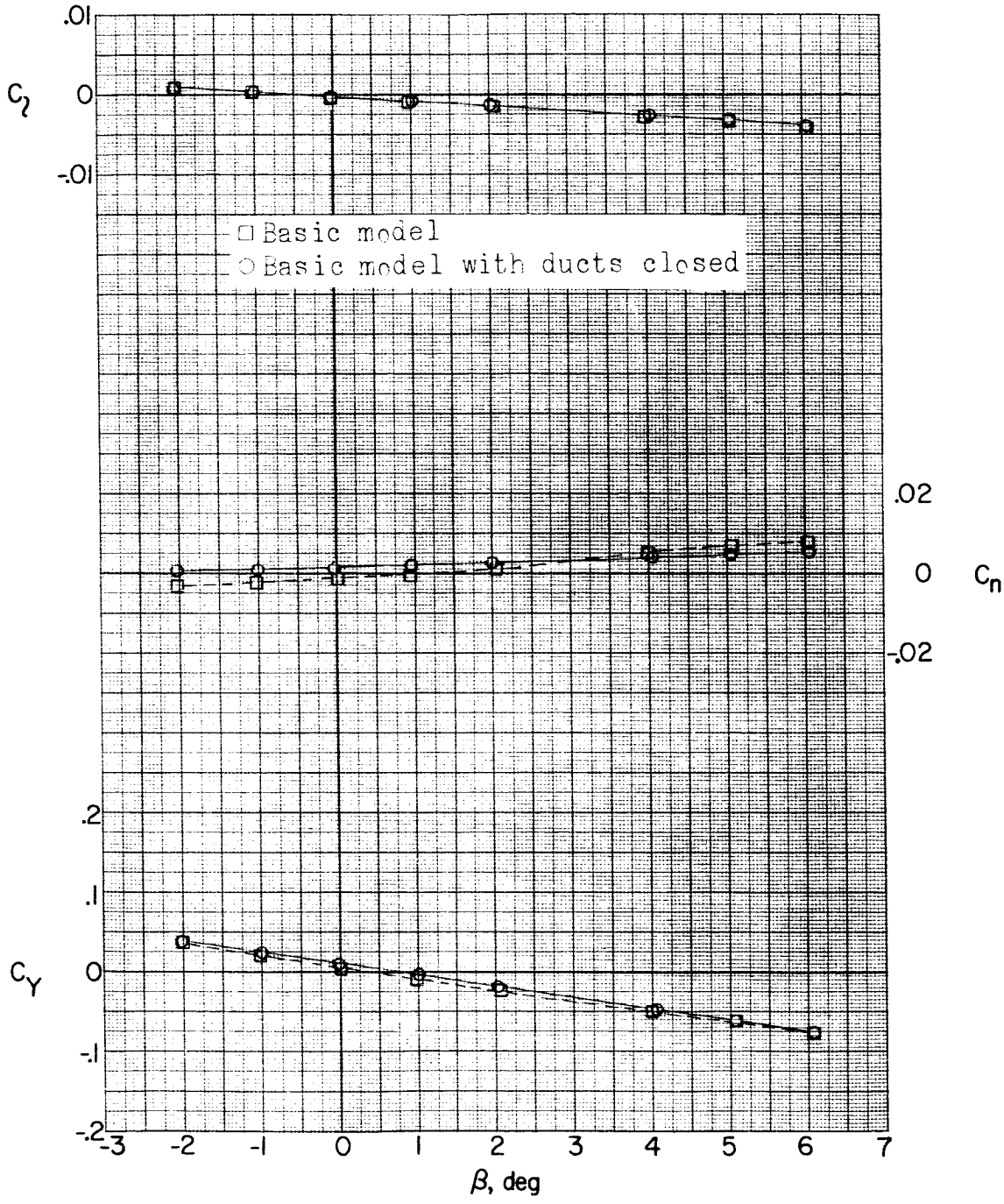

(b) Continued. $\alpha = 5.2^{\circ}$.

Figure 23.- Continued.

[redacted]

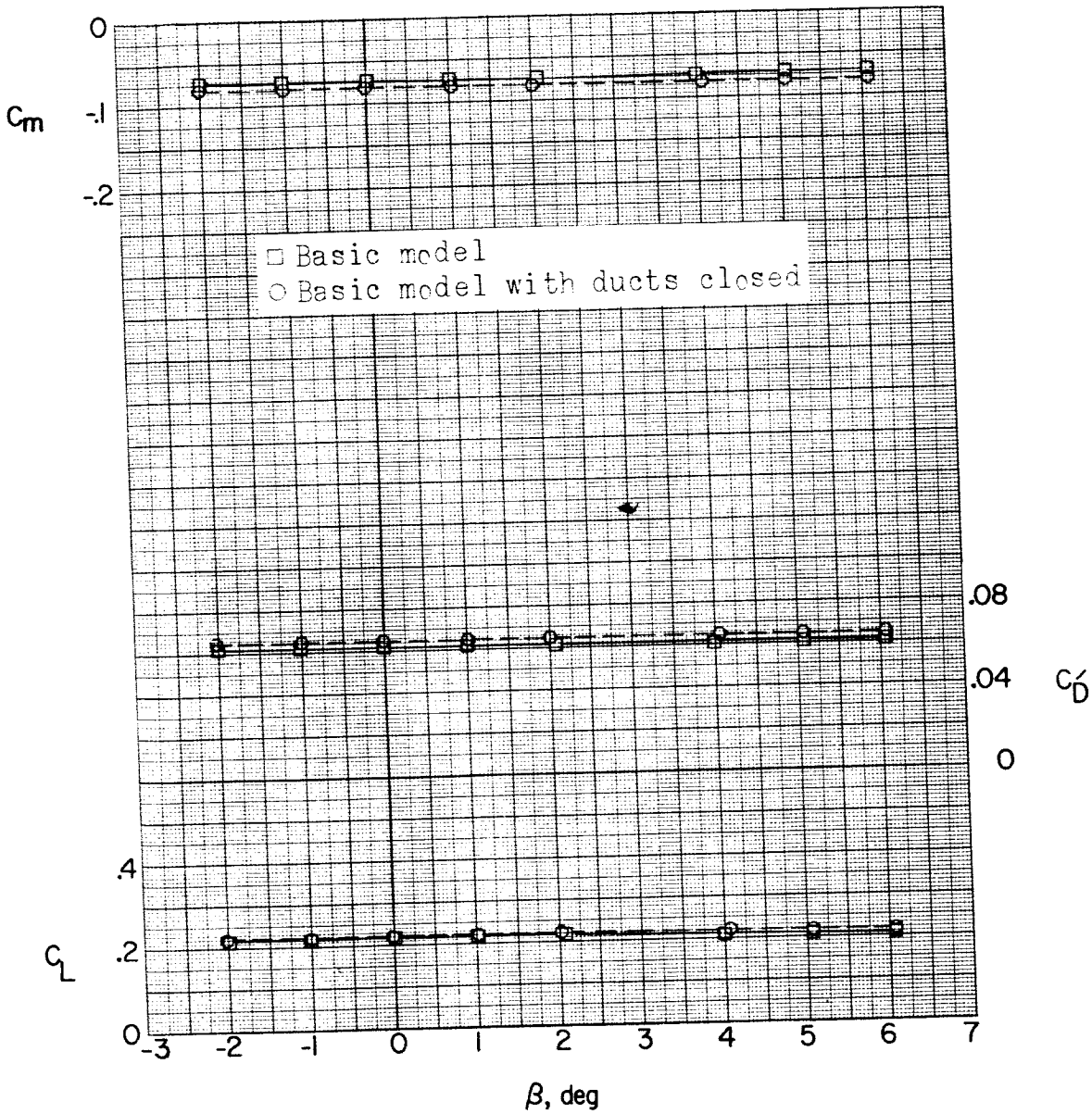

(b) Continued. $\alpha = 5.2^{\circ}$.

Figure 23.- Continued.

DECLASSIFIED

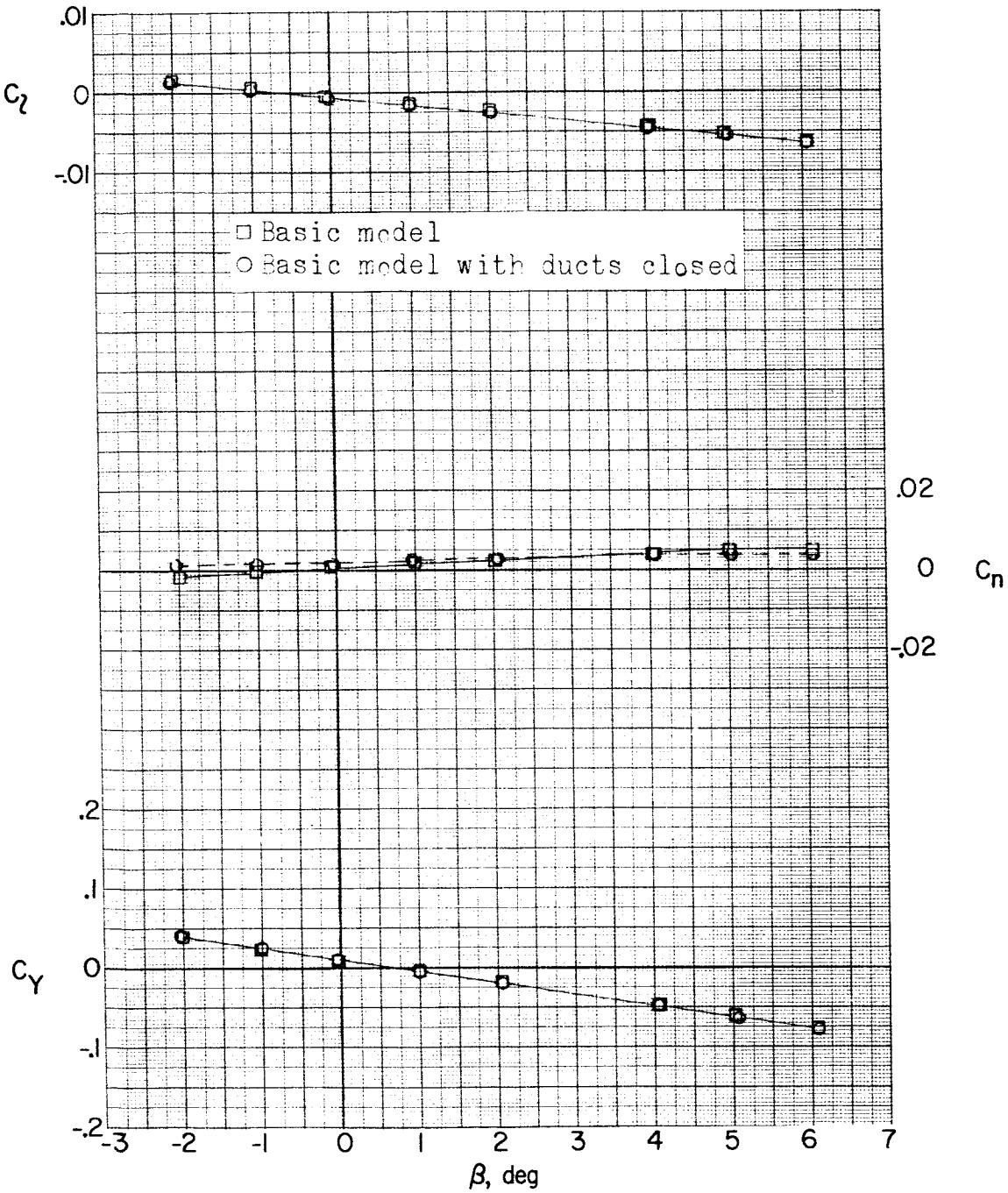

(b) Continued. $\alpha = 10.4^{\circ}$.

Figure 23.- Continued.

[redacted]

DECLASSIFIED

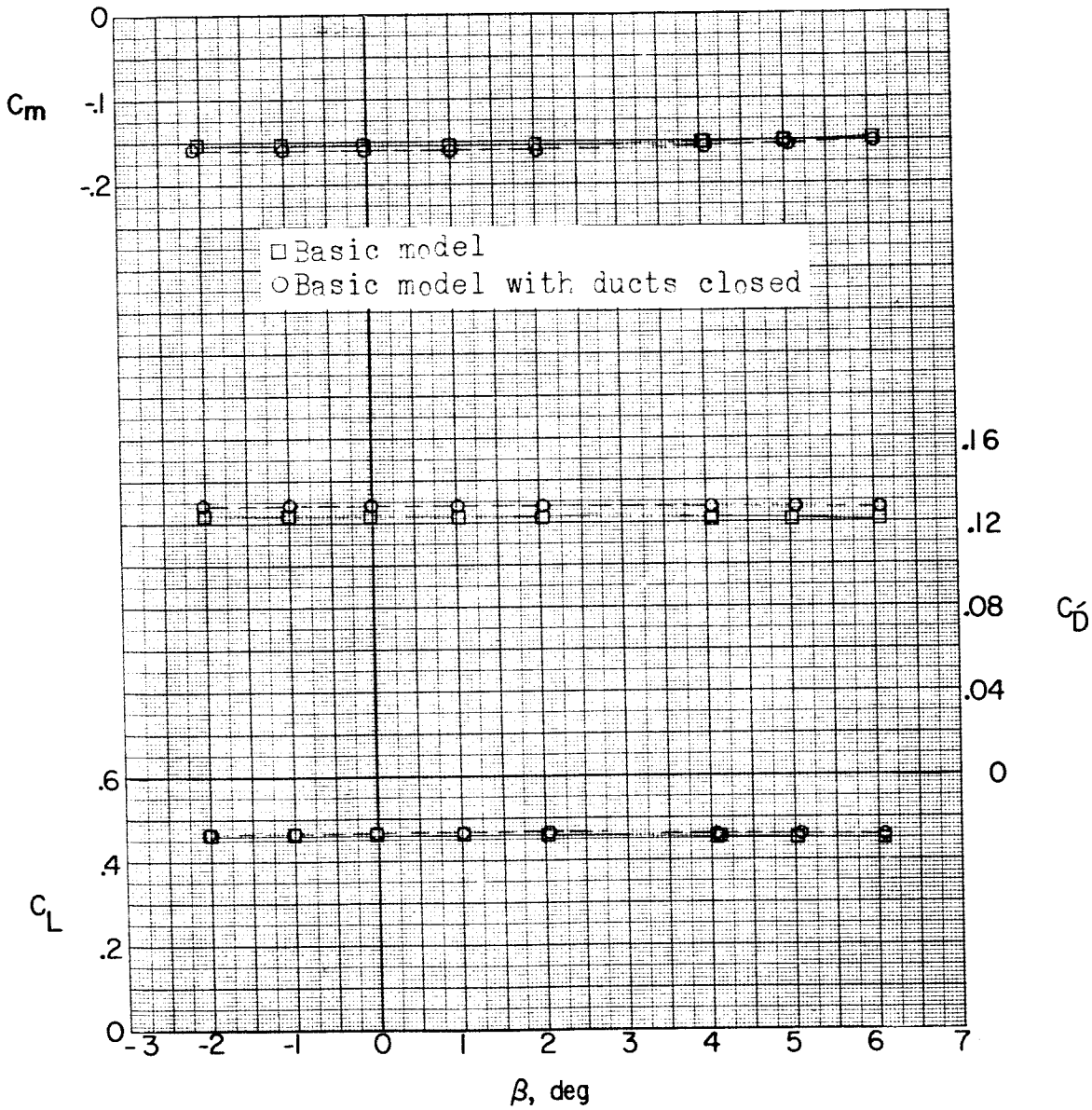

(b) Concluded. $\alpha = 10.4^{\circ}$.

Figure 23.- Concluded.

[redacted]

DECLASSIFIED

INDEX

Subject	Number
Stability, Longitudinal - Static	1.8.1.1.1
Stability, Lateral - Static	1.8.1.1.2
Stability, Directional - Static	1.8.1.1.3
Control, Longitudinal	1.8.2.1

ABSTRACT

An investigation has been conducted in the Langley Unitary Plan wind tunnel at Mach numbers of 1.56, 1.76, 2.06, and 2.53 to determine the drag and static longitudinal and lateral stability characteristics of a 1/15-scale model of the Grumman F11F-1F airplane. Configurations consisting of a wing-root leading-edge fillet and horizontal tails with negative dihedral of 10° and 30° were also investigated. The model had a wing with 35° sweepback of the quarter chord, an aspect ratio of 4, a taper ratio of 0.5, and dihedral of -2.5°.

[redacted]